### **Springer Theses**Recognizing Outstanding Ph.D. Research

Tim Langen

# Non-equilibrium Dynamics of One-Dimensional Bose Gases



### **Springer Theses**

Recognizing Outstanding Ph.D. Research

### Aims and Scope

The series "Springer Theses" brings together a selection of the very best Ph.D. theses from around the world and across the physical sciences. Nominated and endorsed by two recognized specialists, each published volume has been selected for its scientific excellence and the high impact of its contents for the pertinent field of research. For greater accessibility to non-specialists, the published versions include an extended introduction, as well as a foreword by the student's supervisor explaining the special relevance of the work for the field. As a whole, the series will provide a valuable resource both for newcomers to the research fields described, and for other scientists seeking detailed background information on special questions. Finally, it provides an accredited documentation of the valuable contributions made by today's younger generation of scientists.

### Theses are accepted into the series by invited nomination only and must fulfill all of the following criteria

- They must be written in good English.
- The topic should fall within the confines of Chemistry, Physics, Earth Sciences, Engineering and related interdisciplinary fields such as Materials, Nanoscience, Chemical Engineering, Complex Systems and Biophysics.
- The work reported in the thesis must represent a significant scientific advance.
- If the thesis includes previously published material, permission to reproduce this must be gained from the respective copyright holder.
- They must have been examined and passed during the 12 months prior to nomination.
- Each thesis should include a foreword by the supervisor outlining the significance of its content.
- The theses should have a clearly defined structure including an introduction accessible to scientists not expert in that particular field.

More information about this series at http://www.springer.com/series/8790

### Tim Langen

## Non-equilibrium Dynamics of One-Dimensional Bose Gases

Doctoral Thesis accepted by the Technische Universität Wien, Austria



Author
Dr. Tim Langen
JILA, NIST and University of Colorado
Boulder, CO
USA

Supervisor
Prof. Dr. Jörg Schmiedmayer
Atominstitut
TU Wien
Vienna
Austria

ISSN 2190-5053 ISSN 2190-5061 (electronic) Springer Theses ISBN 978-3-319-18563-7 ISBN 978-3-319-18564-4 (eBook) DOI 10.1007/978-3-319-18564-4

Library of Congress Control Number: 2015939812

Springer Cham Heidelberg New York Dordrecht London © Springer International Publishing Switzerland 2015

This work is subject to copyright. All rights are reserved by the Publisher, whether the whole or part of the material is concerned, specifically the rights of translation, reprinting, reuse of illustrations, recitation, broadcasting, reproduction on microfilms or in any other physical way, and transmission or information storage and retrieval, electronic adaptation, computer software, or by similar or dissimilar methodology now known or hereafter developed.

The use of general descriptive names, registered names, trademarks, service marks, etc. in this publication does not imply, even in the absence of a specific statement, that such names are exempt from the relevant protective laws and regulations and therefore free for general use.

The publisher, the authors and the editors are safe to assume that the advice and information in this book are believed to be true and accurate at the date of publication. Neither the publisher nor the authors or the editors give a warranty, express or implied, with respect to the material contained herein or for any errors or omissions that may have been made.

Printed on acid-free paper

Springer International Publishing AG Switzerland is part of Springer Science+Business Media (www.springer.com)

### Parts of this thesis have been published in the following publications:

- M. Gring, M. Kuhnert, T. Langen, T. Kitagawa, B. Rauer, M. Schreitl, I. Mazets, D. Adu Smith, E. Demler, and J. Schmiedmayer Relaxation and prethermalization in an isolated quantum system Science 337, 1318 (2012), arXiv:1112.0013
- M. Kuhnert, R. Geiger, T. Langen, M. Gring, B. Rauer, T. Kitagawa, E. Demler,
   D. Adu Smith, and J. Schmiedmayer
   Multimode dynamics and emergence of a characteristic length-scale in a one-dimensional quantum system
  - Phys. Rev. Lett. 110, 090405 (2013), arXiv:1211.5323
- T. Langen, M. Gring, M. Kuhnert, B. Rauer, R. Geiger, D. Adu Smith, I. Mazets, and J. Schmiedmayer
  - Prethermalization in one-dimensional Bose gases: description by a stochastic Ornstein-Uhlenbeck process
  - Eur. Phys. J. Special Topics 217, 43 (2013), arXiv:1211.0016
- D. Adu Smith, M. Gring, T. Langen, M. Kuhnert, B. Rauer, R. Geiger, T. Kitagawa, I. Mazets, E. Demler, and J. Schmiedmayer Prethermalization revealed by the relaxation dynamics of full distribution functions
  - New J. Phys. 15, 075011 (2013), arXiv:1212.4645
- T. Langen, R. Geiger, M. Kuhnert, B. Rauer, and J. Schmiedmayer Local emergence of thermal correlations in an isolated quantum many-body system
  - Nature Phys. 9, 640-643 (2013), arXiv:1305.3708
- R. Geiger, T. Langen, I. Mazets, and J. Schmiedmayer

  Local relaxation and light-cone-like propagation of correlations in a trapped

  1D Bose gas
  - New J. Phys. 16, 053034 (2014), arXiv:1312.7568
- T. Langen, M. Gring, M. Kuhnert, B. Rauer, R. Geiger, I. Mazets, D. Adu Smith, T. Kitagawa, E. Demler, and J. Schmiedmayer Studying non-equilibrium many-body dynamics using 1D Bose gases AIP Conf. Proc. 1633, 11 (2014)
- T. Langen, S. Erne, R. Geiger, B. Rauer, T. Schweigler, M. Kuhnert, W. Rohringer, I.E. Mazets, T. Gasenzer, and J. Schmiedmayer
   *Experimental observation of a generalized Gibbs ensemble* Science 348, 207 (2015), arXiv:1411.7185
- J. F. Schaff, T. Langen, and J. Schmiedmayer
   *Interferometry with Atoms* Proc. Internat. School Phys. Enrico Fermi, 188, 1 (2014)
   also published as Riv. Nuovo Cimento 34, 509 (2014), arXiv:1504.04285
- T. Langen, R. Geiger, and J. Schmiedmayer *Ultracold atoms out of equilibrium* to be published in Annu. Rev. Cond. Mat. Phys. 6, 201 (2015), arXiv:1408.6377

### Supervisor's Foreword

The relaxation of isolated quantum many-body systems is a major unsolved problem at the interface of statistical and quantum physics. It is of high relevance in many diverse fields, ranging from electron dynamics in condensed matter, and decoherence in quantum information and metrology, to the complex dynamics in high-energy physics and cosmology. Moreover, relaxation processes are intimately related to the question of if and how the classical world at the macro-scale can emerge from the unitary quantum evolution at the micro-scale.

The thesis of Tim Langen investigates a series of questions that are highly contested in this context: how and to which extent does an isolated quantum many body system relax? To what extent and through which processes is the memory of an initial state erased during a time-evolution? How does a classical ensemble description in the sense of statistical physics emerge from the underlying quantum evolution, even when an actual environment is absent?

Over the last years, ultracold gases have been established as ideal model systems to study these questions, as there is a large set of methods available to isolate, manipulate and probe these gases. In particular, one-dimensional (1D) gases allow probing of their many-body physics in a very controlled setting, as detailed theoretical models exist to compare to. Furthermore, these 1D gases show very rich dynamics because of a large number of conserved quantities, which constraint their evolution and have a profound effect on the relaxation processes.

In his thesis, Tim Langen prepares, controls and probes such systems using a socalled atom chip. On this chip micro-fabricated wires allow the precise manipulation of ultracold gases using static, radio and microwave magnetic fields. For example, splitting a single 1D quantum gas into two parallel 1D halves by introducing a double-well potential initializes a well-controlled and reproducible nonequilibrium evolution. The resulting dynamics can be investigated in great detail through matter-wave interference between the two halves.

When Tim Langen started his thesis one of the key questions was how to extract information about this non-equilibrium evolution. For his investigations he developed powerful methods to probe the dynamics of the many-body system through

full distribution functions of interference contrast, or through measurements of phase correlation functions to high order. These methods, in conjunction with a significant progress in the theoretical modeling, allowed him to reveal that the observed relaxation does not follow a simple path, but exhibits a plethora of complex phenomena.

For example, the experiments demonstrated the emergence of a so-called prethermalized state. Instead of relaxing directly to thermal equilibrium, the system stays trapped in this intermediate quasi-steady state, which already shares certain properties with thermal equilibrium but still differs significantly from it. By a careful investigation, the different notions of equilibration, thermalization and prethermalization could be carefully explained. Studying the relaxation process in further detail revealed that thermal correlations in the system emerge locally in their final form and then propagate in a light-cone-like evolution with a specific velocity set by the quasi-particles in the system. This provided a striking visualization of how information is distributed in quantum many-body systems and represents the first experimental study of this process in a continuous system. Moreover, while the thermal equilibrium state can be described by the well-known thermodynamical ensembles, Tim Langen was able to show that a whole class of prethermalized states has to be described by generalized ensembles taking into account the many conserved quantities of the 1D system. In contrast to the single temperature characterizing thermal equilibrium, these ensembles can exhibit many temperatures at once. The most remarkable conclusion of the latter experiment is that it provides an explicit connection between the unitary quantum evolution of the system to its description in terms of statistical mechanics. These results challenge our understanding of isolated quantum systems and as such open a new chapter in the study of relaxation processes.

The thesis of Tim Langen is an significant piece of work. I am convinced that it will become an important reference and a stepping stone for new experiments bringing deep insight in the quantum world.

Vienna January 2015 Prof. Dr. Jörg Schmiedmayer

### **Abstract**

Understanding the non-equilibrium dynamics of isolated quantum many-body systems is an open problem on vastly different energy, length, and time scales. Examples range from the dynamics of the early universe and heavy-ion collisions to the subtle coherence and transport properties in condensed matter physics. However, realizations of such quantum many-body systems, which are both well isolated from the environment and accessible to experimental study are scarce.

This thesis presents a series of experiments with ultracold one-dimensional Bose gases. These gases combine a nearly perfect isolation from the environment with many well-established methods to manipulate and probe their quantum states. This makes them an ideal model system to explore the physics of quantum many body systems out of equilibrium.

In the experiments, a well-defined non-equilibrium state is created by splitting a single one-dimensional gas coherently into two parts. The relaxation of this state is probed using matter-wave interferometry. The observations reveal the emergence of a prethermalized steady state which differs strongly from thermal equilibrium. Such thermal-like states had previously been predicted for a large variety of systems, but never been observed directly. Studying the relaxation process in further detail shows that the thermal correlations of the prethermalized state emerge locally in their final form and propagate through the system in a light-cone-like evolution. This provides first experimental evidence for the local relaxation conjecture, which links relaxation processes in quantum many-body systems to the propagation of correlations. Furthermore, engineering the initial state of the evolution demonstrates that the prethermalized state is described by a generalized Gibbs ensemble, an observation which substantiates the importance of this ensemble as an extension of standard statistical mechanics. Finally, preliminary results of an experiment are presented, where pairs of gases with an atom number difference appear to have thermalized, while they still remain in a non-thermal state.

The results presented in this thesis demonstrate both the wide range of phenomena that can occur in non-equilibrium quantum many-body systems, and the great potential of one-dimensional Bose gases to explore these phenomena. This paves the way for the further study of a universal framework for non-equilibrium dynamics.

### Acknowledgments

At this point I would like to thank all those who have supported me during my time as a Ph.D. student and who have substantially contributed, both on a scientific and on a personal level, to the success of this thesis. I am especially grateful to:

- My supervisor Jörg Schmiedmayer, who gave me the opportunity to work on this fascinating subject in his group.
- Our post-doc Remi Geiger, who joined us with enthusiasm and commitment. He deserves particular acknowledgment for his contribution to the results that are presented in Chaps. 5 and 6.
- Our post-doc David Adu Smith, who coordinated the construction of the setup and the experiments that are presented in Chap. 4. Many thanks in particular for the careful proof reading of parts of this manuscript.
- My Ph.D. collegues Michael Gring and Maximilian Kuhnert, as well as our diploma student Matthias Schreitl, with whom I was fortunate enough to realize the experiments presented in this thesis. Moreover, our successors Bernhard Rauer and Thomas Schweigler who will hopefully draw many more exciting results from the new experimental setup.
- I am indebted to our many theoretical collaborators, without whom this thesis would not have been possible: Igor Mazets, Eugene Demler, Takuya Kitagawa, Thomas Gasenzer and Sebastian Erne. Special thanks to Igor for his careful proofreading of the theory chapter.
- I am grateful to Christophe Salomon for his assistance as external advisor and for having welcomed me in his group in Paris for a very insightful time.
- My Parisian colleagues Benno Rem, Andrew Grier, Igor Ferrier-Barbut, Ulrich Eismann and Fréderic Chevy from whom I was able to learn a lot about strongly-interacting gases of Lithium.
- Aurélien Perrin, Christian Koller, Hannes Majer, Jean-François Schaff, Tarik Berrada, Thomas Betz, Stephanie Manz, Stephan Schneider, Thorsten Schumm, Wolfgang Rohringer and all other members of the atom chip group for lab supplies, codes, advice and discussions.

xii Acknowledgments

• Hanns-Christoph Nägerl for his willingness to take over the role of being my thesis examiner.

• Stefanie Barz for her ongoing support and motivation.

This work was supported by the Austria Science Fund (FWF) through the Doctoral Programme CoQuS (W1210).

### **Contents**

1	Intr	oductio	n to One-Dimensional Bose Gases	1		
	1.1	From	Quantum to Statistical Mechanics	1		
	1.2	Therm	al Equilibrium	3		
	1.3	1.3 Bose Statistics				
		1.3.1	The Ideal Bose Gas	5		
		1.3.2	The Interacting Bose Gas	7		
	1.4	erate One-Dimensional Bose Gases	9			
		1.4.1	The Ideal One-Dimensional Bose Gas	10		
		1.4.2	The Interacting One-Dimensional Bose Gas	10		
		1.4.3	Luttinger Liquid Theory	13		
		1.4.4		16		
		1.4.5	Trapped Quasi-condensates in the 1D/3D Crossover 1	17		
		1.4.6	Description by a Stochastic Process	18		
	1.5	Bose (	Gases in a Double-Well Potential	20		
		1.5.1	Matter-Wave Interference of One-Dimensional			
			Bose Gases	22		
		1.5.2	Equilibrium States	26		
	Refe	erences		30		
2	Exp			39		
	2.1	Magne	11 6	39		
		2.1.1	Magnetic Trapping	39		
		2.1.2	1	40		
	2.2	Theory	, , , , , , , , , , , , , , , , , , , ,	12		
		2.2.1	A Double-Well Potential for Ultracold Atoms 4	13		
		2.2.2	Beyond the Rotating-Wave Approximation	15		
	2.3	Experi	mental Setup and Cooling Sequence	17		
		2.3.1	Atom Source and Precooling	18		
		2.3.2	Science Chamber and Mirror Magneto-optical Trap 4	18		
		2.3.3		19		

xiv Contents

		2.3.4	The Atom Chip	49						
		2.3.5	Imaging Systems	51						
		2.3.6	Making and Probing Degenerate Gases	54						
	2.4	Experi	ments with Atoms in a Tunable Double-Well Potential	56						
		2.4.1	Characterization of the Radio-Frequency Dressing	57						
		2.4.2	Turning Off the Double Well	57						
		2.4.3	Equilibrium States: Cooling into the Double Well	59						
	Refe	erences .		63						
3	Isolated Quantum Systems Out of Equilibrium									
_	3.1		nics Following a Quench	67 67						
	0.1	3.1.1	Scenario I: No Relaxation	69						
		3.1.2	Scenario II: Relaxation with One Timescale	70						
		3.1.3	Scenario III: (Partial) Relaxation with More	, 0						
		3.1.3	Timescales	71						
	3.2	The Ro	ole of Integrability	71						
			·····	73						
	Dala	4!	and Bush amaslimation in One Dimensional							
4	Relaxation and Prethermalization in One-Dimensional									
	4.1		ant Splitting as a Quanch	75 76						
	4.1		ent Splitting as a Quench	70 79						
	4.2		vation of a Non-thermal Steady State	82						
	4.3		etical Discussion and Interpretation	82						
	4.4			87						
	4.5		S	90						
		•	nics Beyond Prethermalization							
	кет	erences .		93						
5	Loc	al Emer	gence of Thermal Correlations	97						
	5.1		ocal Relaxation Conjecture	97						
	5.2		mental Results	98						
	5.3	Theore	etical Discussion	102						
	5.4	The Ch	haracteristic Velocity	106						
	5.5	Conclu	sion	107						
	Refe	erences .		108						
6	Exp	eriment	al Observation of a Generalized Gibbs Ensemble	111						
	6.1	The Ge	eneralized Gibbs Ensemble	111						
	6.2		mental Results	112						
	6.3	-	ısion	119						
	Refe			120						

Contents xv

7	Relaxation Dynamics in an Imbalanced Pair of One-Dimensional						
	Bose Gases.						
	7.1	Quenching an Imbalanced Pair of One-Dimensional					
		Bose Gases	123				
	7.2	Experimental Results	124				
	7.3	Theoretical Discussion and Interpretation	127				
	7.4	Conclusion	131				
	Refe	erences	132				
8	Conclusion and Outlook						
_	8.1	Cooling, Thermalization and Ultracold Mixtures in 1D	135				
	8.2	Using Prethermalized States for Precision Interferometry	136				
	8.3	From the Coherence Dynamics of Coupled 1D Superfluids					
		to Universality Away from Equilibrium	136				
	References						
Δı	nend	lices	141				

### Chapter 1 Introduction to One-Dimensional Bose Gases

### 1.1 From Quantum to Statistical Mechanics

Statistical mechanics has proven to be one of the most comprehensive theories in physics. From a boiling pot of water to the complex dynamics of quantum many-body systems it provides a successful connection between the microscopic dynamics of atoms and molecules to the macroscopic properties of matter [1, 2].

However, despite almost a century of efforts to explain the foundations of statistical mechanics through the underlying laws of quantum mechanics [3, 4], these foundations still rely on assumptions rather then exact derivations. Moreover, statistical mechanics only describes the thermal equilibrium situation of a system, but there is no general consensus on the framework to describe how equilibrium is reached or under which circumstances it can be reached at all [5].

In classical mechanics, dynamical processes and thermalization are intimately connected to chaotic behavior [6, 7]. Entropy grows until its maximum is reached in the thermal equilibrium state [8–10]. This thermal equilibrium state is the same for all initial states with a certain energy.

However, the microscopic world is properly described in terms of quantum mechanics. In principle, all quantum evolution is unitary, and thus isolated quantum systems should never relax to a universal thermal equilibrium state. Nevertheless, experience tells us that many quantum systems can be well described by such a state.

Thus, the central question is how the unitary non-equilibrium evolution of an isolated quantum many-body system can lead to observables which relax to steady, thermal expectation values [11–19].

The answer to this question is an open one on all energy, length, and time scales, from the expansion dynamics of the early universe [20–22] and the physics of quark-gluon plasmas [23–25] to the subtle coherence properties of solid-state materials [26–29] and future quantum information devices [5]. Thus, a thorough understanding could not only shed light on the origins of our universe, but might also lead to important technological advances. Chapter 3 gives a brief introduction into the current framework of non-equilibrium dynamics.

1

From an experimentalist's point of view all these situations have one challenge in common: their study is difficult, since quantum many-body systems are usually hard to isolate from the environment. Only recently, the advances in the manipulation of ultracold atomic clouds have enabled the realization and control of truly isolated quantum many-body systems [30, 31].

For example, confining atoms in optical lattices allows the realization of systems where thousands of atoms behave coherently for times that are much longer than the characteristic time scales of their dynamics [32–37]. To extract information, these systems can be probed down to the single atom level [38–40]. Moreover, quantum gases with tunable interactions [41, 42] now provide benchmarks for the most advanced numerical methods to simulate quantum many-body systems [43–47].

In particular, the realization of low-dimensional quantum gases [48–51] has enabled the detailed experimental study of textbook examples of statistical physics, for example, Ising chains [52], Tonks-Girardeau [53–56] and Yang-Yang gases [57], Luttinger liquids [58, 59], as well as the quantum Sine-Gordon [60], the Hubbard [61] and the Yang-Gaudin models [62].

In this thesis the non-equilibrium dynamics of isolated quantum many-body systems are investigated using a one-dimensional (1D) Bose gas of ultracold <sup>87</sup>Rb atoms. To this end, an experiment was set up to realize such a gas on an atom chip [63–68]. The experimental setup is discussed in detail in Chap. 2.

The micro-fabricated traps on such atom chips enable a wide range of powerful techniques to manipulate and probe ultracold atoms [69–72]. In our experiment we employ matter-wave interferometry as a sensitive probe for fluctuations and manybody dynamics [73–75]. In addition to these experimental benefits, the 1D Bose gas has the favorable property that it shows very rich dynamics, but still remains theoretically tractable [76]. Moreover, the 1D Bose gas is an example of a so-called integrable system, where the existence of many conserved quantities has a strong influence on the dynamics [77–79]. In the experiment, these conserved quantities are realized only approximately, which opens up the possibility of studying relaxation close to an integrable point.

This unique combination of experimental and theoretical properties enables a series of experiments which provide comprehensive insights into the dynamics of isolated quantum many-body systems.

Chapter 4 presents an experiment [59, 80–83], in which a 1D Bose gas is brought out of equilibrium by rapidly splitting it into two parts. The ensuing evolution reveals the emergence of an intermediate, prethermalized state which already exhibits some thermal-like properties, but still contains a strong memory of the initial state. The theoretical analysis reveals that the appearance of this state is closely connected to the near-integrability of the 1D Bose gas, which leads to almost non-interacting quasi-particles [27].

After demonstrating that states with thermal correlations can dynamically emerge in an isolated quantum system, we study in Chap. 5 how these thermal correlations form during the dynamics. It has been conjectured [84, 85] that thermal states will emerge locally and spread in a light-cone-like evolution in systems which exhibit a finite velocity for the propagation of correlations. We observe this local emergence

of thermal correlations for the first time, by using time-resolved measurements of the two-point correlation function of the gas [86].

Having established the two-point correlation function as a very sensitive tool to study the dynamics, it is employed in Chap. 6 to reveal how a variation of the splitting process can change the initial conditions of the non-equilibrium evolution. The preparation of such an alternative initial state demonstrates that the prethermalized state can be described by a generalized Gibbs ensemble [87], a generalization of the usual thermodynamical ensembles to integrable systems.

In Chap. 7 the relaxation dynamics of two gases with an atom number imbalance is studied. The insights of this experiment are twofold: on one hand, imbalancing the gases exposes one of the subtleties of relaxation in the quantum world: depending on the measurement, the relaxation can appear vastly different. Under certain circumstances the system might look completely thermalized, although it is still in a non-equilibrium state. On the other hand, the two 1D Bose gases show interesting similarities with 1D spin chains and could therefore serve as a model system to study spin-charge dynamics within the Luttinger liquid framework [88].

Finally, an outlook on ongoing and future experiments is presented. These experiments include the study of evaporative and sympathetic cooling in 1D, a possible interferometer with ultracold mixtures, as well as experiments investigating the coherence dynamics of two tunnel coupled 1D Bose gases. The latter experiments establish pairs of coupled gases as a promising platform for future investigations, for example the search for universality away from equilibrium [89], quantum simulations of the early universe [90], or as a tool to engineer states for quantum-enhanced metrology [91].

In this first chapter, the physics of Bose gases in equilibrium are reviewed with a particular focus on 1D bosons in a double-well potential. This equilibrium situation allows the introduction of the tools that will later be used to study 1D Bose gases in various non-equilibrium situations.

### 1.2 Thermal Equilibrium

Thermodynamics describes the physics of a quantum system containing a large number of particles by means of a small number of macroscopic variables. Typical examples for these variables are temperature, pressure, and entropy. Thermal equilibrium is defined as the state of the system in which these variables do not change in time. There is no flow of heat or matter, and in the classical limit all degrees of freedom contain the same amount of energy [1, 2].

Statistical mechanics connects this macroscopic description to the underlying microscopic dynamics. In practice, a complete description of the very complex microscopic dynamics is unfeasible. However, this complete description is also unnecessary to describe the macroscopic variables of interest. Instead, a statistical approach is much more useful, where the macroscopic variables are derived from the average over an ensemble that represents all possible microscopic states.

The fundamental hypothesis of statistical mechanics is that a system is equally likely to be found in any of these microscopic states [1]. This hypothesis has no rigorous justification and has therefore recently been the subject of intense study [14, 92]. Starting from this hypothesis, it is central to observe that many microscopic states of a system result in the same macroscopic properties. The thermal equilibrium state then simply follows as the most probable macroscopic state in the ensemble.

Typical examples of statistical ensembles that are appropriate for the description are the microcanonical, canonical, or grand-canonical ensembles [1]. In the following, we describe the grand canonical ensemble formulation, as the statistics of Bose gases follow from it in a natural way.

To this end, we consider a generic system with a certain volume  $\mathcal{V}$  that is in contact with a bath, with which it can exchange particles and energy. The fact that the system is connected to a bath has no particular importance in standard statistical mechanics. The reason for this is that the mean values of all physical observables are identical in the thermodynamic limit, independent of whether the system is described as being completely isolated (using the microcanonical ensemble) or coupled to a bath (using the canonical or the grand canonical ensemble) [1, 2].

The total energy, described by the Hamiltonian  $\hat{H}$  of the system, and the total particle number, described by the particle number operator  $\hat{N}$  are conserved quantities. The state of the system can be described by a density matrix

$$\hat{\rho} = \frac{1}{Z} \exp(-\beta [\hat{H} - \mu \hat{N}]), \tag{1.1}$$

where  $\beta$  and  $\mu$  are parameters to be determined and  $Z={\rm Tr}(\exp(-\beta[\hat{H}-\mu\hat{N}]))$  is the grand partition function.

Following the standard knowledge of quantum statistical mechanics, the thermal equilibrium state of this system is the unique state  $\hat{\rho}_{eq}$  which maximizes the entropy

$$S = -k_B \operatorname{Tr}(\hat{\rho}_{eq} \log \hat{\rho}_{eq}), \tag{1.2}$$

under the constraints imposed by the conserved quantities. In the maximization of the entropy,  $\beta$  and  $\mu$  play the role of Lagrange multipliers, which are connected to the conserved quantities  $\hat{H}$  and  $\hat{N}$ , respectively. One can identify  $\mu$  as the chemical potential, which governs the exchange of particles with the bath, and  $\beta = 1/k_BT$  as the inverse temperature of the system, which governs the exchange of energy. Here,  $k_B$  is Boltzmann's constant and T is the temperature. The expectation value of a generic observable  $\hat{A}$  follows via  $\langle \hat{A} \rangle = \text{Tr}(\hat{\rho}_{eq}\hat{A})/\text{Tr}(\hat{\rho}_{eq})$ .

The density matrix  $\hat{\rho}_{eq}$  describes a mixed state. How such a mixed state can emerge from a pure state through a unitary non-equilibrium evolution is subject to an ongoing debate [13, 15]. Several possible mechanisms will be discussed in Chap. 3. In fact, we will see later that this entropy maximization scheme can be generalized to describe also the more complex steady states which emerge in the non-equilibrium dynamics of systems with many more conserved quantities.

1.3 Bose Statistics 5

### 1.3 Bose Statistics

In quantum mechanics identical particles are indistinguishable and, as a result, exhibit completely different statistical properties than their distinguishable classical counterparts [93]. This fact was first pointed out by Bose in a derivation of Planck's law for photons [94]. As Einstein realized soon thereafter [95], arbitrary particles with an integer spin, now called bosons [96], will under certain conditions accumulate in the energetic ground state and form a single coherent object, a Bose-Einstein condensate (BEC). This BEC is the starting point for the experiments presented in this thesis.

### 1.3.1 The Ideal Bose Gas

We start by considering a homogeneous, non-interacting gas of bosonic particles. From the equilibrium density matrix in Eq. 1.1 one derives [1, 97] that for a bosonic system the occupation of a non-degenerate quantum state with energy  $E_k \ge 0$  is given by the Bose-Einstein distribution

$$N(E_k) \equiv N_k = \frac{1}{\zeta^{-1} \exp(E_k/k_B T) - 1},$$
 (1.3)

where  $\zeta = \exp(\mu/k_BT)$  is the fugacity and k is an index labeling the discrete energy eigenvalues. As the occupation  $N_k$  of a state cannot be negative, the chemical potential  $\mu$  of the ideal Bose gas always has to remain negative. Consequently, the fugacity must fulfil  $0 < \zeta < 1$ , where the limit  $\zeta \to 0$  corresponds to classical Boltzmann statistics and  $\zeta \to 1$  to the quantum regime.

In a semi-classical approximation, the discrete level structure  $E_k$  can be approximated by a continuous spectrum. As the Bose-Einstein distribution is normalized to the total number of atoms  $N = \sum_k N_k$  one finds the equation of state [1]

$$n = n_0 + n' = n_0 + \frac{1}{\lambda_{dB}^3} g_{3/2}(\zeta).$$
 (1.4)

Here,

$$g_n(\zeta) = \sum_{i=1}^{\infty} \frac{\zeta^j}{j^n}$$
 (1.5)

is the Bose function and  $\lambda_{\rm dB} = \sqrt{2\pi\hbar/mk_BT}$  denotes the thermal de Broglie wavelength, with  $\hbar$  being Planck's constant h divided by  $2\pi$  and m the mass of the atoms. Furthermore,  $n=N/\mathcal{V}$  is the total density of the atoms,  $n'=N'/\mathcal{V}$  is the density of atoms in the excited states and  $n_0=N_0/\mathcal{V}$  is the density of atoms in the ground state.

The central aspect of this result is that the Bose function is bounded from above by  $g_{3/2}(1) \simeq 2.612$  for  $\zeta = 1$ . For a given temperature, there can thus only be a limited number of atoms in the excited states. Turning this argument around, for a system with a certain total number N of particles, there exists a critical temperature  $T_c$  below which the excited states of the system are saturated. All other atoms will have to collectively accumulate in the ground state. The corresponding critical temperature is given by

$$k_B T_c = \frac{2\pi\hbar^2}{m} \left(\frac{n}{2.612}\right)^{3/2}.$$
 (1.6)

In terms of the density this can be expressed as

$$n\lambda_{\rm dB}^3 = 2.612.$$
 (1.7)

This condition allows for a very intuitive interpretation, namely that Bose-Einstein condensation will occur when the de Broglie wavelength  $\lambda_{\rm dB}$  becomes on the order of the mean inter-particle spacing  $n^{-1/3}$ .

For alkali atoms, like  $^{87}$ Rb which is used in this work, this condition results in the need to achieve temperatures in the sub- $\mu$ K range to reach the quantum degenerate regime.

In experiments the atoms are confined in a harmonic trapping potential

$$V(x, y, z) = \frac{1}{2}m\omega_x^2 x^2 + \frac{1}{2}m\omega_y^2 y^2 + \frac{1}{2}m\omega_z^2 z^2,$$
 (1.8)

where  $\omega_{x,y,z}$  are the trap frequencies in the three spatial directions r=(x,y,z). As the resulting system is inhomogeneous, not all atoms in the gas will reach the condensation threshold at the same time. This situation can be captured in the equation of state (Eq. 1.4) using a local density approximation, where the chemical potential is replaced by a local chemical potential  $\mu(r) = \mu - V(r)$  in the expression for the fugacity  $\zeta$ . The maximum of  $\zeta$ , and thus of the density, is located in the center of the trap. Therefore, the condensate will start to form once  $n_0 \lambda_{\rm dB}^3 = 2.612$ , where  $n_0$  is the density in the center of the trap.

In the limit of zero temperature, all N atoms will condense into the ground state. They can thus be described by the single-particle Gaussian ground state wave function  $\psi_0$  of the harmonic trapping potential. The width of this wave function, and thus the size of the condensate is given by the harmonic oscillator lengths

$$a_{\text{ho},i} = \sqrt{\frac{\hbar}{m\omega_i}},\tag{1.9}$$

in the respective directions  $i = \{x, y, z\}$ . The total wave function is the product of these single particle wave functions, resulting in a density profile given by [97]

$$n(\mathbf{r}) = N \left| \psi_0(\mathbf{r}) \right|^2. \tag{1.10}$$

1.3 Bose Statistics 7

### 1.3.2 The Interacting Bose Gas

As we have just seen, the Bose-Einstein condensation of an ideal bosonic gas is a purely statistical effect. However, thermal equilibrium, which is assumed in the above treatment, cannot be reached without interactions. For a realistic description, we thus have to introduce interactions between the atoms. The many-body Hamiltonian of such an interacting bosonic gas is of the form [97]

$$\hat{H} = \int d^3r \,\hat{\Psi}^{\dagger}(\mathbf{r}, t) \left( -\frac{\hbar^2 \nabla^2}{2m} + V(\mathbf{r}) - \mu \right) \hat{\Psi}(\mathbf{r}, t) +$$

$$+ \frac{1}{2} \int d^3r \, d^3r' \,\hat{\Psi}^{\dagger}(\mathbf{r}, t) \hat{\Psi}^{\dagger}(\mathbf{r}', t) U(\mathbf{r} - \mathbf{r}') \hat{\Psi}(\mathbf{r}', t) \hat{\Psi}(\mathbf{r}, t). \quad (1.11)$$

Here,  $U(\mathbf{r} - \mathbf{r}')$  is the effective interatomic interaction potential and the  $\hat{\Psi}(\mathbf{r}, t)$  are the time-dependent field operators, which create a particle at position  $\mathbf{r}$ .

The fact that the gases have to be cooled to extremely low temperatures to achieve quantum degeneracy reduces the possible collisional processes to simple s-wave scattering [97, 98]. In this case, the interactions can be described by a single number, the s-wave scattering length  $a_s$ . For  $^{87}$ Rb,  $a_s \simeq 5.24$  nm > 0, which makes the interactions repulsive [99]. The effective interaction potential itself can be represented by a contact potential  $U(\mathbf{r} - \mathbf{r}') = g_{3D}\delta(\mathbf{r} - \mathbf{r}')$ , where

$$g_{\rm 3D} = \frac{4\pi\hbar^2}{m} a_s \tag{1.12}$$

is the 3D interaction constant.

The dynamics of the field operators  $\hat{\Psi}({m r},t)$  can be calculated from the many-body Hamiltonian by approximating them with  $\hat{\Psi}({m r},t)=\hat{\Phi}({m r},t)+\delta\hat{\psi}({m r},t)$ , and replacing  $\hat{\Phi}({m r},t)$  by its expectation value  $\langle \hat{\Phi}({m r},t) \rangle = \Phi({m r},t)$ . Here,  $\Phi({m r},t)$  is a macroscopic wave function and the term  $\delta\hat{\psi}$  describes small fluctuations around that wave function [100, 101]. In a first approximation these small fluctuations can be neglected and the gas can be described by  $\Phi({m r},t)$ , which is determined by the non-linear Schrödinger equation

$$i\hbar \frac{\partial}{\partial t} \Phi(\mathbf{r}, t) = \left( -\frac{\hbar^2}{2m} \nabla^2 + V(\mathbf{r}) + g_{3D} |\Phi(\mathbf{r}, t)|^2 \right) \Phi(\mathbf{r}, t). \tag{1.13}$$

In this so-called Gross-Pitaevski equation (GPE) the mean-field term  $g_{3D}|\Phi(\mathbf{r},t)|^2$  describes the interactions between the atoms [97, 102, 103]. A separational ansatz  $\Phi(\mathbf{r},t) = \Phi(\mathbf{r}) \exp(-i\mu t/\hbar)$  yields the stationary GPE [104]

$$\left(-\frac{\hbar^2}{2m}\nabla^2 + V(\mathbf{r}) + g_{3D}|\Phi(\mathbf{r})|^2\right)\Phi(\mathbf{r}) = \mu\Phi(\mathbf{r}). \tag{1.14}$$

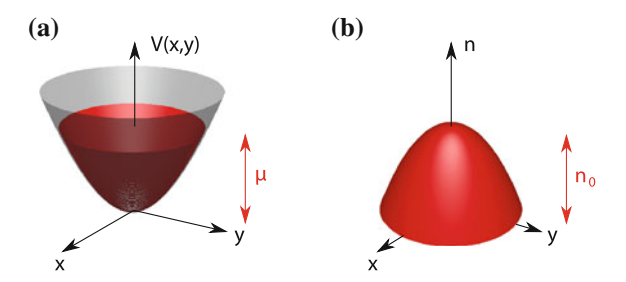


Fig. 1.1 Thomas-Fermi approximation. a If the kinetic energy term in the Gross-Pitaevski equation (Eq. 1.14) can be neglected compared to the mean-field energy term, an analytic solution for the atomic density profile can be found (Eq. 1.15). The atoms uniformly fill the potential up to the chemical potential  $\mu$ . b In a harmonic trap, this results in an inverted parabola for the atomic density n, with the peak density given by  $n_0 = \mu/q_{\rm 3D}$ 

For the interacting gas, the chemical potential no longer has to remain negative and is now given by the solution of the GPE, which can easily be obtained numerically [105]. Note that, while Bose-Einstein condensation is still statistically favored, the picture in which the excited states of a trapped gas are saturated is fully valid only in the limit of no interactions [106].

A very good analytical approximation to the GPE can be found in the limit where the mean-field term is much stronger than the kinetic energy [107]. This so-called Thomas-Fermi approximation allows the algebraic solution of the GPE for the atomic density

$$n(\mathbf{r}) = |\Phi(\mathbf{r})|^2 = \frac{1}{g_{3D}} \max(\mu - V(\mathbf{r}), 0).$$
 (1.15)

The atoms fill the trapping potential uniformly up to the chemical potential. In a harmonic trapping potential this leads to an atomic density profile which has the form of an inverted parabola (Fig. 1.1). The surface of the atomic cloud is defined by the condition  $\mu = V(\mathbf{r})$ , which yields the Thomas-Fermi radius  $R_{\text{TF},i}$  in each direction  $i = \{x, y, z\}$ 

$$\mu = \frac{1}{2} m \omega_i^2 R_{\text{TF},i}^2. \tag{1.16}$$

Due to repulsive interactions, these radii are generally larger than the oscillator length (Eq. 1.9) characterizing the non-interacting gas.

Excitations can be described as small thermal or quantum fluctuations  $\delta\hat{\psi}$  around the mean-field  $\Phi$ . This description was developed by Bogoliubov [100] and de Gennes [108] and will play a central role in the description of 1D gases. In the homogeneous case, or in local density approximation, one finds for the dispersion relation of these excitations

$$\epsilon_k = \sqrt{E_k(E_k + 2\mu)},\tag{1.17}$$

1.3 Bose Statistics 9

with  $E_k=\hbar^2k^2/2m$  the dispersion relation of a free particle. At high energies the dispersion relation can be approximated by  $\epsilon_k=E_k+\mu$  and the excitations behave like free particles. At low energies one finds  $\epsilon_k=ck$ , such that the excitations are phonons with a speed of sound  $c=\sqrt{g_{3D}n/m}$ . The crossover energy between these two regimes is located at the chemical potential. The corresponding excitation energies in the trapped Thomas-Fermi limit are given in Ref. [109].

The Bose-Einstein condensate is a coherent quantum object. This fact can be captured using the one-body density matrix of the gas [110]

$$\hat{\rho}(\mathbf{r}, \mathbf{r}', t) = \langle \hat{\Psi}^{\dagger}(\mathbf{r}, t) \hat{\Psi}(\mathbf{r}', t) \rangle. \tag{1.18}$$

The eigenvalues of this matrix describe the number of particles occupying the corresponding eigenfunction. The defining feature of a BEC is that this matrix remains finite for  $|\mathbf{r} - \mathbf{r}'| \to \infty$ , corresponding to a macroscopic occupation of the ground state. This property is called off-diagonal long-range order. As the one-body density matrix is directly related to the two-point correlation function

$$C(\mathbf{r}, \mathbf{r}', t) = \frac{\langle \hat{\Psi}^{\dagger}(\mathbf{r}, t) \hat{\Psi}(\mathbf{r}', t) \rangle}{\sqrt{\langle \hat{\Psi}^{\dagger}(\mathbf{r}, t) \hat{\Psi}(\mathbf{r}, t) \rangle} \sqrt{\langle \hat{\Psi}^{\dagger}(\mathbf{r}', t) \hat{\Psi}(\mathbf{r}', t) \rangle}},$$
(1.19)

it implies that a BEC exhibits long-range phase coherence.

### 1.4 Degenerate One-Dimensional Bose Gases

Low-dimensional quantum systems show fundamentally different behavior than their higher-dimensional counterparts. Examples include the transport properties in atomic or molecular chains [111–114] and carbon nanotubes [115–117], the quantum hall effect [118–120], high- $T_c$  superconductivity [121, 122], or the unusual electronic properties of graphene [123]. As we will see in the following, the dimensionality also has a strong influence on the character of the Bose-Einstein condensation in low-dimensional quantum gases [124–126].

In experiments, a 1D Bose gas can be realized if the confinement in two directions is strong enough such that the temperature and the chemical potential of the system are smaller than the excited energy levels of the trapping potential. This can be expressed by the condition

$$k_B T, \mu \lesssim \hbar \omega_{\perp},$$
 (1.20)

where  $\omega_{\perp}$  denotes the trap frequency in the two strongly confining directions. In the following, we will use the convention that the strongly confining trap directions are the *x*-direction and the *y*-direction, such that  $\omega_{\perp} = \omega_x = \omega_y$ .

### 1.4.1 The Ideal One-Dimensional Bose Gas

We start by considering an ideal homogeneous 1D Bose gas. In analogy with the 3D case (Eq. 1.4), the equation of state is given by [127]

$$n_{\rm 1D} = \frac{1}{\lambda_{\rm dB}} g_{1/2}(\zeta).$$
 (1.21)

Again, quantum effects become important when the de Broglie wavelength  $\lambda_{\rm dB}$  becomes comparable to the particle separation  $n_{\rm 1D}^{-1}$ . From this condition, one defines the degeneracy temperature

$$T_D = \frac{\hbar^2 n_{1D}^2}{2mk_R}. (1.22)$$

In contrast to the critical temperature in 3D, the degeneracy temperature does not mark a phase transition, but only loosely defines a temperature scale for the quantum regime. The fact that there is no BEC phase transition in 1D can be seen in the equation of state, where  $g_{1/2}(z)$ , in contrast to its counterpart  $g_{3/2}(z)$  in the 3D case, does not converge for  $z \to 1$ . There is thus no saturation of the exited states and the ideal 1D Bose gas can always be described as a thermal gas.

Even more importantly, we immediately learn that in 1D many momentum modes are occupied, in contrast to the single momentum state in 3D BECs. These many momentum modes are the origin of strong density and phase fluctuations in 1D Bose gases. It has been shown rigorously by Mermin, Wagner and Hohenberg [124, 125] that because of this enhanced role of fluctuations no off-diagonal long-range order and thus no BEC can exist in ideal 1D Bose gases, even at zero temperature.

### 1.4.2 The Interacting One-Dimensional Bose Gas

Similar to the 3D case (Eq. 1.11) the interacting 1D Bose gas can be described by the many-body Hamiltonian

$$\hat{H} = \int dz \,\hat{\Psi}^{\dagger}(z,t) \left( -\frac{\hbar^2}{2m} \frac{\partial^2}{\partial z^2} \right) \hat{\Psi}(z) +$$

$$+ \frac{1}{2} \int dz \, dz' \,\hat{\Psi}^{\dagger}(z,t) \hat{\Psi}^{\dagger}(z',t) U(z-z') \hat{\Psi}(z',t) \hat{\Psi}(z,t). \tag{1.23}$$

Here, we have omitted the chemical potential and the zero-point fluctuations of the two radial directions. The fact that the 1D nature of the gas is achieved by strongly confining it in two directions of the three-dimensional space is reflected in the scattering properties of the atoms. These are still 3D for the parameters reached in our experiments with 1D Bose gases. For temperatures below the degeneracy temperature  $T_D$  and sufficiently high density, a mean-field description is applicable to model these properties. In this case, the 1D dynamics can be described by integrating out the two strongly confining directions, leading to an effective scattering potential  $U(z-z')=g\delta(z-z')$ . Here,

$$g = \frac{2\hbar a_s \omega_{\perp}}{1 - C a_s \sqrt{\frac{m\omega_{\perp}}{\hbar}}} \tag{1.24}$$

is the 1D interaction parameter, with C a constant of order unity and  $\omega_{\perp}$  the trapping frequency of the transversal confinement [128, 129]. For our typical parameters  $a_s \ll a_{\text{ho},\perp}$ , such that Eq. 1.24 can be approximated by

$$g = 2\hbar a_s \omega_{\perp}. \tag{1.25}$$

The homogeneous 1D Bose gas with such delta function interactions is one of the prime models of mathematical and statistical physics. An exact solution based on the Bethe Ansatz [130] was found by Girardeau, Lieb and Liniger [77, 131, 132]. Moreover, Yang and Yang used this solution to predict the properties of the 1D Bose gas at finite temperature [78, 79]. This is an important point in the context of this thesis, because the exact solution leads to a large number of conserved quantities. In analogy to classical systems, the existence of these conserved quantities means that the system is integrable and that thermalization is strongly inhibited in 1D Bose gases [34, 133]. However, this point is very delicate, as integrability is a concept that is only well-defined for classical systems. No generally accepted definition exists in the quantum case [134–136]. We will discuss the important consequences for the non-equilibrium dynamics of these systems in Chap. 3.

In the exact solutions [77, 78, 132], the strength of the interactions is parametrized by the Lieb-Liniger parameter  $\gamma$  which is defined as

$$\gamma = \frac{mg}{\hbar^2 n_{1D}}.\tag{1.26}$$

The 1D Bose gas thus becomes more strongly interacting for lower density. For  $\gamma\gg 1$  the system is in the strongly correlated Tonks-Girardeau regime, for  $\gamma\ll 1$  it is in the weakly-interacting regime.

Similarly to the interaction parameter  $\gamma$ , one defines a reduced temperature  $\tau=T/T_D$  to characterize the system at finite temperature. For  $\tau\gg 1$  the gas behaves in a manner similar to a classical ideal gas. For  $\tau\ll 1$  quantum effects become important. In contrast to the 3D case, different regimes of quantum degeneracy exist at finite temperature and weak interactions [137]. At high temperatures ( $\tau>\sqrt{\gamma}$ ) both phase and density fluctuations can play an important role, leading to a decoherent quantum regime. For lower temperatures, the gas is a quasi-condensate characterized by suppressed density fluctuations. The phase, on the other hand, strongly fluctuates.

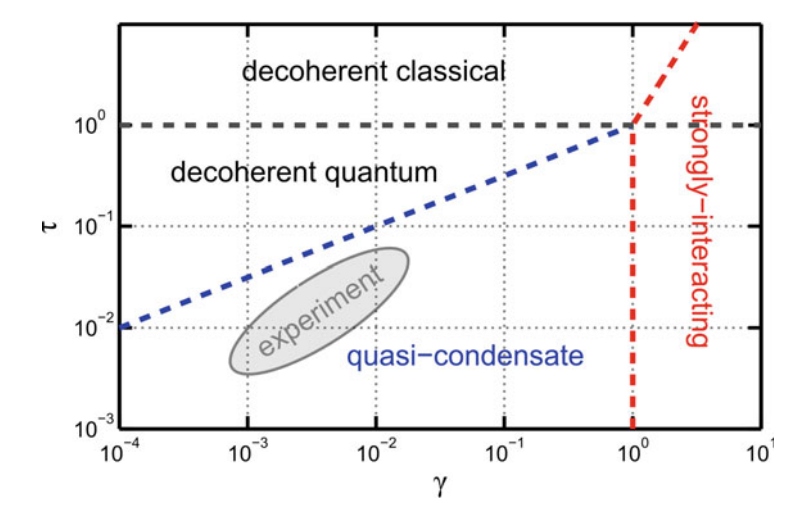


**Fig. 1.2** Finite temperature diagram of states for the interacting 1D Bose gas. Several regimes exist as a function of the Lieb-Liniger parameter  $\gamma = mg/\hbar^2 n_{1D}$  and the rescaled temperature  $\tau = T/T_D$  [137]. These regimes are separated by smooth crossovers. The shaded area indicates the range of parameters covered in the experiments that are presented in this thesis

The corresponding finite-temperature diagram of states is presented in Fig. 1.2. For the typical parameters of the experiments presented in this thesis,  $\gamma$  is on the order of  $10^{-2}-10^{-3}$  and  $\tau$  is approximately  $10^{-2}$ . The gas is thus a weakly-interacting quasi-condensate.

The phase-fluctuating nature of the quasi-condensate plays a central role for the non-equilibrium experiments presented in this thesis. In equilibrium, the phase correlations are characterized by an exponentially decaying two-point phase correlation function (see Eq. 1.19)

$$C(z, z') = \frac{\langle \hat{\Psi}(z) \hat{\Psi}^{\dagger}(z') \rangle}{\langle |\hat{\Psi}(z)|^2 \rangle} = \exp\left(-\bar{z}/\lambda_T^{(s)}\right). \tag{1.27}$$

This function measures the correlations between two arbitrary points z and z' in the gas, with  $\bar{z} = z - z'$  their distance and

$$\lambda_T^{(s)} = \frac{2\hbar^2 n_{1D}}{mk_B T} \tag{1.28}$$

the thermal coherence length of a single 1D Bose gas.

In experiment, the phase fluctuations of a quasi-condensate can be observed in two different ways. First, two quasi-condensates can be made to interfere, revealing a fluctuating relative phase in their interference pattern. This situation will be discussed in detail in Sect. 1.5. Second, in an expanding single 1D Bose gas, the varying phase

 $\phi(z)$  corresponds to a velocity field  $v = \nabla \phi(z)$  for the atoms. In time-of-flight expansion the phase fluctuations will thus turn into density fluctuations, similar to an optical speckle pattern [138, 139]. In this thesis, measurements of the correlation properties of these *density ripples* are the standard method to measure the temperature of the gas. This is made possible by the fact that the interactions between the atoms can be neglected in the expansion. As a consequence, the correlation properties of the density ripples can directly be related to the correlation properties of the in situ phase fluctuations, and thus to the temperature (see Eq. 1.28).

### 1.4.3 Luttinger Liquid Theory

While the existence of an exact solution gives valuable insights about the 1D Bose gas, it is not very convenient to make predictions about its dynamics. For a quantitative analysis it is more practical to use effective models, which capture the complex many-body problem using its low-energy excitations. While it is well understood why this is possible in equilibrium, the non-equilibrium case is not obvious, as, in principle, high-energy eigenstates might be populated in the dynamics. As we will see later, the experimental results suggest that this low-energy approach also works very well for dynamical problems.

The origins of such effective models lie in the description of electrons. In 3D it is well known that many-body interactions of electrons can be reduced to quasi-particles. This is the principle of Landau's Fermi liquid approach [140]. Instead of dealing with the whole many-body interactions in a solid, the problem is recast as a set of quasi-particles which behave almost like free fermions. Surprisingly, the only effect of the many-body interactions is to dress these particles, giving them a new, effective mass.

Intuition tells us that this approach is problematic to describe electrons in 1D, because particles can only move along one direction: perturbing one of them, will immediately affect also all the other particles. One thus needs a more collective description of the dynamics, which is provided by the Luttinger liquid formalism [141–145]. This formalism can be generalized to describe a large class of 1D systems, both bosonic or fermionic, with a gapless, linear dispersion relation. It describes the excitations of the system as non-interacting bosonic particles. As the excitations can be identified with collective low-energy phonons this approach is also called the harmonic fluid approach.

Beyond cold atoms, experimental evidence for Luttinger liquid behavior was found in 1D quantum wires formed by GaAs/AlGaAs heterostructures [113, 146] and SrCuO<sub>2</sub> compounds [147], self-assembled atomic chains on surfaces [111], 1D crystals [148], or carbon nanotubes [117, 149] (for a review see Ref. [145]). The Luttinger liquid thus has high technological relevance as a description for electronic conductors in the atomic limit.

In the case of 1D Bose gases, a derivation of the Luttinger description is possible using the previously introduced Bogoliubov theory [76, 150–152]. To this end one writes the field operators in a phase-density representation as

$$\hat{\Psi} = \exp(i\hat{\phi})\sqrt{\hat{n}},\tag{1.29}$$

with  $\hat{n}$  and  $\hat{\phi}$  describing density and phase fluctuations in the 1D Bose gas. These operators are conjugate variables  $[\hat{n}(z), \hat{\phi}(z')] = i\delta(z-z')$ . With this definition, the Hamiltonian for a 1D Bose gas can be written as

$$\hat{H} = \int_{-\mathcal{L}/2}^{\mathcal{L}/2} dz \left[ \frac{\hbar^2 n_{1D}}{2m} \left( \nabla \hat{\phi}(z) \right)^2 + \frac{g}{2} \left( \hat{n}(z) \right)^2 \right], \tag{1.30}$$

with  $\mathcal{L}$  the length of the system. In general, the properties of a Luttinger liquid are described by the Luttinger parameter K and the speed of sound c, which contain the specific properties of the system under study. For a 1D Bose gas, the exact solutions make it possible to obtain the analytic expressions

$$c = \sqrt{\frac{gn_{1D}}{m}}, \quad K^{(s)} = \hbar\pi\sqrt{\frac{n_{1D}}{mg}} = \pi\gamma^{-1/2},$$
 (1.31)

which are valid in the limit of  $\gamma \ll 1$ . Inserting this in Eq. 1.30 results in the general form of the Luttinger liquid Hamiltonian

$$\hat{H} = \frac{\hbar c}{2} \int_{-\mathcal{L}/2}^{\mathcal{L}/2} dz \left[ \frac{\pi}{K^{(s)}} \hat{n}^2(z) + \frac{K^{(s)}}{\pi} \left( \frac{\partial}{\partial z} \hat{\phi}(z) \right)^2 \right]. \tag{1.32}$$

The operators  $\hat{\phi}(z)$  and  $\hat{n}(z)$  describing density and phase fluctuations are coarse-grained in the sense that they represent the physics in the long-wavelength limit beyond a cutoff [88]. For 1D bosons the typical cutoff is defined by the inverse of the healing length  $\xi_h = \hbar/mc$ . We develop these operators in plain waves

$$\hat{\phi}(z) = \frac{1}{\sqrt{\mathcal{L}}} \sum_{k} e^{ikz} \hat{\phi}_{k}, \quad \hat{n}(r) = \frac{1}{\sqrt{\mathcal{L}}} \sum_{k} e^{ikz} \hat{n}_{k}, \tag{1.33}$$

with  $k = n \times 2\pi/\mathcal{L}$  ( $n \neq 0$  integer), and the expansion coefficients

$$\hat{n}_k = \sqrt{\frac{n_{1D}S_k}{2}} \left( \hat{b}_k(t) + \hat{b}_{-k}^{\dagger}(t) \right), \tag{1.34}$$

and

$$\hat{\phi}_k = \frac{-i}{\sqrt{2n_{1D}S_k}} \left( \hat{b}_k(t) - \hat{b}_{-k}^{\dagger}(t) \right). \tag{1.35}$$

Here  $\hat{b}_k^{\dagger}$  and  $\hat{b}_k$  are the creation and annihilation operators for an excitation with momentum  $\hbar k$ . The expansion coefficients fulfill  $[\hat{\phi}_k^{\dagger}, \hat{n}_{k'}] = [\hat{\phi}_{-k}, \hat{n}_{k'}] = -i\delta_{kk'}$ . The structure factor in the phononic regime is given by  $S_k = \hbar |k|/2mc = |k|K^{(s)}/2\pi n_{1D}$ . It is related to the usual Bogoliubov coefficients  $(u_k, v_k)$  via  $\sqrt{S_k} = (u_k - v_k)^{-1}$  [151, 153]. Here, we neglect the k = 0 mode, as the spatial correlations in 1D are determined by the modes with  $k \neq 0$ . In the new basis, the Hamiltonian takes the form

$$\hat{H} = \frac{\hbar c}{2} \sum_{k \neq 0} \left( \frac{K^{(s)}}{\pi} k^2 \hat{\phi}_k^{\dagger} \hat{\phi}_k + \frac{\pi}{K^{(s)}} \hat{n}_k^{\dagger} \hat{n}_k \right) = \sum_k \hbar \omega_k \hat{b}_k^{\dagger} b_k. \tag{1.36}$$

In the Luttinger liquid approximation the complex interacting system can thus be identified with uncoupled harmonic oscillators. Their excitations are sound waves which travel with the speed of sound  $c = \sqrt{gn_{1D}/m}$ .

Solving the Heisenberg equations of motion for the phase yields its variance

$$\langle |\hat{\phi}_k(t)|^2 \rangle = \frac{m^2 c^2}{\hbar^2 k^2 n_{1D}^2} \langle |\hat{n}_k(0)|^2 \rangle \sin^2(\omega_k t) + \langle |\hat{\phi}_k(0)|^2 \rangle \cos^2(\omega_k t). \tag{1.37}$$

The phase correlation function (Eq. 1.27) can be calculated using the approximation for the field operators in Eq. 1.29. This results in

$$C(z, z', t) \simeq \langle e^{i\hat{\phi}(z, t) - i\hat{\phi}(z', t)} \rangle = e^{-\frac{1}{2}\langle [\hat{\phi}(z, t) - \hat{\phi}(z', t)]^2 \rangle}, \tag{1.38}$$

which is translation invariant and can be rewritten as

$$C(\bar{z},t) = \exp\left[-\int_0^\infty \frac{dk}{\pi} \langle |\hat{\phi}_k(t)|^2 \rangle (1 - \cos k\bar{z})\right]. \tag{1.39}$$

where  $\bar{z} = z - z'$ .

In thermal equilibrium the fluctuations of density and phase are given by [151]

$$\langle |\hat{\phi}_k(0)|^2 \rangle = \frac{mk_B T}{n_{1D}\hbar^2 k^2}, \qquad \langle |\hat{n}_k(0)|^2 \rangle = \frac{k_B T n_{1D}}{mc^2}.$$
 (1.40)

Inserting this into Eq. 1.39 and using the identity  $\int_0^\infty \frac{dk}{\pi} \frac{a}{k^2} [1 - \cos(kz)] = \frac{1}{2} a |z|$ , we find exactly the time-independent, exponentially decaying thermal correlation function Eq. 1.27, with the correlation length  $\lambda_T^{(s)}$ . In Chap. 4, we will use these

expressions to describe various non-equilibrium settings, where the initial values  $\langle |\hat{\phi}_k(0)|^2 \rangle$  and  $\langle |\hat{n}_k(0)|^2 \rangle$  deviate from their equilibrium values.

### 1.4.4 Luttinger Liquid in a Trap

Similar regimes of quantum degeneracy as in the homogeneous case can be found when the longitudinal confinement of the trap is taken into account [126, 154]. In particular, the longitudinal density profile in the quasi-condensate regime is well described by a Thomas-Fermi parabola (Eq. 1.15). In contrast to the exact Bethe Ansatz solutions, the low-energy approximation for the trapped 1D Bose gas is still integrable. The general procedure for the solution is the same as in the homogeneous case, as outlined below.

Assuming harmonic trapping in the longitudinal direction the Luttinger Hamiltonian (Eq. 1.32) takes the form [154]

$$\hat{H} = \frac{\hbar}{2\pi} \int dz \left[ v_N(z) (\pi \hat{n})^2 + v_J(z) (\partial_z \hat{\phi})^2 \right]. \tag{1.41}$$

In the local density approximation, the generalized velocities  $v_N$  and  $v_J$  can be written as

$$v_N = \frac{c(z)}{K(z)} = \frac{g}{\pi\hbar},\tag{1.42}$$

$$v_J(z) = c(z)K(z) = \frac{\pi\hbar}{2m}n(z). \tag{1.43}$$

These velocities fulfill the relation  $v_N v_J = c(z)^2$ , where c(z) denotes the local speed of sound, K(z) is the local Luttinger parameter and  $n(z) = n_0[1 - (z/R_{\rm TF})^2]$  is the local density in the longitudinal direction. To diagonalize this Hamiltonian we expand the phase and density operators as

$$\hat{\phi}(z,t) = -i \sum_{j>1} \left( \frac{\pi v_N}{2\omega_j R_{\text{TF}}} \right)^{1/2} f_j(z) \hat{b}_j + \text{H.c.},$$
 (1.44)

$$\hat{n}(z,t) = \sum_{j \ge 1} \left( \frac{2\pi n(z)^2 v_N}{\omega_j R_{\text{TF}}} \right)^{1/2} f_j(z) \hat{b}_j + \text{H.c.}$$
 (1.45)

where  $\hat{b}_j^{\dagger}$  and  $\hat{b}_j$  denote operators that create or destroy a bosonic excitation in the jth eigenmode. The eigenmodes  $f_j(z)$  are proportional to the Legendre polynomials

 $P_i(z/R_{\rm TF})$  [155]. Explicitly, they are given by

$$f_j(z) = \sqrt{j + \frac{1}{2}} \times P_j(z/R_{\text{TF}}),$$
 (1.46)

with  $R_{TF}$  the Thomas-Fermi radius of the cloud. The corresponding eigenenergies are given by

$$\epsilon_i = \hbar \omega_i = \hbar \omega_z \sqrt{j(j+1)/2},$$
(1.47)

resulting in the Hamiltonian

$$\hat{H} = \sum_{j>1} \hbar \omega_j \hat{b}_j^{\dagger} \hat{b}_j, \tag{1.48}$$

which again describes a simple set of independent harmonic oscillators.

From these results one obtains the phase variance as

$$\Delta \phi_{zz'}(t)^{2} = \langle \left[ \phi(z, t) - \phi(z', t) \right]^{2} \rangle$$

$$= \frac{\pi v_{N}}{2R_{TF}} \sum_{j>1} \frac{\left[ f_{j}(z) - f_{j}(z') \right]^{2}}{\omega_{j}} (1 + 2N_{j}). \tag{1.49}$$

where  $N_j = \langle \hat{b}_j^\dagger \hat{b}_j \rangle = [\exp(\epsilon_j/k_BT) - 1]^{-1}$  is the thermal occupation number for the excitations, and  $1 + 2N_j \approx 2k_BT/\hbar\omega_j$ . Here, we have neglected the factor of 1, which corresponds to shot noise and can be accounted for separately, if necessary. Inserting this into the expression for the phase correlation function, one closely recovers the exponential decay of Eq. 1.27. Generally, finite size effects only play a role close to the edge of the cloud. However, one important consequence is that the coherence length can now become larger than the system size, leading to the formation of a true BEC with off-diagonal long-range order. The corresponding characteristic temperature is given by

$$T_{\phi} = T_D \times \frac{\hbar \omega_z}{\mu}.\tag{1.50}$$

For typical parameters ( $\mu \sim 100 \, \hbar \omega_z$ ) this corresponds to a temperature well below the ones reached in experiments.

### 1.4.5 Trapped Quasi-condensates in the 1D/3D Crossover

In some of the experiments performed in this thesis the system is not strictly 1D but the temperature or the chemical potential are comparable to the transverse level spacing. In both cases, the 1D criterion introduced in Eq. 1.20 is not strictly fulfilled

anymore and the transverse excited states can be populated. The gas is in a crossover regime between 1D and 3D physics.

This problem has been theoretically studied in a mean-field treatment in Refs. [156–158]. It was found that the chemical potential relative to the ground state of the trap can be approximated by

$$\mu = \hbar\omega_{\perp} \left( \sqrt{1 + 4a_s n} - 1 \right). \tag{1.51}$$

Using the local density approximation, the density profile is given by [159]

$$n(z) = \frac{\alpha}{16a_s} \left( 1 - \frac{z^2}{R^2} \right) \left[ \alpha \left( 1 - \frac{z^2}{R^2} \right) + 4 \right], \tag{1.52}$$

where the radius of the gas is  $R = a_{ho,z}^2/a_{ho,\perp}\sqrt{\alpha}$ , with  $\alpha$  determined from the equation  $\alpha^3(\alpha+5)^2 = (15Na_sa_{ho,\perp}/a_{ho,z}^2)^2$ . For our usual parameters this density profile is very close to the normal Thomas-Fermi parabola. A comparison between the two is presented in Fig. 1.3.

The thermal equilibrium situation of a Bose gas in the 1D/3D crossover has recently been studied experimentally with the conclusion that 1D effects persist far into the crossover [160]. We will see in Sect. 4.5 that the same is also true away from equilibrium.

### 1.4.6 Description by a Stochastic Process

To compare the experiment with theory it is often necessary to simulate single realizations of the experiment and to take into account technical aspects, such as the expansion of the gases or the limited resolution of the imaging system. Also, as the number of times the experiment can be repeated is limited, it is desirable to be able to predict how this finite statistics affects the results. To this end, a powerful simulation technique was developed that models the in situ fluctuations of a quasi-condensate using a stochastic process [159, 161, 162]. For a single gas this stochastic process is a simple diffusion process. Thanks to an exact updating formula [163] this approach is numerically very efficient. It can also take the trap into account using the local density approximation. After the simulation of the in situ gas, a numerical time-propagation of the wave function allows the modeling of the time-of-flight expansion and the imaging process [105, 159, 164]. In the following, we present the basic concepts of the modeling [159]. Alternative possibilities to simulate single realizations in equilibrium are the stochastic sampling of excitations [153, 165], stochastic versions of the Gross-Pitaevskii equation [166] or Metropolis sampling algorithms [167].

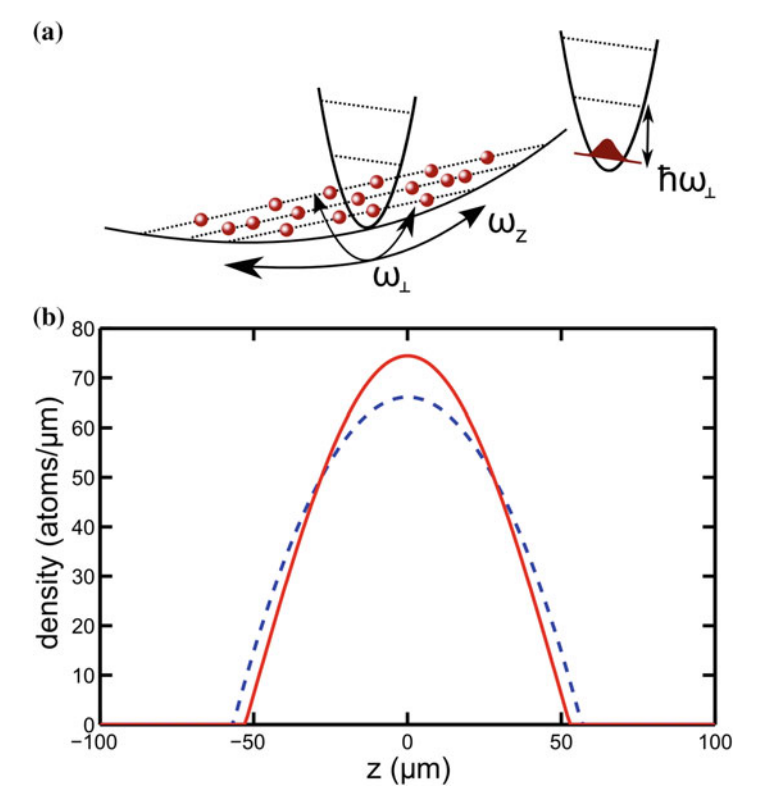


Fig. 1.3 The trapped 1D Bose gas. a A trapped Bose gas behaves one-dimensional, if  $k_BT$ ,  $\mu < \hbar\omega_{\perp}$ . Consequently, all atoms are radially in the ground state of the trapping potential. Longitudinally, many modes are occupied. b Longitudinal density profile, calculated in the Thomas-Fermi approximation (*dashed line*) and using Eq. 1.52 (*solid line*) for N=5000,  $\omega_{\perp}=2\pi\times 2$  kHz and  $\omega_z=2\pi\times 10$  Hz. The results of the two calculations closely resemble each other. For lower atom numbers they become identical

As the statistical properties of the phase fluctuations in a quasi-condensate are Gaussian, the spatial variation of the phase can be described by a Gaussian diffusion process

$$\frac{d}{dz}\phi(z) = f(z). \tag{1.53}$$

The basic idea is to model the stochastic force f(z) in such a way that it reproduces the correct exponentially decaying correlation properties of Eq. 1.27. To this end we define f(z) such that it fulfills  $\langle f(z)f(z')\rangle = 2\delta(z-z')/\lambda_T^{(s)}$  and  $\langle f(z)\rangle = 0$ . Given the phase at a certain position z in the gas, the phase at another position z' can then be found using the exact updating formula [163]

$$\phi(z') = \phi(z) + \sqrt{\frac{2|z - z'|}{\lambda_T^{(s)}}} \times \mathcal{N}$$
 (1.54)

where  $\mathcal{N}$  is a random number drawn from a Gaussian distribution with zero mean and unit standard deviation. Using this updating formula, it is possible to simulate a single phase profile on a discrete grid, by randomly choosing a starting phase at one end of the cloud and generating the rest of the phase profile pixel by pixel. To take the trapping potential into account, the thermal phase correlation length can be changed in each step, following a local density approximation approach. Finally, all correlation properties can be calculated by averaging over many realizations of the stochastic process.

### 1.5 Bose Gases in a Double-Well Potential

Interference is one of the hallmark features all wave theories. From the first experiments demonstrating the wave-like nature of light [168, 169] to the ground-breaking achievements of matter-wave interferometry with electrons [170], neutrons [171], atoms [172] and even large molecules [173], interference has led to new insights into the laws of nature and served as a sensitive tool for metrology. In the context of Bose-Einstein condensates, interference was demonstrated in one of the first experiments, providing a striking demonstration of the macroscopic phase coherence of the wave function [174].

In this thesis we use the interference of two 1D Bose gases to learn about their dynamics. Each gas is trapped in one well of a double-well potential. A first simple picture is obtained by describing the two Bose gases as spatially separate wave packets.

The situation is depicted in Fig. 1.4a. After a time of free expansion t that is large enough to neglect the initial size and the initial separation d of the wave packets, their wave functions can be written as [97, 175]

$$\psi^{(1,2)}(\mathbf{r},t) \sim \exp\left(i \, \mathbf{Q}_{1,2}(\mathbf{r} \pm \mathbf{d}/2)\right) \exp\left(-\frac{i}{\hbar} \frac{\mathbf{Q}_{1,2}^2}{2m}t\right) \exp(i \, \phi^{(1,2)}),$$
 (1.55)

where  $\phi^{(1,2)}$  denotes the initial phases of the two wave packets and  $Q_{1,2} = m(r \pm d/2)/\hbar t$  the momenta of atoms that are released from one of the condensates and detected at a point r. The resulting interference signal is given by

$$S \equiv \left| \psi^{(1)} + \psi^{(2)} \right|^2 = \left| \psi^{(1)}(r,t) \right|^2 + \left| \psi^{(2)}(r,t) \right|^2 + 2 \operatorname{Re} \left[ \psi^{(1)}(r,t) \psi^{(2)*}(r,t) \right]. \tag{1.56}$$

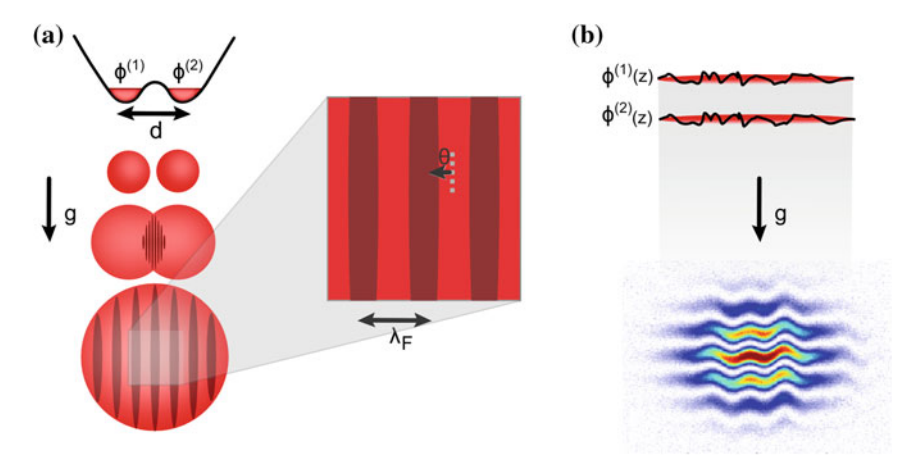


Fig. 1.4 Matter-wave interference. a Double-slit experiment with two atomic wave packets in a double well. After releasing the wave packets from the trap, they expand, overlap and form an interference pattern. The fringe spacing of this interference pattern is related to the initial separation of the two wave packets via  $\lambda_F = ht/md$ , where t is the expansion time and m is the mass of the atoms. The position of the interference fringes with respect to the center of the interference pattern (dashed line) is set by the relative phase  $\theta = \phi^{(1)} - \phi^{(2)}$  of the two wave packets. b The interference of two phase-fluctuating 1D Bose gases can be understood in exactly the same terms. The two gases expand and form a locally displaced interference pattern. The local position of the interference fringes at every point z is determined by the local relative phase  $\theta(z)$  at this point. The interference pattern thus directly reflects the in situ distribution of the relative phase between the interfering 1D Bose gases. In both pictures, g denotes the direction of gravity

It is thus proportional to the oscillating function

$$S \sim \cos\left(\frac{md}{\hbar t}r + \theta\right),$$
 (1.57)

with the relative phase  $\theta=\phi^{(1)}-\phi^{(2)}$ . This function exhibits periodic maxima separated by a distance

$$\lambda_F = ht/md = 1/|Q_1 - Q_2|.$$
 (1.58)

In the following, these maxima will be referred to as the interference fringes. Their position relative to the center of the cloud is defined by the relative phase  $\theta$ . This is directly analogous to Young's double-slit experiment with light [168, 169]. By measuring the position of the interference fringes it is thus possible to infer the relative phase between the original wave packets. Note however, that phase coherence between the two gases is not a necessary requirement for the observation of high-contrast interference in a single-shot measurement. Interference can also appear for completely independent sources, where a relative phase is spontaneously and randomly fixed during the measurement [97, 176, 177]. Averaging over many

such independent-source measurements therefore washes out the interference [73]. however, the fluctuations of the phase contain important information about the system, as we shall see below.

### 1.5.1 Matter-Wave Interference of One-Dimensional Bose Gases

Similar to the simple interference of the two Gaussian wave packets, 1D Bose gases in a double well can be studied using matter-wave interferometry. This approach has previously been used to characterize their equilibrium states [162, 178]. In the following, we review typical techniques and observables in equilibrium and then extend the approach to non-equilibrium states.

The situation we want to study are pairs of 1D Bose gases in a double well. In this case, each gas can be described by an individual Luttinger Hamiltonian

$$\hat{H} = \hat{H}^{(1)} + \hat{H}^{(2)} \tag{1.59}$$

$$\hat{H}^{(1)} = \int_{-L/2}^{L/2} dz \left[ \frac{\hbar^2 n_{1D}^{(1)}}{2m} \left( \nabla \hat{\phi}(z)^{(1)} \right)^2 + \frac{g}{2} \left( \hat{n}(z)^{(1)} \right)^2 \right]$$
(1.60)

$$\hat{H}^{(2)} = \int_{-L/2}^{L/2} dz \left[ \frac{\hbar^2 n_{1D}^{(2)}}{2m} \left( \nabla \hat{\phi}(z)^{(2)} \right)^2 + \frac{g}{2} \left( \hat{n}(z)^{(2)} \right)^2 \right], \tag{1.61}$$

where the superscript labels the gases. Usually, this situation is studied using symmetric and anti-symmetric superpositions of the individual fluctuations, i.e.

$$\hat{\nu}(z) = [\hat{n}^{(1)}(z) - \hat{n}^{(2)}(z)]/2, \tag{1.62}$$

$$\hat{\nu}^{(+)}(z) = [\hat{n}^{(1)}(z) + \hat{n}^{(2)}(z)]/2, \tag{1.63}$$

for the density fluctuations and

$$\hat{\theta}(z) = [\hat{\phi}^{(1)}(z) - \hat{\phi}^{(2)}(z)], \tag{1.64}$$

$$\hat{\theta}^{(+)}(z) = [\hat{\phi}^{(1)}(z) + \hat{\phi}^{(2)}(z)], \tag{1.65}$$

for the phase fluctuations. In the most general case this leads to

$$\hat{H} = \hat{H}^{(-)} + \hat{H}^{(+)} + \hat{H}_{\text{mix}}.$$
 (1.66)

with

$$\hat{H}^{(-)} = \int_{-L/2}^{L/2} dz \left[ \frac{\hbar^2 (n_{1D}^{(1)} + n_{1D}^{(2)})}{8m} \left( \nabla \hat{\theta}(z) \right)^2 + \frac{g}{2} \left( \hat{\nu}(z) \right)^2 \right]$$
(1.67)

$$\hat{H}^{(+)} = \int_{-L/2}^{L/2} dz \left[ \frac{\hbar^2 (n_{1\mathrm{D}}^{(1)} + n_{1\mathrm{D}}^{(2)})}{8m} \left( \nabla \hat{\theta}^{(+)}(z) \right)^2 + \frac{g}{2} \left( \hat{\nu}^{(+)}(z) \right)^2 \right]$$
(1.68)

$$\hat{H}_{\text{mix}} = \int_{-L/2}^{L/2} dz \left[ \frac{\hbar^2 (n_{1\text{D}}^{(1)} - n_{1\text{D}}^{(2)})}{4m} \left( \nabla \hat{\theta}^{(+)}(z) \nabla \hat{\theta}(z) \right) \right]. \tag{1.69}$$

There are thus two cases to study. If the mean densities  $n_{\rm 1D}^{(1,2)}$  of the two gases are different  $\hat{H}_{\rm mix} \neq 0$ , leading to mixing between symmetric and anti-symmetric degrees of freedom. This case is studied in Chap. 7. If the mean densities of the two gases are identical  $\hat{H}_{\rm mix} = 0$ , and symmetric and anti-symmetric degrees of freedom decouple. This case will be discussed in the following.

If  $\hat{H}^{(-)}$  and  $\hat{H}^{(+)}$  decouple, they can be diagonalized independently, using the same procedure as in the case of a single gas in Sect. 1.4.3. Expanding  $\hat{\theta}(z)$  and  $\hat{\nu}(z)$  into plain waves we obtain

$$\hat{\theta}(z) = \sum_{k} \hat{\theta}_{k} \frac{e^{ikz}}{\sqrt{\mathcal{L}}}, \quad \hat{\nu}(z) = \sum_{k} \hat{\nu}_{k} \frac{e^{ikz}}{\sqrt{\mathcal{L}}}, \tag{1.70}$$

$$\hat{\theta}_k = -i\frac{\hat{b}_k - \hat{b}_{-k}^{\dagger}}{\sqrt{2n_{1D}S_k}}, \quad \hat{\nu}_k = \sqrt{\frac{n_{1D}S_k}{2}}(\hat{b}_k + \hat{b}_{-k}^{\dagger}), \tag{1.71}$$

where  $\hat{b}_k^{\dagger}$  and  $\hat{b}_k$  are again creation and annihilation operators for an elementary excitation with the momentum  $\hbar k$ . Note that the Luttinger parameter for the relative degrees of freedom is defined as

$$K = \frac{\hbar\pi}{2} \sqrt{\frac{n_{\rm 1D}}{mg}}. (1.72)$$

For the corresponding Hamiltonian one finds

$$\hat{H}^{(-)} = \sum_{k \neq 0} \hbar c |k| \hat{b}_k^{\dagger} \hat{b}_k + \frac{\hbar \pi c}{2K} \hat{n}_{k=0}^2.$$
 (1.73)

Here we have included the contribution of the k = 0 mode, as it can be identified with the phase diffusion discussed in the coherence properties of 3D BECs in double wells [73, 179–181]. The resulting phase variance is given by

$$\langle |\hat{\theta}_k(t)|^2 \rangle = \frac{4m^2c^2}{\hbar^2k^2n_{1D}^2} \langle |\hat{\nu}_k(0)|^2 \rangle \sin^2(\omega_k t) + \langle |\hat{\theta}_k(0)|^2 \rangle \cos^2(\omega_k t). \tag{1.74}$$

For the trapped gas we find

$$\Delta \hat{\theta}_{zz'}(t)^{2} = \langle [\hat{\theta}(z,t) - \hat{\theta}(z',t)]^{2} \rangle$$

$$= \frac{\pi v_{N}}{2R_{\text{TF}}} \sum_{j \ge 1} \sin^{2}(\omega_{j}t) \frac{\left[f_{j}(z) - f_{j}(z')\right]^{2}}{\omega_{j}} (1 + 2N_{j}). \tag{1.75}$$

In a typical experimental sequence the gases are released from the trap and allowed to expand freely under gravity. After a certain time of flight they will form an interference pattern, just as the wave packets in the simple example. However, now the gases are extended in the z-direction and the relative phase  $\theta(z)$  fluctuates along their length. For every point in the interference pattern the local position of the fringes is thus different, as determined by  $\theta(z)$ . In a simple picture, every point along the length of the gas acts like an independent interference experiment. In every individual experiment, the position of the fringes is determined by the local relative phase of the matter waves emitted from the two wells. Stacking all these experiments together results in the observed interference pattern, as shown in Fig. 1.4b. This simple view neglects the effects of the expansion, but remains accurate for typical experimental parameters.

More formally, in analogy with the simple interference experiment discussed above, we can write the interference signal of two 1D Bose gases as

$$(\hat{\Psi}^{(1)} + \hat{\Psi}^{(2)})^{\dagger} (\hat{\Psi}^{(1)} + \hat{\Psi}^{(2)})$$

$$= \langle |\hat{\Psi}^{(1)}|^2 \rangle + \langle |\hat{\Psi}^{(2)}|^2 \rangle + \hat{\Psi}^{(1)\dagger} \hat{\Psi}^{(2)} + \hat{\Psi}^{(2)\dagger} \hat{\Psi}^{(1)}.$$
(1.76)

Here,  $\hat{\Psi}(\boldsymbol{r},z) = \hat{\Psi}^{(1)}(z)e^{i\,Q_1(\boldsymbol{r}+\boldsymbol{d}/2)-i\,Q_1^2t/2\hbar m} + \hat{\Psi}^{(2)}(z)e^{i\,Q_2(\boldsymbol{r}-\boldsymbol{d}/2)-i\,Q_2^2t/2\hbar m}$  denotes the field operator after expansion [182]. Again, the cross terms are responsible for the interference. To formally describe the interference pattern we introduce the operator [175, 182]

$$\hat{A}(L) = \int_{-L/2}^{L/2} dz \,\hat{\Psi}^{(1)\dagger}(z,t) \hat{\Psi}^{(2)}(z,t), \tag{1.77}$$

where L denotes a length scale over which the interference pattern is integrated in the z-direction. The complex phase of this operator can be identified with the

integrated phase  $\theta(L)$  of the interference pattern, its magnitude  $|\hat{A}|$  is connected to the contrast. For independent gases the expectation value of this operator vanishes, as the total phase is different in each individual realization. However, one can still observe high-contrast interference in these individual realizations. Consequently, the variance

$$\langle |\hat{A}(L)|^2 \rangle = \int_{-L/2}^{L/2} \int_{-L/2}^{L/2} dz dz' \left\langle \hat{\Psi}^{(2)\dagger}(z) \hat{\Psi}^{(1)}(z) \hat{\Psi}^{(1)\dagger}(z') \hat{\Psi}^{(2)}(z') \right\rangle$$
(1.78)

is finite.

The operator  $\langle |\hat{A}(L)|^2 \rangle$  is directly related to the mean squared contrast observed in experiment via  $\langle C^2(L) \rangle = \langle |\hat{A}(L)|^2 \rangle / n_{1D}^2 L^2$ , where  $n_{1D} = \langle |\Psi_1(z)|^2 \rangle$  is the mean density in the two gases.

The argument of the integral in Eq. 1.78 can be identified with the two-point correlation function of the relative phase

$$C(z, z') = \frac{\langle \hat{\Psi}^{(2)\dagger}(z) \hat{\Psi}^{(1)}(z) \hat{\Psi}^{(1)\dagger}(z') \hat{\Psi}^{(2)}(z') \rangle}{\langle |\Psi^{(1)}(z)|^2 \rangle \langle |\Psi^{(2)}(z')|^2 \rangle}.$$
 (1.79)

The mean squared contrast is thus the double integral over the two-point correlation function. Neglecting the typically weak density fluctuations by using  $\hat{\Psi}^{(1,2)} = \sqrt{n_{1D}} \exp(\hat{\phi}^{(1,2)})$ , the phase correlation function can be rewritten as

$$C(z, z') = \langle e^{i\hat{\theta}(z) - i\hat{\theta}(z')} \rangle, \tag{1.80}$$

with  $\hat{\theta}(z) = \hat{\phi}^{(1)}(z) - \hat{\phi}^{(2)}(z)$  denoting the local relative phase. In experiment, the relative phase profile is directly inferred from the interference pattern. Therefore, Eq. 1.80 can be used to calculate the experimental phase correlation function. To calculate the corresponding theoretical correlation function, we make use of the fact that the fluctuations of  $\hat{\theta}(z)$  are Gaussian, leading to [159]

$$C(z, z') = e^{-\frac{1}{2} \left\langle [\hat{\theta}(z) - \hat{\theta}(z')]^2 \right\rangle}.$$
 (1.81)

The argument of the exponential function is the phase variance  $\Delta \hat{\theta}_{zz'}^2 = \langle [\hat{\theta}(z) - \hat{\theta}(z')]^2 \rangle$ . This enables the calculation of the phase correlation function using the results obtained in Eqs. 1.74 and 1.75.

Further information about the system beyond the two-point correlation function can be obtained from the shot-to-shot fluctuations of the contrast. Such noise measurements have a long and rich history in the characterization of quantum systems [63]. Examples range from the Hanbury Brown-Twiss effect in light [183, 184] and matter-waves [185, 186] to the study of current fluctuations in quantum-Hall systems [187] and the coherence properties of atomic systems [188–190].

The shot-to-shot fluctuations of the contrast can be characterized by the moments of the full distribution function (FDF)  $P(\alpha)$  of fringe contrast [178, 191]

$$\frac{\langle |\hat{A}|^{2m} \rangle}{\langle |\hat{A}|^2 \rangle^m} \equiv \langle \alpha^m \rangle = \int_0^\infty P(\alpha) \alpha^m d\alpha, \tag{1.82}$$

where  $P(\alpha)d\alpha$  measures the probability to observe a contrast in the interval between  $\alpha$  and  $\alpha+d\alpha$ . The normalized moments on the left hand side are each connected to a correlation function  $\langle |\hat{A}|^{2m} \rangle$  of order 2m, which is the reason why the FDF, in general, contains more information about the many-body state than the mean contrast. To calculate the full distribution function one has to calculate all moments, or equivalently, all even correlation functions. For the equilibrium situation powerful insights were obtained by mapping this problem onto a quantum impurity problem and to a generalized Coulomb gas model [192]. Experimentally, the FDFs have successfully been used before to study 1D gases in thermal equilibrium [178], as well as the dynamics of an unstable quantum pendulum [193].

#### 1.5.2 Equilibrium States

For the anti-symmetric degrees of freedom of a balanced pair of 1D gases in thermal equilibrium the initial conditions are given by [151, 153]

$$\langle |\hat{\theta}_k(0)|^2 \rangle = \frac{k_B T}{2n_{1D} \frac{\hbar^2 k^2}{4m}} = \frac{2mk_B T}{n_{1D} \hbar^2 k^2}$$
 (1.83)

$$\langle |\hat{\nu}_k(0)|^2 \rangle = \frac{k_B T}{mc^2} \frac{n_{1D}}{2},$$
 (1.84)

where  $n_{1D}$  denotes the mean density in each of the gases. Inserting these expressions into Eq. 1.74 results in the correlation function

$$C(z, z') = \exp(-|z - z'|/\lambda_T), \qquad (1.85)$$

where  $\lambda_T = \hbar^2 n_{\rm 1D}/mk_BT$  is the thermal correlation length. Note the missing factor of two in the definition, compared to the thermal coherence length  $\lambda_T^{(s)}$  of a single gas (Eq. 1.39). This factor arises because we now deal with a two-body density matrix, instead of the one-body density matrix for a single gas.

In the trapped case

$$C(z, z') = \exp\left(\frac{g}{\hbar^2 R_{\text{TF}}} \sum_{j \ge 1} \frac{\left[f_j(z) - f_j(z')\right]^2}{\omega_j} \frac{2k_B T}{\hbar \omega_j}\right). \tag{1.86}$$

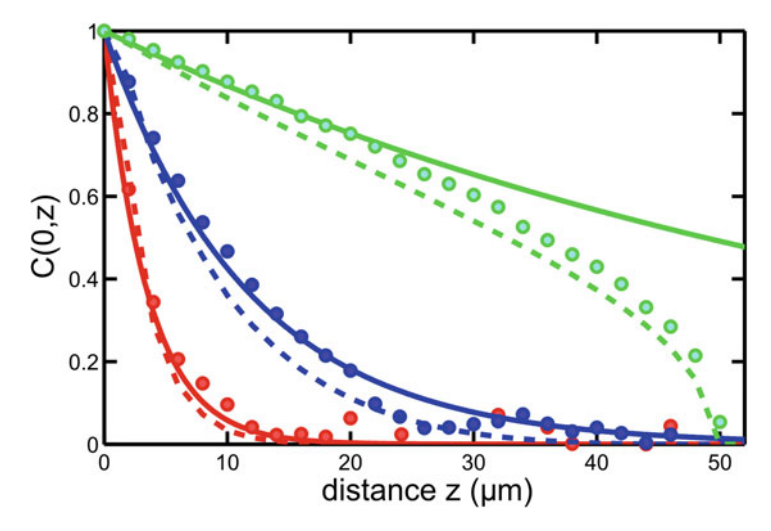


Fig. 1.5 Relative two-point phase correlation functions in equilibrium. Parameters are 4000 atoms per well,  $T=100\,\mathrm{nK}$  (red),  $T=30\,\mathrm{nK}$  (blue) and  $T=5\,\mathrm{nK}$  (green). Dashed lines represent the full trapped theory (Eq. 1.86), points the result of an Ornstein-Uhlenbeck simulation averaging over 200 realizations. The solid lines correspond to the homogeneous theory (Eq. 1.85) with a density corresponding to the peak density of the trapped simulation. Finite size effects are generally small and only play a significant role at very low temperature or close to the edge of the cloud ( $R_{\mathrm{TF}}\sim50\,\mu\mathrm{m}$ )

A comparison of different results is shown in Fig. 1.5, revealing that trap effects are usually weak and only play a role close to the edge of the system.

The result for the equilibrium correlation function (Eq. 1.85) also allows the derivation of the mean contrast as a function of integration length, which yields

$$\langle C^{2}(L)\rangle \equiv \frac{1}{L^{2}} \int \int_{-L/2}^{L/2} dz_{1} dz_{2} \, \mathcal{C}(z_{1}, z_{2})$$

$$= 2R \left[ \frac{\lambda_{T}}{L} - \left( \frac{\lambda_{T}}{L} \right)^{2} \left( 1 - \exp\left( -\frac{L}{\lambda_{T}} \right) \right) \right]. \tag{1.87}$$

Here,  $R=e^{-1/4K}\approx 1$  is a reduction of the interference contrast due to the contributions of high-energy excitations [88].

In a more general case, we can also allow for tunnel coupling between the two gases. This leads to a large variety of effects and has strong analogies with the quantum Sine-Gordon model (see Outlook). For the phase correlation function one finds [153]

$$C_J(z, z') = \exp\left[-\frac{l_J}{\lambda_T} \left(1 - e^{-|z - z'|/l_J}\right)\right],\tag{1.88}$$

where  $\lambda_T$  is again the thermal coherence length. It characterizes the thermal fluctuations which lead to a randomization of the phase along the longitudinal direction of the system. The new length scale  $l_J = \sqrt{\hbar/4mJ}$  is related to the tunnel coupling J, which counteracts the randomization of the relative phase [153, 162]. In the limit of vanishing tunnel coupling  $l_J \rightarrow \infty$ , and the exponential decay of Eq. 1.85 is recovered.

As in the previous chapter the system can also be described using a stochastic process. If we include coupling, the stochastic force is not sufficient anymore to describe the fluctuations and an additional friction force is needed. In the case of the relative phase, the simple stochastic diffusion process thus has to be replaced by a full Ornstein-Uhlenbeck process, which is defined via

$$\frac{d}{dz}\theta(z) = f(z) - \frac{1}{l_I}\theta(z). \tag{1.89}$$

Here, we have assumed a vanishing mean of the phase  $\langle \theta(z) \rangle = 0$ . The correct correlation properties of the stochastic force f(z) are given by  $\langle f(z)f(z') \rangle = \frac{2}{\lambda_T} \delta(z-z')$  and  $\langle f(z) \rangle = 0$ . The differential equation Eq. 1.89 has a simple interpretation in terms of the two stochastic forces. While temperature randomizes the phase profile as characterized by  $\lambda_T$ , the coupling acts as a restoring force characterized by  $l_J$ . The corresponding updating formula is given by

$$\theta(z') = \beta \,\theta(z) + \sqrt{\frac{l_J}{\lambda_T} (1 - \beta^2)} \times \mathcal{N},\tag{1.90}$$

with  $\beta=\exp(-\left|z-z'\right|/l_J)$ . For the numerical simulation of the experiment it is, however, necessary to simulate not only the relative phase, but also the two individual phase profiles. It can be shown that these single phase fields cannot be simulated using the updating formula given by Eq. 1.90 if the gases are coupled. However, the common phase  $\theta^{(+)}(z)=\phi^{(1)}(z)+\phi^{(2)}(z)$  can be simulated using the updating formula

$$\theta^{(+)}(z') = \theta^{(+)}(z) + \sqrt{\frac{2|z - z'|}{\lambda_T}} \times \mathcal{N}.$$
 (1.91)

As the phase profiles of the individual gases are given by

$$\phi^{(1,2)}(z) = \frac{\theta^{(+)}(z) \pm \theta(z)}{2},\tag{1.92}$$

they can be obtained from the combination of two stochastic processes, one for the relative phase and one for the common phase. The remaining treatment of expansion and imaging follows in exactly the same way as for a single gas. Repeating the procedure described by Eq. 1.91 many times allows the reproduction of all correlation

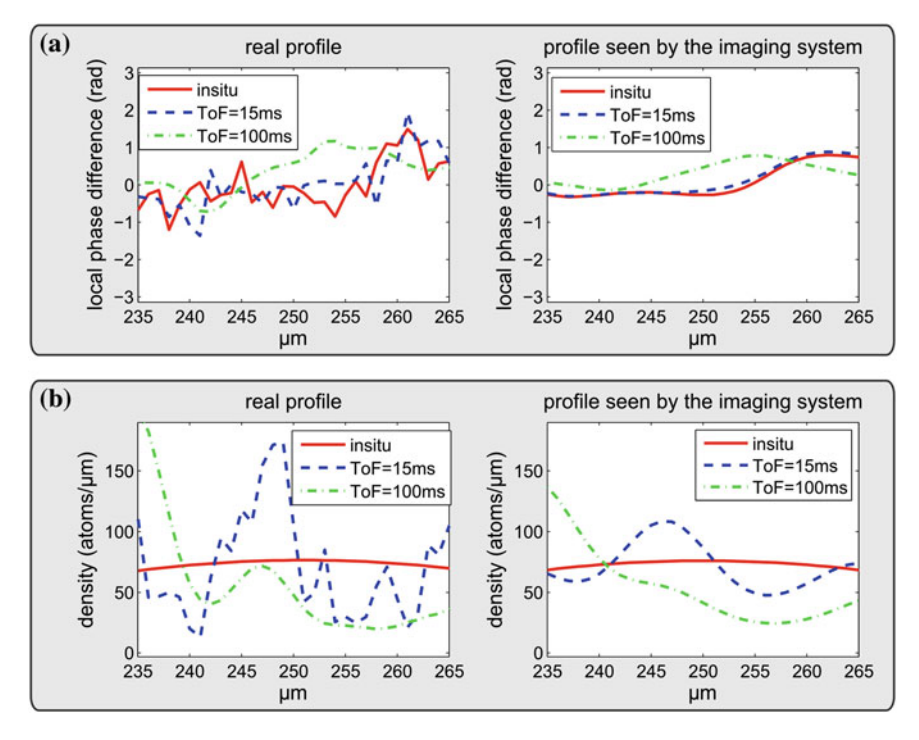


**Fig. 1.6** Simulation of realistic interference between two 1D Bose gases. The images reveal the effect of time-of-flight expansion and limited imaging resolution on phase and density profiles. **a** The phase fluctuates both in situ and in time-of-flight. For very long times of flight, fluctuations get washed out. Consequently, we limit the time of flight to approximately 15 ms in experiment. Similarly, the limited resolution of the imaging system strongly reduces the amount of visible fluctuations and thus has to be taken into account. In the theoretical analysis this is accomplished by convolving the phase profile with the point spread function of the imaging system. **b** The in situ density profile is smooth, as fluctuations are strongly suppressed in the quasi-condensate regime. However, the phase gradient leads to a velocity field for the atoms, resulting in increasing density fluctuations in time-of-flight. This effect can be observed both for a single gas or for two gases and can be used for thermometry. Similar to the phase profile, the density fluctuations are reduced due to the limited imaging resolution. Figure adapted from [63]

properties of the system, including the two-point correlation function (see Fig. 1.5) or the FDFs.

Typical results are presented in Fig. 1.6. One observes that the longitudinal relative phase after time-of-flight closely reflects the in situ relative phase. The reason for this is the typically low trapping frequency in the longitudinal direction, which results in a negligible expansion in this direction. The strongest effect of the expansion is a loss in effective resolution with increasing time of flight. In the experiments we therefore image the gases after relatively short times of flight of  $\sim 15\,\mathrm{ms}$ .

In equilibrium, the resulting density profile after time-of-flight expansion is the incoherent sum of the two gases. As in the case of a single gas, this density profile shows pronounced density ripples as a result of the in situ phase fluctuations, enabling thermometry of a pair of gases in equilibrium [162].

#### References

- 1. K. Huang, Statistical Mechanics (Wiley, 1987)
- 2. F. Reif, Fundamentals of Statistical and Thermal Physics (McGraw-Hill, 1965)
- J.V. Neumann, Beweis des Ergodensatzes und des H-Theorems in der neuen Mechanik. Z. Phys. 57, 30–70 (1929)
- 4. D. Ter Haar, Foundations of statistical mechanics. Rev. Mod. Phys. 27, 289–338 (1955)
- A. Polkovnikov, K. Sengupta, A. Silva, M. Vengalattore, Colloquium: nonequilibrium dynamics of closed interacting quantum systems. Rev. Mod. Phys. 83, 863–883 (2011)
- E. Fermi, J. Pasta, S. Ulam, Studies of nonlinear problems. Los Alamos scientific laboratory report No. LA-1940 (1955)
- G. Gallavotti, Statistical Mechanics: A Short Treatise. Texts and Monographs in Physics (Springer, 1999)
- L. Boltzmann, Weitere Studien über das Wärmegleichgewicht unter Gasmolekülen (Sitzungsberichte der Akademie der Wissenschaften, 1872)
- 9. E.T. Jaynes, Information theory and statistical mechanics. Phys. Rev. 106, 620–630 (1957)
- R. Balian, From Microphysics to Macrophysics: Methods and Applications of Statistical Physics (Springer, 2007)
- 11. M. Srednicki, Chaos and quantum thermalization. Phys. Rev. E 50, 888–901 (1994)
- J.M. Deutsch, Quantum statistical mechanics in a closed system. Phys. Rev. A 43, 2046–2049 (1991)
- P. Reimann, Foundation of statistical mechanics under experimentally realistic conditions. Phys. Rev. Lett. 101, 190403 (2008)
- S. Popescu, A.J. Short, A. Winter, Entanglement and the foundations of statistical mechanics. Nat. Phys. 2, 754–758 (2006)
- M. Rigol, V. Dunjko, M. Olshanii, Thermalization and its mechanism for generic isolated quantum systems. Nature 452, 854–858 (2008)
- C. Gogolin, M.P. Müller, J. Eisert, Absence of thermalization in nonintegrable systems. Phys. Rev. Lett. 106, 040401 (2011)
- M. Rigol, M. Fitzpatrick, Initial-state dependence of the quench dynamics in integrable quantum systems. Phys. Rev. A 84, 033640 (2011)
- A. Riera, C. Gogolin, J. Eisert, Thermalization in nature and on a quantum computer. Phys. Rev. Lett. 108, 080402 (2012)
- M. Rigol, M. Srednicki, Alternatives to eigenstate thermalization. Phys. Rev. Lett. 108, 110601 (2012)
- D. Podolsky, G. Felder, L. Kofman, M. Peloso, Equation of state and beginning of thermalization after preheating. Phys. Rev. D 73, 023501 (2006)
- L. Kofman, A. Linde, A.A. Starobinsky, Reheating after Inflation. Phys. Rev. Lett. 73, 3195–3198 (1994)
- 22. A. Arrizabalaga, J. Smit, A. Tranberg, Equilibration in  $\varphi^4$  theory in 3+ 1 dimensions. Phys. Rev. D **72**, 025014 (2005)
- 23. J. Berges, Sz. Borsányi, C. Wetterich, Prethermalization. Phys. Rev. Lett. 93, 142002 (2004)
- 24. P. Braun-Munzinger, D. Magestro, K. Redlich, S.J. Hadron, Production in Au-Au collisions at RHIC. Phys. Lett. B **518**, 41–46 (2001)
- 25. U. Heinz, P. Kolb, Early thermalization at RHIC. Nucl. Phys. A 702, 269–280 (2002)

References 31

 C. Kollath, A.M. Läuchli, E. Altman, Quench dynamics and nonequilibrium phase diagram of the Bose-Hubbard model. Phys. Rev. Lett. 98, 180601 (2007)

- M. Eckstein, M. Kollar, P. Werner, Thermalization after an interaction quench in the Hubbard model. Phys. Rev. Lett. 103, 056403 (2009)
- M. Moeckel, S. Kehrein, Crossover from adiabatic to sudden interaction quenches in the Hubbard model: prethermalization and non-equilibrium dynamics. New J. Phys. 12, 055016 (2010)
- R. Barnett, A. Polkovnikov, M. Vengalattore, Prethermalization in quenched spinor condensates. Phys. Rev. A 84, 023606 (2011)
- 30. I. Bloch, J. Dalibard, W. Zwerger, Many-body physics with ultracold gases. Rev. Mod. Phys. **80**, 885–964 (2008)
- T. Langen, R. Geiger, J. Schmiedmayer, Ultracold atoms out of equilibrium. Annu. Rev. Cond. Mat. Phys. 6, 201 (2015)
- 32. M. Greiner, O. Mandel, T. Esslinger, T.W. Hänsch, I. Bloch, Quantum phase transition from a superfluid to a Mott insulator in a gas of ultracold atoms. Nature **415**, 39–44 (2002)
- M. Greiner, O. Mandel, T.W. Hänsch, I. Bloch, Collapse and revival of the matter wave field of a Bose-Einstein condensate. Nature 419, 51 (2002)
- 34. T. Kinoshita, T. Wenger, D. Weiss, A quantum Newton's cradle. Nature 440, 900–903 (2006)
- N. Strohmaier, D. Greif, R. Jördens, L. Tarruell, H. Moritz, T. Esslinger, R. Sensarma, D. Pekker, E. Altman, E. Demler, Observation of elastic doublon decay in the Fermi-Hubbard model. Phys. Rev. Lett. 104, 080401 (2010)
- S. Will, T. Best, U. Schneider, L. Hackermüller, D.-S. Lühmann, I. Bloch, Time-resolved observation of coherent multi-body interactions in quantum phase revivals. Nature 465, 197– 201 (2010)
- S. Will, D. Iyer, M. Rigol, Observation of coherent quench dynamics in a metallic many-body state of fermionic atoms. Nat. Commun. 6, 6009 (2015)
- W.S. Bakr, A. Peng, M.E. Tai, R. Ma, J. Simon, J.I. Gillen, S. Fölling, L. Pollet, M. Greiner, Probing the superfluid-to-Mott insulator transition at the single-atom level. Science 329, 547 (2010)
- 39. J.F. Sherson, C. Weitenberg, M. Endres, M. Cheneau, I. Bloch, S. Kuhr, Single-atom-resolved fluorescence imaging of an atomic Mott insulator. Nature **467**, 68–72 (2010)
- 40. F. Serwane, G. Zürn, T. Lompe, T.B. Ottenstein, A.N. Wenz, S. Jochim, Deterministic preparation of a tunable few-Fermion system. Science 332, 336 (2011)
- C. Chin, R. Grimm, P. Julienne, E. Tiesinga, Feshbach resonances in ultracold gases. Rev. Mod. Phys. 82, 1225–1286 (2010)
- B.S. Rem, A.T. Grier, I. Ferrier-Barbut, U. Eismann, T. Langen, N. Navon, L. Khaykovich, F. Werner, D.S. Petrov, F. Chevy, C. Salomon, Lifetime of the bose gas with resonant interactions. Phys. Rev. Lett. 110, 163202 (2013)
- 43. S. Nascimbène, N. Navon, K.J. Jiang, F. Chevy, C. Salomon, Exploring the thermodynamics of a universal Fermi gas. Nature **463**, 1057 (2010)
- S. Trotzky, Y.-A. Chen, A. Flesch, I.P. McCulloch, U. Schöllwöck, J. Eisert, I. Bloch, Probing the relaxation towards equilibrium in an isolated strongly correlated one-dimensional Bose gas. Nat. Phys. 8, 325–330 (2012)
- M.J.H. Ku, A.T. Sommer, L.W. Cheuk, M.W. Zwierlein, Revealing the superfluid lambda transition in the universal thermodynamics of a unitary Fermi gas. Science 335, 563–567 (2012)
- K. Van Houcke, F. Werner, E. Kozik, N. Prokof'ev, B. Svistunov, M.J.H. Ku, A.T. Sommer, L.W. Cheuk, A. Schirotzek, M.W. Zwierlein, Feynman diagrams versus Fermi-gas Feynman emulator. Nat. Phys. 8, 366–370 (2012)
- 47. T. Yefsah, A.T. Sommer, M.J.H. Ku, L.W. Cheuk, W. Ji, W.S. Bakr, M.W. Zwierlein, Heavy solitons in a fermionic superfluid. Nature **499**, 426–430 (2013)
- A. Görlitz, J.M. Vogels, A.E. Leanhardt, C. Raman, T.L. Gustavson, J.R. Abo-Shaeer, A.P. Chikkatur, S. Gupta, S. Inouye, T. Rosenband, W. Ketterle, Realization of Bose-Einstein condensates in lower dimensions. Phys. Rev. Lett. 87, 130402 (2001)

- 49. M. Greiner, I. Bloch, O. Mandel, T.W. Hänsch, T. Esslinger, Exploring phase coherence in a 2D lattice of Bose-Einstein condensates. Phys. Rev. Lett. **8716**, 160405 (2001)
- J. Esteve, J.-B. Trebbia, T. Schumm, A. Aspect, C.I. Westbrook, I. Bouchoule, Observations
  of density fluctuations in an elongated bose gas: ideal gas and quasicondensate regimes. Phys.
  Rev. Lett. 96, 130403 (2006)
- 51. Z. Hadzibabic, P. Krüger, M. Cheneau, B. Battelier, J. Dalibard, Berezinskii-Kosterlitz-Thouless crossover in a trapped atomic gas. Nature **441**, 1118–1121 (2006)
- 52. J. Simon, W.S. Bakr, R. Ma, M.E. Tai, P.M. Preiss, M. Greiner, Quantum simulation of antiferromagnetic spin chains in an optical lattice. Nature **472**, 307–312 (2011)
- 53. T. Kinoshita, T. Wenger, D.S. Weiss, Observation of a one-dimensional Tonks-Girardeau gas. Science **305**, 1125–1128 (2004)
- B. Paredes, A. Widera, V. Murg, O. Mandel, S. Fölling, I. Cirac, G.V. Shlyapnikov, T.W. Hänsch, I. Bloch, Tonks-Girardeau gas of ultracold atoms in an optical lattice. Nature 429, 277–281 (2004)
- E. Haller, M. Gustavsson, M.J. Mark, J.G. Danzl, R. Hart, G. Pupillo, H.-C. Nägerl, Realization of an excited, strongly-correlated quantum gas phase. Science 325, 1224–1227 (2009)
- T. Jacqmin, J. Armijo, T. Berrada, K.V. Kheruntsyan, I. Bouchoule, Sub-poissonian fluctuations in a 1D Bose gas: from the quantum quasicondensate to the strongly interacting regime. Phys. Rev. Lett. 106, 230405 (2011)
- 57. A.H. van Amerongen, J.J.P. van Es, P. Wicke, K.V. Kheruntsyan, N.J. van Druten, Yang-Yang thermodynamics on an atom chip. Phys. Rev. Lett. **100**, 090402 (2008)
- A. Widera, S. Trotzky, P. Cheinet, S. Fölling, F. Gerbier, I. Bloch, V. Gritsev, M.D. Lukin,
   E. Demler, Quantum spin dynamics of mode-squeezed Luttinger liquids in two-component atomic gases. Phys. Rev. Lett. 100, 140401 (2008)
- M. Gring, M. Kuhnert, T. Langen, T. Kitagawa, B. Rauer, M. Schreitl, I.E. Mazets, D. Adu Smith, E. Demler, J. Schmiedmayer, Relaxation and prethermalization in an isolated quantum system. Science 337, 1318–1322 (2012)
- E. Haller, R. Hart, M.J. Mark, J.G. Danzl, L. Reichsollner, M. Gustavsson, M. Dalmonte, G. Pupillo, H.-C. Nagerl, Pinning quantum phase transition for a Luttinger liquid of strongly interacting bosons. Nature 466, 597–600 (2010)
- 61. T. Stöferle, H. Moritz, C. Schori, M. Köhl, T. Esslinger, Transition from a strongly interacting 1D superfluid to a Mott insulator. Phys. Rev. Lett. **92**, 130403 (2004)
- 62. H. Moritz, T. Stöferle, K. Günter, M. Köhl, T. Esslinger, Confinement induced molecules in a 1D Fermi gas. Phys. Rev. Lett. **94**, 210401 (2005)
- 63. M. Gring, Prethermalization in an Isolated Many-Body System. Ph.D. thesis (Vienna University of Technology, 2012)
- 64. M. Kuhnert, Thermalization and Prethermalization in an ultracold Bose Gas. Ph.D. thesis (Vienna University of Technology, 2013)
- 65. W. Hänsel, P. Hommelhoff, T.W. Hänsch, J. Reichel, Bose-Einstein condensation on a microelectronic chip. Nature **413**, 498–501 (2001)
- H. Ott, J. Fortagh, G. Schlotterbeck, A. Grossmann, C. Zimmermann, Bose-Einstein condensation in a surface microtrap. Phys. Rev. Lett. 87, 230401 (2001)
- 67. J. Reichel, V. Vuletic (eds.), Atom Chips (Wiley, VCH, 2011)
- 68. R. Folman, P. Kruger, J. Schmiedmayer, J. Denschlag, C. Henkel, Microscopic atom optics: from wires to an atom chip. Adv. At. Mol. Opt. Phys. 48, 263–356 (2002)
- 69. Y. Colombe, T. Steinmetz, G. Dubois, F. Linke, D. Hunger, J. Reichel, Strong atom-field coupling for Bose-Einstein condensates in an optical cavity on a chip. Nature **450**, 272–276 (2007)
- D. Heine, W. Rohringer, D. Fischer, M. Wilzbach, T. Raub, S. Loziczky, X. Liu, S. Groth, B. Hessmo, J. Schmiedmayer, A single-atom detector integrated on an atom chip: fabrication, characterization and application. New J. Phys. 12, 095005 (2010)
- J. Verdú, H. Zoubi, Ch. Koller, J. Majer, H. Ritsch, J. Schmiedmayer, Strong magnetic coupling of an ultracold gas to a superconducting waveguide cavity. Phys. Rev. Lett. 103, 043603 (2009)

R. Amsüss, Ch. Koller, T. Nöbauer, S. Putz, S. Rotter, K. Sandner, S. Schneider, M. Schramböck, G. Steinhauser, H. Ritsch, J. Schmiedmayer, J. Majer, Cavity QED with magnetically coupled collective spin states. Phys. Rev. Lett. 107, 060502 (2011)

- T. Schumm, S. Hofferberth, L.M. Andersson, S. Wildermuth, S. Groth, I. Bar-Joseph, J. Schmiedmayer, P. Kruger, Matter-wave interferometry in a double well on an atom chip. Nat. Phys. 1, 57–62 (2005)
- A.D. Cronin, J. Schmiedmayer, D. Pritchard, Optics and interferometry with atoms and molecules. Rev. Mod. Phys. 81, 1051–1129 (2009)
- J.F. Schaff, T. Langen, J. Schmiedmayer, Interferometry with atoms. In: M.A. Kasevich, G.M. Tino (eds.) Proceedings of the International School of Physics Enrico Fermi (Varenna, Italy, 2014), pp. 1–87
- M.A. Cazalilla, R. Citro, T. Giamarchi, E. Orignac, M. Rigol, One dimensional bosons: from condensed matter systems to ultracold gases. Rev. Mod. Phys. 83, 1405–1466 (2011)
- 77. E.H. Lieb, W. Liniger, Exact analysis of an interacting Bose gas. I. The general solution and the ground state. Phys. Rev. **130**, 1605–1616 (1963)
- C.N. Yang, Thermodynamics of a one-dimensional system of bosons with repulsive deltafunction interaction. J. Mat. Phys. 10, 1115 (1969)
- V.E. Korepin, Quantum Inverse Scattering Method and Correlation Functions (Cambridge University Press, 1997)
- M. Kuhnert, R. Geiger, T. Langen, M. Gring, B. Rauer, T. Kitagawa, E. Demler, D. Adu Smith,
   J. Schmiedmayer, Multimode dynamics and emergence of a characteristic length scale in a one-dimensional quantum system. Phys. Rev. Lett. 110, 090405 (2013)
- D. Adu Smith, M. Gring, T. Langen, M. Kuhnert, B. Rauer, R. Geiger, T. Kitagawa, I. Mazets,
   E. Demler, J. Schmiedmayer, Prethermalization revealed by the relaxation dynamics of full distribution functions. New J. Phys. 15, 075011 (2013)
- T. Langen, M. Gring, M. Kuhnert, B. Rauer, R. Geiger, D. Adu Smith, I. E. Mazets, J. Schmiedmayer, Prethermalization in one-dimensional Bose gases: description by a stochastic Ornstein-Uhlenbeck process. Eur. Phys. J. Spec. Top. 217, 43–53 (2013)
- T. Langen, M. Gring, M. Kuhnert, B. Rauer, R. Geiger, I. Mazets, D. Adu Smith, T. Kitagawa,
   E. Demler, J. Schmiedmayer, Studying non-equilibrium many-body dynamics using one-dimensional Bose gases. AIP Conf. Proc. 1633, 11 (2014) (2013)
- 84. P. Calabrese, J. Cardy, Time dependence of correlation functions following a quantum quench. Phys. Rev. Lett. **96**, 011368 (2006)
- 85. M. Cramer, C.M. Dawson, J. Eisert, T.J. Osborne, Exact relaxation in a class of nonequilibrium quantum lattice systems. Phys. Rev. Lett. **100**, 030602 (2008)
- 86. T. Langen, R. Geiger, M. Kuhnert, B. Rauer, J. Schmiedmayer, Local emergence of thermal correlations in an isolated quantum many-body system. Nat. Phys. **9**, 640–643 (2013)
- 87. M. Rigol, V. Dunjko, V. Yurovsky, M. Olshanii, Relaxation in a completely integrable many-body quantum system: an ab initio study of the dynamics of the highly excited states of 1d lattice hard-core bosons. Phys. Rev. Lett. **98**, 050405 (2007)
- 88. T. Kitagawa, A. Imambekov, J. Schmiedmayer, E. Demler, The dynamics and prethermalization of one-dimensional quantum systems probed through the full distributions of quantum noise. New. J. Phys. **13**, 073018 (2011)
- E. G. Dalla Torre, E. Demler, A. Polkovnikov, Universal rephasing dynamics after a quantum quench via sudden coupling of two initially independent condensates. Phys. Rev. Lett. 110, 090404 (2013)
- C. Neuenhahn, F. Marquardt, Quantum simulation of expanding space-time with tunnelcoupled condensates. arXiv: 1208.2255v1 (2013)
- J. Grond, J. Schmiedmayer, U. Hohenester, Optimizing number squeezing when splitting a mesoscopic condensate. Phys. Rev. A 79, 021603 (2009)
- 92. S. Goldstein, J.L. Lebowitz, R. Tumulka, N. Zanghì, Canonical typicality. Phys. Rev. Lett. 96, 050403 (2006)
- J.J. Sakurai, Modern Quantum Mechanics (Addison-Wesley Publishing Company, Reading, 1994)

- 94. S.N. Bose, Plancks Gesetz und Lichtquantenhypothese. Z. Phys. 26, 178 (1924)
- 95. A. Einstein, Zur Quantentheorie des idealen Gases. Sitzungsberichte der Preußischen Akademie der Wissenschaften 3, 18 (1925)
- 96. W. Pauli, The connection between spin and statistics. Phys. Rev. 58, 716 (1940)
- C.J. Pethick, H. Smith, Bose-Einstein Condensation in Dilute Gases (Cambridge University Press, 2001)
- 98. J.T.M. Walraven, Thermodynamic and Collisional Properties of Trapped Atomic Gases. Lecture Notes of the Ecole de Physique des Houches (2008)
- 99. D.A. Steck, Rubidium 87 D Line Data (2003), http://steck.us/alkalidata
- 100. N.N. Bogoliubov, On the theory of superfluidity. J. Phys. (USSR) 11, 4–2 (1947)
- F. Dalfovo, S. Giorgini, L.P. Pitaevskii, S. Stringari, Theory of Bose-Einstein condensation in trapped gases. Rev. Mod. Phys. 71, 463–512 (1999)
- 102. E.P. Gross, Structure of a quantized vortex in boson systems. Nuovo Cimento **20**, 454–477 (1961)
- 103. L.P. Pitaevskii, Vortex lines in an imperfect Bose gas. Zh. Eksp. Teor. Fiz. 40, 646 (1961)
- 104. T. Langen, Addressing of ultracold atoms in optical lattices. Diplomarbeit (Johannes Gutenberg-Universität Mainz, 2008)
- W. Bao, D. Jaksch, P.A. Markowich, Numerical solution of the Gross-Pitaevskii equation for Bose-Einstein condensation. J. Comp. Phys. 187, 318–342 (2003)
- N. Tammuz, R.P. Smith, R.L.D. Campbell, S. Beattie, S. Moulder, J. Dalibard, Z. Hadzibabic, Can a Bose gas be saturated? Phys. Rev. Lett. 106, 230401 (2011)
- 107. G. Baym, C.J. Pethick, Ground-state properties of magnetically trapped Bose-condensed Rubidium gas. Phys. Rev. Lett. **76**, 6–9 (1996)
- 108. P. de Gennes, Superconductivity of Metals and Alloys (Addison-Wesley New York, 1989)
- S. Stringari, Collective excitations of a trapped Bose-condensed gas. Phys. Rev. Lett. 77, 2360–2363 (1996)
- O. Penrose, L. Onsager, Bose-Einstein condensation and liquid helium. Phys. Rev. 104, 576– 584 (1956)
- 111. C. Blumenstein, J. Schäfer, S. Mietke, S. Meyer, A. Dollinger, M. Lochner, X.Y. Cui, L. Patthey, R. Matzdorf, R. Claessen, Atomically controlled quantum chains hosting a Tomonaga-Luttinger liquid. Nat. Phys. 776–780 (2011)
- M. Dressel, A. Schwartz, G. Grüner, L. Degiorgi, Deviations from Drude response in lowdimensional metals: electrodynamics of the metallic state of (TMTSF)<sub>2</sub>PF<sub>6</sub>. Phys. Rev. Lett. 77, 398–401 (1996)
- Y. Jompol, C.J.B. Ford, J.P. Griffiths, I. Farrer, G.A.C. Jones, D. Anderson, D.A. Ritchie, T.W. Silk, A.J. Schofield, Probing spin-charge separation in a Tomonaga-Luttinger liquid. Science 325, 597–601 (2009)
- P. Segovia, D. Purdie, M. Hengsberger, Y. Baer, Observation of spin and charge collective modes in one-dimensional metallic chains. Nature 402, 504–507 (1999)
- 115. S. Iijima, Helical microtubules of graphitic carbon. Nature **354**, 56–58 (1991)
- Z. Yao, H.W.C. Postma, L. Balents, C. Dekker, Carbon nanotube intramolecular junctions. Nature 402, 273–276 (1999)
- M. Bockrath, D.H. Cobden, J. Lu, A.G. Rinzler, R.E. Smalley, L. Balents, P.L. McEuen, Luttinger-liquid behaviour in carbon nanotubes. Nature 397, 598–601 (1999)
- K. von Klitzing, G. Dorda, M. Pepper, New method for high-accuracy determination of the fine-structure constant based on quantized hall resistance. Phys. Rev. Lett. 45, 494

  –497 (1980)
- 119. X.G. Wen, Chiral Luttinger liquid and the edge excitations in the fractional quantum Hall states. Phys. Rev. B **41**, 12838–12844 (1990)
- 120. A.M. Chang, L.N. Pfeiffer, K.W. West, Observation of chiral luttinger behavior in electron tunneling into fractional quantum Hall edges. Phys. Rev. Lett. **77**, 2538–2541 (1996)
- J.G. Bednorz, K.A. Müller, Possible high-Tc superconductivity in the Ba-La-Cu-O system. Z. Phys. B 64, 189–193 (1986)
- K. Takada, H. Sakurai, E. Takayama-Muromachi, F. Izumi, R.A. Dilanian, T. Sasaki, Superconductivity in two-dimensional CoO<sub>2</sub> layers. Nature 422, 53–55 (2003)

References 35

- 123. A.K. Geim, Graphene: status and prospects. Science **324**, 1530–1534 (2009)
- N.D. Mermin, H. Wagner, Absence of ferromagnetism or antiferromagnetism in one- or twodimensional isotropic Heisenberg models. Phys. Rev. Lett. 17, 1133–1136 (1966)
- P.C. Hohenberg, Existence of long-range order in one and two dimensions. Phys. Rev. 158, 383–386 (1967)
- D.S. Petrov, G.V. Shlyapnikov, J.T.M. Walraven, Regimes of quantum degeneracy in trapped 1D gases. Phys. Rev. Lett. 85, 3745–3749 (2000)
- D.S. Petrov, D.M. Gangardt, G.V. Shlyapnikov, Low-dimensional trapped gases. J. Phys. IV France 116, 5–44 (2004)
- M. Olshanii, Atomic scattering in the presence of an external confinement. Phys. Rev. Lett. 81, 938–941 (1998)
- E. Haller, M.J. Mark, R. Hart, J.G. Danzl, L. Reichsöllner, V. Melezhik, P. Schmelcher, H.-C. Nägerl, Confinement-induced resonances in low-dimensional quantum systems. Phys. Rev. Lett. 104, 153203 (2010)
- 130. H. Bethe, Zur Theorie der Metalle. Z. Phys. **71**, 205–226 (1931)
- 131. M. Girardeau, Relationship between systems of impenetrable bosons and fermions in one dimension. J. Math. Phys. 1, 516 (1960)
- 132. E.H. Lieb, Exact analysis of an interacting Bose gas. II. The excitation spectrum. Phys. Rev. 130, 1616–1624 (1963)
- 133. M. Rigol, Breakdown of thermalization in finite one-dimensional systems. Phys. Rev. Lett. **103**, 100403 (2009)
- 134. V.I. Arnol'd, Mathematical Methods of Classical Mechanics. Graduate Texts in Mathematics (Springer, 1989)
- 135. J.-S. Caux, J. Mossel, Remarks on the notion of quantum integrability. J. Stat. Mech. Theor. Exp. **2011**, P02023 (2011)
- 136. B. Sutherland, Beautiful models: 70 years of exactly solved quantum many-body problems (World Scientific, 2004)
- K. Kheruntsyan, D. Gangardt, P. Drummond, G. Shlyapnikov, Pair correlations in a finite-temperature 1D Bose gas. Phys. Rev. Lett. 91, 040403 (2003)
- A. Imambekov, I.E. Mazets, D.S. Petrov, V. Gritsev, S. Manz, S. Hofferberth, T. Schumm, E. Demler, J. Schmiedmayer, Density ripples in expanding low-dimensional gases as a probe of correlations. Phys. Rev. A 80, 033604 (2009)
- 139. S. Manz, Density correlations of expanding one-dimensional Bose gases. Ph.D. thesis (Vienna University of Technology, 2011)
- 140. L.D. Landau, E.M. Lifshitz, Course of Theoretical Physics, vol. 9 (Pergamon, 1980)
- 141. S. Tomonaga, Remarks on Bloch's method of sound waves applied to many-fermion problems. Prog. Theo. Phys. **5**, 544–569 (1950)
- 142. J.M. Luttinger, An exactly soluble model of a many-fermion system. J. Math. Phys. 4, 1154–1162 (1963)
- 143. D.C. Mattis, E.H. Lieb, Exact solution of a many-fermion system and its associated boson field. J. Math. Phys. **6**, 304 (1965)
- 144. F.D.M. Haldane, Effective harmonic-fluid approach to low-energy properties of onedimensional quantum fluids. Phys. Rev. Lett. 47, 1840–1843 (1981)
- V.V. Deshpande, M. Bockrath, L.I. Glazman, A. Yacoby, Electron liquids and solids in one dimension. Nature 464, 209–216 (2010)
- O.M. Auslaender, A. Yacoby, R. de Picciotto, K.W. Baldwin, L.N. Pfeiffer, K.W. West, Tunneling spectroscopy of the elementary excitations in a one-dimensional wire. Science 295, 825–828 (2002)
- C. Kim, A.Y. Matsuura, Z.-X. Shen, N. Motoyama, H. Eisaki, S. Uchida, T. Tohyama, S. Maekawa, Observation of spin-charge separation in one-dimensional SrCuO<sub>2</sub>. Phys. Rev. Lett. 77, 4054 (1996)
- 148. R. Claessen, M. Sing, U. Schwingenschlögl, P. Blaha, M. Dressel, C.S. Jacobsen, Spectroscopic signatures of spin-charge separation in the quasi-one-dimensional organic conductor TTF-TCNQ. Phys. Rev. Lett. 88, 096402 (2002)

- 149. H. Ishii, H. Kataura, H. Shiozawa, H. Yoshioka, H. Otsubo, Y. Takayama, T. Miyahara, S. Suzuki, Y. Achiba, M. Nakatake et al., Direct observation of Tomonaga-Luttinger-liquid state in carbon nanotubes at low temperatures. Nature 426, 540–544 (2003)
- H. Monien, M. Linn, N. Elstner, Trapped one-dimensional Bose gas as a Luttinger liquid. Phys. Rev. A 58, R3395 (1998)
- C. Mora, Y. Castin, Extension of Bogoliubov theory to quasicondensates. Phys. Rev. A 67 (2003)
- 152. Y. Castin, Simple theoretical tools for low dimension Bose gases. J. Phys. IV (Proceedings) 116, 89–132 (2004)
- 153. N.K. Whitlock, I. Bouchoule, Relative phase fluctuations of two coupled one-dimensional condensates. Phys. Rev. A **68**, 053609 (2003)
- D.M. Gangardt, G.V. Shlyapnikov, Stability and phase coherence of trapped 1D Bose gases. Phys. Rev. Lett. 90, 010401 (2003)
- M. Abramowitz, I.A. Stegun, Handbook of Mathematical Functions (U.S, Department of Commerce, 1964)
- 156. F. Gerbier, Quasi-1D Bose-Einstein condensates in the dimensional crossover regime. Eur. Phys. Lett. **66**, 771–777 (2004)
- J.N. Fuchs, X. Leyronas, R. Combescot, Hydrodynamic modes of a one-dimensional trapped Bose gas. Phys. Rev. A 68, 043610 (2003)
- A. Muñoz Mateo, V. Delgado, Effective mean-field equations for cigar-shaped and disk-shaped Bose-Einstein condensates. Phys. Rev. A 77, 013617 (2008)
- 159. T. Betz, Phase correlations of coupled one-dimensional Bose gases. Ph.D. thesis (Vienna University of Technology, 2011)
- J. Armijo, T. Jacqmin, K. Kheruntsyan, I. Bouchoule, Mapping out the quasicondensate transition through the dimensional crossover from one to three dimensions. Phys. Rev. A 83, 021605 (2011)
- H.-P. Stimming, N.J. Mauser, J. Schmiedmayer, I.E. Mazets, Fluctuations and stochastic processes in one-dimensional many-body quantum systems. Phys. Rev. Lett. 105, 015301 (2010)
- 162. T. Betz, S. Manz, R. Bücker, T. Berrada, C. Koller, G. Kazakov, I.E. Mazets, H.-P. Stimming, A. Perrin, T. Schumm, J. Schmiedmayer, Two-point phase correlations of a one-dimensional bosonic Josephson junction. Phys. Rev. Lett. 106, 020407 (2011)
- D.T. Gillespie, Exact numerical simulation of the Ornstein-Uhlenbeck process and its integral. Phys. Rev. E 54, 2084–2091 (1996)
- S. Hofferberth, Coherent Manipulation of Bose-Einstein condensates with radio-frequency adiabatic potentials on atom chips. Ph.D. thesis (University of Heidelberg, 2007)
- 165. T. Berrada, PhD Thesis (Vienna University of Technology, 2014)
- S.P. Cockburn, D. Gallucci, N.P. Proukakis, Quantitative study of quasi-one-dimensional Bose gas experiments via the stochastic Gross-Pitaevskii equation. Phys. Rev. A 84, 023613 (2011)
- P. Grišins, I.E. Mazets, Metropolis-Hastings thermal state sampling for numerical simulations of Bose-Einstein condensates. Comp. Phys. Comm. 185(7), 2014
- T. Young, A Course of Lectures on Natural Philosophy and the Mechanical Arts (Taylor and Walton, 1845)
- 169. M. Born, E. Wolf, Principles of Optics (Cambridge University Press, 1997)
- C. Davisson, L.H. Germer, Diffraction of electrons by a crystal of nickel. Phys. Rev. 30, 705 (1927)
- 171. H. Rauch, W. Treimer, U. Bonse, Test of a single crystal neutron interferometer. Phys. Lett. A 47, 369–371 (1974)
- 172. D.W. Keith, C.R. Ekstrom, Q.A. Turchette, D.E. Pritchard, An interferometer for atoms. Phys. Rev. Lett. 66, 2693 (1991)
- 173. M. Arndt, O. Nairz, J. Vos-Andreae, C. Keller, G. van der Zouw, A. Zeilinger, Wave-particle duality of C<sub>60</sub> molecules. Nature 401, 680–682 (1999)
- 174. M.R. Andrews, C.G. Townsend, H.-J. Miesner, D.S. Durfee, D.M. Kurn, W. Ketterle, Observation of interference between two bose condensates. Science 275, 637 (1997)

References 37

175. A. Imambekov, V. Gritsev, E. Demler, Ultracold Fermi gases, Proc. Internat. School Phys. Enrico Fermi, (Fundamental noise in matter interferometers (IOS Press, Amsterdam, The Netherlands, 2006), p. 2007

- 176. J. Javanainen, S.M. Yoo, Quantum phase of a Bose-Einstein condensate with an arbitrary number of atoms. Phys. Rev. Lett. **76**, 161–164 (1996)
- 177. Y. Castin, Bose-Einstein Condensates in Atomic Gases: Simple Theoretical Results. Lecture Notes of Les Houches Summer School (2001)
- S. Hofferberth, I. Lesanovsky, T. Schumm, A. Imambekov, V. Gritsev, E. Demler, J. Schmiedmayer, Probing quantum and thermal noise in an interacting many-body system. Nat. Phys. 4, 489–495 (2008)
- R. Bistritzer, E. Altman, Intrinsic dephasing in one-dimensional ultracold atom interferometers. Proc. Natl. Acad. Sci. 104, 9955 (2007)
- 180. M. Lewenstein, L. You, Quantum phase diffusion of a Bose-Einstein condensate. Phys. Rev. Lett. **77**, 3489–3493 (1996)
- Y. Shin, M. Saba, T.A. Pasquini, W. Ketterle, D.E. Pritchard, A.E. Leanhardt, Atom interferometry with Bose-Einstein condensates in a double-well potential. Phys. Rev. Lett. 92, 050405 (2004)
- A. Polkovnikov, E. Altman, E. Demler, Interference between independent fluctuating condensates. Proc. Natl. Acad. Sci. 103, 6125–6129 (2006)
- 183. R. Hanbury-Brown, R.Q. Twiss, Correlation between photons in two coherent beams of light. Nature 177, 27–29 (1956)
- 184. R. Glauber, Photon correlations. Phys. Rev. Lett. **10**, 84–86 (1963)
- 185. T. Jeltes, J.M. McNamara, W. Hogervorst, W. Vassen, V. Krachmalnicoff, M. Schellekens, A. Perrin, H. Chang, D. Boiron, A. Aspect, C.I. Westbrook, Comparison of the Hanbury Brown-Twiss effect for bosons and fermions. Nature 445, 402–405 (2007)
- A. Perrin, R. Bucker, S. Manz, T. Betz, C. Koller, T. Plisson, T. Schumm, J. Schmiedmayer, Hanbury Brown and Twiss correlations across the Bose-Einstein condensation threshold. Nat. Phys. 8, 195–198 (2012)
- 187. L. Saminadayar, D. Glattli, Y. Jin, B. Etienne, Observation of the e/3 fractionally charged laughlin quasiparticle. Phys. Rev. Lett. **79**, 2526–2529 (1997)
- 188. A. Öttl, S. Ritter, M. Köhl, T. Esslinger, Correlations and counting statistics of an atom laser. Phys. Rev. Lett. 95, 090404 (2005)
- S. Fölling, F. Gerbier, A. Widera, O. Mandel, T. Gericke, I. Bloch, Spatial quantum noise interferometry in expanding ultracold atom clouds. Nature 434, 481 (2005)
- T. Rom, Th Best, D. van Oosten, U. Schneider, S. Fölling, B. Paredes, I. Bloch, Free fermion antibunching in a degenerate atomic Fermi gas released from an optical lattice. Nature 444, 733 (2006)
- V. Gritsev, E. Altman, E. Demler, A. Polkovnikov, Full quantum distribution of contrast in interference experiments between interacting one dimensional Bose liquids. Nat. Phys. 2, 705–709 (2006)
- 192. A. Imambekov, V. Gritsev, E. Demler, Mapping of Coulomb gases and sine-Gordon models to statistics of random surfaces. Phys. Rev. A 77, 063606 (2008)
- 193. C.S. Gerving, T.M. Hoang, B.J. Land, M. Anquez, C.D. Hamley, M.S. Chapman, Non-equilibrium dynamics of an unstable quantum pendulum explored in a spin-1 Bose-Einstein condensate. Nat. Commun. **3**, 1169 (2012)

# Chapter 2 Experimental Realization of One-Dimensional Bose Gases

In this chapter we review the basic concepts necessary for the realization of a degenerate 1D Bose gas, as well as the actual experimental implementation of these concepts.

#### 2.1 Magnetic Trapping of Ultracold Atoms

In order to achieve a 1D system of ultracold atoms, it is necessary to confine atoms very strongly in two directions. To date, two well-established techniques exist to realize such a strong confinement: optical lattices [1–3] and micro-traps [4, 5]. As discussed in the previous chapter, we aim to study single realizations of 1D Bose gases to have direct access to their intrinsic fluctuations. While optical lattices typically allow the realization of many slightly different copies in parallel, micro-traps are ideally suited to prepare and manipulate single realizations. In the following, we theoretically introduce the basic working principles of magnetic micro-traps that are realized using an atom chip. We then present the experimental apparatus to realize 1D Bose gases.

# 2.1.1 Magnetic Trapping

An atom with angular momentum F exhibits a magnetic moment  $\mu = -g_F \mu_B F$ , where  $g_F$  is the Landé g-Factor,  $\mu_B$  is the Bohr magneton. If a weak magnetic field B is present, the Zeeman effect causes a linear shift of the atomic energy levels, which is given by

$$V(\mathbf{r}) = -\boldsymbol{\mu} \cdot \boldsymbol{B}(\mathbf{r}) = m_F g_F \mu_B B(\mathbf{r}). \tag{2.1}$$

If the magnitude  $B = |\mathbf{B}|$  of the field varies slowly enough such that  $dB/dt < \omega_L B$  is fulfilled, the atoms will adiabatically follow the shift of the Zeeman levels.

<sup>©</sup> Springer International Publishing Switzerland 2015 T. Langen, *Non-equilibrium Dynamics of One-Dimensional Bose Gases*, Springer Theses, DOI 10.1007/978-3-319-18564-4\_2

Here,  $\omega_L = m_F g_F \mu_B B/\hbar$  is the Larmor frequency of the atoms. Depending on the value of the magnetic quantum number  $m_F$  and the g-factor  $g_F$  of the atomic state, this will either lead to an attraction of the atom towards regions of lower magnetic field or to an attraction towards regions of higher magnetic field. Correspondingly, atomic states where  $g_F m_F > 0$ , are called low-field seeking states and states where  $g_F m_F < 0$  are called high-field seeking states. As Maxwell's equations forbid local maxima for static magnetic fields, only low-field seeking states can be trapped in a purely magnetic trap [6].

The most basic form of a magnetic trapping potential can be created by using a 3D quadrupole field. In the center of the quadrupole configuration the magnetic field vanishes, forming a trap for atoms in low-field seeking states. This field configuration can, for example, be realized using a pair of coils in anti-Helmholtz configuration. While this method is very efficient for the trapping of hot atoms, problems arise when the atoms are cooled down. The reason for this is that when the atoms get colder, the probability to find them at the position of zero magnetic field in the center of the trap increases drastically [7]. If the magnetic field vanishes, the adiabatic approximation introduced above is not valid anymore, the spin of the atoms can flip and they end up in an untrapped state. These so-called Majorana losses make it impossible to obtain a Bose-Einstein condensate of alkali atoms in a pure quadrupole trap [8].

The magnetic field zero in the center of the trap can be removed by adding an additional homogeneous bias field. The most common implementation of this enhanced trap is the Ioffe trap, where the quadrupole is created by four bars and the homogeneous offset field is created by two coils perpendicular to these bars. This realizes a trap with approximately harmonic confinement in all three spatial directions [6, 9].

# 2.1.2 Atom Chips

In typical experiments, macroscopic conductors are employed to create the fields that are used to trap the atoms. This has the disadvantage that the atoms usually have to be trapped far from these structures. As the magnetic field of a conductor decreases with distance, high currents are needed to create sizable field strengths. This makes experimental setups complex and difficult to handle. An alternative approach are magnetic micro-traps, where the atoms are intentionally trapped close to microscopic, current carrying structures. Micro-fabrication allows the routine creation of such structures on substrates, reaching nanometer sizes. In analogy to computer chips these devices are called atom chips. The scale reduction that is achieved by trapping the atoms close to the surface of such chips, facilitates the creation of very tight and robust traps with moderate currents. This enables the realization of compact and flexible setups, which allow for a large range of complex trap geometries [10–14], with applications ranging from atom interferometry [15, 16] and the study of gases in reduced dimensions [5, 17, 18] to quantum information processing [19–21].

The most simple of such traps, the so-called wire guide, can be formed by using a single wire and a perpendicular bias field. This situation is depicted in Fig. 2.1a. The

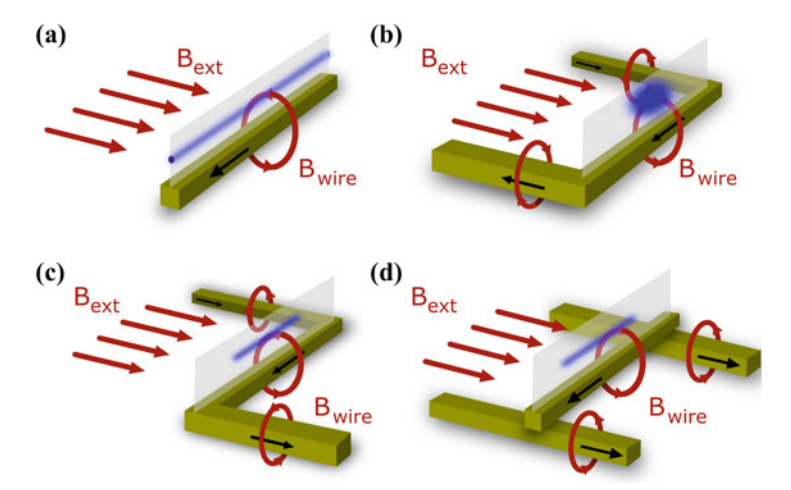


**Fig. 2.1** Different geometries to trap atoms using wires. The trapping volume is indicated in *blue*. **a** A wire guide, formed using a single straight wire and a perpendicular magnetic field. This results in a 2D quadrupole potential above the wire, as detailed in Fig. 2.2. **b** A U-trap, realizing a 3D quadrupole potential above the central segment of the wire. **c** The Z-trap combines the 2D quadrupole confinement of the wire guide with longitudinal confinement that is created using the bend segments of the wire. **d** Independently tunable longitudinal confinement can be realized by adding more wires

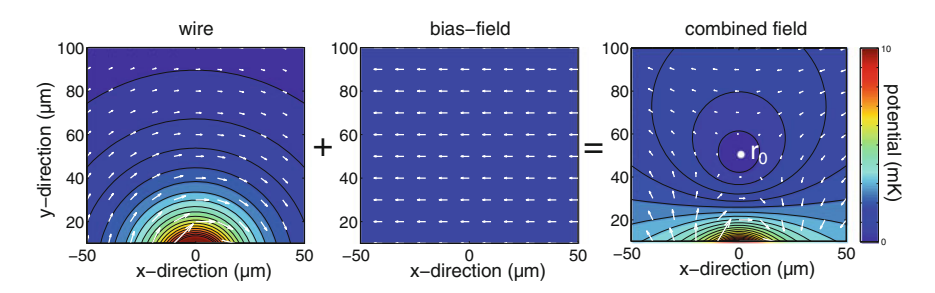


Fig. 2.2 Magnetic field of a wire guide. A current flowing through a wire (in z-direction) creates a circular magnetic field around the wire. A homogeneous bias field is added perpendicular to the wire. At a distance  $r_0$  from the wire, the two fields cancel, creating a zero in the magnetic field which can be used to trap atoms in low-field seeking states. Figure adapted from [22]

corresponding field configuration is shown in Fig. 2.2. The bias field  $\mathbf{B}_{\text{Bias}} = B_0 \hat{\mathbf{e}}_x$  in x-direction exactly cancels the circular magnetic field  $\mathbf{B} = \mu_0 I/(2\pi r)\hat{\mathbf{e}}_r$  of the wire at a distance

$$r_0 = \frac{\mu_0}{2\pi} \frac{I}{B_0} \tag{2.2}$$

from the wire. The superposition of these fields forms a two-dimensional quadrupole field around the point of vanishing magnetic field. Here, *I* is the current flowing

through the wire and  $\mu_0 = 4\pi \times 10^7 \, \text{Vs/(Am)}$  denotes the vacuum permeability.  $\hat{e}_r$  and  $\hat{e}_x$  denote unit vectors in the radial and x-direction, respectively.

The quadrupole field results in a force that confines the atoms in the plane perpendicular to the wire. To confine the atoms also in the third direction the trapping wire can be bend in a U-shape (Fig. 2.1b). This approximately realizes a three-dimensional quadrupole potential located above the central wire segment, which can be further optimized by flattening this part of the wire [23]. This trap configuration, in combination with appropriate laser light, is well-suited to create a magneto-optical trap close to the wires [14].

Bending the wire in a Z-shape closes the trap also in the direction along the wire (Fig. 2.1c). This realizes a trapping potential which is equivalent to that of a Ioffe-Pritchard trap [9]. An additional homogeneous bias field  $B_z$  in the z-direction allows the tuning of the field minimum to avoid Majorana losses. In the center, this trap can be very well approximated by an harmonic confinement in all three spatial directions.

More flexible trap shapes can be created by combining the single wire waveguide with additional wires. Adding wires perpendicular to the main trapping wire, as depicted in Fig. 2.1d, leads to a trap that is similar to the Z-trap. It has the advantage that the longitudinal confinement can be tuned with very little influence on the radial confinement. An equivalent configuration that avoids the necessity of wires to cross, is realized by sets of U-shaped wires next to the main trapping wire.

Our experiment includes a variety of wire arrangements to realize these different trapping configurations. In the experimental setup both macroscopic wire structures and micro-fabricated wires on an atom chip are employed. The setup will be presented in detail in Sect. 2.3. Note that in the simple examples discussed in this section, we have assumed infinitely thin wires. However, for the experiments presented in this thesis, a precise knowledge of the trapping potential created by realistic, extended wires is necessary. This situation and its detailed simulation are discussed in Appendix A.

# 2.2 Theory of Radio-Frequency Dressed-State Potentials

One particular advantage of atom chips is that they enable the creation of trapping potentials that go beyond what is possible with simple static magnetic fields. For example, a wide range of potentials can be created using near-field radio-frequency (RF) fields [24–26]. These potentials are based on the dressed-state formalism which is well known from cavity QED, where it describes the interaction of atoms with a light-field. Analyzing the interaction of the atoms with the RF radiation in a similar way, one finds new dressed eigenstates, which are superpositions of the original Zeeman levels [27–29]. If the RF radiation is turned on adiabatically, the atoms follow these new eigenstates of the system. As the dressed level structure is widely tunable via the properties of the radiation, this leads to a great flexibility in the design of the trapping geometry.

#### 2.2.1 A Double-Well Potential for Ultracold Atoms

To calculate the effect of the RF dressing, we start with the semi-classical Hamiltonian of an atom in a time-dependent magnetic field

$$H = \frac{\mathbf{p}^2}{2m} + g_F \mu_B \mathbf{F} \cdot \mathbf{B}(\mathbf{r}, t). \tag{2.3}$$

The magnetic field B(r, t) can be separated into a part  $B_S(r)$  which realizes the static trap for the atoms, and additional, rapidly oscillating terms  $B_{RF}(r, t)$ 

$$B(\mathbf{r},t) = B_{S}(\mathbf{r}) + B_{RF}(\mathbf{r},t)$$

$$= B_{S}(\mathbf{r}) + \sum_{n} B_{RF,n}(\mathbf{r}) \cos(\omega_{RF}t - \delta_{n}), \qquad (2.4)$$

with  $\delta_n$  denoting the phase offsets between the oscillating fields. Note that we assume the same frequency  $\omega_{RF}$  for all RF fields. To diagonalize this Hamiltonian, one transfers the problem into a local coordinate system where the static field  $\boldsymbol{B}_{S}(\boldsymbol{r})$  defines the quantization direction at every point  $\boldsymbol{r}$ . Subsequently, one applies the rotating-wave approximation (RWA) [26, 30], resulting in the Hamiltonian

$$\hat{H}_{\text{RWA,final}} = \frac{\mathbf{p}^2}{2m} + g_F \mu_B \mathbf{F} \cdot \mathbf{B}_{\text{eff}}(\mathbf{r})$$
 (2.5)

$$= \frac{\mathbf{p}^2}{2m} + g_F \mu_B |\mathbf{B}_{\text{eff}}(\mathbf{r})| F_z = \frac{\mathbf{p}^2}{2m} + V_{\text{ad}}(\mathbf{r}). \tag{2.6}$$

Equation 2.6 describes the motion of a particle in an effective magnetic field given by

$$\mathbf{B}_{\text{eff}}(\mathbf{r}) = \left(\frac{|B_{\text{RF},\perp}|}{2}, 0, |\mathbf{B}_{S}(\mathbf{r})| - \frac{\hbar\omega}{\mu_{B}|g_{F}|}\right)^{T}.$$
 (2.7)

Here,  $B_{\text{RF},\perp}(r,t)$  is the component of the RF fields that is perpendicular to the static field. This field is not a real magnetic field and thus does not have to fulfill Maxwell's equations. For this reason, it enables the creation of trapping potentials that are not possible using static fields alone. In general, the effective field is the sum of the single RF fields projected onto some direction in the xy-plane. For the nth field, this direction is defined by the angle  $\gamma_n = -g_F \delta_n/|g_F|$ . This dependence of the effective field on the sign of the g-factor makes the potentials state- and also species-selective [26].

The resulting adiabatic potential in Eq. 2.6 is given by

$$V_{\text{ad}}(\mathbf{r}) = \tilde{m}_F g_F \mu_B \sqrt{\Delta(\mathbf{r})^2 + \Omega(\mathbf{r}, \delta)^2}$$
$$= \tilde{m}_F g_F \mu_B \sqrt{\left(|\mathbf{B}_S(\mathbf{r})| - \frac{\hbar \omega_{\text{RF}}}{\mu_B |g_F|}\right)^2 + \left(\frac{B_{\text{RF}\perp}}{2}\right)^2}, \tag{2.8}$$

with  $\tilde{m}_F$  being defined along the local magnetic field component  $B_{\rm eff,z}$ . The new atomic states  $\tilde{m}_F$  are superpositions of the bare  $m_F$  states. If the RF radiation is switched on slowly, the atoms adiabatically follow the new dressed states, such that atoms in a state with quantum number  $m_F$  are transferred into the corresponding state with the quantum number  $\tilde{m}_F$ .

The detuning  $\Delta(\mathbf{r})$  in Eq. 2.8 is the difference between the absolute value of the local static field and the RF frequency. The Rabi-frequency or coupling strength  $\Omega(\mathbf{r})$  defines the local coupling between the different  $\tilde{m}_F$  levels. If  $\Delta$  vanishes, it is responsible for a level repulsion and thus an avoided crossing of the levels. In this situation it acts also as an effective Ioffe field preventing Majorana losses. The fact that the coupling term defines the minima of the potential is an essential feature of the RF potentials, because by shaping its spatial dependence many different trapping geometries can be realized.

With Eq. 2.8, the calculation of the RF potentials reduces to the calculation of the perpendicular part  $B_{\rm RF\perp}$  of the RF fields. Details of this calculation in various trapping geometries can be found in Refs. [24, 26, 29–31]. For example, using a single linear polarized RF field, as it can be realized using the near-field radiation of a single wire, two terms contribute to the adiabatic potential. Neglecting longitudinal confinement and assuming a static quadrupole field in the radial direction, the contribution from the detuning vanishes along the ring where the dressing frequency exactly corresponds to the (radially symmetric) absolute value of the static field. Along this minimum, the only contribution to the effective potential is the coupling term  $\Omega \sim B_{\rm RF\perp}$ . As  $|B_{\rm RF\perp}| \sim |B_S \times B_{\rm RF}|$ , the coupling term becomes minimal when  $B_{\rm RF}$  and  $B_S$  are parallel or anti-parallel. The result is a double well, where the potential minima are located opposite to each other on the ring. This situation is depicted in Fig. 2.3.

For the case of negative detuning  $\Delta$  there will always be a double well. For the case of positive detuning, which is the one usually encountered in our experiments, there will be a splitting once a critical field amplitude  $B_c=2\sqrt{B_I\Delta}$  is reached, with  $B_I$  the Ioffe field of the static trap. The reason behind this are the different gradients of the detuning and the coupling term. This is the second way to make the potentials state- and species-selective. For example, the RF transitions in  $^{40}$ K and  $^{87}$ Rb have different frequencies, thus for a given RF frequency they will experience a different detuning. If the frequency is chosen in the correct way, only one species is split while the other remains unsplit.

More flexibility can be achieved using two linearly polarized RF fields. To obtain the resulting total RF field, the two individual fields have to be added vectorially. For example, with the appropriate phase offset, the sum of the two fields can be

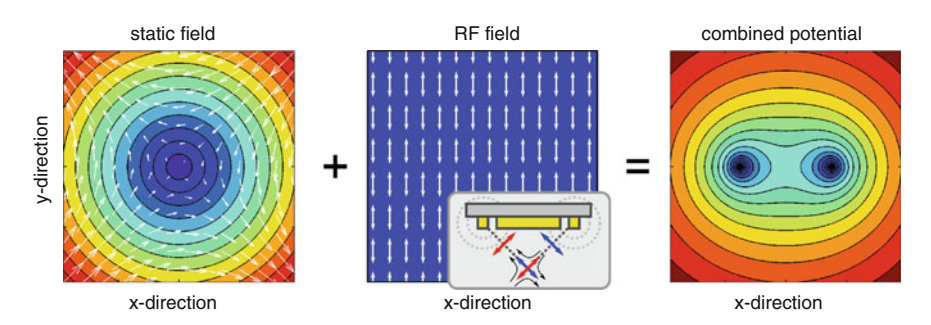


Fig. 2.3 Creation of a horizontal double-well potential. The static trapping fields form a quadrupole potential in the xy-plane. *Arrows* indicate the local direction of the field. The RF field is linearly polarized along the y-direction. As shown in the *inset*, this polarization can, for example, be achieved by combining the RF fields of two wires with a  $\pi$  phase shift. The resulting dressed-state potential exhibits two minima at the positions where the static and the RF field are parallel. Rotating the linear polarization of the RF field leads to a rotation of the double well

made linearly polarized in the horizontal or in the vertical direction, which changes the orientation of the double well accordingly. In our setup with two RF wires, we employ currents with a phase shift of  $\delta=\pi$  to realize the vertical polarization that forms a horizontal double well. Rotating the double well in arbitrary directions is possible by using different amplitudes for the two RF fields.

Further trapping geometries can be realized using circular or elliptical polarizations. For example, circular polarization ( $\delta = \pi/2$ ) leads to a ring shaped trap, where the atoms explore a 2D surface with periodic boundary condition. Elliptical polarization, on the other hand is well-suited to create state- and species-dependent potentials [31].

# 2.2.2 Beyond the Rotating-Wave Approximation

For <sup>87</sup>Rb in the F=2 state, the dressing within the RWA turns five bare  $m_F$  states into five dressed  $\tilde{m}_F$  states. However, in a diagonalization of the full Hamiltonian (Eq. 2.3), many more of these manifolds, each containing five  $\tilde{m}_F$  states appear (see Appendix A and Refs. [29, 32, 33]). A quantum mechanical analysis reveals that every manifold can be associated with a fixed, but large number of photons in the RF field. Adjacent manifolds are therefore separated by the energy  $\hbar\omega_{RF}$  of a single RF photon. This is in complete analogy to the analysis of dressed states in cavity QED [27].

The full diagonalization shows that the rotating-wave approximation provides a good approximation of the dressed-state level structure as long as

$$\Omega, \Delta \ll \omega.$$
 (2.9)

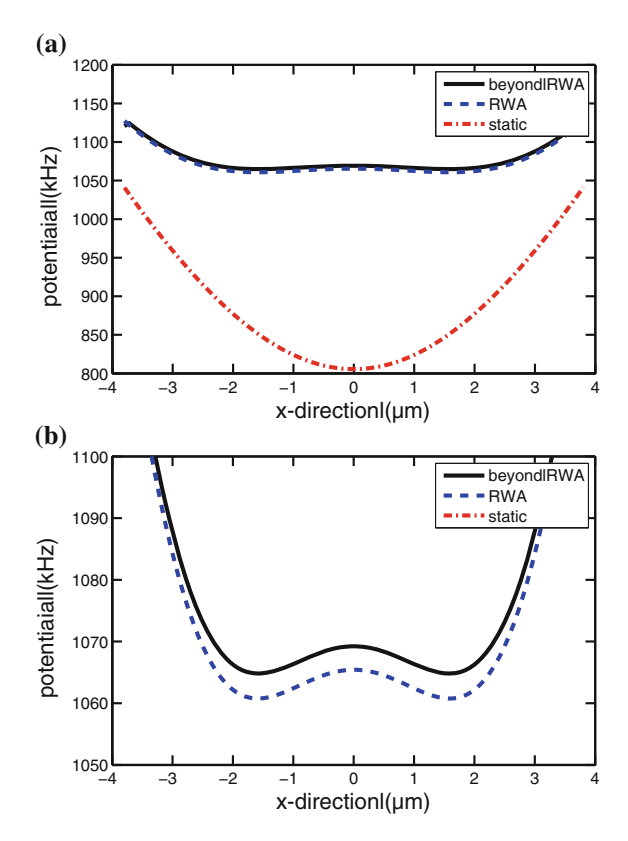


Fig. 2.4 Typical trapping potentials. Simulated trapping potentials for the static fields as well as the RF fields in a rotating-wave approximation (RWA) calculation and a beyond RWA calculation. a The RF dressing shifts the static level up in energy, forming the dressed double well. b Zoom into the double-well potential, revealing the differences between RWA and beyond RWA calculation. Parameters of the double well, such as barrier height or the distance between the two wells can be tuned using the applied RF radiation. Here, the RF current is  $I_{\rm RF}=20\,{\rm mA}$  and the detuning from the  $m_F=2 \to m_F=1$  transition is 30 kHz. The static trap is located 100  $\mu$ m from the chip surface. For details on the choice of parameters, see Chap. 4

Here,  $\omega$  is the atomic transition frequency between the bare  $m_F$  states. This condition can be understood from the fact that the dressed  $\tilde{m}_F$  states in each manifold are separated by an energy  $\hbar \tilde{\omega} = \hbar \sqrt{\Delta^2 + \Omega^2}$ , which remains smaller than the separation of different manifolds as long as Eq. 2.9 is fulfilled. If this is not the case, different manifolds overlap and it is not possible to analyze them separately anymore.

The atom chip easily enables couplings  $\Omega$  which are much larger than  $\omega$ , violating the condition in Eq. 2.9. Moreover, the detuning can locally become on the order of  $\omega$ . To obtain a precise description of the potentials in these cases therefore requires the diagonalization of the full Hamiltonian. Exemplary results are presented in Fig. 2.4.

Labeling the  $\tilde{m}_F$  manifolds with the index  $\kappa$ , off-resonant contributions from the overlap of the different manifolds lead to many possible transitions between the dressed states. These transitions can be summarized by the resonance condition

$$\omega_{\rm res} = \Delta \kappa \, \omega_{\rm RF} + \Delta \tilde{m}_F \, \tilde{\omega}, \tag{2.10}$$

Here,  $\omega_{RF}$  is the frequency of the RF radiation and  $\hbar\tilde{\omega}$  denotes the energy difference between the  $\tilde{m}_F$  states of a single manifold. The selection rules for these transitions are given by  $\Delta\kappa=0,\pm 1,\pm 2,\ldots$  and  $\Delta\tilde{m}_F=\pm 1$ .

#### 2.3 Experimental Setup and Cooling Sequence

This chapter describes the experimental realization of a 1D quantum gas of bosonic <sup>87</sup>Rb atoms on an atom chip.

The setup consists of two vacuum chambers, a design widely used in many cold atom experiments. In principle, the fast cooling cycles on an atom chip also allow for single chamber designs. The two chamber setup was chosen to allow also for multi-species experiments with fermionic <sup>40</sup>K or bosonic <sup>39</sup>K. The first chamber is used as an efficient source for cold atoms, which are then transferred to the second science chamber where the actual experiments take place. Details of the design are described in [31, 34, 35]. An overview is depicted in Fig. 2.5.

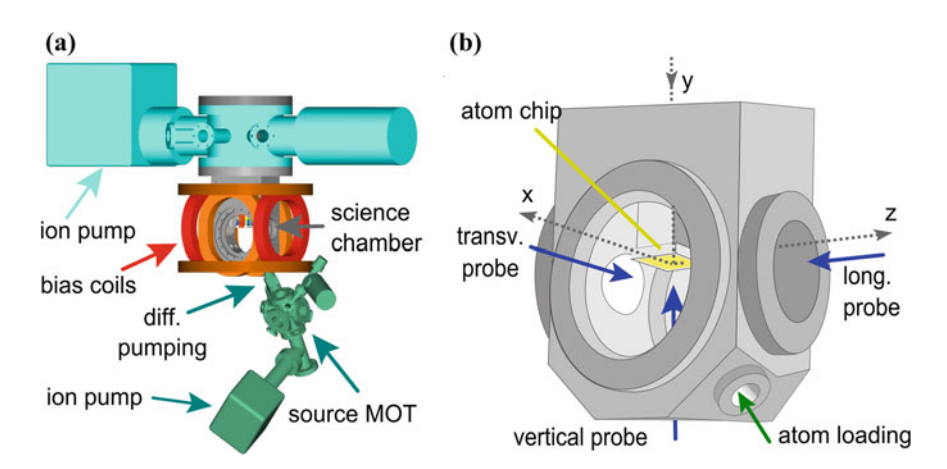


**Fig. 2.5** Experimental setup. **a** Source-MOT and science chamber with the vacuum system [34]. The two chambers are connected by a differential pumping stage. A resonant push beam is used to transfer the atoms from a 3D source-MOT in the lower chamber to a mirror-MOT in the science chamber. The setup is designed such that it allows for good optical access to the science chamber from all directions. **b** Close-up of the science chamber with the atom chip mounted upside down in the center [37]. Large windows enable absorption imaging in all three spatial directions

In the course of this thesis, the first degenerate Bose gases of <sup>87</sup>Rb were realized in the new machine. In the following we present a short summary of the typical experimental procedure. Details can be found in Refs. [22, 36].

#### 2.3.1 Atom Source and Precooling

The experimental cycle starts with a source of cold atoms. The source consists of a 3D magneto-optical (3DMOT) trap that is created in a stainless steel chamber with six CF40 and eight CF16 flanges. The chamber houses commercial rubidium dispensers which are continuously operated at a current of 7.5 A to achieve a high Rb background pressure. One CF40 flange is connected to an ion pump, resulting in a typical pressure of  $10^{-8}$  mBar. The 3DMOT uses a six-beam configuration, where the lasers are detuned by 22 Mhz from the  $F=2 \rightarrow F'=3$  transition of the  $^{87}$ Rb  $D_2$  line ( $\lambda_{D2} \sim 780$  nm). The laser power of 15 mW per beam is derived from a single cooling laser, which also provides most of the other light used in the experiment. Additional repumping light on the  $F=1 \rightarrow F=2$  transition is derived from a home-built diode laser system. During the operation of the source-MOT a resonant pushbeam is used to continuously transfer atoms into the science chamber through a differential pumping stage.

#### 2.3.2 Science Chamber and Mirror Magneto-optical Trap

The science chamber has a size of  $25 \times 16 \times 9\,\mathrm{cm}$  and is produced from a single block of stainless steel (Fig. 2.5b). It is pumped by an ion pump, <sup>4</sup> resulting in a typical pressure of  $10^{-10}$ – $10^{-11}\,\mathrm{mBar}$ . Additional pumping can be provided using a titanium sublimation pump. The main feature of the science chamber are two 100 mm diameter windows which allow for good optical access in what later will be the transversal direction of the 1D gases. Further view ports on all other sides of the chamber allow for additional optical access in all other directions. The chamber is surrounded by large bias coils in all three spatial directions. The microfabricated atom chip is mounted upside down in the center of the chamber. Several macroscopic copper structures are located behind the actual atom chip and are used for additional trapping and cooling. The first of these is a U-shaped structure which, together with an external magnetic bias field, creates a quadrupole field that is centered less than 1 cm away from the chip surface. This quadrupole field and four laser beams are used to create a second MOT. To this end, two of the laser

<sup>&</sup>lt;sup>1</sup>SEAS Getter, Inc.

<sup>&</sup>lt;sup>2</sup>Varian 20 l/s Star-Cell.

<sup>&</sup>lt;sup>3</sup>Coherent MBR 110 Ti:Sa laser, pumped by a Coherent Verdi V18, output 1.2 W @ 780 nm.

<sup>&</sup>lt;sup>4</sup>Varian 1501/s Star-Cell.

beams are reflected from the atom chip's highly reflective surface under an angle of 45°. This represents a mirror-MOT which is equivalent to the usual six-beam MOT configuration [14, 23]. Typical powers per beam are 20 mW. The light for the cooling, as well as for additional repumping is derived from the same lasers as for the source-MOT. The mirror-MOT is continuously loaded for 10 s using the push beam from the lower chamber.

#### 2.3.3 Wire Traps and Evaporative Cooling

In the next step, the atoms are transferred to a first magnetic trap formed by two Z-shaped copper structures with cross-sections of  $(1 \times 1)$  mm<sup>2</sup> and  $(2 \times 1)$  mm<sup>2</sup>, which are located behind the chip. To this end, we first compress the mirror-MOT by increasing the bias fields. This prepares the MOT for a good mode-matching with the magnetic trap. Subsequently, all magnetic fields are turned off and a 8 ms long stage of sub-Doppler cooling in an optical molassis is used to decrease the temperature of the atoms. This yields  $10^8$  atoms at temperatures around  $50 \,\mu$  K. The optical molassis is followed by a 1 ms pulse of  $\sigma^+$  light on the  $F=2 \rightarrow F'=2$  transition to optically pump the atoms into the trappable F=2,  $m_F=2$  state. We then ramp up a current of (60–70) A in both copper structures to form a trap that has a depth of approximately 1.6 mK and estimated trap frequencies of  $\omega_7 = 2\pi \times 17$  Hz and  $\omega_{\perp} = 2\pi \times 50$  Hz. At this point,  $7 \times 10^7$  atoms are trapped, corresponding to a transfer efficiency of about 70 % from the MOT. This number depends critically on the efficiency of the optical pumping. The current in the larger Z-structure is subsequently ramped down within 350 ms, followed by a 2 s compression of the Z-trap. This results in a trap which is characterized by  $\omega_z \sim 2\pi \times 24$  Hz and  $\omega_\perp \sim 2\pi \times 800$  Hz. Subsequently, evaporative cooling is initiated by applying RF radiation via the U-shaped structure. The radiation is created using an arbitrary wave-form generator. Typical coupling strengths of the RF are (2-6) kHz. Starting from a frequency of around 15 MHz, we decrease the frequency of the RF radiation roughly exponentially to 0.75 MHz within 6.1 s. This increases the phase space density close to unity, with a temperature of about  $10 \,\mu\text{K}$  and  $10^6$  atoms.

# 2.3.4 The Atom Chip

Typically the cold cloud in the macroscopic trap is not cooled further to quantum degeneracy, but transferred to the microscopic traps on the atom chip. To this end we linearly ramp up the current in the chip structures within 500 ms, while in the mean time decreasing the current in the macroscopic Z-structure. This allows for a nearly

<sup>&</sup>lt;sup>5</sup>Tabor Electronics WW1071.

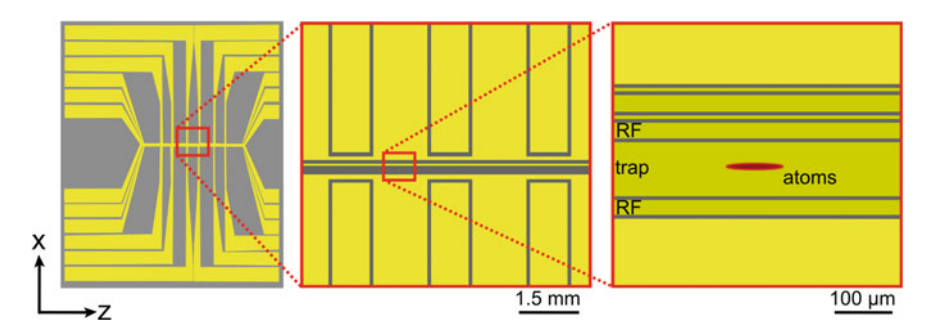


Fig. 2.6 Layout of the atom chip. The atom chip consists of approximately  $1.2\,\mu m$  thick, single layer gold structures that have been evaporated on a  $35.7\times0.525\times29.7$  mm sized silicon substrate by means of photo lithography. Six wires of different widths are available to realize variable trapping geometries for the atoms. For the experiments presented this thesis, we use a  $100\,\mu m$  wire together with external bias fields to create the static trapping potential. Tunable longitudinal confinement is realized using 4 of the  $6\,100\,\mu m$  wide U-shaped wires. Two parallel  $30\,\mu m$  wide wires adjacent to the main trapping wire are used to apply radio frequency fields. A detailed description of the design and the fabrication process can be found in [31]

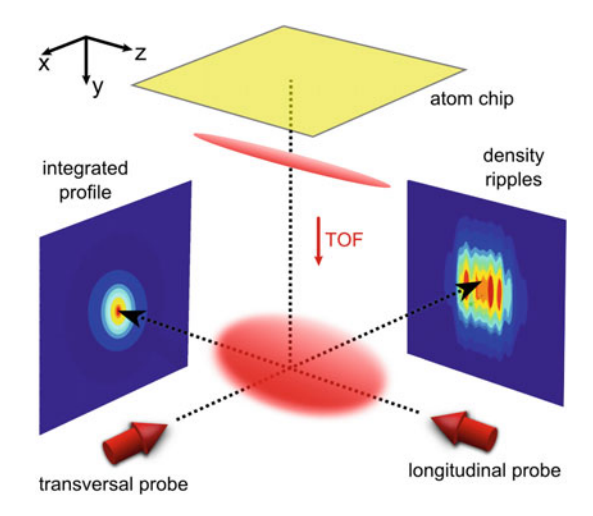
loss-less transfer of the atoms to the chip, much better than what could be achieved by loading the chip directly from the large volume mirror-MOT.

The atom chip employed is a single layer gold chip fabricated on a silicon substrate. The wire layout is shown in Fig. 2.6. It allows for a large variety of traps, formed using 100 or 30  $\mu$ m wide main trapping wires, in conjunction with external bias fields. Each of the trapping wires is combined with two additional smaller parallel wires, which are used for RF manipulation of the atoms. Flexible longitudinal trapping is created using 6 U-shaped wire structures.

After transferring the atoms to the chip, further evaporative cooling is performed. For the experiments presented in this thesis, we typically employ a trap formed using the  $100\,\mu\mathrm{m}$  wide main trapping wire and two neighboring pairs of U-structures. Typical currents are 810 mA in the  $100\,\mu\mathrm{m}$  wire and 295 mA in each of the U-structures. To minimize fluctuations, the chip currents are supplied by car batteries. A bias field in x-direction is used to set the properties of the trap. It ranges from 12 to 16 G, realizing a trap located between 120 and 90  $\mu\mathrm{m}$  below the chip surface, with radial trapping frequencies of  $\omega_{\perp}=2\pi\times(1.4-2.5)\,\mathrm{kHz}$ . The longitudinal trapping freqency is  $\omega_z=2\pi\times(7-12)\,\mathrm{Hz}$ . Further evaporative cooling in this trap leads to degenerate gases with temperatures in the range of  $(20-200)\,\mathrm{nK}$ , and containing  $10^3-10^4$  atoms. This realizes a single 1D Bose gas that can be further manipulated in the experiments.

<sup>&</sup>lt;sup>6</sup>Produced by M. Trinker at Zentrum für Mikro- und Nanostrukturen (ZMNS) of TU Wien.

Fig. 2.7 Imaging setup for a single 1D Bose gas. A cloud of phase fluctuating 1D bosons is prepared below the atom chip. Upon its release it falls under gravity and expands in time-of-flight (TOF). The cloud can be illuminated transversally to obtain an image of the density ripples that form in expansion, or longitudinally, to obtain an integrated image of the atomic density profile. Figure adapted from [22]



#### 2.3.5 Imaging Systems

Independent of the particular experiment that is performed, information is always extracted using standard absorption imaging [9]. After rapidly turning off all trapping potentials, the atoms fall under gravity and expand for a variable time-of-flight. The observation is performed using three different imaging systems, each pointing along one spatial direction. For all imaging systems, we use the  $F=2 \rightarrow F'=3$  transition of the  $D_2$  line of <sup>87</sup>Rb with an intensity corresponding to about 10% of the saturation intensity. The finite resolution of the imaging process can be described by a radially symmetric Gaussian point spread function [22, 38]

$$f(r) = \frac{1}{\sqrt{2\pi\sigma_{\rm PSF}^2}} \exp\left(-\frac{r^2}{2\sigma_{\rm PSF}^2}\right),\tag{2.11}$$

where  $\sigma_{PSF}$  is the width of the point spread function.

An overview of the imaging process for a single 1D Bose gas is shown in Fig. 2.7. The corresponding procedure for two gases in a double well is presented in Fig. 2.8. A detailed description of the absorption signal for each imaging system can be found in Ref. [22].

#### **Longitudinal Imaging System**

The longitudinal imaging records the integrated atomic density distribution along the y-direction using a standard CCD camera. It uses a two-lens setup, resulting in a field of view of  $2.5 \times 1.67$  mm and a pixelsize of  $2.45 \,\mu m$ . As the optical access is shared with the MOT beams, the optical setup limits the numerical aperture of this

<sup>&</sup>lt;sup>7</sup>Andor DV435-BV-958, serial number CCD5302.

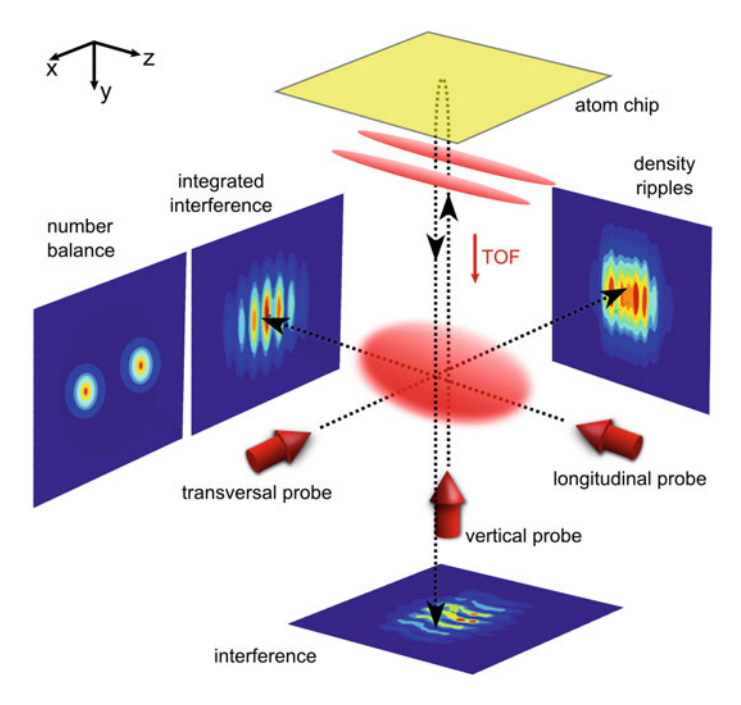


Fig. 2.8 Imaging setup for two interfering 1D Bose gases. After turning off all trapping potentials, the clouds expand and form a matter-wave interference pattern. This pattern can be imaged using the vertical imaging, or by integration of the cloud along its longitudinal axis. As the line of sight of the vertical imaging is blocked by the atom chip, the imaging beam is reflected before passing the atoms. The transversal imaging system records the sum of the density ripples in both gases. Alternatively, the double-well trap can be turned off before the static trap (see text for details). After time-of-flight expansion (TOF), this leads to two well-separated clouds which can be individually resolved using the longitudinal imaging system. This procedure can thus be used to count the number balance of atoms in the left or right gas. Figure adapted from [22]

imaging system to approximately 0.096 [36]. The imaging system is used to record integrated pictures of interfering 1D gases. It is also used to measure the number balance of atoms trapped in a double well. Focusing is accomplished using a detuned imaging beam, which results in characteristic near-field diffraction effects [22, 39]. For example, imaging an interference pattern will result in a constant interference contrast as a function of detuning only if the imaging is focused. If it is defocused, a linear variation of the contrast with detuning can be observed.

#### **Transversal Imaging System**

The second imaging system is used to study the atoms along their transversal direction. To benefit from the large optical access in this direction, the imaging system uses a high-resolution objective with a numerical aperture of 0.26 [40, 41]. It images

the atoms onto a standard CCD camera, and has a field of view of  $0.7 \times 1$  mm and a pixel size of  $1.05\,\mu m$  [22]. The system is optimized for high-resolution in situ imaging, but can also be used to image the density ripple patterns that form after time-of-flight expansion of a phase-fluctuating 1D Bose gas. Examples of temperature measurements based on these patterns are presented in Sect. 2.3.6. Coarse focusing is accomplished by detuning the imaging beam, fine tuning using the density ripple spectrum [42, 43]. From this density ripple spectrum, the resolution can be determined to be  $\sigma_{PSF} = (2.55 \pm 0.10)\,\mu m$ .

Additionally, this imaging system can be used for a high-resolution optical pumping scheme, which spatially selects subsections of clouds for the longitudinal imaging system [37, 44]. In this scheme atoms are illuminated by a beam resonant to the  $F=2 \rightarrow F'=1$  transition. After scattering on average only 1–2 photons they decay into the F=1 state, which renders them invisible to further imaging light on the  $F=2 \rightarrow F'=3$  transition. By imaging a target with variable size onto the atoms through the high-resolution objective, parts of the cloud can be protected from this state change. This scheme is used together with the longitudinal imaging to perform matter-wave interference experiments with variable integration length in Chap. 4.

Moreover, this imaging system can be easily replaced by an overview imaging system using a flip mirror. The overview imaging system has a field of view of  $4\times5.3$  mm, a pixel size of  $3.84\,\mu\text{m}$  and uses a Pixelfly CCD camera. Due to the large field of view it is particularly useful for the calibration of the molassis and the optical pumping, where the atomic clouds are too large to be observed with the other imaging systems.

#### **Vertical Imaging System**

The third imaging system records the atomic density distribution from below. This is of particular importance for the experiments presented in this thesis, as it enables the direct imaging of the local interference pattern of two 1D Bose gases. While imaging this interference pattern is, in principal, also possible using the optical pumping scheme presented above, the vertical imaging directly provides the full spatial information including all integration lengths at once and down to the resolution limit. It is this feature which enables the measurement of phase correlation functions, which is central to Chaps. 5 and 6.

A conventional absorption imaging setup in this direction is rendered impossible by the atom chip, which directly blocks the line of sight. This problem can be circumvented by using the chip as a mirror, before collecting the light on a electron multiplying CCD (EMCCD) camera<sup>9</sup> which is currently used without the amplification stage. The EMCCD camera was chosen to prepare this imaging system for future single-atom sensitive fluorescence imaging [45].

Special care has to be taken as the structures on the chip can severely degrade the image quality through diffraction of the light beam. Therefore, the imaging beam

<sup>&</sup>lt;sup>8</sup>Andor DV435-BV-958, serial number CCD5303.

<sup>&</sup>lt;sup>9</sup>Andor iXon DV887.

is focused such that only the central trapping wire is illuminated. The focus of the beam is positioned close to the atoms such that they are only illuminated once by the beam, after it has been reflected from the atom chip surface. This results in a circular field of view with a radius of about  $100\,\mu\text{m}$ . The pixel size is  $2.02\,\mu\text{m}$ . As for the longitudinal imaging, focusing is achieved by imaging an interference pattern with a detuned imaging beam. Note that due to the imaging beam focusing, the focal position of this imaging system is fixed and corresponds to a time-of-flight of 15.7 ms. The resolution can be determined using measurements of phase correlation functions (see Sect. 2.4) and corresponds to  $\sigma_{PSF} = (3.6 \pm 0.1)\,\mu\text{m}$ .

#### 2.3.6 Making and Probing Degenerate Gases

The emergence of a quasi-condensate is shown in Fig. 2.9. The transversal images reveal strong density fluctuations, which become less pronounced with decreasing temperature. These density fluctuations are a direct consequence of the in situ phase fluctuations of the quasi-condensate and were first observed in elongated 3D condensates [46]. In low-dimensional gases, interactions during the expansion are negligible and thus the spectrum and the correlation properties of the density fluctuations after expansion can be calculated [47]. Interestingly, the scaling laws governing the

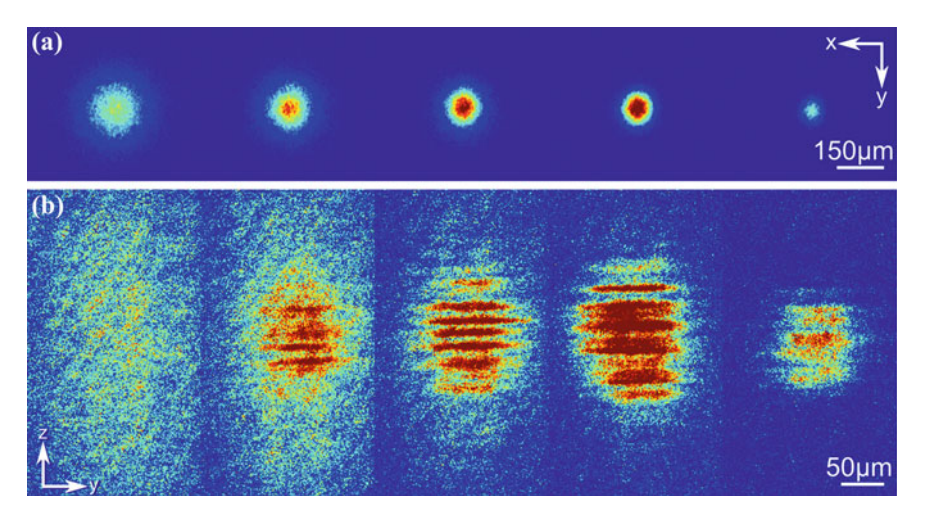


**Fig. 2.9** Emergence of a quasi-condensate. Absorption images after 12 ms time-of-flight. From *left* to *right* the final RF evaporation frequency decreases from 450 to 410 kHz in steps of 10 kHz. **a** Images using the longitudinal imaging system reveal the transition from a Gaussian thermal cloud to a strongly peaked quantum degenerate gas. **b** Images using the transversal imaging system show how density ripples slowly emerge withing the thermal background, signaling the emergence of the quasi-condensate. Decreasing the RF frequency the thermal background vanishes and the quasi-condensate grows. As temperature decreases the density ripples become less pronounced

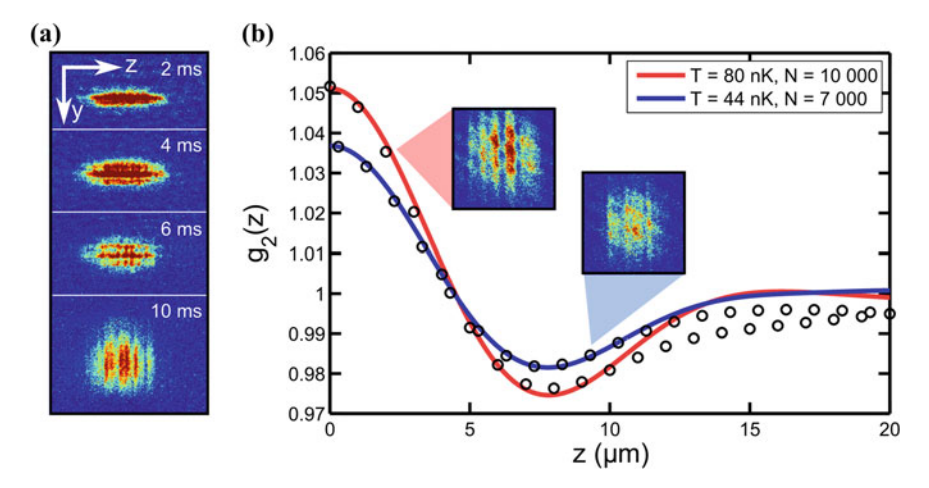


**Fig. 2.10** Thermometry using density fluctuations in expansion. **a** In situ phase fluctuations lead to density fluctuations of a quasi-condensate in time-of-flight expansion. **b** The density-density-correlation function of these fluctuations can be used for thermometry [47, 50]. If the temperature is high, phase fluctuations are strong, leading to strong density fluctuations in time-of-flight. If the temperature is low, phase fluctuations are reduced

spectra in 1D and 2D Bose gases have been predicted to be identical, a topic which is currently under intense study [42, 48, 49]. In our experiment we use the correlation properties of the density ripples to measure the temperature of the gas.

To this end the experiment is repeated approximately 100 times to extract the density-density correlation function [36, 42, 47, 50]. The result is compared to Ornstein-Uhlenbeck simulations for quasi-condensates of different temperatures to fit the temperature of the gas. Examples are presented in Fig. 2.10.

It is well known that the proximity of the atoms to the wires makes the trapping potentials on atom chips very sensitive to imperfections of the wire structures [51]. Information about the trapping potential can be obtained by using the atoms as a probe for these corrugations. To this end, cold but still thermal clouds are imaged after a short time of flight. Averaging over many realizations, structures in the density profile directly reveal deviations from a smooth trapping potential. Examples are presented in Fig. 2.11a. The overall potential closely follows a harmonic potential. In the center, small deviations can be observed which are the result of wire corrugations. These corrugations become more pronounced the closer the atoms are located to the wires. To minimize this effect we exclusively use traps which are formed at least  $100\,\mu\mathrm{m}$  from the chip.

The harmonic confinement of the trap can be further characterized using trap frequency measurements. A short step in the current of the trapping wires displaces the trap and induces collective oscillations of the atoms. Fitting position and width of the cloud after time-of-flight expansion for varying evolution times after

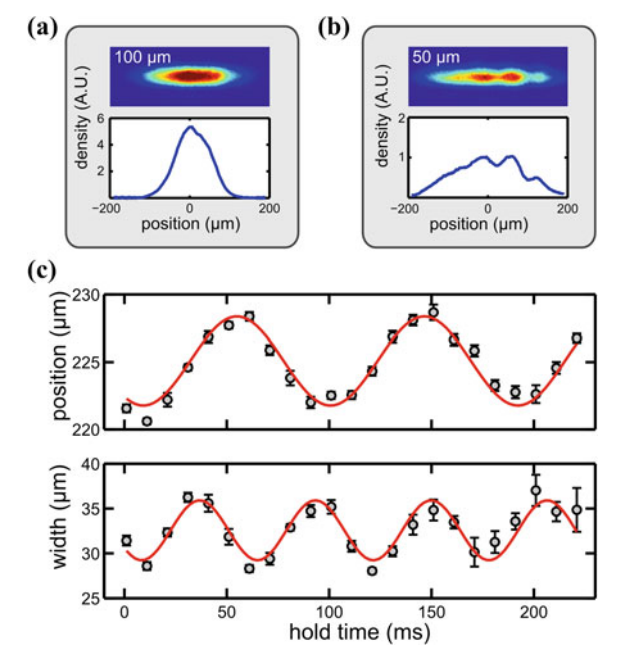


Fig. 2.11 Characterization of the trapping potential. Wire corrugations can lead to a deformation of the potential. The effect can be probed using the density profile of thermal atoms. **a** At a distance of 100  $\mu$ m from the chip, the integrated profile is almost smooth, corresponding to a smooth trapping potential. **b** Moving the atoms closer to the chip wire corrugations are revealed. To minimize the effect of these corrugations all experiments presented in this thesis have been performed at distances around 100  $\mu$ m from the chip. **c** The (approximately) harmonic confinement of the trap in (**a**) is characterized using trap frequency measurements. For the trap in this example, we find frequencies of  $\omega_D = \omega_z = 2\pi \times (10.94 \pm 0.14)$  Hz for the collective dipole oscillations (*top*) and  $\omega_B = 2\pi \times (17.67 \pm 0.26)$  Hz for the collective breathing oscillations (*bottom*) of the atoms. The ratio  $\omega_B/\omega_D = 1.61 \pm 0.03$  is close to the predicted value of  $\sqrt{3}$  [52]. Similarly, the radial trapping frequency can be measured. Typical values are  $\omega_\perp = 2\pi \times (2-2.1)$  kHz

the displacement, we obtain the frequencies of dipole and breathing oscillations, respectively. As expected for a trapped 1D Bose gas, we find a ratio close to  $\omega_B/\omega_D\sim\sqrt{3}$  [52, 53]. Exemplary results are shown in Fig. 2.11b.

# 2.4 Experiments with Atoms in a Tunable Double-Well Potential

Having produced and characterized a single harmonically trapped 1D Bose gas provides a solid starting ground for experiments in a double-well potential. In this chapter, this double-well potential is characterized. Subsequently, we introduce the

tools to probe the equilibrium state of 1D bosons in this potential via matter-wave interference.

#### 2.4.1 Characterization of the Radio-Frequency Dressing

To create the dressed-state potentials we use two parallel 30  $\mu$ m wide wires adjacent to the main trapping wire. The RF radiation is provided by a two-channel arbitrary wave-form generator<sup>10</sup> which allows the individual control of both phase and amplitude in each of the wires. Typical RF currents for the creation of a double well located 100  $\mu$ m below the chip surface are  $I_{RF} = (20-25)$  mA per wire. To characterize the applied RF fields we first monitor the 5-level Rabi oscillations in the bare state basis by mapping the populations of the different  $m_F$  states using a Stern-Gerlach experiment. To this end, we turn on the RF for a fixed time at a variable frequency. Then the trapping potentials are switched off and a field gradient is applied via one of the macroscopic Z-wires during the ensuing time-of-flight expansion. As the different  $m_F$  states have different magnetic moments they are spatially separated and can be imaged individually using the longitudinal imaging system. To fit the results, we solve the 5-level Rabi problem and find typical coupling strengths on the order of several hundred kHz.

To precisely study the dressed-state level structure we perform spectroscopy with an additional weak RF field [29]. This RF field is applied via the U-wire, as in the normal evaporative cooling sequence. It couples the different dressed states, just as it would with the bare states, leading to pronounced loss features in the atom number. The results of this RF spectroscopy are shown in Fig. 2.12. We use the position of the resonances to calibrate our simulation of the potentials (see Appendix B). Another benchmark for the simulation can be obtained by measuring the distance between the wells as a function of RF current.

The trap frequencies in the double well are characterized in the same way as in the static trap. Typically, both longitudinal and radial trap frequency are about 30 % lower than in the static trap. The exact value depends on the applied RF current and can be very well estimated using the simulation of the potentials.

### 2.4.2 Turning Off the Double Well

When loading the double well the RF can be ramped up slowly, thus transferring the atoms adiabatically from the bare states to the dressed states. This is not possible when the atoms are released from the trap, as all potentials have to be switched off immediately. The rapid change of the quantization axis leads to a decomposition of the atoms into the various bare states. This has significant implications for interference

<sup>&</sup>lt;sup>10</sup>Tabor Electronics WW5062.

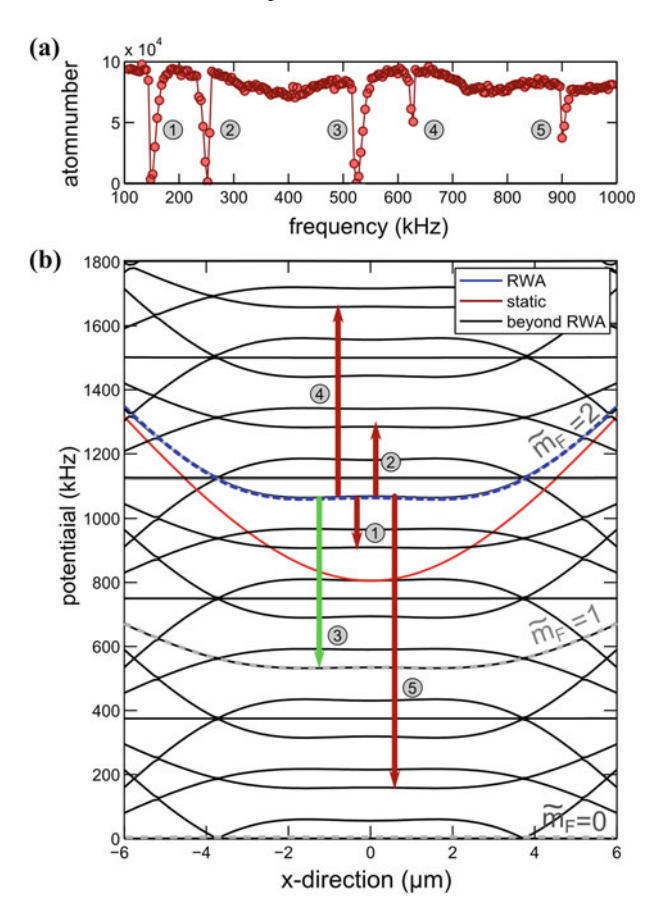
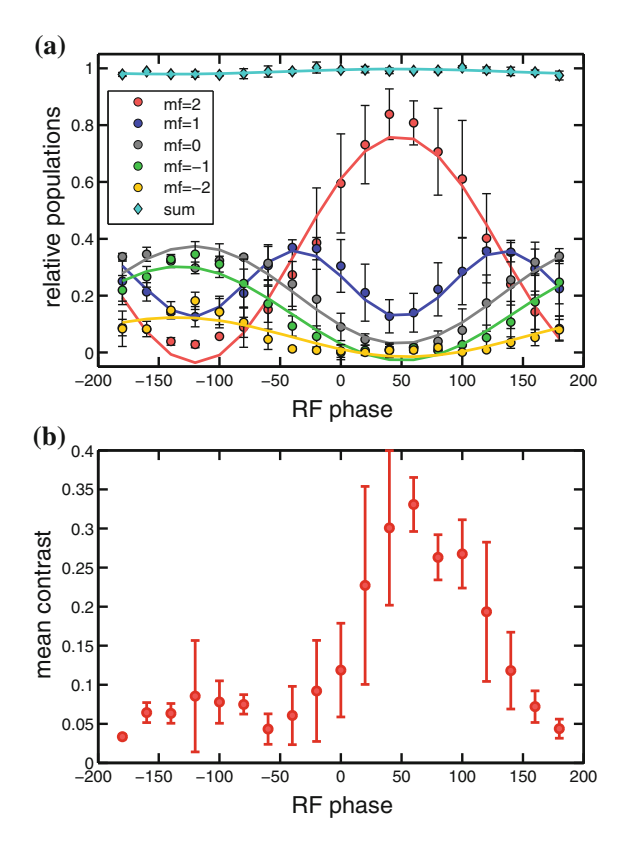


Fig. 2.12 RF spectroscopy of the dressed states. **a** A weak additional RF field is used to outcouple atoms from the dressed trap. Resonances appear whenever the RF field is resonant with a transition between the different dressed states. **b** Simulation of the level structure in the dressed trap, which enables the identification of the transitions (1)  $\Delta \kappa = +1$ ,  $\Delta \tilde{m}_F = -1$ , (2)  $\Delta \kappa = +2$ ,  $\Delta \tilde{m}_F = -1$ , (3)  $\Delta \kappa = +0$ ,  $\Delta \tilde{m}_F = -1$ , (4)  $\Delta \kappa = +3$ ,  $\Delta \tilde{m}_F = -1$ , and (5)  $\Delta \kappa = -1$ ,  $\Delta \tilde{m}_F = -1$ . *Gray dashed lines* indicate the sub levels of the  $\Delta \kappa = 0$  manifold. The *green line* indicates transition (3), which is typically used for RF cooling in the experiments. Note that resonances (2) and (4) to states with higher energy are shifted by approximately 25 kHz because of the high temperature of the atoms used in this measurement

experiments as the different  $m_F$  states have different magnetic moments. Any small residual field during expansion will displace the different  $m_F$  states with respect to each other, leading to a decrease in interference contrast. Note that this does not change the dynamics that are observed, it just reduces the experimental sensitivity to small changes in contrast. The decomposition can be optimized by properly choosing the phase of the RF field. Typical observations are shown in Fig. 2.13. From these

Fig. 2.13 RF potential switch-off. a For the ideal choice of the RF phase, most atoms are projected back into the  $m_F = 2$  bare state. Solid lines are a guide to the eye. b This leads to a maximization of the interference contrast

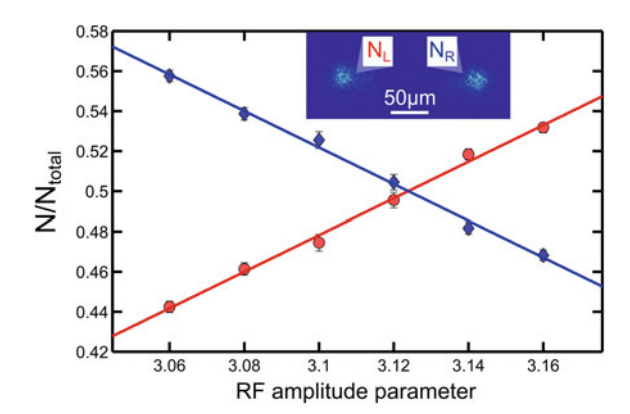


results we extract the best value for the phase, where most of the atoms are transferred into the  $m_F = 2$  bare state, resulting in the highest contrast.

# 2.4.3 Equilibrium States: Cooling into the Double Well

To prepare a pair of gases in equilibrium we change the experimental sequence and let the evaporative cooling in the static chip trap end at a frequency which is significantly higher than the one needed to create a degenerate gas. We then ramp up the RF potentials in 10 ms. As the trapping frequency is reduced during the splitting process, special care is taken not to cool the gas to degeneracy by adiabatic expansion [9]. Subsequently, the RF cooling is resumed using one of the resonances identified in the RF spectroscopy. Typically, the  $\Delta \kappa = 0$ ,  $\Delta \tilde{m}_F = -1$  resonance at approximately 520 kHz is used for 300 ms of further cooling, creating two degenerate gases in the individual double wells, which, by definition, are completely independent of each other. This is the thermal equilibrium situation of two gases in a double well.

Fig. 2.14 Atom number imbalance. By changing the relative amplitude of the two RF currents the double well can be tilted. This leads to a mean atom number imbalance between the two wells. The imbalance can be measured by turning off the RF currents before the static currents. This leads to a separation of the two wave packets in time-of-flight (details see text)



For example, symmetric and anti-symmetric degrees of freedom exhibit the same temperatures and are thus in equilibrium.

At this point we can perform two complimentary measurements. First, to access the atom number imbalance between the two gases, the RF amplitude is ramped down over 40 periods, corresponding to a time scale of 0.1 ms. This transfers the atoms back into the bare states, while the static trapping potential is still present. As the ramp-down is fast compared to the radial trapping frequency ( $\omega_{\perp} \sim 2\pi \times 2 \text{ kHz}$ ), the resulting two clouds are displaced from the energy minimum of the static trap. Similar to classical balls they will thus roll down the potential. Turning off the trap at the time when they reach the potential minimum prepares two clouds with opposite momenta. These momenta are large enough to separate the two clouds spatially after time-of-flight, enabling the measurement of the respective atom numbers using the longitudinal imaging system. Examples are shown in Fig. 2.14. Controllable atom number imbalances can be prepared by using a small asymmetry in the two RF currents that are used to create the double well.

Second, information about the relative coherence of the gases is obtained by matter-wave interference (Fig. 2.15). To this end, all potentials are turned off at the same time. The atoms drop and form an interference pattern after a time-of-flight expansion. As discussed in Sect. 1.5, the location of the fringes in this interference pattern is a direct measure for the relative phase between the two gases. Due to the low trapping frequency in the longitudinal direction, the expansion of the gases in this direction is negligible and the local displacement of the interference fringes indeed reflects the in situ phase distribution.

To extract the interference contrast C(L) the absorption image is summed over a length L and fitted with the cosine-modulated Gaussian function [54]

$$f_L(x) = A \cdot \exp\left(-\frac{(x - x_0)^2}{2\sigma^2}\right) \cdot \left[1 + C\left(L\right)\cos\left(\frac{2\pi(x - x_0)}{\lambda_F} + \theta\left(L\right)\right)\right], \quad (2.12)$$

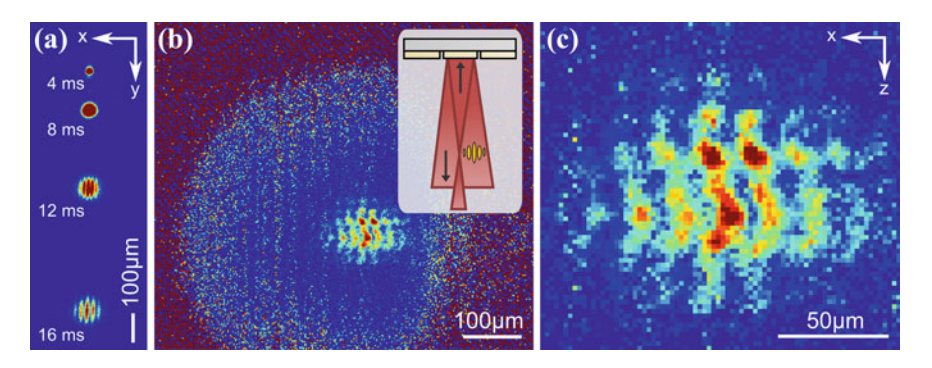


Fig. 2.15 Matter-wave interference of two 1D Bose gases. a Emergence of the interference pattern in time-of-flight as seen from the longitudinal imaging system. b Imaging of the local fluctuations of the interference pattern using the vertical imaging system after 15.7 ms time-of-flight. The limited field of view results from the focusing of the imaging beam onto the trapping wire. The beam path is shown in the *inset* [44]. c Zoom into the image shown in (b). Fitting the local interference pattern allows the determination of the relative phase  $\theta(z)$  and the contrast C(L), where L is the integration length

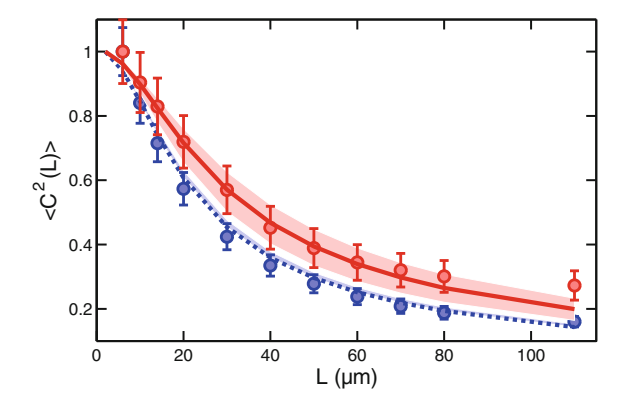


Fig. 2.16 Decay of the mean contrast squared. *Points* represent experimental data for  $\langle C^2(L) \rangle$ , normalized to  $\langle C^2(6 \, \mu m) \rangle$ . *Lines* are the theory prediction (Eq. 1.87). Parameters are  $n_{1D} = 35/\mu m$ ,  $T = (27 \pm 7) \, \text{nK}$  (red dashed line) and  $n_{1D} = 45/\mu m$ ,  $T = (117 \pm 7) \, \text{nK}$  (blue dashed line). A bootstrapped fit of the experimental data [36, 55] is used to extract the values  $\lambda_T = (7.02 \pm 2.45) \, \mu \text{m}$  (red solid line) and  $\lambda_T = (2.99 \pm 0.7) \, \mu \text{m}$ , in good agreement with the expected 7.2 and 2 μm

where  $\sigma$  is the rms radius of the Gaussian profile,  $x_0$  is its center of mass, and  $\lambda_F$  is the fringe spacing. The results are shown in Fig. 2.16. To extract the relative phase profile  $\theta(z)$ , the integration length L is set to the size of one pixel.

To extract the FDFs, we repeat the experiment many times with the same conditions and measure the different outcomes of the contrast. Examples of measured FDFs in equilibrium are shown in Fig. 2.17. Note that this procedure is fundamentally different to the averaging performed in a 2D optical lattice. There, typically many

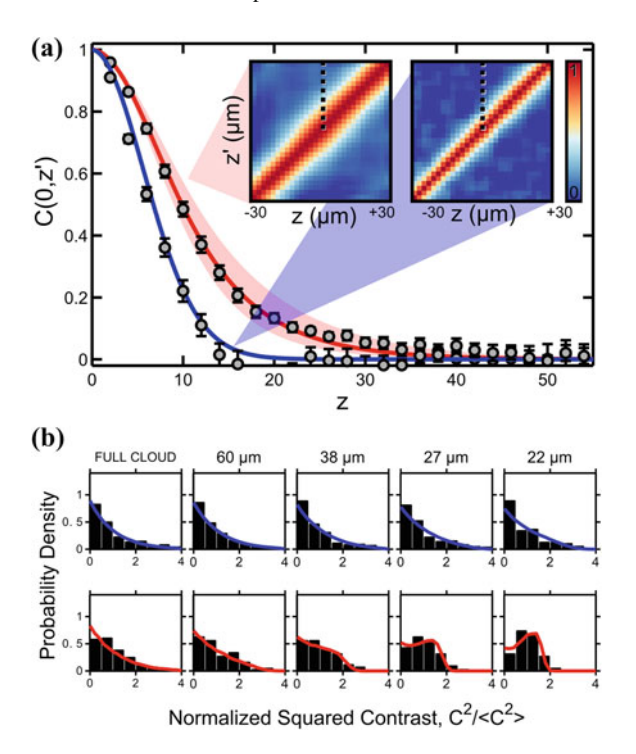


Fig. 2.17 A pair of 1D Bose gases in thermal equilibrium. a Two-point phase correlation functions C(0,z') for  $n_{1D}=35/\mu m$ ,  $T=(27\pm7)\,\mathrm{nK}$  (red) and for  $n_{1D}=45/\mu m$ ,  $T=(117\pm7)\,\mathrm{nK}$  (blue). Solid lines denote the theory predictions (Eq. 1.85), including the optical resolution. Points are the experimental results, averaged over approximately 100 realizations. The temperatures used for the theory lines have been independently determined using density ripples, demonstrating that the gases are in equilibrium. For the hotter dataset, the correlation function is completely determined by the optical resolution. Such high-temperature datasets thus enable an independent determination of the point spread function width  $\sigma_{\mathrm{PSF}}$  (Eq. 2.11). The insets show the corresponding full two-point correlation functions C(z,z'), with the dashed lines indicating the C(0,z') lines. b The corresponding FDFs are exponentially decaying on all length scales for hot temperatures and show a crossover from exponentially decaying to Gumbel-like for lower temperatures [56], both in very good agreement with theory [57, 58]. Figure (b) adapted from [44]

1D gases are realized and probed in parallel which means that only ensemble averages are available. Due to the central limit theorem the statistics of such averages is approximately Gaussian, meaning that the information contained in the higher moments of the FDFs is not accessible in this way.

As in the case of a single 1D Bose gas, we can further image the atoms transversally to extract information using the resulting density fluctuations in time-of-flight. As the two gases are completely independent, the resulting density ripple pattern is an incoherent superposition of two single density ripple patterns. We simulate this situation using the Ornstein-Uhlenbeck process technique and use it to extract a

temperature (see Sect. 1.4.6). As expected for thermal equilibrium, we find exactly the same temperature as for the anti-symmetric mode.

#### References

- T. Kinoshita, T. Wenger, D.S. Weiss, Observation of a one-dimensional Tonks-Girardeau gas. Science 305, 1125–1128 (2004)
- M. Greiner, I. Bloch, O. Mandel, T.W. Hänsch, T. Esslinger, Exploring phase coherence in a 2D lattice of Bose-Einstein condensates. Phys. Rev. Lett. 8716, 160405 (2001)
- E. Haller, R. Hart, M.J. Mark, J.G. Danzl, L. Reichsollner, M. Gustavsson, M. Dalmonte, G. Pupillo, H.-C. Nagerl, Pinning quantum phase transition for a Luttinger liquid of strongly interacting bosons. Nature 466, 597–600 (2010)
- F. Serwane, G. Zürn, T. Lompe, T.B. Ottenstein, A.N. Wenz, S. Jochim, Deterministic preparation of a tunable few-Fermion system. Science 332, 336 (2011)
- P. Krüger, S. Hofferberth, I.E. Mazets, I. Lesanovsky, J. Schmiedmayer, Weakly interacting Bose gas in the one-dimensional limit. Phys. Rev. Lett. 105, 265302 (2010)
- 6. C. Foot, *Atomic Physics* (Oxford University Press, Oxford, 2008)
- C.V. Sukumar, D.M. Brink, Spin-flip transitions in a magnetic trap. Phys. Rev. A 56, 2451–2454 (1997)
- 8. K.B. Davis, M.-O. Mewes, M.A. Joffe, M.R. Andrews, W. Ketterle, Evaporative cooling of sodium atoms. Phys. Rev. Lett. **74**, 5202 (1995)
- W. Ketterle, D.S. Durfee, D.M. Stamper-Kurn, in *Making, Probing and Understanding Bose-Einstein Condensates*, ed. by M. Inguscio, S. Stringari, C.E. Wieman. Bose-Einstein Condensation in Atomic Gases, Proceedings of the International School of Physics Enrico Fermi (IOS Press, Amsterdam, 1999), pp. 67–176
- W. Hänsel, P. Hommelhoff, T.W. Hänsch, J. Reichel, Bose-Einstein condensation on a microelectronic chip. Nature 413, 498–501 (2001)
- H. Ott, J. Fortagh, G. Schlotterbeck, A. Grossmann, C. Zimmermann, Bose-Einstein condensation in a surface microtrap. Phys. Rev. Lett. 87, 230401 (2001)
- 12. R. Folman, P. Kruger, J. Schmiedmayer, J. Denschlag, C. Henkel, Microscopic atom optics: from wires to an atom chip. Adv. At. Mol. Opt. Phys. **48**, 263–356 (2002)
- 13. J. Reichel, V. Vuletic (eds.), *Atom Chips* (Wiley-VCH, New York, 2011)
- J. Reichel, W. Hänsel, T.W. Hänsch, Atomic micromanipulation with magnetic surface traps. Phys. Rev. Lett. 83, 3398–3401 (1999)
- T. Schumm, S. Hofferberth, L.M. Andersson, S. Wildermuth, S. Groth, I. Bar-Joseph, J. Schmiedmayer, P. Kruger, Matter-wave interferometry in a double well on an atom chip. Nat. Phys. 1, 57–62 (2005)
- M.F. Riedel, P. Böhi, Y. Li, T.W. Hänsch, A. Sinatra, P. Treutlein, Atom-chip-based generation of entanglement for quantum metrology. Nature 464, 1170–1173 (2010)
- T. Jacqmin, J. Armijo, T. Berrada, K.V. Kheruntsyan, I. Bouchoule, Sub-Poissonian fluctuations in a 1D Bose gas: from the quantum quasicondensate to the strongly interacting regime. Phys. Rev. Lett. 106, 230405 (2011)
- A.H. van Amerongen, J.J.P. van Es, P. Wicke, K.V. Kheruntsyan, N.J. van Druten, Yang-Yang thermodynamics on an atom chip. Phys. Rev. Lett. 100, 090402 (2008)
- J. Verdú, H. Zoubi, Ch. Koller, J. Majer, H. Ritsch, J. Schmiedmayer, Strong magnetic coupling of an ultracold gas to a superconducting waveguide cavity. Phys. Rev. Lett. 103, 043603 (2009)
- R. Amsüss, Ch. Koller, T. Nöbauer, S. Putz, S. Rotter, K. Sandner, S. Schneider, M. Schramböck, G. Steinhauser, H. Ritsch, J. Schmiedmayer, J. Majer, Cavity QED with magnetically coupled collective spin states. Phys. Rev. Lett. 107, 060502 (2011)
- P. Treutlein, T.W. Hänsch, J. Reichel, A. Negretti, M.A. Cirone, T. Calarco, Microwave potentials and optimal control for robust quantum gates on an atom chip. Phys. Rev. A 74, 022312 (2006)

- M. Gring, Prethermalization in an isolated many-body system. Ph.D. thesis, Vienna University of Technology, 2012
- S. Wildermuth, P. Krüger, C. Becker, M. Brajdic, S. Haupt, A. Kasper, R. Folman, J. Schmiedmayer, Optimized magneto-optical trap for experiments with ultracold atoms near surfaces. Phys. Rev. A 69, 030901 (2004)
- 24. O. Zobay, B.M. Garraway, Atom trapping and two-dimensional Bose-Einstein condensates in field-induced adiabatic potentials. Phys. Rev. A 69, 023605 (2004)
- Y. Colombe, E. Knyazchyan, O. Morizot, B. Mercier, V. Lorent, H. Perrin, Ultracold atoms confined in RF-induced two-dimensional trapping potentials. Eur. Phys. Lett. 67, 593 (2004)
- I. Lesanovsky, T. Schumm, S. Hofferberth, L.M. Andersson, P. Krüger, J. Schmiedmayer, Adiabatic radio frequency potentials for the coherent manipulation of matter waves. Phys. Rev. A 73, 033619 (2006)
- 27. R. Loudon, *The Quantum Theory of Light* (Oxford University Press, Oxford, 2000)
- 28. S. Will, Atom optical experiments with ultracold sodium atoms. Diplomarbeit, Johannes Gutenberg-Universität Mainz, 2006
- 29. S. Hofferberth, Coherent manipulation of Bose-Einstein condensates with radio-frequency adiabatic potentials on atom chips. Ph.D. thesis, University of Heidelberg, 2007
- 30. I. Lesanovsky, S. Hofferberth, J. Schmiedmayer, P. Schmelcher, Manipulation of ultracold atoms in dressed adiabatic RF-potentials. Phys. Rev. A. **74**, 033619 (2006)
- 31. M. Göbel, Low Dimensional Traps for Bose-Fermi Mixtures. Ph.D. thesis, Ruperto-Carola University of Heidelberg (2008)
- 32. S. Hofferberth, B. Fischer, T. Schumm, J. Schmiedmayer, I. Lesanovsky, Ultracold atoms in radio-frequency dressed potentials beyond the rotating-wave approximation. Phys. Rev. A 76, 013401 (2007)
- 33. J.H. Shirley, Solution of the Schrödinger equation with a Hamiltonian periodic in time. Phys. Rev. **138**, B979–B987 (1965)
- 34. C. vom Hagen, Towards a low-dimensional degenerate Fermi-Fermi-Bose mixture. Ph.D. thesis, Ruperto-Carola University of Heidelberg, 2008
- 35. M. Kuhnert, A dual-species two-MOT setup for preparing a Bose-Fermi mixture on an atom chip. Diplomarbeit, Vienna University of Technology, 2008
- M. Kuhnert, Thermalization and prethermalization in an ultracold Bose gas. Ph.D. thesis, Vienna University of Technology, 2013
- T. Langen, M. Gring, M. Kuhnert, B. Rauer, R. Geiger, D. Adu Smith, I.E. Mazets,
   J. Schmiedmayer, Prethermalization in one-dimensional Bose gases: description by a stochastic
   Ornstein-Uhlenbeck process. Eur. Phys. J. Special Topics 217, 43–53 (2013)
- 38. M. Born, E. Wolf, *Principles of Optics* (Cambridge University Press, Cambridge, 1997)
- A. Marte, Feshbach-Resonanzen bei Stößen ultrakalter Rubidiumatome. Ph.D. thesis, Technische Universität, München, 2003
- 40. B. Stix, A new imaging system for dual-species atomchip experiments. Diplomarbeit, Vienna University of Technology, 2008
- 41. W. Alt, An objective lens for efficient fluoresence detection of single atoms. Optik **113**, 142 (1996)
- 42. T. Langen, Comment on "Probing phase fluctuations in a 2D degenerate Bose gas by free expansion". Phys. Rev. Lett. **111**, 159601 (2013)
- 43. A. Putra, D.L. Campbell, R.M. Price, S. De, I.B. Spielman, Optimally focused cold atom systems obtained using density-density correlations. Rev. Sci. Instrum. **85**, 013110 (2014)
- D. Adu Smith, M. Gring, T. Langen, M. Kuhnert, B. Rauer, R. Geiger, T. Kitagawa, I. Mazets,
   E. Demler, J. Schmiedmayer, Prethermalization revealed by the relaxation dynamics of full distribution functions. New J. Phys. 15, 075011 (2013)
- R. Bücker, A. Perrin, S. Manz, T. Betz, Ch. Koller, T. Plisson, J. Rottmann, T. Schumm, J. Schmiedmayer, Single-particle-sensitive imaging of freely propagating ultracold atoms. New J. Phys. 11, 103039 (2009)
- S. Dettmer, D. Hellweg, P. Ryytty, J. Arlt, W. Ertmer, K. Sengstock, D.S. Petrov, G. Shlyapnikov,
   H. Kreutzmann, L. Santos, M. Lewenstein, Observation of phase fluctuations in elongated Bose-Einstein condensates. Phys. Rev. Lett. 87, 160406 (2001)

References 65

A. Imambekov, I.E. Mazets, D.S. Petrov, V. Gritsev, S. Manz, S. Hofferberth, T. Schumm,
 E. Demler, J. Schmiedmayer, Density ripples in expanding low-dimensional gases as a probe of correlations. Phys. Rev. A 80, 033604 (2009)

- 48. J.-Y. Choi, S.W. Seo, W.J. Kwon, Y. Shin, Probing phase fluctuations in a 2D degenerate Bose gas by free expansion. Phys. Rev. Lett. **109**, 125301 (2012)
- 49. I.E. Mazets, Two-dimensional dynamics of expansion of a degenerate Bose gas. Phys. Rev. A **86**, 055603 (2012)
- S. Manz, R. Bücker, T. Betz, Ch. Koller, S. Hofferberth, I.E. Mazets, A. Imambekov, E. Demler, A. Perrin, J. Schmiedmayer, T. Schumm, Two-point density correlations of quasicondensates in free expansion. Phys. Rev. A 81, 031610 (2010)
- T. Schumm, J. Esteve, C. Figl, J.B. Trebbia, C. Aussibal, H. Nguyen, D. Mailly, I. Bouchoule, C.I. Westbrook, A. Aspect, Atom chips in the real world: the effects of wire corrugation. Eur. Phys. J. D 32, 171–180 (2005)
- 52. C. Menotti, S. Stringari, Collective oscillations of a one-dimensional trapped Bose-Einstein gas. Phys. Rev. A **66**, 043610 (2002)
- 53. H. Moritz, T. Stöferle, M. Köhl, T. Esslinger, Exciting collective oscillations in a trapped 1D gas. Phys. Rev. Lett. **91**, 250402 (2003)
- M. Kuhnert, R. Geiger, T. Langen, M. Gring, B. Rauer, T. Kitagawa, E. Demler, D. Adu Smith,
   J. Schmiedmayer, Multimode dynamics and emergence of a characteristic length scale in a one-dimensional quantum system. Phys. Rev. Lett. 110, 090405 (2013)
- 55. I. Hughes, T. Hase, Measurements and Their Uncertainties: A Practical Guide to Modern Error Analysis (Oxford University Press, Oxford, 2010)
- S. Hofferberth, I. Lesanovsky, T. Schumm, A. Imambekov, V. Gritsev, E. Demler, J. Schmiedmayer, Probing quantum and thermal noise in an interacting many-body system. Nat. Phys. 4, 489–495 (2008)
- 57. V. Gritsev, E. Altman, E. Demler, A. Polkovnikov, Full quantum distribution of contrast in interference experiments between interacting one dimensional Bose liquids. Nat. Phys. **2**, 705–709 (2006)
- H.-P. Stimming, N.J. Mauser, J. Schmiedmayer, I.E. Mazets, Fluctuations and stochastic processes in one-dimensional many-body quantum systems. Phys. Rev. Lett. 105, 015301 (2010)

# **Chapter 3 Isolated Quantum Systems Out of Equilibrium**

In this chapter we present a brief summary of the current framework of non-equilibrium dynamics in isolated quantum many-body systems, focusing, in particular, on the aspects that are of relevance to the dynamics of 1D Bose gases.

#### 3.1 Dynamics Following a Quench

The term non-equilibrium dynamics encompasses many different protocols and phenomena. Topics that are studied range from dynamical phase transitions and the exact time-evolution, to the emergence of a thermodynamical description in this time-evolution [1–8]. In the context of this thesis, we focus on the response of a system to a sudden perturbation as the conceptually most simple approach to an isolated system's non-equilibrium dynamics.

The general scheme of such a so-called *quantum quench* is depicted in Fig. 3.1. We start with a system that is described by a Hamiltonian  $\hat{H}$ . The initial state of the system can be a pure or a thermal state. The evolution is initialized by rapidly changing the Hamiltonian

$$\hat{H} \to \hat{H}',$$
 (3.1)

for example by varying an external field or, as in our case, by deforming the trapping potential. If the new state  $|\psi_0\rangle$  of the system after the quench is not an Eigenstate of the new Hamiltonian H', the quench will lead to a dynamical evolution of the system. For the expectation value of a generic observable  $\hat{A}$  this evolution is given by

$$\langle \hat{A}(t) \rangle = \langle \psi(t) | \hat{A} | \psi(t) \rangle$$
 (3.2)

where

$$|\psi(t)\rangle = \exp\left(-\frac{i}{\hbar}\hat{H}'t\right)|\psi_0\rangle.$$
 (3.3)

<sup>©</sup> Springer International Publishing Switzerland 2015 T. Langen, *Non-equilibrium Dynamics of One-Dimensional Bose Gases*, Springer Theses, DOI 10.1007/978-3-319-18564-4\_3

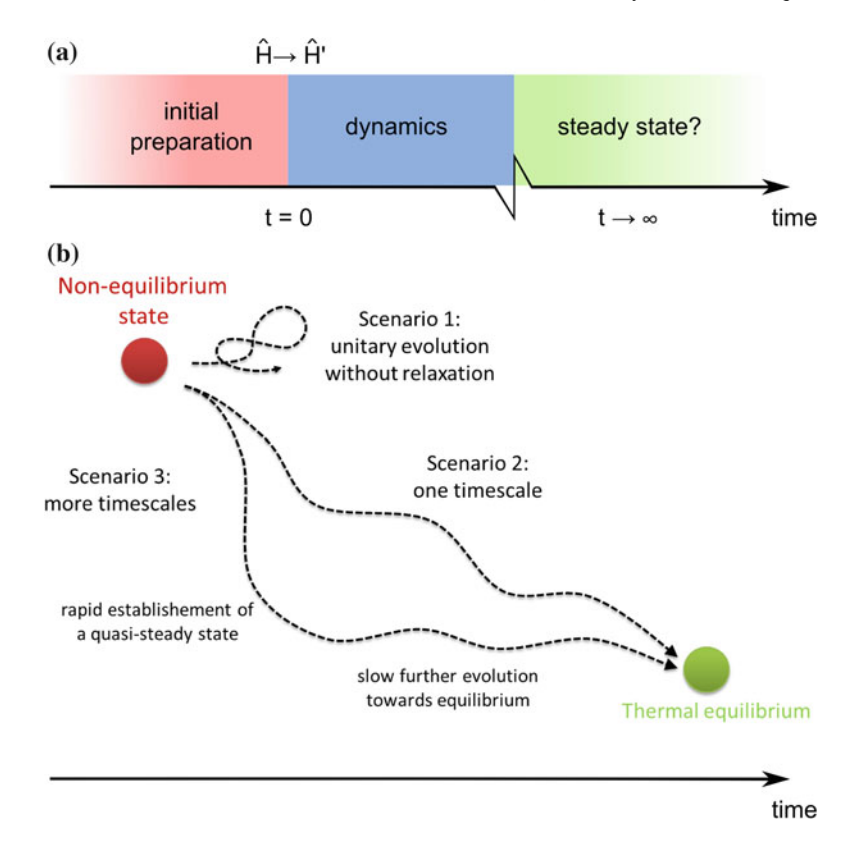


**Fig. 3.1** Dynamics following a quench. **a** The generic protocol of a quench. After the preparation of an initial state, the Hamiltonian of the system is rapidly changed, creating a non-equilibrium state. This induces a dynamical evolution. The question under study is whether a steady state emerges and if so, what kind of steady state is established. Figure adapted from [9]. **b** Several scenarios are conceivable for the dynamics. Following the strictly unitary evolution of quantum mechanics, thermal equilibrium can never be reached. However, alternative scenarios have been put forward, where the expectation values of observables might come arbitrarily close to their thermal values. The corresponding relaxation could happen on a single timescale, but also be more complex with one or more intermediate states that already share certain properties with the thermal equilibrium state

Based on this time evolution, a series of seemingly simple, yet very fundamental questions can be asked [10]:

- 1. Will the system relax?
- 2. If it relaxes, what are the properties of the steady state? Can the steady state be thermal?
- 3. If it is thermal, how are these thermal properties established? In other words, how is the memory of the initial state erased?

For a general Hamiltonian the time evolution (Eq. 3.3) is a very hard problem to solve. Thus, so far, no general answers to these questions exist [10]. From the theoretical

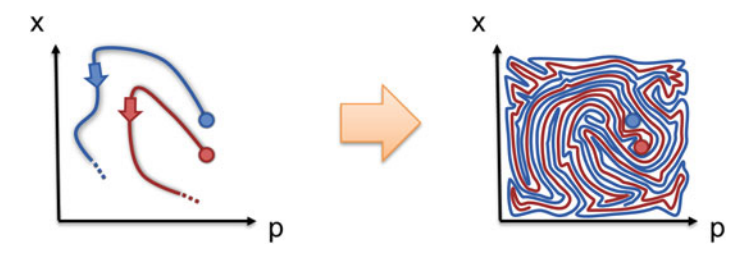


**Fig. 3.2** A sketch of classical ergodicity. Thermal equilibrium is independent of the initial state of a non-equilibrium evolution. After a sufficiently long time, both initial trajectories come arbitrarily close to any point in the position-momentum (x-p) phase space. This leads to the law of equal a priori probabilities for all microscopic states within a certain energy window. In the process, all memory of the initial state is dynamically erased

side, several scenarios are conceivable for the dynamics, which will be outlined in the following.

#### 3.1.1 Scenario I: No Relaxation

In many cases, a classical isolated system that is perturbed will relax to a unique thermal state that is defined by the system's energy. The most notable exception are integrable systems, which we will discuss separately in Sect. 3.2.

The microscopic mechanism responsible for the relaxation is the dynamical chaos that is present in the classical equations of motion. It results in dynamics, in which the system ergodically explores the whole phase space. The system is thus equally likely to be found at any point in phase space (see Fig. 3.2). This leads to a state that is independent of the initial conditions and can be described by the usual ensembles of statistical mechanics.

From a very purist point of view any evolution in the quantum world is unitary and reversible. The absence of chaos in the Schrödinger equation thus prevents thermalization in the classical sense. Consequently, as complicated as the time-evolution may be when many particles are involved, it should never lead to a unique thermal state that is independent of the initial state. In particular, if the system is in a pure state in the beginning of the evolution, it should never reach the mixed thermal state discussed in Chap. 1.

In a more mathematical formulation, thermalization corresponds to a situation where the time-average of a quantum evolution of an observable  $\hat{A}$  coincides with the expectation values of the thermodynamical ensembles [11]

$$\bar{A} = \lim_{\tau \to \infty} \frac{1}{\tau} \int_{\tau} d\tau' \left\langle \psi(\tau') \middle| \hat{A} \middle| \psi(\tau') \right\rangle \stackrel{!}{=} \frac{\text{Tr}(\hat{\rho}_{\text{eq}} \hat{A})}{\text{Tr}(\hat{\rho}_{\text{eq}})}. \tag{3.4}$$

Expanding the states  $|\psi(t)\rangle = \sum c_n |n\rangle$  in the Eigenstates of the new Hamiltonian  $\hat{H}'|n\rangle = E_n |n\rangle$ , with  $c_n = \langle \psi_0 | n \rangle$ , one finds that

$$\langle \hat{A} \rangle = \sum_{n,m} c_n^* c_m e^{i(E_n - E_m)t/\hbar} \langle n | \hat{A} | m \rangle.$$
 (3.5)

For non-degenerate Eigenstates the time average of this expression is given by the diagonal ensemble [6]

$$\bar{A} = \sum_{n} |c_n|^2 \langle n | \hat{A} | n \rangle \neq \frac{\text{Tr}(\hat{\rho}_{eq} \hat{A})}{\text{Tr}(\hat{\rho}_{eq})}.$$
 (3.6)

This result is markedly different from the prediction of any of the thermodynamical ensembles and, in particular, depends on the initial state for all times via the coefficients  $c_n$ . It thus seems to contradict the very essence of thermalization, as the thermal expectation value must be the same for any initial state. In the next scenario, we will see how this apparent contradiction can be resolved.

#### 3.1.2 Scenario II: Relaxation with One Timescale

Despite this contradiction, many quantum many-body systems relax to states where at least some observables are well described by thermal equilibrium. It was suggested that the relaxation can be understood by the fact that the Hilbert space of a large number of interacting atoms quickly becomes untraceably large and complex, leading to an apparent relaxation. In a single run, the total system evolves in a unitary way, but when calculating observables, their expectation values might become arbitrarily close to a thermal value. The key is to find observables that reach thermal steady states in a way that is robust with respect to the initial conditions.

Ideas how to grasp this intuition more formally have been around for a long time, for example in the form of a quantum ergodic theorem [12]. A particular well studied scenario is the Eigenstate thermalization hypothesis (ETH) [5, 6, 13]. To resolve the contradiction in Eq. 3.6, the ETH conjectures that the initial state of a non-equilibrium evolution already has thermal properties on the level of individual many-body Eigenstates. In other words,  $\langle n|\hat{A}|n\rangle$  coincides with the thermal expectation value for any Eigenstate  $|n\rangle$ . In terms of the density matrix this means that the diagonal elements contain the thermal properties while the off-diagonal terms correspond to the non-equilibrium physics. As described in Eq. 3.5, the off-diagonal terms vanish over time because of dephasing. Consequently, only a thermal state remains in the end. The range of applicability of the ETH is a topic of ongoing research. Numerical results in some systems (in particular ones with a chaotic classical limit) indicate that the ETH is fulfilled for generic few-body observables, i.e. observables that only act on

a small subsystem of the total system [6, 11]. An intuitive picture for this observation is that the isolated total system acts as a bath for its few-body subsystems [14].

#### 3.1.3 Scenario III: (Partial) Relaxation with More Timescales

Another possibility is that the relaxation might be more complex. For example, there might be partial relaxation only, where instead of a complete loss of memory, the system only partially forgets the initial conditions. Also, there might be different stages of relaxation connected to different time scales. The properties of these different relaxation stages are believed to contain important information about the properties of the system [15].

In general, the question to answer is what properties a system needs to be qualified as thermal. This question was first put forward by Berges and coworkers to describe the collision products observed in heavy-ion collisions [16, 17]. It was shown that some thermal aspects of a quantum many-body system might already form very early in the evolution, long before the system has actually reached thermal equilibrium. How this relaxation looks like in detail, depends on the observable under study.

Relaxation with different time scale has been predicted to occur in many systems [15, 16, 18–23]. It is important to note that this is different from the dynamics in systems which simply relax on different time scales because of the presence of different energy scales, like it is the case, for example, in an ensemble composed of electron and nuclear spins.

#### 3.2 The Role of Integrability

A special role in the context of non-equilibrium dynamics is played by the class of integrable systems.

The discovery and study of integrability and its consequences played an important role in the understanding of thermalization in classical mechanics. In one of the first numerical experiments, Fermi, Pasta, and Ulam studied the evolution of a chain of harmonic oscillators with non-linear couplings without observing any signs of thermalization [24]. This surprising result ultimately led to the development of chaos theory, which now forms the basis for the understanding of classical thermalization [25].

In classical systems the notion of integrability is well-defined by the existence of a full set of conserved quantities, which restricts the system to a sub-part of the total phase space. This precludes any chaotic behavior and thus makes thermalization impossible.

In quantum mechanics the definition is less clear. Different definitions that have been used include the existence of a complete set of linearly or algebraically independent operators, the existence of either a Bethe Ansatz or in any other way *exact* solution, or the occurrence of non-diffractive scattering processes [26–28].

Despite this lack of a clear definition, it is generally accepted that also in the quantum case, conserved quantities will strongly inhibit thermalization. <sup>1</sup>

Despite the absence of thermalization, relaxation and the emergence of thermal properties are still possible. It has been suggested that the relaxed state of such an integrable evolution can be described by the density matrix of a generalized Gibbs ensemble (GGE) [30]

 $\hat{\rho} = \frac{1}{Z} \exp\left(-\sum_{m} \lambda_{m} \hat{\mathcal{I}}_{m}\right) \tag{3.7}$ 

where  $\{\hat{\mathcal{I}}_m\}$  denotes a full set of conserved quantities,  $Z=\mathrm{Tr}[\exp(-\sum_m \lambda_m \hat{\mathcal{I}}_m)]$  is the partition function and m is a positive integer. The numbers  $\lambda_m$  are Lagrange multipliers associated with the conserved quantities. They are obtained by maximization of the entropy, under the condition that the expectation values of the conserved quantities are fixed to their initial values [31, 32]. The GGE is a direct generalization of the well-known thermodynamical ensembles. For example, in the case where only the total energy and the particle number are conserved, it reduces to the grand-canonical ensemble, where temperature and chemical potential play the role of the respective Lagrange multipliers (see Sect. 1.2 and Ref. [33]). If only the total energy is conserved, we recover the canonical or Gibbs ensemble. The reason why non-integrable systems, in contrast to integrable systems, can successfully be described by such a small number of conserved quantities so far remains unknown.

The generalized Gibbs ensemble is believed to be the final state of relaxation for an integrable system. However, a natural follow-up question is what happens if certain quantities are only approximately conserved. It has been conjectured that in this case the system will first relax to a meta-stable state described by a GGE. Subsequently, evolution towards thermal equilibrium will happen on a much slower time-scale [23, 34]. However, it is completely unclear in which way and how far the integrability has to be perturbed.

The question is of large theoretical interest, as this problem is very well studied in classical mechanics. In that case, the famous Kolmogorow-Arnold-Moser (KAM) theorem quantifies the effect of a weak non-integrability on the dynamics [10, 35]. No such theorem exists in the quantum case.

Experiments are ideally suited to study this issue, as the trapping potential that is used to confine the atoms automatically makes the systems slightly non-integrable [35–38]. One thus expects the interplay of thermalization and integrability to have a strong effect on the dynamics.

<sup>&</sup>lt;sup>1</sup>An interesting counterexample that illustrates the difficulty of the definition is given by the integrable Gross-Pitaevskii equation with periodic boundary conditions, which has such involved conserved quantities that thermalization can be observed in its phononic modes [29].

References 73

#### References

 P. Barmettler, M. Punk, V. Gritsev, E. Demler, E. Altman, Relaxation of antiferromagnetic order in spin-1/2 chains following a quantum quench. Phys. Rev. Lett. 102, 130603 (2009)

- 2. M. Heyl, A. Polkovnikov, S. Kehrein, Dynamical quantum phase transitions in the transverse-field ising model. Phys. Rev. Lett. **110**, 135704 (2013)
- 3. M. Eckstein, M. Kollar, P. Werner, Thermalization after an interaction quench in the Hubbard model. Phys. Rev. Lett. **103**, 056403 (2009)
- 4. D. Muth, B. Schmidt, M. Fleischhauer, Fermionization dynamics of a strongly interacting one-dimensional Bose gas after an interaction quench. New J. Phys. 12, 083065 (2010)
- 5. M. Srednicki, Chaos and quantum thermalization. Phys. Rev. E **50**, 888–901 (1994)
- M. Rigol, V. Dunjko, M. Olshanii, Thermalization and its mechanism for generic isolated quantum systems. Nature 452, 854–858 (2008)
- P. Reimann, Foundation of statistical mechanics under experimentally realistic conditions. Phys. Rev. Lett. 101, 190403 (2008)
- 8. S. Popescu, A.J. Short, A. Winter, Entanglement and the foundations of statistical mechanics. Nat. Phys. **2**, 754–758 (2006)
- M. Heyl, Nonequilibrium phenomena in many-body quantum systems. Ph.D. thesis, Ludwig-Maximilians-Universität, München, 2012
- A. Polkovnikov, K. Sengupta, A. Silva, M. Vengalattore, Colloquium: nonequilibrium dynamics of closed interacting quantum systems. Rev. Mod. Phys. 83, 863–883 (2011)
- M. Rigol, M. Srednicki, Alternatives to Eigenstate thermalization. Phys. Rev. Lett. 108, 110601 (2012)
- 12. J.V. Neumann, Beweis des Ergodensatzes und des H-Theorems in der neuen Mechanik. Z. Phys. **57**, 30–70 (1929)
- J.M. Deutsch, Quantum statistical mechanics in a closed system. Phys. Rev. A 43, 2046–2049 (1991)
- 14. M. Cramer, C.M. Dawson, J. Eisert, T.J. Osborne, Exact relaxation in a class of nonequilibrium quantum lattice systems. Phys. Rev. Lett. **100**, 030602 (2008)
- M. Moeckel, S. Kehrein, Crossover from adiabatic to sudden interaction quenches in the Hubbard model: prethermalization and non-equilibrium dynamics. New J. Phys. 12, 055016 (2010)
- 16. J. Berges, Sz. Borsányi, C. Wetterich, Prethermalization. Phys. Rev. Lett. 93, 142002 (2004)
- P. Braun-Munzinger, D. Magestro, K. Redlich, J. Stachel, Hadron production in Au-Au collisions at RHIC. Phys. Lett. B 518, 41–46 (2001)
- 18. D. Podolsky, G. Felder, L. Kofman, M. Peloso, Equation of state and beginning of thermalization after preheating. Phys. Rev. D 73, 023501 (2006)
- C. Kollath, A.M. Läuchli, E. Altman, Quench dynamics and nonequilibrium phase diagram of the Bose-Hubbard model. Phys. Rev. Lett. 98, 180601 (2007)
- R. Barnett, A. Polkovnikov, M. Vengalattore, Prethermalization in quenched spinor condensates. Phys. Rev. A 84, 023606 (2011)
- 21. A. Arrizabalaga, J. Smit, A. Tranberg, Equilibration in  $\varphi^4$  theory in 3 + 1 dimensions. Phys. Rev. D **72**, 025014 (2005)
- T. Kitagawa, A. Imambekov, J. Schmiedmayer, E. Demler, The dynamics and prethermalization of one-dimensional quantum systems probed through the full distributions of quantum noise. New. J. Phys. 13, 073018 (2011)
- M. Kollar, F.A. Wolf, M. Eckstein, Generalized Gibbs ensemble prediction of prethermalization plateaus and their relation to nonthermal steady states in integrable systems. Phys. Rev. B 84, 054304 (2011)
- E. Fermi, J. Pasta, S. Ulam, Studies of Nonlinear Problems. Los Alamos Scientific Laboratory Report No. LA-1940 (1955)
- N.P. Proukakis, S.A. Gardiner, M.J. Davis and M.H. Szymanska (eds.), Quantum Gases: Finite Temperature and Non-Equilibrium Dynamics. Cold Atoms Series, Vol. 1 (Imperial College Press, London, 2013)

- J.-S. Caux, J. Mossel, Remarks on the notion of quantum integrability. J. Stat. Mech. Theor. Exp. 2011, P02023 (2011)
- 27. B. Sutherland, Beautiful Models: 70 Years of Exactly Solved Quantum Many-Body Problems (World Scientific, Singapore, 2004)
- 28. C. Gogolin, M.P. Müller, J. Eisert, Absence of thermalization in nonintegrable systems. Phys. Rev. Lett. **106**, 040401 (2011)
- P. Grisins, I.E. Mazets, Thermalization in a one-dimensional integrable system. Phys. Rev. A 84, 053635 (2011)
- M. Rigol, V. Dunjko, V. Yurovsky, M. Olshanii, Relaxation in a completely integrable manybody quantum system: an Ab initio study of the dynamics of the highly excited states of 1D lattice hard-core bosons. Phys. Rev. Lett. 98, 050405 (2007)
- 31. E.T. Jaynes, Information theory and statistical mechanics. Phys. Rev. 106, 620–630 (1957)
- 32. R. Balian, From Microphysics to Macrophysics: Methods and Applications of Statistical Physics (Springer, Heidelberg, 2007)
- 33. K. Huang, Statistical Mechanics (Wiley, New York, 1987)
- 34. M. Stark, M. Kollar, Kinetic description of thermalization dynamics in weakly interacting quantum systems. arXiv:1308.1610 (2013)
- 35. T. Kinoshita, T. Wenger, D. Weiss, A quantum Newton's cradle. Nature 440, 900–903 (2006)
- M. Gring, M. Kuhnert, T. Langen, T. Kitagawa, B. Rauer, M. Schreitl, I.E. Mazets, D. Adu Smith, E. Demler, J. Schmiedmayer, Relaxation and prethermalization in an isolated quantum system. Science 337, 1318–1322 (2012)
- 37. T. Langen, R. Geiger, M. Kuhnert, B. Rauer, J. Schmiedmayer, Local emergence of thermal correlations in an isolated quantum many-body system. Nat. Phys. 9, 640–643 (2013)
- 38. J.P. Ronzheimer, M. Schreiber, S. Braun, S.S. Hodgman, S. Langer, I.P. McCulloch, F. Heidrich-Meisner, I. Bloch, U. Schneider, Expansion dynamics of interacting Bosons in homogeneous lattices in one and two dimensions. Phys. Rev. Lett. **110**, 205301 (2013)

## Chapter 4 Relaxation and Prethermalization in One-Dimensional Bose Gases

The study of relaxation processes remains a challenge despite considerable theoretical and experimental efforts [1]. Their difficulty is exacerbated by the scarcity of experimental tools for characterizing complex transient states. In this context, ultracold atoms provide unique opportunities to understand non-equilibrium phenomena because of the large set of available methods to probe and manipulate these systems.

As outlined in Chap. 3, the trapped 1D Bose gas is a particularly interesting system to study in experiments, because one expects a strong influence of its near-integrability on the non-equilibrium dynamics. Indeed the total absence of thermalization was observed in a landmark experiment by Kinoshita et al. [2]. In that experiment an array of 1D Bose gases in an optical lattice was taken out of equilibrium by transferring momentum to the atoms via a short Bragg pulse. Following this quench, the momentum distribution of the gases remained non-thermal even after thousands of collisions. It was later conjectured that this system had relaxed to a generalized Gibbs ensemble [3]. In contrast to that, without the presence of the lattice the system was three-dimensional, non-integrable and thus immediately thermalized.

Here, we make use of an atom chip to produce a 1D Bose gas. This has the advantage that a single system can be realized, which allows direct access to the intrinsic fluctuations of the 1D Bose gas.

The system is quenched by coherently splitting it into two parts. Matter-wave interferometry between the two parts is used to extract information about the dynamics. Measuring the full probability distributions of interference contrast reveals the prethermalization of the system to a non-thermal steady state, which can be characterized by an effective temperature.

This chapter is based on and also uses parts of Refs. [4–8]. Further information on this experiment can be found in the theses of Michael Gring and Maximilian Kuhnert [9, 10].

- M. Gring, M. Kuhnert, T. Langen, T. Kitagawa, B. Rauer, M. Schreitl, I. Mazets, D. Adu Smith, E. Demler, and J. Schmiedmayer Relaxation and Prethermalization in an Isolated Quantum System Science 337, 1318 (2012)
- T. Langen, M. Gring, M. Kuhnert, B. Rauer, R. Geiger, D. Adu Smith, I. Mazets, and J. Schmiedmayer Prethermalization in one-dimensional Bose gases: description by a stochastic Ornstein-Uhlenbeck process Eur. Phys. J. Special Topics 217, 43 (2013)
- D. Adu Smith, M. Gring, T. Langen, M. Kuhnert, B. Rauer, R. Geiger, T. Kitagawa, I. Mazets, E. Demler, and J. Schmiedmayer Prethermalization Revealed by the Relaxation Dynamics of Full Distribution Functions New J. Phys. 15, 075011 (2013)
- T. Langen, M. Gring, M. Kuhnert, B. Rauer, R. Geiger, I. Mazets,
   D. Adu Smith, T. Kitagawa, E. Demler and J. Schmiedmayer
   Studying Non-Equilibrium Many-Body Dynamics Using 1D Bose Gases
   AIP Conf. Proc. 1633, 11 (2014)

#### 4.1 Coherent Splitting as a Quench

A prerequisite for non-equilibrium experiments is the ability to precisely prepare and characterize both the initial non-equilibrium state and the expected thermal equilibrium state of the system under study. It is one of the key advantages of coherently split 1D Bose gases that both these states can be prepared and described with high precision.

In Chap. 3 we introduced a quench as the rapid change of a system's Hamiltonian. Using our atom chip this rapid change is realized by transforming the initial harmonic trapping potential of the gas into a double-well potential. The change of the potential splits an initial single 1D Bose gas coherently into two uncoupled parts with almost identical longitudinal phase profiles. The situation is depicted in Fig. 4.1. While the two resulting gases contain all the thermal fluctuations of the initial gas in their symmetric degrees of freedom, the anti-symmetric or *relative* degrees of freedom are influenced only by very weak fluctuations which result from the halving of the atom number during the splitting. As the different degrees of freedom are populated according to completely different energy scales, the system is intuitively expected to relax, eventually leading to a randomization of the relative phase profile [11–13]. The question we address here, is how far this randomization proceeds.

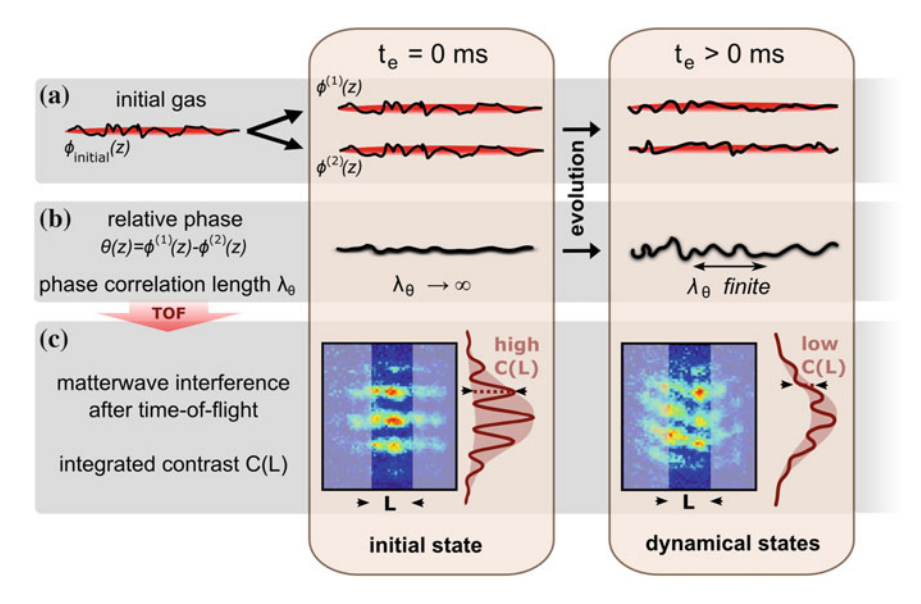


Fig. 4.1 Experimental scheme. a A single phase-fluctuating 1D Bose gas is coherently split into two uncoupled parts with almost identical phase distributions  $\phi^{(1)}(z)$  and  $\phi^{(2)}(z)$  (phases represented by the *black solid lines*). These evolve for a variable time t. b At t=0 ms, fluctuations in the local phase difference  $\theta(z)$  between the two gases are very small, but start to randomize during the evolution. The question we study is if, and if yes, how this randomization leads to the thermal equilibrium situation of completely uncorrelated gases. c shows typical experimental matter-wave interference patterns obtained by overlapping the two gases in time-of-flight (TOF). Differences in the local relative phase lead to a locally displaced interference pattern. Integrated over a length L, the contrast C(L) in these interference patterns is a direct measure of the strength of the relative phase fluctuations and thus enables the investigation of the dynamics. Figure taken from Ref. [8]

In other words: do the two gases completely forget their initial correlations as commonly associated with the approach to thermal equilibrium, or not? A comparison of the thermal equilibrium and the initial non-equilibrium state is presented in Fig. 4.2. It is interesting to note that thermalization in this system shows similarities with the emergence of a classical description. The splitting process initializes the atoms in a coherent superposition of being in either one of the gases. In thermal equilibrium they can only be located in a single gas. If the two gases thermalize, they thus dynamically emerge as two completely separate entities.

The experiment starts with a single 1D Bose gas that is prepared using our standard procedure which was described in Sect. 2.3.6. We typically prepare degenerate gases containing  $(2-10)\times 10^3$  atoms, corresponding to a peak linear density of  $n_{1D}=(20-80)$  atoms/ $\mu$ m and a chemical potential  $\mu/\hbar=2\pi\times(0.3-1)$  kHz. The trap frequencies are typically  $\omega_{\perp}=2\pi\times(2.0\pm0.1)$  kHz in the radial direction and  $\omega_z=2\pi\times(10\pm0.5)$  Hz in the longitudinal direction, respectively. The temperatures determined from density ripple measurements are in the range of  $T_{\rm in}=(20-120)$  nK. Thus the 1D condition  $k_BT_{\rm in},\,\mu<\hbar\omega_{\perp}$  is typically well fulfilled.

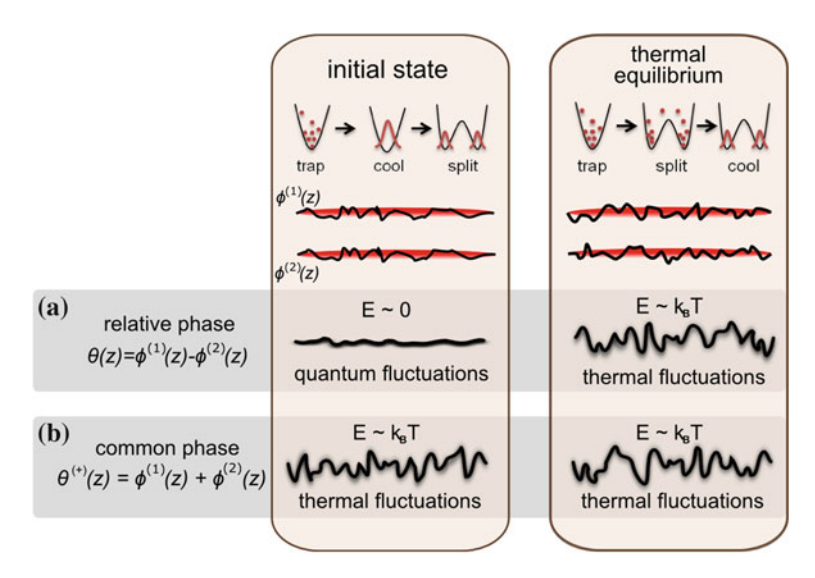


Fig. 4.2 Initial and thermal equilibrium state. Comparison of the initial non-equilibrium state prepared by the coherent splitting process and the thermal equilibrium state of two independent quasi-condensates. The system can be described by a combination of anti-symmetric degrees of freedom (a) and symmetric degrees of freedom (b). After the coherent splitting, the symmetric degrees of freedom contain all the thermal energy  $E \sim k_B T$  of the system, whereas the anti-symmetric degrees of freedom contain only the quantum noise resulting from the splitting process. In thermal equilibrium, all degrees of freedom contain the same amount of thermal energy and are thus characterized by the same temperature. Figure adapted from [5]

To realize the coherent splitting process, the static harmonic trap of the atoms is deformed into a fully controllable double-well potential by applying radio-frequency (RF) radiation via additional wires on the atom chip. Specifically, the RF current is linearly increased to an amplitude of 24 mA in 17 ms (Fig. 4.3). This creates a double well which is characterized by  $\omega_{\perp}=2\pi\times(1.4\pm0.1)$  kHz and  $\omega_{z}=2\pi\times(7.5\pm0.5)$  Hz in the longitudinal direction.

We characterize the evolution of the tunnel coupling between the two gases during the RF ramp using measurements of the relative phase correlation function of an equilibrium system of two coupled condensates, following the method presented in Ref. [14]. The equilibrium systems are prepared by splitting and subsequent cooling of a thermal gas using various double-well configurations, identical to the ones that are realized during the non-equilibrium splitting ramp. This enables an estimation of the tunnel coupling J as a function of RF current. These experiments indicate that the tunnel coupling decreases rapidly during the ramp and that the decoupling of the two gases happens on a timescale of less than  $500\,\mu\text{s}$ , about  $(2.5\pm0.5)$  ms before the end of the RF current ramp. This measurement is in good agreement with a simulation of the trapping potential (see Appendix B). The decoupling is thus faster than the characteristic timescale of the dynamics ( $\sim10\,\text{ms}$ ) and therefore realizes a quench [15].

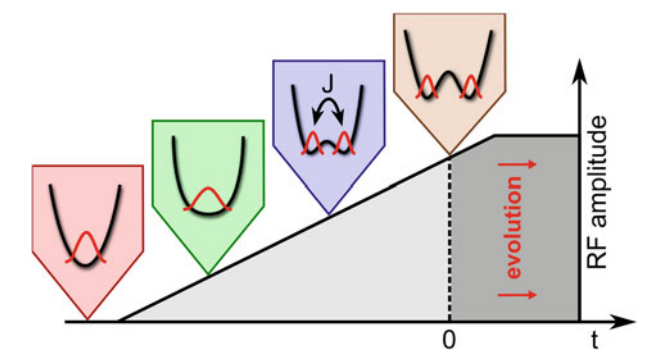


Fig. 4.3 Splitting process. An initial single gas is split into two parts by increasing the RF amplitude linearly to 24 mA. For low RF amplitudes, the radial harmonic confinement is deformed into a quartic potential. For higher RF amplitudes, a double well emerges. Initially, the two parts of the system are coupled with a tunnel coupling J. Increasing the RF amplitude further, this tunnel coupling rapidly decreases until the two parts are uncoupled at t = 0. To make the experiment robust again small changes in the double-well parameters, the RF amplitude is increased slightly further, before the gases are left to evolve. Note that many more splitting protocols can be achieved by tuning the RF ramp, e.g. a realization of the Unruh effect [16]

#### 4.2 Observation of a Non-thermal Steady State

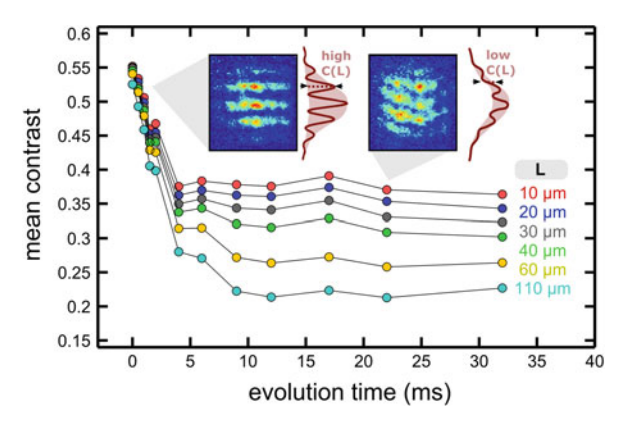
Similar to the equilibrium situation presented in Chap. 2, the dynamics of this system can be probed using matter-wave interferometry [17, 18]. In the following, we demonstrate that this allows for a comprehensive characterization of the transient states that are reached during the evolution.

After the splitting, the atoms are let to evolve in the double-well potential for a variable time. To study the resulting matter-wave interference pattern between the two parts of the system, all trapping potentials are turned off and the two gases expand and overlap in time-of-flight. The resulting interference pattern is imaged via absorption imaging after 15.7 ms.

For the data presented in this chapter, both the integrated imaging along the gases and the direct imaging of the interference pattern were used (see Sect. 2.3.5). As they give equivalent results, we restrict the discussion to the direct imaging in the following. Further details about the integrated imaging can be found in Refs. [5, 6, 9].

To study the dynamics we extract the mean interference contrast C(L) as a function of integration length L and evolution time t. The observations are summarized in Fig. 4.4. The mean contrast shows a rapid decay over a timescale of approximately  $10 \, \mathrm{ms}$ , before settling to a steady state. The decay depends strongly on integration length, which suggests that the dynamics are caused by an interplay of the many momentum modes that are occupied in 1D Bose gases. A detailed study of this length-scale dependent decay is presented in Refs. [10, 15].

Fig. 4.4 Evolution of the mean contrast. Following the quench, the system shows a rapid, length dependent loss of contrast, before reaching a steady state. Insets show examples of interference pictures obtained using the vertical imaging system



The observations demonstrate that the relative phase does indeed randomize and that the system relaxes to a steady state. However, the mere decay of the mean contrast does not provide any information about the nature of the steady state or about the processes that are responsible for the relaxation.

To extract more information, we thus go beyond simple mean values and measure the full quantum mechanical probability distribution function  $P(C^2)$  of the mean squared contrast  $\langle C(L)^2 \rangle$ . This is accomplished by repeating the experiment many times with identical initial conditions. As outlined in Sect. 1.5.1, the mean contrast is related to the two-point phase correlation function of the system. The FDFs contain also information about all even higher-order correlation functions and consequently allow the characterization of the many-body states in much more detail.

The results of this procedure are shown in Fig. 4.5. At t=0, we find peaked contrast distributions on all length scales, directly reflecting the coherence of the initial state. The distributions develop markedly different forms for different L during the evolution. For an integration over the whole length of the cloud ( $L=110\,\mu\text{m}$ ) they quickly develop an exponential shape. This exponential shape is characteristic for a state where the correlation length is much shorter than L [9]. On long length scales, the interferometer thus seems to have lost all its initial correlations. On the other hand, on short length scales ( $L=22\,\mu\text{m}$ ) the distributions remain peaked for all times probed although L is still significantly larger than the thermal coherence length. This shows that some of the high correlations that were prepared with the initial state did remain in the system. Intermediate length scales interpolate between these two extrema. Similar to the mean contrast, the FDFs change strongly during the first 10 ms of the evolution, but then reach a steady state.

The FDFs can be used to directly demonstrate that the emerging steady state is not the thermal equilibrium state. For a system of two uncoupled quasi-condensates the thermal equilibrium state is characterized by the fact that both gases are completely independent. In this case, anti-symmetric and symmetric degrees of freedom have identical temperatures, as expected for a thermal equilibrium state. As demonstrated in Sect. 2.4, we can prepare this situation in experiment by splitting

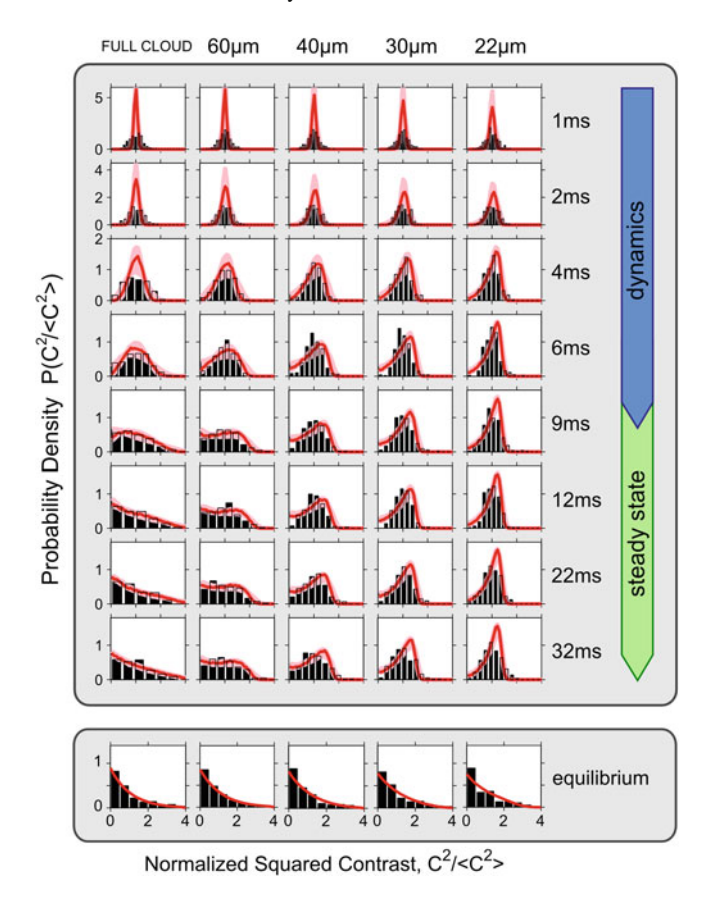


Fig. 4.5 Time evolution of the full distribution functions. Comparison of distributions of the normalized squared contrast  $C^2/\langle C^2 \rangle$  obtained in experiment to the theoretical description based on the homogeneous Luttinger liquid formalism [11]. The experimental data are plotted using histograms and the theoretical simulations using *solid red lines*. The *light red shaded* areas denote the errors resulting from the uncertainty of the experimentally measured theory input parameters. These input parameters were the experimentally measured values of the density in a single well  $n_{1D}=(32\pm4)/\mu m$ , the atom number imbalance  $\Delta N=(0.1\pm0.7)\%$ , the temperature  $T_{in}=(78\pm10)$  nK of the unsplit system, and the uncertainty of  $\pm0.5$  ms for the point in time where t=0. The significantly different behavior on short and long length scales directly visualizes the multimode nature of 1D Bose gases [15]. After a rapid evolution the FDFs settle to a steady state which is markedly different from a thermal equilibrium state at a temperature comparable to  $T_{in}$ . The relaxed state can thus not be thermal equilibrium. Figure adapted from [5]

a thermal, non-condensed gas using the same double-well potential as the one used in the non-equilibrium experiment. Subsequently, we perform evaporative cooling of the two thermal gases in the double well. This produces two completely independent quasi-condensates which have no mutual knowledge of each other. Mapping the FDFs in this situation, we find the characteristic exponential decay on all length

scales probed (see Fig. 4.5), as expected for a situation where the thermal coherence length  $\lambda_T$  is much smaller than any of the investigated length scales L. This behavior in thermal equilibrium differs strongly from the observations for the steady-state of the non-equilibrium evolution. We thus conclude, without the need to refer to any theoretical model that the observed state is not the thermal equilibrium state of the system.

#### 4.3 Theoretical Discussion and Interpretation

It is one of the advantages of 1D Bose gases that their physics can be described using simple, yet powerful tools. In the following, we use the Luttinger liquid formalism that was introduced in Sect. 1.4.3, to model the non-equilibrium evolution of the system.

In the experiment, the splitting is performed fast in comparison to the timescale set by the inverse chemical potential  $t_{\rm split} < \hbar/\mu = \xi_{\rm h}/c$ . Here  $\xi_{\rm h} = \hbar/mc$  denotes the healing length and  $c = \sqrt{gn_{\rm 1D}/m}$  is the speed of sound. Thus, there is no time for the atoms to correlate along the length of the gases and the longitudinal density fluctuations are completely random. For each of the N atoms the decision of going to either one of the gases is therefore random and uncorrelated. This leads to a binomial distribution of atom number fluctuations in each small segment of the 1D system, as illustrated in Fig. 4.6. In detail, the probability of finding  $N^{(1)}$  atoms in one gas, and  $N^{(2)}$  in the other one, is given by [9]

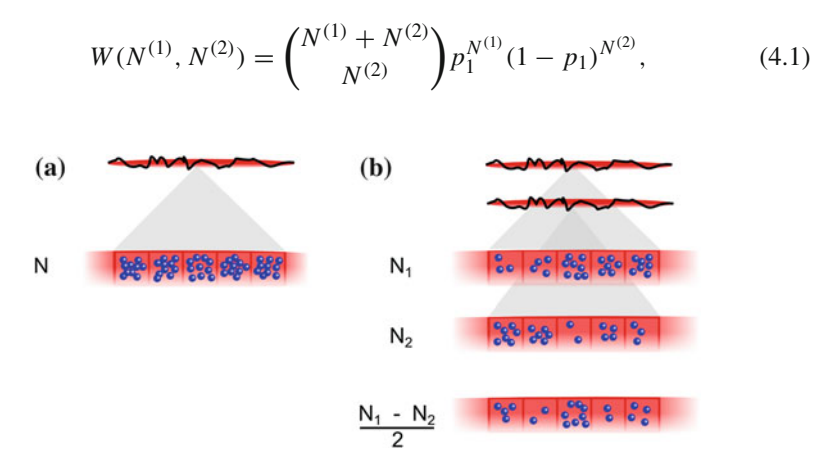


**Fig. 4.6** Local number fluctuations. The splitting distributes atoms into the two parts of the system. The probability of finding an atom in either one of the two parts is given by a binomial distribution. For a fixed atom number N in each small segment of the initial gas (a) the relative fluctuations after the split (b) are given by  $\langle |(N^{(1)} - N^{(2)})/2|^2 \rangle = N/4$  (see text and Ref. [9]). These fluctuations are introduced into the system in addition to the thermal fluctuations which are already present. This brings the system out of equilibrium

where  $p_1$  is the probability of an atom to go to one particular well. For a balanced splitting this probability is given by  $p_1 = 1/2$ . The probability for a certain atom number difference  $\Delta N = (N^{(1)} - N^{(2)})/2$  between the two gases can thus be found from

$$W(N/2 - \Delta N, N/2 + \Delta N) = \binom{N}{N/2 - \Delta N} p_1^{N/2 - \Delta N} (1 - p_1)^{N/2 + \Delta N}.$$
 (4.2)

The variance of this distribution is  $\langle |\Delta N|^2 \rangle = N/4$ . As the number of atoms in a segment of length L is given by  $N = 2n_{1D}L$ , one finds

$$\langle \hat{\nu}(z)\hat{\nu}(z')\rangle = \frac{n_{1D}}{2}\delta(z-z')$$
 (4.3)

for the density fluctuations  $\hat{\nu}(z)$  created in the splitting process. In the Luttinger liquid description (see Sect. 1.5.1) these fluctuations can be associated to the phonon modes in momentum space. This yields

$$\langle \hat{\nu}_k \hat{\nu}_{k'} \rangle = \frac{n_{1D}}{2} \delta_{k,-k'}, \tag{4.4}$$

which means that no correlations between modes with different momenta are present in the initial state. Consequently, all phonon modes are populated with the same amount of energy. Because of the linear dispersion relation, this leads to a 1/k dependence of their occupation numbers.

The relative phase profile  $\hat{\theta}(z)$  is almost zero after the splitting. Its fluctuations follow via the minimum uncertainty relation  $[\hat{\phi}_k^{\dagger}, \hat{n}_{k'}] = [\hat{\phi}_{-k}, \hat{n}_{k'}] = -i\delta_{k,k'}$ , and are given by

$$\langle \hat{\theta}_k \hat{\theta}_{k'} \rangle = \frac{1}{2n_{1D}} \delta_{k,-k'}. \tag{4.5}$$

The initial conditions for phase and density fluctuations can be used to calculate the evolution of the relative phase. A comparison with Eq. 1.74 reveals the non-equilibrium dynamics of the system [11]

$$\langle |\hat{\theta}_{k}|^{2} \rangle = \frac{4m^{2}c^{2}}{\hbar^{2}k^{2}n_{1D}} \frac{n_{1D}}{2} \sin(\omega_{k}t) + \frac{1}{2n_{1D}} \cos(\omega_{k}t)$$

$$= \frac{\pi}{2|k|K} \frac{\sin^{2}(c|k|t) + S_{k}^{2} \cos^{2}(c|k|t)}{S_{k}} \quad (k \neq 0), \tag{4.6}$$

$$\langle |\hat{\theta}_0|^2 \rangle = \frac{1}{2n_{1D}} + \left(\frac{c\pi t}{K}\right)^2 \frac{n_{1D}}{2} \quad (k=0),$$
 (4.7)

where  $S_k = kK/\pi n_{\rm 1D}$  is the structure factor. For the density fluctuations, one finds the same result, just with different initial conditions. In other words, at t=0 we have a squeezed state: the relative phase fluctuations are suppressed with respect to their

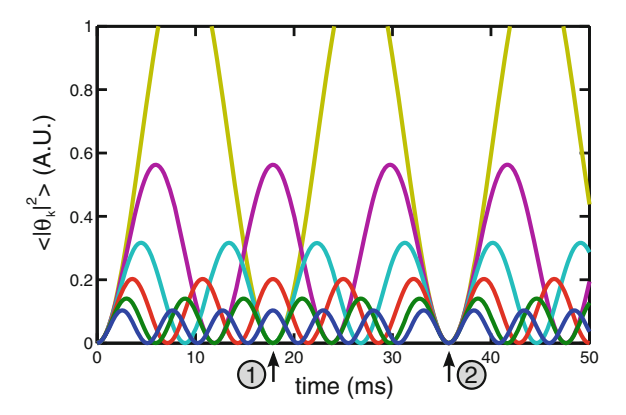


Fig. 4.7 Multimode nature of 1D Bose gases: Oscillations. At early times, the energy stored in the density fluctuations is transferred to the phase fluctuations, leading to a rapid increase of  $\langle |\theta_k|^2 \rangle$  for all  $k=2\pi/\mathcal{L}\times n$ , where  $\mathcal{L}$  is the system size and  $n\neq 0$  is an integer. In the plot, different colors depict the different values of k. Later, the dynamics of the system is characterized by oscillations of fluctuations between phase and density. As all excitations oscillate with different frequencies  $\omega_k=ck$ , they dephase over time. Maximum dephasing and thus the establishment of a steady state is achieved on a time scale given by the quarter of an oscillation period  $T=\mathcal{L}/4c$  of the n=1 mode (1). In this simplified homogeneous model, the periodic boundary conditions result in a perfect rephasing of all modes after 2T. This leads to a perfect revival of the initial state (2). In experiment, these revivals are not observed, as the trap makes the spectrum more complex than assumed in this simple model [20]. The parameters in this plot are c=1.4 mm/s,  $\mathcal{L}=100\,\mu\text{m}$ . Figure adapted from [9]

equilibrium value. On the contrary, there is a huge excess of noise in the relative density fluctuations.

Over time, density fluctuations oscillate into phase fluctuations and vice versa. Similar oscillations have recently been observed in a 2D Bose gas after an interaction quench [19]. As the oscillations have different characteristic frequencies  $\omega_k$  corresponding to their momenta k, they dephase over time. The resulting time evolution of the phase variance  $\langle |\phi_k|^2 \rangle$  is illustrated in Fig. 4.7.

For a single realization of the relative phase profile one finds

$$\theta(z, \{\lambda_k, \lambda_{\theta k}\}) = \frac{1}{\sqrt{\mathcal{L}}} \sum_{k} \sqrt{\langle |\hat{\theta}_k|^2 \rangle} \lambda_k \sin(kz + \lambda_{\theta k}), \tag{4.8}$$

where  $\lambda_k$  and  $\lambda_{\theta k}$  are random variables which are used in the numerical simulation of the dynamics [11].

This expression describes the superposition of many sinusoidal waves, which modulate the phase profile on a length scale  $\sim 2\pi/k$ . Experimentally probing the system on different length scales therefore corresponds to a filtering of the effects of different modes. This is illustrated in Fig. 4.8. The observation of a length dependent

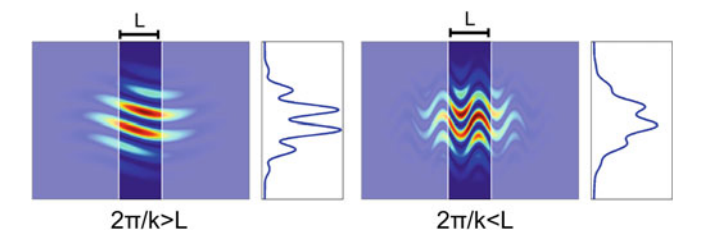


Fig. 4.8 Multimode nature of 1D Bose gases: Interference. The phase profile is a superposition of many sinusoidal oscillations corresponding to the eigenmodes  $\omega_k = ck$  of the system. Integrating the interference pattern over a certain length L acts as a filter for these oscillations. The figure shows two artificial interference patterns in which only one mode with a momentum  $k = 2\pi/\lambda$  is populated. If  $L < \lambda$  the phase only varies slowly within L, resulting in a high contrast of the integrated line profile. The only consequence is a shift of the mean relative phase  $\theta(L)$ . If, however,  $L > \lambda$ , phase fluctuations within L lead to a decrease in the integrated contrast. Figure from [5, 9]

decay of contrast thus is a direct visualization of the multimode nature of 1D Bose gases [10, 15].

The individual sinusoidal waves are populated with a certain amplitude, which is given by the phase variance  $\langle |\hat{\theta}_k(t)|^2 \rangle$ . Over time, the dephasing of the excitations leads to an increase (decrease) of the amplitude of the phase (density) fluctuations. This results in a progressive randomization of the relative phase field  $\theta(z)$ . Eventually, the energy associated with the phase fluctuations equilibrates with the energy associated with the density fluctuations and the system reaches a steady state.

The phase variance is of utmost importance for the understanding of the dynamics, as it allows the direct calculation of the two-point phase correlation function using Eq. 1.81. We find that the state resulting after a dephasing of all modes has exponentially decaying correlations

$$C(z, z') = \exp(-|z - z'|/\lambda_{\text{eff}}), \tag{4.9}$$

resembling the thermal equilibrium state. However, it decays with an effective coherence length  $\lambda_{\rm eff}=\hbar^2 n_{\rm 1D}/mk_BT_{\rm eff}$  instead of the thermal coherence length. This effective coherence length is connected to an effective temperature

$$k_B T_{\text{eff}} = \frac{g n_{\text{1D}}}{2}.\tag{4.10}$$

This effective temperature is determined by the initial conditions of the splitting. It corresponds to the energy  $\langle \hat{H}^{(-)}(t=0) \rangle = \frac{\pi}{K} \frac{\hbar c}{2} \langle |\nu_k(0)|^2 \rangle$  which is initially stored in each mode via the density fluctuations (Eq. 4.4). Note that this initial energy is independent of k, which means the splitting equally distributes energy among the excitations [7, 11]. Together with the dephasing this emulates thermal statistics in the steady state.

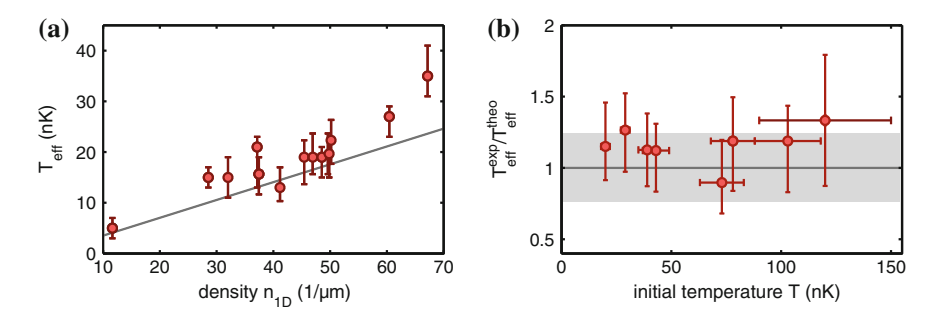


**Fig. 4.9** Scaling laws for the effective temperature. **a** Measuring the effective temperature for a large set of densities we verify that  $T_{\rm eff} = g n_{\rm 1D}/2$ . **b** Independence of the effective temperature from the temperature of the initial gas. Figure adapted from [4, 5]

The two-point correlation function as well as all higher-order correlation functions are contained in the full distribution function (FDF) of the phase  $\theta$  and the contrast C [11]

$$P(C,\theta) = \prod_{k} \int_{-\pi}^{\pi} d\lambda_{k} \frac{d\lambda_{\theta k}}{2\pi} \int_{0}^{\infty} \lambda_{k} e^{-\lambda_{k}^{2}/2} \times \delta\left(C(L)e^{i\theta(L)} - n_{1D} \int_{-L/2}^{L/2} dr e^{i\theta(r,\{\lambda_{k}\lambda_{\theta k}\})}\right), \tag{4.11}$$

where L denotes the integration length over which the system is probed.

A detailed discussion of the functional form of the FDF can be found in Ref. [9]. The distribution of the phase is investigated in Refs. [10, 15]. Here, we study the distribution of the mean contrast squared  $P(C^2)$ . As shown in Fig. 4.5, the description of Eq. 4.11 is in very good agreement with the experimental data for all times and length scales that were investigated. As the two-point correlation function, the FDFs approach a thermal form with an effective temperature, once the excitations have dephased [18, 21].

Although it is not the thermal equilibrium state, the quasi-steady state still shows thermal properties in all even correlation functions. This can be further elaborated by fitting the experimental data with the theoretically expected shape for a thermal equilibrium state of a certain temperature. For the experimentally prepared thermal equilibrium state this procedure yields, as expected, a temperature which corresponds to the temperature measured independently using the density ripples. In contrast to this, the quasi-steady state reveals thermal FDFs corresponding to the effective temperature  $T_{\rm eff}$ , which can be significantly lower than the temperature of the system. For the data presented in Fig. 4.5, we find  $T_{\rm eff}=14\,{\rm nK}$ , almost an order of magnitude lower than the temperature of the initial gas  $T_{\rm in}=100\,{\rm nK}$ . Repeating the experiment for different initial densities and temperatures allows the confirmation of the scaling properties of the effective temperature (Eq. 4.10) for a wide range of parameters. The results are shown in Fig. 4.9 and provide further evidence for our theoretical analysis of the dynamics.

To summarize: the system relaxes to a non-thermal steady state. This non-thermal steady state already exhibits pronounced thermal features. The mechanism leading to this state is a simple dephasing of the non-interacting excitations of the system.

Such thermal-like non-equilibrium states are called prethermalized states. They have first been predicted to explain the unexpected results in heavy-ion collision experiments, where the reaction products appear to be in equilibrium long before this is physically possible [22, 23]. It has further been suggested that they play a role in the description of the early, inflationary phase of the universe [24–26] and in many solid-state systems [27–30]. The experiments with ultracold atoms presented in this thesis and in Refs. [4–6, 9, 10] are the first direct observation of such a state. The similarities of prethermalized states in different types of systems might play a central role in the establishment of a general framework for non-equilibrium dynamics.

A direct connection can also be made to the relaxation dynamics of integrable systems. As discussed in Chap. 3, such systems are predicted to relax to a generalized Gibbs ensemble (GGE). In contrast to the thermal equilibrium state, where only one temperature is needed to describe the system, integrable systems should exhibit more temperatures. These additional temperatures are directly connected to the conserved quantities of the integrable system. Our observation of different temperatures for the anti-symmetric modes and symmetric modes thus leads us to conjecture that the observed state can be described by a GGE. A detailed investigation of this subject is presented in Chap. 6.

### 4.4 Approximate Description Using an Ornstein-Uhlenbeck Process

The derivation of the analytical result for the FDFs (Eq. 4.11) is mathematically demanding as, in principle, an infinite number of even correlation functions has to be calculated [21]. However, a simple approximate description can be found by identifying analogies with tunnel coupled gases in equilibrium. This complementary approach was developed by Igor Mazets and is based on an effective classical field model [6]. It provides valuable insights into the correlation properties of the non-equilibrium states, is numerically very efficient, and enables a simple modeling of the technical aspects of the experimental setup. It is directly based on the Ornstein-Uhlenbeck description that was introduced in Sects. 1.4.6 and 1.5.2 to study equilibrium properties of 1D gases [31–33], providing a straightforward link between equilibrium and non-equilibrium dynamics.

In this model, the operators  $\hat{\nu}_k$  and  $\hat{\theta}_k$  describing density and phase fluctuations, respectively, are approximated using classical fields  $\nu_k$  and  $\theta_k$ . The equations of motion for these fields describe two coupled harmonic oscillators [34, 35]

$$\dot{\nu}_k = n_{1D} \left( \frac{\hbar k^2}{2m} \right) \theta_k, \quad \dot{\theta}_k = -\frac{1}{\hbar n_{1D}} \left( \frac{\hbar^2 k^2}{2m} + 2mc^2 \right) \nu_k.$$
 (4.12)

Neglecting the small initial phase fluctuations, their solution yields

$$\theta_k(t) = -\frac{\hbar^2 k^2 / (2m) + 2mc^2}{n_{1D}\hbar\omega_k} \nu_k(0) \sin(\omega_k t), \tag{4.13}$$

where the eigenfrequency of a mode with momentum k is given by

$$\omega_k = \sqrt{\left(\frac{\hbar k^2}{2m}\right)\left(\frac{\hbar k^2}{2m} + \frac{2mc^2}{\hbar}\right)} = ck\sqrt{1 + \xi_h^2 k^2/4} \approx ck. \tag{4.14}$$

Here,  $\xi_h$  denotes the healing length and we have used the long-wavelength approximation  $k \ll \xi_h^{-1}$  in the last step. This yields an expression for the phase variance that is identical to the result obtained in Eq. 4.6. As already described above, the initial high density fluctuations periodically turn into phase fluctuations and dephase, which leads to the observed decrease in interference contrast. For the time-evolution of the phase correlation function we find

$$\begin{split} \mathcal{C}(\bar{z},t) &= \exp\left\{-2\int_{0}^{\xi_{\rm h}^{-1}} dk \, \frac{\sin^{2}(ck\,t)}{\pi n_{\rm 1D}\xi_{\rm h}^{2}k^{2}} [1 - \cos(k\bar{z})]\right\} \\ &= \exp\left\{-\frac{2mc^{2}t}{\hbar\mathcal{K}} \left[\Xi(2c\xi_{\rm h}^{-1}t) + \frac{\bar{z}}{2ct}\Xi(\xi_{\rm h}^{-1}\bar{z}) \right. \\ &\left. - \frac{1}{2} \left|1 - \frac{\bar{z}}{2ct}\right| \Xi(|2ct - \bar{z}|\xi_{\rm h}^{-1}) - \frac{1}{2} \left|1 + \frac{\bar{z}}{2ct}\right| \Xi(|2ct + \bar{z}|\xi_{\rm h}^{-1})\right]\right\}, \end{split}$$

$$(4.15)$$

where  $K^{(s)} = \pi n_{1D} \xi_h$  is the Luttinger liquid parameter for a single gas,  $\Xi(x) = (\cos x - 1)/x + \operatorname{Si}(x)$  and  $\operatorname{Si}(x) = \int_0^x dy \, y^{-1} \sin(y)$  is the sine integral.

If we are not interested in details of the correlation function behavior on the experimentally unresolved length scale  $\bar{z} \lesssim \xi_{\rm h}$ , we can simultaneously assume  $\xi_{\rm h}^{-1}ct\gg 1$ ,  $\bar{z}\xi_{\rm h}^{-1}\gg 1$ , and  $|2ct-\bar{z}|\xi_{\rm h}^{-1}\gg 1$ . In this limit we obtain

$$C(\bar{z},t) = \begin{cases} \exp[-\pi \bar{z}/(2K^{(s)}\xi_{h})], & 0 \le \bar{z} < 2ct \\ \exp[-\pi mc^{2}t/(\hbar K^{(s)})], & \bar{z} \ge 2ct. \end{cases}$$
(4.16)

We see from Eq. 4.16 that the phase correlations first decrease exponentially and then stabilize at a certain level. The crossover between exponential decrease and constant values of  $C(\bar{z}, t)$  are time-dependent.

The essence of the approach is to compare Eq. 4.16 to its counterpart  $C_J(\bar{z})$  (Eq. 1.88) in the stationary regime of two tunnel-coupled quasi-condensates at finite temperature T [36]. This comparison leads to the conclusion that the time-dependent correlation function  $C(\bar{z},t)$  during the dephasing emulates that of a coupled equilibrium system with the effective temperature and effective time-dependent phase-locking length

$$T_{\rm eff} = \frac{mc^2}{2k_{\rm B}}, \quad l_J^{\rm eff}(t) = 2ct.$$
 (4.17)

A quasi-steady state is reached on a timescale  $t \gg \tau$ , where the typical evolution time is [12]

$$\tau = \frac{K^{(s)}\xi_{h}}{\pi c} = \frac{\hbar K^{(s)}}{\pi m c^{2}} = \frac{n_{1D}\xi_{h}^{2}}{c}.$$
 (4.18)

For the parameters of the dataset shown in Fig. 4.10 we find  $\tau \sim 5$  ms, in good agreement with our experimental observations that the steady state is reached for  $t \gtrsim 10$  ms. The effective length scale is directly related to an effective coupling  $J_{\rm eff}(t) = \hbar/4m \, l_J^{\rm eff}(t)^2$ . In the limit  $t \gg \tau$  the effective coupling vanishes and we recover the prethermalized state studied in the previous section. Although the system is still far from equilibrium, it appears thermal-like and can be characterized by an effective temperature  $T_{\rm eff}$ , which is independent of the initial temperature of the gas. In particular, symmetric and anti-symmetric degrees of freedom have not yet equilibrated, but all dynamics can be attributed to dephasing within the relative degrees of freedom [4].

In the approach to the prethermalized state,  $l_J^{\rm eff}$  plays the role of a characteristic length scale over which the system forgets the initial correlations for a given evolution time. The scaling of  $l_J^{\rm eff}$  is that of a light cone [7, 37–40], reflecting that correlations in this many-body quantum system spread with a finite velocity given by the speed of sound. In Chap. 5 the first direct experimental observation of such a light-cone-like emergence of thermal correlations is presented.

The typical correlation length reached in the prethermalized state is

$$\lambda_{\text{eff}} = 2c\tau = \frac{2K^{(s)}\xi_{\text{h}}}{\pi} \equiv \lambda_T(T_{\text{eff}}). \tag{4.19}$$

For our typical parameters  $\lambda_{\rm eff} \gg \lambda_T$ , which corresponds to much higher correlations than expected in thermal equilibrium [15]. This can be interpreted as a signature for the strong memory of the initial state that is present in the prethermalized state.

The effective model enables the simulation of the FDFs for any evolution time t and any sampling length greater then the healing length using an Ornstein-Uhlenbeck stochastic process that develops in space, along the major axis of the trap (see also Sect. 1.4.6). In our case, the ratio  $T_{\rm eff}/n_{1D}$  defines the diffusion, and the effective inter-well coupling provides the restoring force. To construct the FDFs, we use the exact updating formula Eq. 1.90 to simulate individual phase profiles [41]. Properties of the experimental setup, such as finite imaging resolution, trapping potential and time-of-flight expansion are directly taken into account in this procedure [14]. A statistical analysis yields the FDFs. The method is computationally fast and efficient, and especially suited for finite-size atomic clouds. In Fig. 4.10 we compare the results of the Ornstein-Uhlenbeck simulation to our experimental data. We find very good agreement for all length scales and evolution times probed, both for the non-equilibrium and the equilibrium cases.

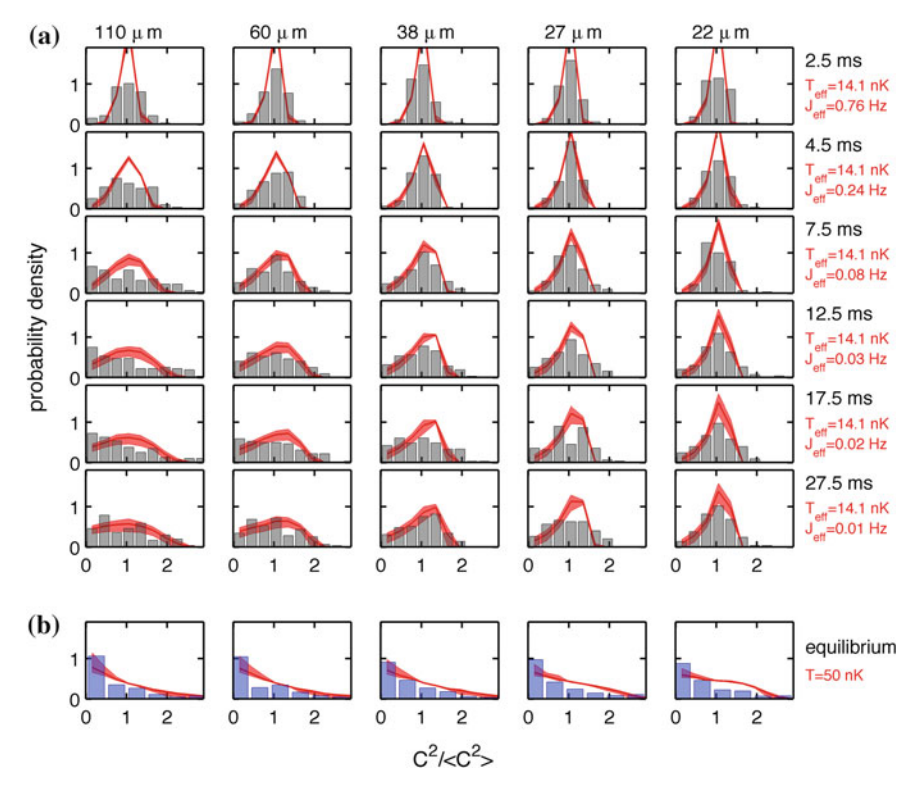


Fig. 4.10 Time evolution of the full distribution functions compared to the classical field model. a The experimental full distribution functions (FDFs) of squared contrast  $C(L)^2/\langle C^2\rangle$  (bars) are well described by the effective Ohrnstein-Uhlenbeck model described in the text (solid line). Compared to the Luttinger liquid calculation presented in Fig. 4.5, this model allows for a more simple approximate description of the dynamics. Shaded areas denote the statistical uncertainty corresponding to the 170 samples used in the experimental data. b Typical equilibrium FDFs measured by splitting a thermal gas and creating two completely independent quasi-condensates. The strong difference in shape of the thermal FDFs and the observed non-equilibrium steady state directly demonstrates that this steady state is not thermal equilibrium. Figure from [6]

#### 4.5 Dynamics Beyond Prethermalization

In classical mechanics the question of near-integrability is well-defined by the Kolmogorow-Arnold-Moser (KAM) theorem. This theorem states that an integrable system will be restricted to a region of phase space which is defined by its conserved quantities, even if these conserved quantities are only approximately realized. In contrast to that, in quantum mechanics, neither the definition of integrability, nor the relaxation of generic integrable systems are properly understood (see Chap. 3). To gain a deeper understanding, it is thus insightful to study quantum systems where the

conserved quantities are perturbed. The general belief is that the resulting dynamics will strongly depend on the type of perturbation.

In Sect. 4.3 we have demonstrated that the 1D Bose gases realized in experiment do not relax to thermal equilibrium. The behavior is very closely connected to the integrability of the Lieb-Liniger gas or, equivalently, the integrability of the Luttinger liquid as the low-energy limit of the Lieb-Liniger gas. However, the 1D Bose gas realized in our experiments is only nearly-integrable, most notably, because radial trapping states can affect the 1D dynamics.

It has been conjectured that in this case the observed prethermalized state is only an intermediate steady state on the way to thermal equilibrium, its lifetime being directly related to the degree of integrability breaking [42, 43]. Alternatively, also the opposite have been suggested, namely that the quasi-particles of the experimentally realized 1D Bose gas could be unaffected by the radial states [44]. Thus, a natural question to study is how long the prethermalized state will persist. A detailed discussion of the measurements that are presented in the following can be found in the thesis of Maximilian Kuhnert [10].

To study this situation, we follow the same experimental procedure as before but let the system evolve for longer evolution times in the double-well trap. The coherent splitting process initializes the system with different energies in the symmetric and anti-symmetric modes. Thermalization requires an equilibration of symmetric and anti-symmetric modes, which would manifest in a rise of the initially very small effective temperature of the prethermalized state. Microscopically, this corresponds to the relaxation of the momentum distribution to a Bose-Einstein distribution.

The dynamical values of  $T_{\rm eff}(t)$  are extracted by fitting the mean squared contrast  $\langle C^2(L) \rangle$  with the prediction of Eq. 1.87 [15]. From the result of this fit, a correlation length and thus a temperature can be obtained. Similar results can be found by studying the corresponding FDFs.

Before studying the raise of  $T_{\rm eff}(t)$ , it is essential to characterize technical heating that is caused by fluctuations of the experimental setup. This is possible using measurements with equilibrium gases. In the double-well trap we find this heating to be negligible for the time scales of the experiments [10]. The maximum evolution times  $t \sim (200-300)\,\rm ms$  are determined by a constant loss of atoms, which is caused by background gas collisions and three-body losses [10]. We note that previous measurements presented in Ref. [4] detected a slow heating of the equilibrium gases with time. These experiments were affected by a higher technical noise in the experiment, as well as a clock offset between the RF source and the control computer. This caused the ideal global phase for the switch-off (see Fig. 2.13) to change with evolution time, leading to a loss of contrast with time, which mimicked heating.

In Fig. 4.11 we present the evolution of  $T_{\rm eff}(t)$  following the splitting of the initial gas. For cold initial temperatures we find almost no change of the effective temperature. From this, we conclude that the integrability breaking mechanisms play a minor role for the dynamics and that the prethermalized state is very stable. Notably, we do not observe any rephasing of the excitations, which is predicted in the homogeneous theory due to the periodic boundary conditions (see Fig. 4.7). The reason for this is that the spectrum in the trapped system is much more complex, leading to rephasing

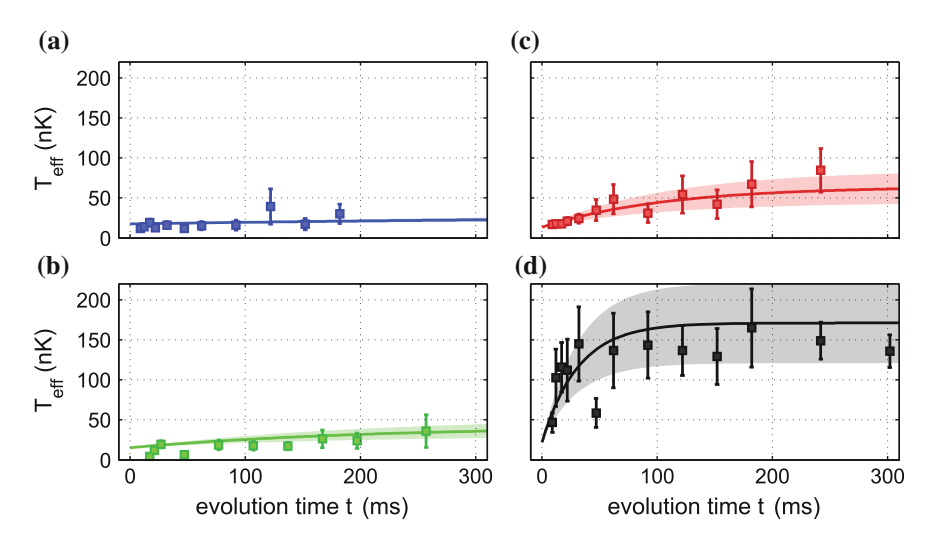


Fig. 4.11 Long-time behavior of the effective temperature. Evolution of the effective temperature  $T_{\rm eff}(t)$  of the anti-symmetric degrees of freedom (*squares*) for various initial temperatures  $T_{\rm in} = (43\pm6)~{\rm nK}$  (a),  $(69\pm11)~{\rm nK}$ (b),  $(115\pm20)~{\rm nK}$  (c), and  $(320\pm50)~{\rm nK}$  (d). The radial trap frequency corresponds to  $\sim$ 70 nK. The data reveals a relaxation to a final temperature  $T_{\rm fin} \approx [T_{\rm in} + T_{\rm eff}(0)]/2$ . *Solid lines* represent fits. Figure adapted from [10]

that is only incomplete and happens at much longer evolution times than predicted from the simplified homogeneous model [20].

The observations change drastically when the temperature of the initial gas is increased above the radial trapping frequency  $k_B T_{\rm in} \geq \hbar \omega_{\perp}$ . As a consequence, a significant increase of  $T_{\rm eff}(t)$  with time can be observed. This eventually leads to a second steady state which appears to be characterized by the temperature

$$T_{\rm fin} \approx \frac{T_{\rm in} + T_{\rm eff}(0)}{2}.\tag{4.20}$$

This temperature describes a situation where the initially different energies of the symmetric and anti-symmetric degrees of freedom have equilibrated [10]. It thus corresponds to the value that is expected in thermal equilibrium. A possible explanation for the system's thermalization is provided by the rate with which  $T_{\rm fin}$  is reached. For the data presented in Fig. 4.11, one possible explanation for the increase in temperature is the scattering of phonons with highly-energetic particles from the radially excited states [45]. In contrast to the simple head-on collisions that are usually associated with two-body scattering processes in 1D, these collisions can lead to a mixing of the momentum distribution. They become important as soon as the thermal energy is high enough to populate radially excited states. For temperatures below the radial trapping frequency they are exponentially suppressed. However, another possible explanation for the observations are nonlinear processes which go

beyond the Luttinger description, but still remain integrable [46]. We note that other predicted integrability breaking processes are either excluded by the data [44, 47], or are negligible for our parameters [48, 49].

Assuming two completely independent gases once the system has relaxed, we can also use density ripples to measure the temperature of the system. As for the relative degrees of freedom we find a temperature  $T_{\rm fin}$ , demonstrating complete equilibration of the system. However, more detailed studies, both theoretically and experimentally, are needed to reveal the detailed dynamics of the relaxation process. Importantly, the emergence of thermal equilibrium can only indirectly be concluded from the observed equilibration. While it appears obvious that the new scattering channels or nonlinear processes lead to a change in the momentum distribution of the particles, and thus to relaxation to thermal equilibrium, we will show in Chap. 7 how also integrable dephasing of the two gases can lead to an equilibrated state without any change in the momentum distribution.

#### References

- A. Polkovnikov, K. Sengupta, A. Silva, M. Vengalattore, Colloquium: nonequilibrium dynamics of closed interacting quantum systems. Rev. Mod. Phys. 83, 863–883 (2011)
- 2. T. Kinoshita, T. Wenger, D. Weiss, A Quantum Newton's Cradle. Nature **440**, 900–903 (2006)
- M. Rigol, V. Dunjko, V. Yurovsky, M. Olshanii, Relaxation in a completely integrable manybody quantum system: an ab initio study of the dynamics of the highly excited states of 1D lattice hard-core bosons. Phys. Rev. Lett. 98, 050405 (2007)
- M. Gring, M. Kuhnert, T. Langen, T. Kitagawa, B. Rauer, M. Schreitl, I.E. Mazets, D. Adu Smith, E. Demler, J. Schmiedmayer, Relaxation and prethermalization in an isolated quantum system. Science 337, 1318–1322 (2012)
- D. Adu Smith, M. Gring, T. Langen, M. Kuhnert, B. Rauer, R. Geiger, T. Kitagawa, I. Mazets, E. Demler, J. Schmiedmayer, Prethermalization revealed by the relaxation dynamics of full distribution functions. New J. Phys. 15, 075011 (2013)
- T. Langen, M. Gring, M. Kuhnert, B. Rauer, R. Geiger, D. Adu Smith, I.E. Mazets, J. Schmiedmayer, Prethermalization in one-dimensional Bose gases: description by a stochastic Ornstein-Uhlenbeck process. Eur. Phys. J. Spec. Top. 217, 43–53 (2013)
- T. Langen, R. Geiger, M. Kuhnert, B. Rauer, J. Schmiedmayer, Local emergence of thermal correlations in an isolated quantum many-body system. Nat. Phys. 9, 640–643 (2013)
- T. Langen, M. Gring, M. Kuhnert, B. Rauer, R. Geiger, I. Mazets, D. Adu Smith, T. Kitagawa, E. Demler, J. Schmiedmayer, Studying non-equilibrium many-body dynamics using one-dimensional Bose gases. AIP Conf. Proc. 1633, 11 (2014) (2013)
- M. Gring, Prethermalization in an isolated many-body system. Ph.D. thesis, Vienna University of Technology, 2012
- M. Kuhnert, Thermalization and prethermalization in an ultracold Bose gas. Ph.D. thesis, Vienna University of Technology, 2013
- T. Kitagawa, A. Imambekov, J. Schmiedmayer, E. Demler, The dynamics and prethermalization of one-dimensional quantum systems probed through the full distributions of quantum noise. New J. Phys. 13, 073018 (2011)
- R. Bistritzer, E. Altman, Intrinsic dephasing in one-dimensional ultracold atom interferometers. Proc. Natl. Acad. Sci. 104, 9955 (2007)
- T. Kitagawa, S. Pielawa, A. Imambekov, J. Schmiedmayer, V. Gritsev, E. Demler, Ramsey interference in one-dimensional systems: the full distribution function of fringe contrast as a probe of many-body dynamics. Phys. Rev. Lett. 104, 255302 (2010)

- T. Betz, S. Manz, R. Bücker, T. Berrada, C. Koller, G. Kazakov, I.E. Mazets, H.-P. Stimming, A. Perrin, T. Schumm, J. Schmiedmayer, Two-point phase correlations of a one-dimensional bosonic Josephson junction. Phys. Rev. Lett. 106, 020407 (2011)
- M. Kuhnert, R. Geiger, T. Langen, M. Gring, B. Rauer, T. Kitagawa, E. Demler, D. Adu Smith,
   J. Schmiedmayer, Multimode dynamics and emergence of a characteristic length scale in a one-dimensional quantum system. Phys. Rev. Lett. 110, 090405 (2013)
- K. Agarwal, E.G. Dalla Torre, B. Rauer, T. Langen, J. Schmiedmayer, E. Demler, Chiral prethermalization in supersonically split condensates. Phys. Rev. Lett. 113, 190401 (2014)
- T. Schumm, S. Hofferberth, L.M. Andersson, S. Wildermuth, S. Groth, I. Bar-Joseph, J. Schmiedmayer, P. Kruger, Matter-wave interferometry in a double well on an atom chip. Nat. Phys. 1, 57–62 (2005)
- S. Hofferberth, I. Lesanovsky, T. Schumm, A. Imambekov, V. Gritsev, E. Demler, J. Schmiedmayer, Probing quantum and thermal noise in an interacting many-body system. Nat. Phys. 4, 489–495 (2008)
- C.-L. Hung, V. Gurarie, C. Chin, From cosmology to cold atoms: observation of Sakharov oscillations in a quenched atomic superfluid. Science 341, 1213–1215 (2013)
- R. Geiger, T. Langen, I.E. Mazets, J. Schmiedmayer, Local relaxation and light-cone-like propagation of correlations in a trapped 1D Bose gas. New J. Phys. 16, 053034 (2014)
- V. Gritsev, E. Altman, E. Demler, A. Polkovnikov, Full quantum distribution of contrast in interference experiments between interacting one dimensional Bose liquids. Nat. Phys. 2, 705– 709 (2006)
- 22. J. Berges, Sz. Borsányi, C. Wetterich, Prethermalization. Phys. Rev. Lett. 93, 142002 (2004)
- P. Braun-Munzinger, D. Magestro, K. Redlich, J. Stachel, Hadron production in Au-Au collisions at RHIC. Phys. Lett. B 518, 41–46 (2001)
- D. Podolsky, G. Felder, L. Kofman, M. Peloso, Equation of state and beginning of thermalization after preheating. Phys. Rev. D 73, 023501 (2006)
- L. Kofman, A. Linde, A.A. Starobinsky, Reheating after inflation. Phys. Rev. Lett. 73, 3195
   3198 (1994)
- 26. A. Arrizabalaga, J. Smit, A. Tranberg, Equilibration in  $\varphi^4$  theory in 3+ 1 dimensions. Phys. Rev. D **72**, 025014 (2005)
- C. Kollath, A.M. Läuchli, E. Altman, Quench dynamics and nonequilibrium phase diagram of the Bose-hubbard model. Phys. Rev. Lett. 98, 180601 (2007)
- M. Eckstein, M. Kollar, P. Werner, Thermalization after an interaction quench in the Hubbard model. Phys. Rev. Lett. 103, 056403 (2009)
- M. Moeckel, S. Kehrein, Crossover from adiabatic to sudden interaction quenches in the Hubbard model: prethermalization and non-equilibrium dynamics. New J. Phys. 12, 055016 (2010)
- R. Barnett, A. Polkovnikov, M. Vengalattore, Prethermalization in quenched spinor condensates. Phys. Rev. A 84, 023606 (2011)
- 31. G.E. Uhlenbeck, L.S. Ornstein, On the theory of the Brownian motion. Phys. Rev. **36**, 823 (1930)
- 32. C.W. Gardiner, Handbook of stochastic methods (Springer, Berlin, 1985)
- H.-P. Stimming, N.J. Mauser, J. Schmiedmayer, I.E. Mazets, Fluctuations and stochastic processes in one-dimensional many-body quantum systems. Phys. Rev. Lett. 105, 015301 (2010)
- C. Mora, Y. Castin, Extension of Bogoliubov theory to quasicondensates. Phys. Rev. A 67, 053615 (2003)
- 35. T. Giamarchi, *Quantum physics in one dimension* (Clarendon Press, Oxford, 2004)
- N.K. Whitlock, I. Bouchoule, Relative phase fluctuations of two coupled one-dimensional condensates. Phys. Rev. A 68, 053609 (2003)
- 37. M. Cramer, C.M. Dawson, J. Eisert, T.J. Osborne, Exact relaxation in a class of nonequilibrium quantum lattice systems. Phys. Rev. Lett. **100**, 030602 (2008)
- 38. P. Calabrese, J. Cardy, Time dependence of correlation functions following a quantum quench. Phys. Rev. Lett. **96**, 011368 (2006)

References 95

 L. Mathey, A. Polkovnikov, Light cone dynamics and reverse Kibble-Zurek mechanism in two-dimensional superfluids following a quantum quench. Phys. Rev. A 81, 60033 (2010)

- M. Cheneau, P. Barmettler, D. Poletti, M. Endres, P. Schauß, T. Fukuhara, C. Gross, I. Bloch, C. Kollath, S. Kuhr, Light-cone-like spreading of correlations in a quantum many-body system. Nature 481, 484–487 (2012)
- 41. D.T. Gillespie, Exact numerical simulation of the Ornstein-Uhlenbeck process and its integral. Phys. Rev. E **54**, 2084–2091 (1996)
- M. Kollar, F.A. Wolf, M. Eckstein, Generalized Gibbs ensemble prediction of prethermalization plateaus and their relation to nonthermal steady states in integrable systems. Phys. Rev. B 84, 054304 (2011)
- 43. M. Stark, M. Kollar, Kinetic description of thermalization dynamics in weakly interacting quantum systems. arXiv:1308.1610 (2013)
- 44. I.E. Mazets, Private communication
- 45. I.E. Mazets, J. Schmiedmayer, Thermalization in a quasi-one-dimensional ultracold bosonic gas. New J. Phys. 12, 055023 (2010)
- 46. H.-P. Stimming, N.J. Mauser, J. Schmiedmayer, I.E. Mazets, Dephasing in coherently split quasicondensates. Phys. Rev. A 83, 023618 (2011)
- 47. A.A. Burkov, M.D. Lukin, E. Demler, Decoherence dynamics in low-dimensional cold atom interferometers. Phys. Rev. Lett. **98**, 200404 (2007)
- 48. S. Tan, M. Pustilnik, L.I. Glazman, Relaxation of a high-energy quasiparticle in a one-dimensional Bose gas. Phys. Rev. Lett. **105**, 090404 (2010)
- 49. I.E. Mazets, T. Schumm, J. Schmiedmayer, Breakdown of integrability in a quasi-1D ultracold bosonic gas. Phys. Rev. Lett. **100**, 210403 (2008)

### **Chapter 5 Local Emergence of Thermal Correlations**

Despite important theoretical effort [1], no generic framework exists yet to understand when and how an isolated quantum system relaxes to a steady state. Regarding the question of how, it has been conjectured [2, 3] that equilibration must occur on a local scale in systems where correlations between distant points can only establish at a finite speed. In this chapter, we provide the first experimental observation of this local equilibration hypothesis. As in the previous chapter, we quench a 1D Bose gas by coherently splitting it into two parts. By monitoring the phase coherence between the two parts we observe that the thermal correlations of the prethermalized state [4, 5] emerge locally in their final form and propagate through the system in a light-cone-like evolution. Our results underline the close link between the propagation of correlations [2, 3, 6, 7] and relaxation processes in quantum many-body systems.

This chapter is based on and also uses parts of Refs. [8, 9].

- T. Langen, R. Geiger, M. Kuhnert, B. Rauer, and J. Schmiedmayer Local emergence of thermal correlations in an isolated quantum many-body system Nature Phys. 9, 640-643 (2013), arXiv:1305.3708
- R. Geiger, T. Langen, I. Mazets, and J. Schmiedmayer
   Local relaxation and light-cone-like propagation of correlations
   in a trapped 1D Bose gas
   New J. Phys. 16, 053034 (2014), arXiv:1312.7568

#### 5.1 The Local Relaxation Conjecture

As outlined in Chap. 3, it has been theoretically suggested that the relaxation in generic isolated quantum many-body systems proceeds through the dephasing of the quantum states populated at the onset of the non-equilibrium evolution [10, 11]. It is generally believed that this dynamically leads to relaxed states which can be well described either by the usual thermodynamical ensembles or by generalized

Gibbs ensembles which take into account dynamical constraints [12]. However, it remains an open question how these relaxed states form dynamically, and in particular, whether they emerge gradually on a global scale, or appear locally and then spread in space and time [3].

#### **5.2 Experimental Results**

The experimental procedure closely follows the one presented in Chap. 4. We start with a single 1D degenerate gas of 4000–12,000 atoms. The trap frequencies are  $\omega_{\perp}=2\pi\times(2.1\pm0.1)$  kHz and  $\omega_{z}=2\pi\times(11\pm0.5)$  Hz. The realized range of atom numbers thus corresponds to peak densities of  $n_{\rm 1D}=50$ –110 atoms/ $\mu$ m and chemical potentials of  $\mu/\hbar\approx2\pi\times(1.1-2.5)$  kHz. The temperature T of the initial gas is estimated using measurements of density fluctuations in time-of-flight [13, 14] and typically lies between 30 and 110 nK.

By applying RF fields via the two main RF wires on the chip, we rapidly transform the initial harmonic trapping potential into a double well. This realizes the matterwave analogue of a coherent beam splitter [15]. To minimize longitudinal excitations of the gas during the splitting, we either carry out the final evaporative cooling of the atoms in a slightly dressed trap ( $I_{RF} = 8 \,\mathrm{mA}$ ) or perform the first part of the splitting ramp very slowly (ramp to  $I_{RF} = 8 \,\mathrm{mA}$  within 30 ms). An RF current of  $I_{RF} = 8 \text{ mA}$  produces a slightly anharmonic trap in the radial direction and a harmonic longitudinal confinement of  $\omega_z = 2\pi \times (7\pm0.5)$  Hz, close to that of the final double-well. Once in this trap, we linearly ramp up the RF current to  $I_{RF} = 24 \text{ mA}$ within 12 ms to create the double-well. This procedure has the advantage that the longitudinal trap frequency is not modified during the splitting. We observe this to reduce spurious longitudinal excitations. The excitation of a breathing mode is intrinsic to this splitting procedure, due to the halving of the atom number [16]. It can be neglected on the timescale of the experiments presented in this chapter. A more detailed investigation of the splitting process and its effect on the initial state is described in Chap. 6.

The system is let to evolve in the double well for a variable time t, before the gases are released by switching off the trapping potential. They expand and interfere after a time-of-flight of 15.7 ms. The resulting interference pattern allows the extraction of the relative phase  $\theta(z,t) = \phi^{(1)}(z,t) - \phi^{(2)}(z,t)$  for every pixel of the image, along the length of the system (see Fig. 5.1). Here  $\phi^{(1)}(z,t)$  and  $\phi^{(2)}(z,t)$  are the phase profiles of the two individual gases. Repeating this procedure many times for each value of t, we determine the two-point relative phase correlation function

$$C(\bar{z} = z - z', t) = \operatorname{Re} \langle e^{i\theta(z,t) - i\theta(z',t)} \rangle. \tag{5.1}$$

This function measures the degree of correlation between the phases at two arbitrary points z and z', separated by a distance  $\bar{z}$  (Refs. [17, 18]). In contrast to the integrated

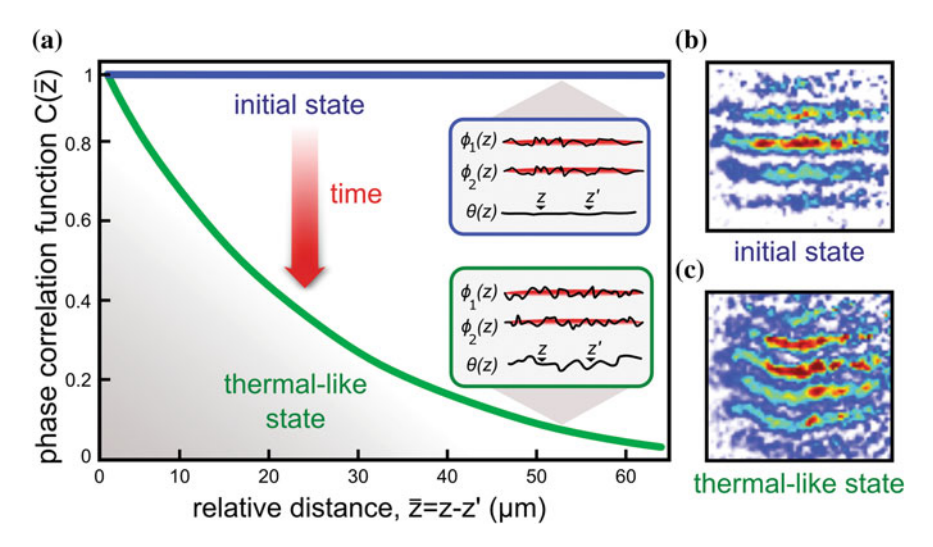


Fig. 5.1 Characterizing the dynamics of correlations in a coherently split 1D Bose gas. a The splitting process creates two 1D gases with almost identical longitudinal phase profiles  $\phi^{(1)}(z)$  and  $\phi^{(2)}(z)$ , corresponding to long-range phase coherence in the relative phase field  $\theta(z) = \phi^{(1)}(z) - \phi^{(2)}(z)$ . The degree of relative phase correlations between two arbitrary points z and z' along the length of the system is characterized by the two-point correlation function  $\mathcal{C}(\bar{z},t)$ . Initially, it is close to unity for any distance  $\bar{z}=z-z'$  between the points. Over time, this strongly phase-correlated state relaxes towards a prethermalized state, characterized by thermal (exponentially decaying) correlations. The aim of this study is to investigate how the thermal correlations locally emerge in time. In the experiment, the relative phase field is probed via matter-wave interferometry between the two gases. b, c Show example interference pictures in the initial and in the prethermalized state, respectively. In these pictures, the relative phase  $\theta(z)$  is directly extracted from the local position of the interference fringes. The phase correlation function is then calculated from an average over  $\sim$ 150 pictures

visibility of the interference pattern, which was used in the previous chapter to identify the prethermalized state [5], the phase correlation function provides a local and much more sensitive probe for the dynamics, and therefore is ideally suited to study the propagation of correlations.

To calculate the phase correlation function from the fitted list of relative phases  $\theta(z_1), \theta(z_2), \ldots$ , we start at the center pixel with index l and compare it to the pixel l+1 for a distance of  $\bar{z}=\sigma_{\rm px}$ . Here,  $\sigma_{\rm px}$  denotes the size of a pixel. We then continue to compare pixel l+1 with pixel l-1 for a distance of  $\bar{z}=2\times\sigma_{\rm px}$  and so on:

$$C(\bar{z} = \sigma_{px}) = \left\langle e^{i\theta(z_{l}) - i\theta(z_{l+1})} \right\rangle$$

$$C(\bar{z} = 2\sigma_{px}) = \left\langle e^{i\theta(z_{l+1}) - i\theta(z_{l-1})} \right\rangle$$

$$C(\bar{z} = 3\sigma_{px}) = \left\langle e^{i\theta(z_{l-1}) - i\theta(z_{l+2})} \right\rangle$$
(5.2)

:

This symmetric evaluation of the phase correlation function allows the study of larger distances  $\bar{z}$  by reducing noise and finite size effects that appear close to the edge of the clouds. As the density changes very little in the center of the cloud, this procedure also ensures that the shape of the phase correlation function typically changes weakly in comparison to the one of an homogeneous system. Note that the trap still has a subtle influence on the characteristic velocity with which the long-range phase coherence decays in the system, as it changes the dispersion relation of the excitations compared to the homogeneous case.

In 1D quantum systems fluctuations play an essential role. Consequently, a large set of experimental runs is needed to evaluate the correlation function. In the experiments, we typically perform 150 measurements for each value of t. To estimate the influence of the finite number of experimental realizations on the uncertainty of the phase correlation function, we simulate single realizations using an Ornstein-Uhlenbeck stochastic process with time-dependent effective parameters as introduced in Sect. 4.4. The results are presented in Fig. 5.2, showing how the statistical uncertainty on  $C(\bar{z})$  becomes more relevant as phase fluctuations develop in time. We therefore neglect large evolution times  $t \gg 8$  ms in the analysis of the dynamics.

Typical experimental data is presented in Fig. 5.3a. Directly after the quench, the phase correlation function  $C(\bar{z},t)$  is close to unity for any distance  $\bar{z}$ . This is a direct manifestation of the long-range phase coherence produced by the splitting process. After a given evolution time t, the phase correlation function decays exponentially up to a characteristic distance  $\bar{z}_c$  and stays nearly constant afterwards:  $C(\bar{z} > \bar{z}_c, t) = C(\bar{z}_c, t)$ . This means that beyond the distance  $\bar{z}_c$  long-range phase coherence is retained across the system. With longer evolution time, the position of  $\bar{z}_c$  shifts to larger distances and the value of  $C(\bar{z} > \bar{z}_c, t)$  gradually decreases.

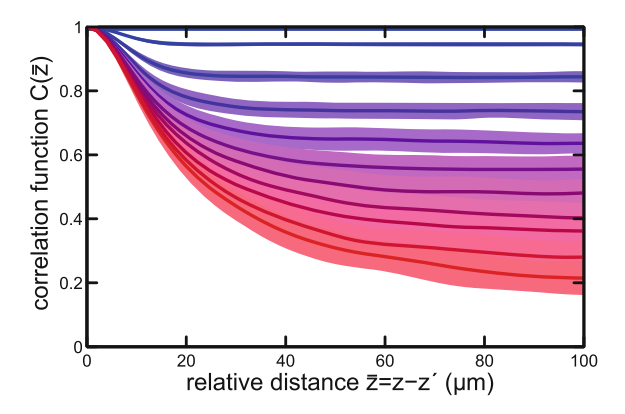


Fig. 5.2 Estimation of the influence of finite statistics. Evolution times increase from 0 to 10 ms in steps of 1 ms from top to bottom. To calculate the phase correlation functions, 150 realizations are used per evolution time. The statistical model is based on a stochastic process (see Sect. 4.4). Shaded areas denote plus/minus one standard deviation. We observe that for evolution times above  $\sim$ 8 ms, the statistical noise becomes comparable to the distance between the plateaus. Consequently, longer evolution times are not taken into account in the analysis

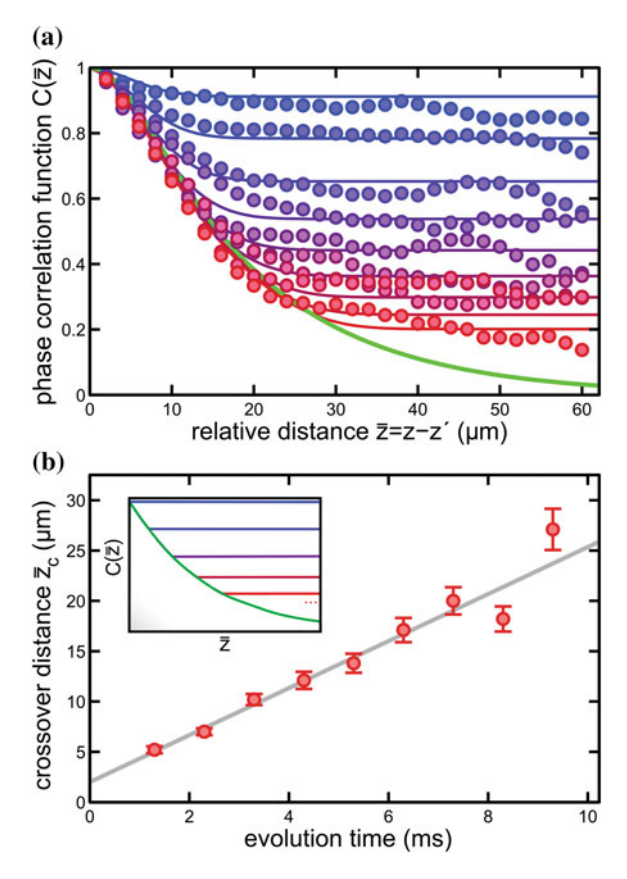


Fig. 5.3 Local emergence of thermal correlations, a Experimental phase correlation functions  $C(\bar{z},t)$  (filled circles) compared to theoretical calculations (solid lines). From top to bottom, the evolution time t increases from 1 to 9 ms in steps of 1 ms. The bottom (green) line is the theoretical correlation function of the prethermalized state. For each t, the constant values of  $C(\bar{z},t)$  at large  $\bar{z}$  can be used to determine the crossover distance  $\bar{z}_c(t)$  up to which the system forgets the initial long-range phase coherence (see Fig. 5.4). **b** Position of the crossover distance  $\bar{z}_c$  as a function of evolution time t, revealing the light-cone-like decay of correlations. The solid line is a linear fit, the slope of which corresponds to twice the characteristic velocity of correlations. Inset schematic visualization of the dynamics. The decay of correlations is characterized by a front moving with a finite velocity: for a given time t,  $C(\bar{z}, t)$  is exponential (thermal) only up to the characteristic distance  $\bar{z}_c(t)$ . Beyond this horizon, long-range phase coherence is retained. In the experimental data shown in (a), these sharp transitions are smeared out by the experimental imaging resolution. Note that there is a finite uncertainty for the decoupling point where t = 0 (see Sect. 4.1). We find best agreement between experiment and theory for a splitting point located 3.3 ms before the end of the ramp. Note that the choice of this particular decoupling point does not affect the extracted value for the characteristic velocity

This evolution continues until the system reaches a quasi-steady state, where the correlations decay exponentially throughout the entire system [19]. This prethermalized state corresponds to the relaxed state of the 1D system [5, 12]. Our observation that the exponentially decreasing parts of the dynamical phase correlation functions match the exponential decay of the relaxed, prethermalized state for  $\bar{z} < \bar{z}_c$ , allows us to conclude that equilibration occurs locally in our system.

Due to the limited resolution of the imaging system, the location of the correlation front  $\bar{z}_c = 2ct$ , which corresponds to a well-defined point in  $\mathcal{C}(\bar{z})$  in theory (see inset of Fig. 5.3), cannot be read off directly from the measured phase correlation functions. Instead, we use the knowledge of the correlation function in the prethermalized state, in conjunction with the observed level of long-range phase coherence remaining at long distances, to determine the position of  $\bar{z}_c(t)$ . Figure 5.4 illustrates the details of the extrapolation procedure.

The results are presented in Fig. 5.3. We observe a clear linear scaling of the position  $\bar{z}_c = 2ct$ , characterizing the local decay of correlations with time. This observation reveals that an arbitrary point in the gas loses its correlations with other points up to a certain separation  $\bar{z}_c$ , while long-range phase coherence persists outside this horizon.

The experimental data thus show that the prethermalized state locally emerges in a light-cone-like evolution, where c plays the role of a characteristic velocity for the propagation of correlations in the quantum many-body system. For the data presented in Fig. 5.3b, a linear fit yields a velocity of  $c = 1.16 \pm 0.09$  mm/s.

#### **5.3** Theoretical Discussion

Light-cone-like effects in quantum many-body dynamics have been previously predicted using results from conformal field theory [2] and for 2D superfluids [20]. Similarly, it is known that some quantum spin models exhibit an intrinsic maximum velocity [6] which limits the propagation of correlations and entanglement to an effective light-cone [7, 21, 22]. It has been conjectured that this leads to a local establishment of thermal properties [3].

The light-cone like emergence of thermal correlations which we observe in our system, can be understood using a homogeneous Luttinger Liquid (LL) model that effectively describes the interacting many-body system in terms of low-energy excitations [23]. Within the LL model, these excitations are superpositions of phase and density fluctuations, as described in Sect. 1.5.1 and Chap. 4. They are characterized by a linear dispersion relation  $\omega_k = c_0|k|$ , with k being the momentum of the excitation and k0 the speed of sound, the latter defining the characteristic velocity in the homogeneous system. For a given evolution time k1, the dephasing of the excitations with different wavelengths k1 and k2 and k3 and k4 randomizes the relative phase field only up to a characteristic distance k5. In a more mathematical formulation, the phase correlation function can be written as k6 cyc, k7 and k8. In the homogeneous limit, the local phase variance is given by (see Sect. 1.5.1 and Refs. [24–26])

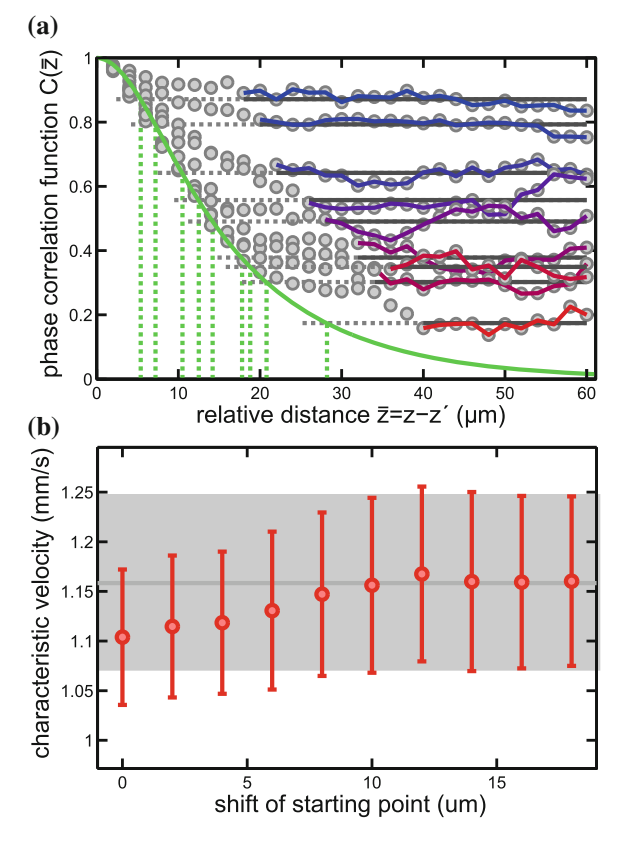


Fig. 5.4 Extraction of the light-cone-like evolution and estimation of the characteristic velocity. a Due to the finite optical resolution the critical distance is extracted by an extrapolation method. For each evolution time t, we consider the region where the correlation function is constant (horizontal blue to red solid lines) and compute its average value (horizontal gray solid lines). We then extrapolate this average value to smaller  $\bar{z}$  to obtain the intersection point  $\bar{z}_c$  with the fitted prethermalized correlation function (exponentially decaying green solid line). To show the robustness of this method against the particular choice of  $\bar{z}$  values used in the averaging of the constant region, we repeat this procedure for different shifts  $\bar{z}_{\text{shift}}$  of the smallest point  $\bar{z}_{\min} = 2c_0t + \bar{z}_{\text{shift}}$  considered for the averaging. The exact value for the speed of sound  $c_0$  used a priori for the starting points does not have an influence on the results. **b** Resulting characteristic velocity for different  $\bar{z}_{\text{shift}}$ . As soon as  $\bar{z}_{\text{shift}}$  is large enough to neglect the effects of the finite imaging resolution, the result for c settles to a constant value. The solid horizontal line denotes the deduced result for c, the shaded area denotes its standard deviation

$$\langle \Delta \theta_{zz'}(t)^2 \rangle = \frac{2\pi^2}{\mathcal{L}K^2} \sum_{k \neq 0} \frac{\sin(\omega_k t)^2}{k^2} \left( 1 - \cos(k\bar{z}) \right), \tag{5.3}$$

with  $\mathcal{L}$  being the length of the system,  $k = 2\pi n/\mathcal{L}$  the momentum of the excitations  $(n \neq 0 \text{ integer})$  and K the Luttinger parameter. The emergence of the sharp light-cone

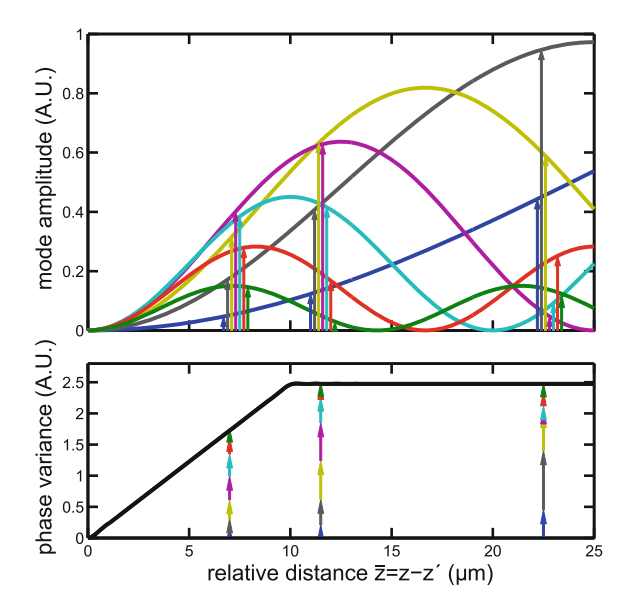


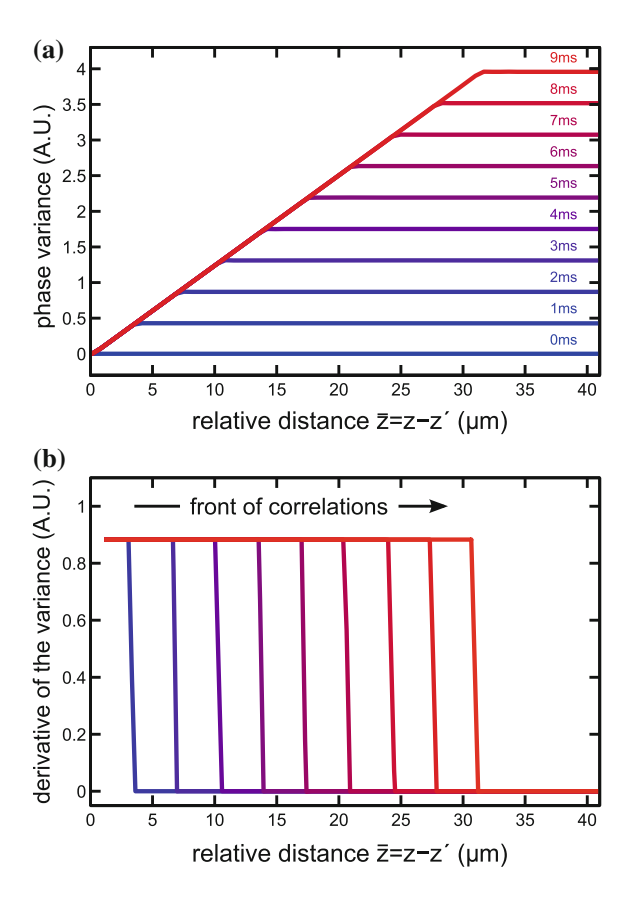
Fig. 5.5 Visualization of the light-cone condition. The relative phase of the system is randomized by a superposition of many modes (solid lines). Initially, the contribution of all these modes grows in amplitude (arrows), leading to a linear increase in the variance of the phase (bottom plot). For the correlation function, this corresponds to the establishment of thermal correlations up to  $\bar{z}_c$ . Beyond  $\bar{z}_c = 2c_0t$ , modes with a wavelength larger than  $\bar{z}_c$  would be needed for a further randomization of the phase. However, while these long-wavelength modes grow in amplitude for  $\bar{z} > \bar{z}_c$ , modes with shorter wavelength start to decrease again in amplitude. Overall, this leads to a constant phase variance beyond  $\bar{z}_c$ . Parameters are  $c_0 = 1$  mm/s and t = 5 ms.

condition can intuitively be understood as a consequence of the superposition of many modes in the sum of Eq. 5.3. The situation is illustrated in Fig. 5.5. For a given time t and speed  $c_0$ , short wavelength modes will grow in amplitude and linearly increase the phase variance up to a distance  $\bar{z}_c = 2c_0t$ . Beyond that point the growth in amplitude of longer wavelength modes with  $\lambda > \bar{z}_c$  and the decrease in amplitude of the shorter wavelength modes with  $\lambda < \bar{z}_c$  exactly compensates, leading to a constant phase variance.

The first term of the sum in Eq. 5.3 represents the growth and subsequent oscillations in the amplitude of the phase fluctuations as they get converted from the initial density fluctuations. The factor  $1/k^2$  in the amplitude reflects the 1/k scaling of the excitation occupation numbers associated with the equipartition of energy induced by the fast splitting. The second term in the sum corresponds to the spatial fluctuations. Equation 5.3 is the Fourier decomposition of a trapezoid with a siding edge at  $\bar{z}_c = 2c_0t$ , which explains the two step feature of the phase correlation function. More rigorously, computing the derivative of the phase variance with respect to the position  $\bar{z}$ , we find

$$\frac{\partial \langle \Delta \theta_{zz'}(t)^2 \rangle}{\partial \bar{z}} \sim \Theta(2c_0t - \bar{z}),\tag{5.4}$$

Fig. 5.6 Time evolution of the phase variance, a Time evolution of the phase variance  $\langle \Delta \theta_{\tau\tau'}^2 \rangle$  for  $c_0 = 1.8 \text{ mm/s}$ . For a given evolution time, the phase variance grows linearly up to a distance  $\bar{z}_c = 2c_0t$ . Beyond that sharp crossover point the phase variance is constant. revealing the persisting long-range phase coherence in the system. b Derivative of the phase variance visualizing how the front of correlations travels through the system



where  $\Theta(x)$  is the Heaviside step function. The phase thus randomizes as a function of  $\bar{z}$  with a constant rate, up to the point where  $\bar{z} = 2c_0t$ . Beyond that point, longrange phase coherence is retained. The full time evolution of the phase variance and its derivative is shown in Fig. 5.6.

Alternatively, the excitations in the LL model can also be identified as pairs of quasi-particles, which propagate in opposite directions with momenta k and -k, respectively [2, 7]. This interpretation naturally leads to the light-cone condition, as two points separated by  $\bar{z}$  can establish thermal correlations if quasi-particles originating from these points meet after a time  $t = \bar{z}/2c_0$ .

In Fig. 5.3a we compare the results of the LL calculation to our measured data, taking into account the finite resolution of the imaging system. We find good agreement, using independently measured experimental parameters as the input for the theory. This quantitative agreement validates our interpretation of the observations as the local emergence of thermal correlations.

### 5.4 The Characteristic Velocity

When increasing the number of particles in our quantum many-body system, we expect interaction effects to play a more important role, leading to a faster local relaxation. In the homogeneous limit, this is captured by the scaling of the speed of sound  $c_0 \sim \sqrt{n_{\rm 1D}}$  with the 1D density  $n_{\rm 1D}$  of each gas [27]. To investigate the scaling of the characteristic velocity, we repeat the experiment for a varying number of atoms N in the system. We observe the light-cone-like emergence of the thermal correlations over the whole range of probed atom numbers ( $N \sim 4000-12,000$ ). In Fig. 5.7 we show the corresponding evolution of the crossover distance  $\bar{z}_c$  for the different datasets, from which we extract the respective characteristic velocities.

In the experimentally realized trapped system, the density varies along the length of the gases, resulting in a spatially dependent speed of sound. Nevertheless, the

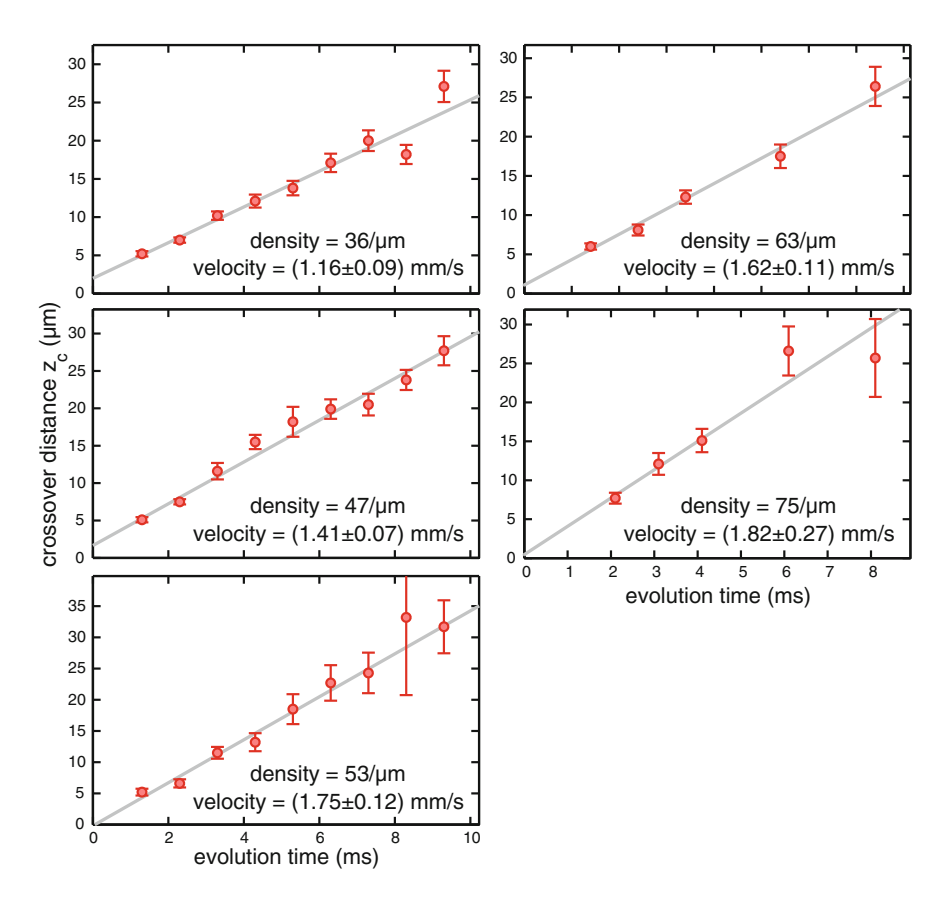
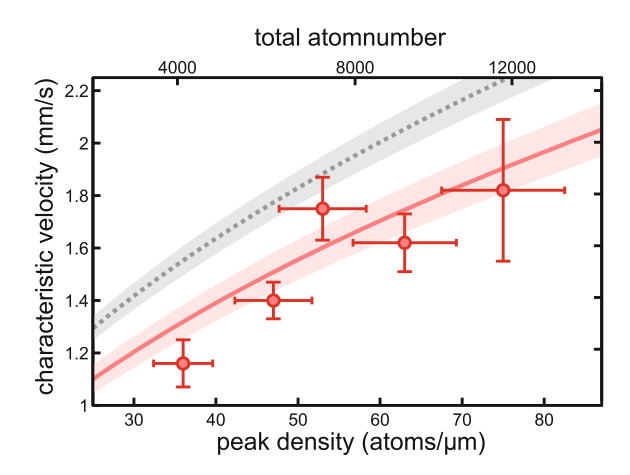


Fig. 5.7 Evolution of the crossover distance  $\bar{z}_c$  for different densities. The light-cone-like emergence of thermal correlations is observed over a large range of densities, revealing a clear scaling of the characteristic velocity with density. This scaling is plotted in Fig. 5.8

Fig. 5.8 Scaling of the characteristic velocity with particle number. The solid red (dashed gray) line is the calculated velocity of correlations for a trapped (homogeneous) system. The peak densities are given for each gas. Shaded areas correspond to the uncertainty on the measured trap frequencies. Error bars denote one standard deviation



superposition of many excitations still leads to a single characteristic velocity for the dynamics, which is slightly reduced with respect to the homogeneous case. In detail, we find that the time evolution of the relative phase variance can be well approximated by [9] (see Eq. 1.75)

$$\langle \Delta \theta_{zz'}(t)^2 \rangle = \frac{2n_0 g^2}{\hbar^2 R_{\text{TF}}} \sum_{i=1}^{\infty} \frac{\sin(\omega_j t)^2}{\omega_j^2} \left[ f_j(z) - f_j(z') \right]^2. \tag{5.5}$$

The structure and interpretation of this expression is exactly the same as in the homogeneous case (Eq. 5.3), but the velocity characterizing the motion of the front of correlations slightly differs. Numerically summing the terms of Eq. 5.5 we find a velocity varying from  $0.84 \times c_0$  to  $0.90 \times c_0$  for the atom numbers probed in the experiment. This velocity results from the interplay of many eigenstates, yielding a non-trivial dependence on the atom number [9]. In Fig. 5.8 we show the measured characteristic velocities. A Luttinger liquid calculation including the trapping potential describes the experimental data within the experimental error, whereas a purely homogeneous calculation clearly overestimates the characteristic velocity.

#### 5.5 Conclusion

In our experiment, thermal correlations emerge locally in their final prethermalized form. This supports the local relaxation hypothesis [3] and indicates a general pathway for the emergence of classical properties in isolated quantum many-body systems. In our system, interactions manifest themselves in excitations with a linear dispersion relation (in the homogeneous limit), resulting in a decay of quantum

coherence which takes the form of an effective light cone. Whether this scenario holds also for systems with non-linear dispersion relations, long-range interactions [28, 29] or systems that are subject to disorder [30] remains a topic of intense study.

#### References

- A. Polkovnikov, K. Sengupta, A. Silva, M. Vengalattore, Colloquium: nonequilibrium dynamics of closed interacting quantum systems. Rev. Mod. Phys. 83, 863–883 (2011)
- 2. P. Calabrese, J. Cardy, Time dependence of correlation functions following a quantum quench. Phys. Rev. Lett. **96**, 011368 (2006)
- M. Cramer, C.M. Dawson, J. Eisert, T.J. Osborne, Exact relaxation in a class of nonequilibrium quantum lattice systems. Phys. Rev. Lett. 100, 030602 (2008)
- 4. J. Berges, Sz. Borsányi, C. Wetterich, Prethermalization. Phys. Rev. Lett. 93, 142002 (2004)
- M. Gring, M. Kuhnert, T. Langen, T. Kitagawa, B. Rauer, M. Schreitl, I.E. Mazets, D. Adu Smith, E. Demler, J. Schmiedmayer, Relaxation and prethermalization in an isolated quantum system. Science 337, 1318–1322 (2012)
- E.H. Lieb, D.W. Robinson, The finite group velocity of quantum spin systems. Commun. Math. Phys. 28, 251–257 (1972)
- M. Cheneau, P. Barmettler, D. Poletti, M. Endres, P. Schauß, T. Fukuhara, C. Gross, I. Bloch, C. Kollath, S. Kuhr, Light-cone-like spreading of correlations in a quantum many-body system. Nature 481, 484–487 (2012)
- 8. T. Langen, R. Geiger, M. Kuhnert, B. Rauer, J. Schmiedmayer, Local emergence of thermal correlations in an isolated quantum many-body system. Nat. Phys. 9, 640–643 (2013)
- 9. R. Geiger, T. Langen, I. E. Mazets, J. Schmiedmayer, Local relaxation and velocity of correlations in a trapped one-dimensional Bose gas (2013)
- 10. M. Srednicki, Chaos and quantum thermalization. Phys. Rev. E 50, 888–901 (1994)
- 11. M. Rigol, V. Dunjko, M. Olshanii, Thermalization and its mechanism for generic isolated quantum systems. Nature **452**, 854–858 (2008)
- M. Rigol, V. Dunjko, V. Yurovsky, M. Olshanii, Relaxation in a completely integrable manybody quantum system: an ab initio study of the dynamics of the highly excited states of 1D lattice hard-core bosons. Phys. Rev. Lett. 98, 050405 (2007)
- A. Imambekov, I.E. Mazets, D.S. Petrov, V. Gritsev, S. Manz, S. Hofferberth, T. Schumm, E. Demler, J. Schmiedmayer, Density ripples in expanding low-dimensional gases as a probe of correlations. Phys. Rev. A 80, 033604 (2009)
- S. Manz, R. Bücker, T. Betz, Ch. Koller, S. Hofferberth, I.E. Mazets, A. Imambekov, E. Demler, A. Perrin, J. Schmiedmayer, T. Schumm, Two-point density correlations of quasicondensates in free expansion. Phys. Rev. A 81, 031610 (2010)
- T. Schumm, S. Hofferberth, L.M. Andersson, S. Wildermuth, S. Groth, I. Bar-Joseph, J. Schmiedmayer, P. Kruger, Matter-wave interferometry in a double well on an atom chip. Nat. Phys. 1, 57–62 (2005)
- H. Moritz, T. Stöferle, M. Köhl, T. Esslinger, Exciting collective oscillations in a trapped 1D gas. Phys. Rev. Lett. 91, 250402 (2003)
- N.K. Whitlock, I. Bouchoule, Relative phase fluctuations of two coupled one-dimensional condensates. Phys. Rev. A 68, 053609 (2003)
- T. Betz, S. Manz, R. Bücker, T. Berrada, C. Koller, G. Kazakov, I.E. Mazets, H.-P. Stimming, A. Perrin, T. Schumm, J. Schmiedmayer, Two-point phase correlations of a one-dimensional bosonic Josephson junction. Phys. Rev. Lett. 106, 020407 (2011)
- M. Kuhnert, R. Geiger, T. Langen, M. Gring, B. Rauer, T. Kitagawa, E. Demler, D. Adu Smith, J. Schmiedmayer, Multimode dynamics and emergence of a characteristic length scale in a one-dimensional quantum system. Phys. Rev. Lett. 110, 090405 (2013)

References 109

 L. Mathey, A. Polkovnikov, Light cone dynamics and reverse Kibble-Zurek mechanism in two-dimensional superfluids following a quantum quench. Phys. Rev. A 81, 60033 (2010)

- S. Bravyi, M.B. Hastings, F. Verstraete, Lieb-Robinson bounds and the generation of correlations and topological quantum order. Phys. Rev. Lett. 97, 050401 (2006)
- A.M. Läuchli, C. Kollath, Spreading of correlations and entanglement after a quench in the one-dimensional Bose-Hubbard model. J. Stat. Mech. P05018 (2008)
- 23. T. Giamarchi, Quantum Physics in One Dimension (Clarendon Press, Oxford, 2004)
- T. Kitagawa, S. Pielawa, A. Imambekov, J. Schmiedmayer, V. Gritsev, E. Demler, Ramsey interference in one-dimensional systems: the full distribution function of fringe contrast as a probe of many-body dynamics. Phys. Rev. Lett. 104, 255302 (2010)
- R. Bistritzer, E. Altman, Intrinsic dephasing in one-dimensional ultracold atom interferometers. Proc. Natl. Acad. Sci. 104, 9955 (2007)
- T. Langen, M. Gring, M. Kuhnert, B. Rauer, R. Geiger, D. Adu Smith, I.E. Mazets, J. Schmied-mayer, Prethermalization in one-dimensional Bose gases: description by a stochastic Ornstein-Uhlenbeck process. Eur. Phys. J. Spec Topics 217, 43–53 (2013)
- D.S. Petrov, G.V. Shlyapnikov, J.T.M. Walraven, Regimes of quantum degeneracy in trapped 1D gases. Phys. Rev. Lett. 85, 3745–3749 (2000)
- 28. P. Hauke, L. Tagliacozzo, Phys. Rev. Lett. 111, 207202 (2013)
- M. van den Worm, B.C. Sawyer, J.J. Bollinger, M. Kastner, Relaxation timescales and decay of correlations in a long-range interacting quantum simulator. New J. Phys. 15, 083007 (2013)
- C.K. Burrell, T.J. Osborne, Bounds on the speed of information propagation in disordered quantum spin chains. Phys. Rev. Lett. 99, 167201 (2007)

# Chapter 6 Experimental Observation of a Generalized Gibbs Ensemble

The connection between the non-equilibrium dynamics of isolated quantum many-body systems and the foundations of statistical mechanics is a fundamental open question. A central role in the answer to this question is played by integrable systems where conserved quantities strongly inhibit thermalization. Instead of relaxing to the thermal equilibrium state that is described by the usual thermodynamical ensembles, it has been conjectured that integrable systems relax to states that are described by generalized Gibbs ensembles. Here, we tune the non-equilibrium state of an ultracold one-dimensional Bose gas to demonstrate that the system indeed relaxes to such an ensemble. This is verified through a detailed study of correlation functions up to 20th order. The applicability of the generalized ensemble description for isolated quantum many-body systems points to a natural emergence of classical statistical properties from the microscopic unitary quantum evolution.

This chapter is based on and also uses parts of [1].

 T. Langen, S. Erne, R. Geiger, B. Rauer, T. Schweigler, M. Kuhnert, W. Rohringer, I.E. Mazets, T. Gasenzer, and J. Schmiedmayer Experimental observation of a generalized Gibbs ensemble Science 348, 207 (2015), arXiv:1411.7185

#### 6.1 The Generalized Gibbs Ensemble

The Lieb-Liniger gas of 1D bosons is one of the prototypical examples of an integrable system in the quantum world. The existence of an exact Bethe Ansatz solution [2, 3] leads to an infinite number of conserved quantities, which make it impossible for a gas to forget the initial state of a non-equilibrium evolution. This renders relaxation to thermal equilibrium, as it is described by the thermodynamical ensembles of statistical mechanics, impossible [4]. As outlined in Chap. 3, it has been suggested that the relaxed state of an integrable system can instead be described by

a generalized Gibbs ensemble (GGE) [5]. The density matrix of this ensemble is given by

 $\hat{\rho} = \frac{1}{Z} \exp\left(-\sum_{m} \lambda_{m} \hat{\mathcal{I}}_{m}\right) \tag{6.1}$ 

where  $Z = \text{Tr}[\exp(-\sum_m \lambda_m \hat{\mathcal{I}}_m)]$  is the partition function,  $\{\hat{\mathcal{I}}_m\}$  denotes a full set of conserved quantities and the numbers  $\lambda_m$  are Lagrange multipliers associated with these conserved quantities (see also Eq. 3.7). Here,  $m \geq 1$  is an integer. In analogy with the well-established procedures of statistical physics (see Sect. 1.2), the values of the Lagrange multipliers are obtained by maximization of the system's entropy under the condition that the expectation values of the conserved quantities are fixed to their initial values [6–9]. It is important to note that the emergence of such a maximum-entropy state is not in contradiction to a unitary evolution according to quantum mechanics. It rather reflects that the true quantum state is indistinguishable from the maximum-entropy ensemble with respect to a set of measurable observables [4].

Recent experiments have shown that also the nearly-integrable 1D Bose gases that are realized by confining clouds of ultracold atoms to strong optical [10] or magnetic trapping potentials [11, 12] behave integrable for very long time scales, enabling the detailed experimental investigation of integrable dynamics [13–16]. From the theoretical side, the 1D Bose gas further has the favorable property that it remains tractable away from equilibrium [17]. Here, we combine these benefits to investigate the relaxation of a coherently split 1D Bose gas. To demonstrate the emergence of a GGE, we prepare the system in different initial non-equilibrium states and observe how they each relax to steady states that maximize entropy according to the initial values of the conserved quantities.

# **6.2 Experimental Results**

Our experiments start with a phase fluctuating 1D Bose gas which is prepared and trapped using our standard procedure (see Sect. 2.3.6). We initialize the non-equilibrium dynamics by splitting this single gas coherently into two halves. Information about the system is extracted using matter-wave interferometry [14, 15, 18, 19]. This enables the time-resolved measurement of individual two-point and higher-order *N*-point phase correlation functions

$$C(z_1, z_2, \dots, z_N)$$

$$\sim \langle \Psi_1(z_1) \Psi_2^{\dagger}(z_1) \Psi_1^{\dagger}(z_2) \Psi_2(z_2) \cdots \Psi_1^{\dagger}(z_N) \Psi_2(z_N) \rangle$$

$$\sim \langle e^{i\theta(z_1) - i\theta(z_2) + \dots - i\theta(z_N)} \rangle, \tag{6.2}$$

where  $z_1, z_2, \dots, z_N$  are N coordinates along the length of the system, and  $\theta(z)$  the relative phase between the two halves. As we show in the following, these correlation

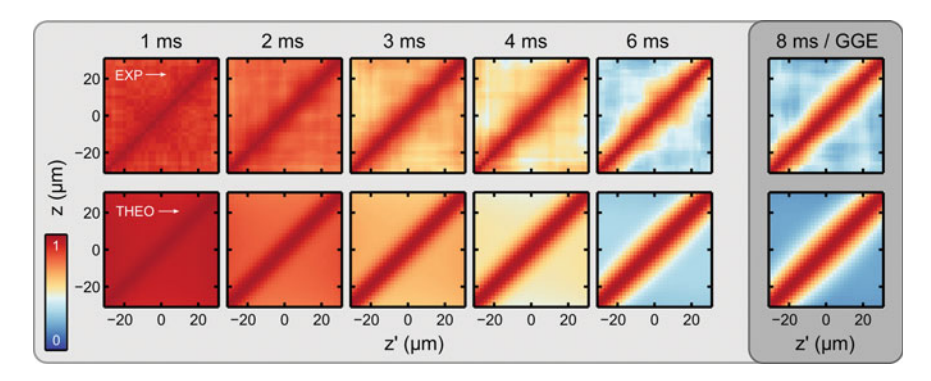


**Fig. 6.1** Relaxation dynamics of a coherently split 1D Bose gas with equal mode populations. Two-point phase correlation functions  $\mathcal{C}(z,z')$  for increasing evolution time, showing a characteristic maximum on the diagonal and a light-cone-like decay of correlations away from the diagonal. The center of the system is located at z=z'=0. *Color* marks the amount of correlations between 0 and 1. The experimental observations (*top row*) are in very good agreement with the theoretical model assuming equal mode populations (*bottom row*). This demonstrates that the system can be described by a single temperature

functions reveal detailed information about the dynamics and the steady states of the system, as for example the relaxation of the system to a prethermalized state [14, 20–22].

We start with the two-point correlation function  $C(z, z') \sim \langle e^{i\theta(z)-i\theta(z')} \rangle$ . In Chap. 5, this correlation function was studied in regimes where the system is approximately translationally invariant [15, 23]. Here, more information about generic many-body states is obtained by mapping the two-point phase correlation function C(z, z') for any combination of z and z' along the length of the gas.

The time-evolution of the system is shown in Fig. 6.1. As every point in the system is perfectly correlated with itself, the correlation functions exhibit a maximum on the diagonal  $z_1 = z_2$  for all times. Away from the diagonal, the system shows a light-cone-like decay of correlations [15] leading to a steady state. From a theoretical point of view, the emergence of this steady state is due to prethermalization [14, 21, 22, 24–26], which in the present case can be described as the dephasing of phononic excitations [22, 26–28]. The occupation numbers  $\hat{b}_m^{\dagger}\hat{b}_m$  of these excitations being the conserved quantities  $\hat{\mathcal{I}}_m$  of the integrable model (see Sect. 1.5.1 for the theoretical description).

Given these conserved quantities, we can directly calculate the Lagrange multipliers for the GGE describing the prethermalized state. In the basis formed by the Fock states of the excitations, the partition function of the GGE takes the form

$$Z = \prod_{m} \sum_{n_m \ge 0} e^{-\lambda_m n_m} = \prod_{m} \frac{1}{1 - e^{-\lambda_m}}.$$
 (6.3)

Inverting the expression for the average occupation,  $\mathcal{I}_m = -Z^{-1}\partial_{\lambda_m}Z$ , the Lagrange multipliers can be found from

$$\lambda_m = \ln\left(1 + \mathcal{I}_m^{-1}\right) \,. \tag{6.4}$$

In terms of the excitation energies  $\epsilon_m$ , the  $\lambda_m$  can be written as  $\lambda_m = \beta_m \epsilon_m$ . This defines effective temperatures  $\beta_m$  for every excitation mode. In the relevant long-wavelength limit of small m, we find the proportionality factor  $\beta_m \approx \beta_{\rm eff} = 1/k_B T_{\rm eff}$  for the prethermalized state. This is independent of m and thus describes a state which, while being a GGE in principle, is formally equivalent to the usual Gibbs ensemble with a single temperature  $T_{\rm eff}$ .

To obtain direct experimental signatures that a GGE emerges, we modify the splitting process such that the initial state exhibits different temperatures for different excitation modes. The details of this procedure are as follows (see also Fig. 4.3). For the single-temperature data presented in Fig. 6.1, we linearly increased the RF amplitude to 8 mA over a time of  $t_1 = 30$  ms. This was followed by a faster increase to 25 mA in 12 ms. The excitation of a breathing mode is intrinsic to this splitting procedure, due to the halving of the atom number. It can be neglected on the timescale of the experiments presented in this chapter. For the data presented in the following, the RF amplitude is increased linearly to the final 25 mA within a single 17 ms long ramp (corresponding to  $t_1 = 5$  ms). For both RF ramp protocols the rapid decoupling of the two gases happens approximately 3 ms before the end of the RF amplitude ramp and within a period of less than 500  $\mu$ s. After the splitting, the tunnel coupling between the two gases is negligible.

The results of the modified splitting process are shown in Fig. 6.2. In addition to the maximum of correlations on the diagonal, we observe a pronounced second

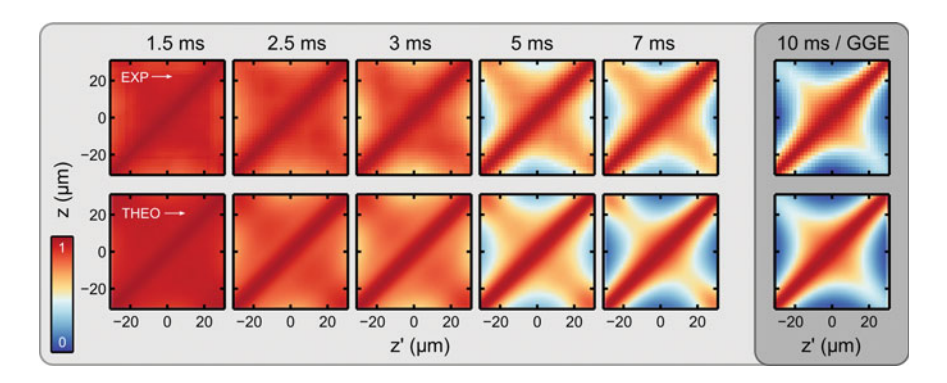


Fig. 6.2 Relaxation dynamics of a coherently split 1D Bose gas with different populations for different modes. Two-point correlation functions  $\mathcal{C}(z,z')$  for increasing evolution time, showing maxima on the diagonal and the anti-diagonal. The experimental observations ( $top\ row$ ) are in very good agreement with the theoretical model ( $bottom\ row$ ) assuming different occupation numbers for the different modes. The occupation numbers used in this plot were obtained from a fit to the steady state, their values are shown in Fig. 6.4. While they result in a reduced  $\chi^2$  close to 1, the best single-temperature model leads to a reduced  $\chi^2 \approx 25$  and thus clearly fails to describe the data

maximum on the anti-diagonal. This corresponds to enhanced correlations of the points  $z_1 = -z_2$ , which are located symmetrically around the center of the system. Interestingly, investigating the correlation function for a fixed value of z reveals that we have imprinted correlations outside of the relaxation light-cone which persist during the dynamics.

Note that only the phase correlation function, but not the integrated interference contrast as studied in the previous chapters, is sensitive enough to reveal the subtle differences between the two splitting protocols. The reason for this is that the effect of the two different temperatures on the contrast is only a small offset, which is negligible for the given experimental precision. Studying the contrast one is thus not able to observe the differences in the splitting process.

The enhanced correlations on the anti-diagonal are a direct consequence of an increased (decreased) population of quasi-particle modes that are even (odd) under a mirror-reflection with respect to the longitudinal trap center. Consequently, the observations can be described, to a first approximation, by the above theoretical model but with different temperatures, i.e. with  $\beta_{2m} = 1/[k_B(T_{\rm eff} + \Delta T)]$  for the even and  $\beta_{2m-1} = 1/[k_B(T_{\rm eff} - \Delta T)]$  for the odd modes, respectively. Fitting the experimental data of the steady state with this model we find  $k_B T_{\rm eff} = (0.64 \pm 0.01) \times \mu$ ,  $\Delta T = (0.48 \pm 0.01) \times T_{\rm eff}$  and a reduced  $\chi^2 \approx 6$ .

We observe that these properties of the GGE can be tuned by varying the speed of the splitting ramp. In Fig. 6.3 we present the corresponding measurements of the

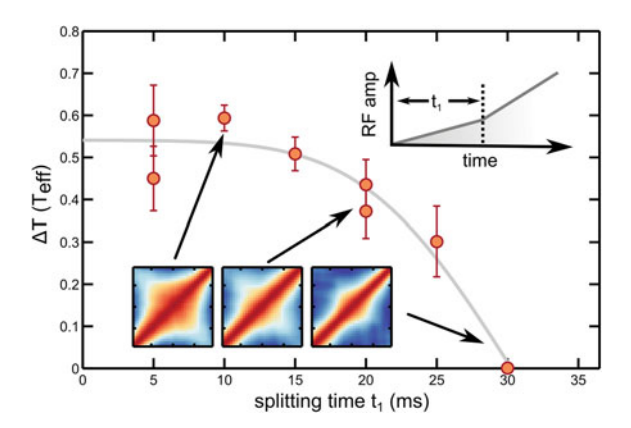


Fig. 6.3 Temperatures of the relaxed states. To split the initial 1D Bose gas into two halves, the amplitude of the dressing RF is increased in a two step ramp (see *Inset*). The longitudinal trap frequency  $\omega_z$  is rapidly changed from  $2\pi \times 11$  Hz to  $2\pi \times 7.5$  Hz during the first ramp segment, while the radial trapping potential still is close to the initial harmonic one. Changing the length  $t_1$  of this segment modifies the populations of even and odd modes. This leads to temperatures  $\beta_{2m} = 1/[k_B(T_{\rm eff} + \Delta T)]$  for the even modes and  $\beta_{2m-1} = 1/[k_B(T_{\rm eff} - \Delta T)]$  for the odd modes, where  $T_{\rm eff}$  is the temperature of the prethermalized state in the equally populated case. A fit to the relaxed state after  $(10 \pm 0.5)$  ms of evolution, allows the determination of the temperatures for even and odd modes. For longer times  $t_1$ , more complex states are created that cannot be described using the simple two-temperature model anymore. The *solid line* is a guide to the eye

temperatures for even and odd excitation modes as a function of the time scale  $t_1$  of the first ramp segment. In detail, an increasing ramp duration leads to a decreasing imbalance between even and odd modes. In the limit of a very slow splitting we recover the balanced situation studied in Fig. 6.1.

Unraveling the exact microscopic mechanism of this preparation requires a detailed simulation of the splitting process, including all details of the realistic chip trap. It is currently under investigation by several theory groups. In the most simple picture an infinitely fast splitting process can be understood as a binomial distribution of the atoms into the two halves of the system, as described by Sect. 4.3. This simple picture leads to the emergence of a single temperature. However, it has previously been shown that complex non-linearities can appear in realistic splitting protocols [29]. They result in the creation of squeezed states where the binomial atom number fluctuations predicted by the simple model are strongly reduced [30]. Our observation of multiple temperatures could be explained along these lines using locally reduced atom number fluctuations at the edges of the cloud.

Due to the non-linearities in the splitting process, the resulting local atom number fluctuations have to be determined numerically. In this context, the splitting process has previously been simulated using classical field methods or (Multi-Layer) Multiconfigurational Time-Dependent Hartree for Bosons (MCTDHB) [29, 31, 32]. However, a full theoretical model including the longitudinal degree of freedom has so far remained elusive. While classical fields can only account for thermal fluctuations using stochastic methods, MCTDHB has been used to study the creation of squeezing during the splitting of gases containing up to  $\mathcal{O}(100)$  particles in zero dimensions. A modeling of the experimental splitting process involving the 1D direction and thousands of particles is far beyond reach of current computational resources. Consequently, we understand our measurements as an important benchmark for future simulations. Moreover, the observed tunability suggests that such a detailed modeling could in the future be used to find splitting protocols which prepare well-defined initial states.

More detailed insights and a more accurate description of the experimental data are found by fitting the steady state with the individual occupations of the lowest modes as free parameters. We observe that including the first 9 modes in the fit and using one common occupation number for all higher modes leads to a very good description of the experimental data, with the reduced  $\chi^2$  close to 1 (see Fig. 6.2). The fact that 9+1 modes are needed is in good agreement with the decreasing contribution of higher modes and the effect of the optical resolution on the phase variance (Eq. 5.5). As expected from our intuitive two-temperature model, the fitting confirms that the occupation of even modes is strongly enhanced, whereas the occupation of odd modes is reduced (see Fig. 6.4). Given these occupation numbers extracted from the steady state, our theoretical model also describes the complete dynamics very well. This clearly demonstrates that the different populations of the modes were imprinted onto the system by the splitting quench and are conserved during the dynamics. Most importantly, it provides a visualization of the fact that the conflicting descriptions in terms of quantum mechanics (for the dynamics) and in terms of statistical physics (for the steady state) can be reconciled. In contrast to that, a usual Gibbs ensemble

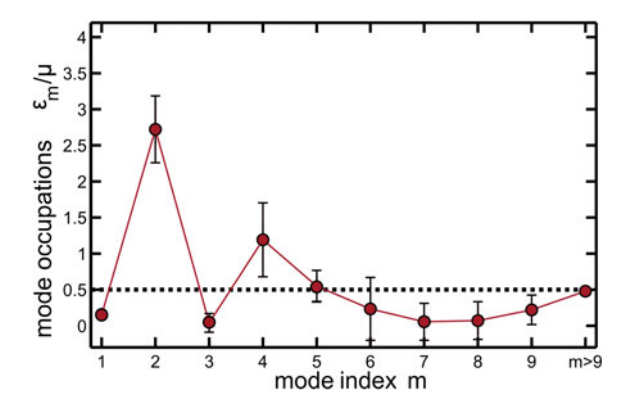
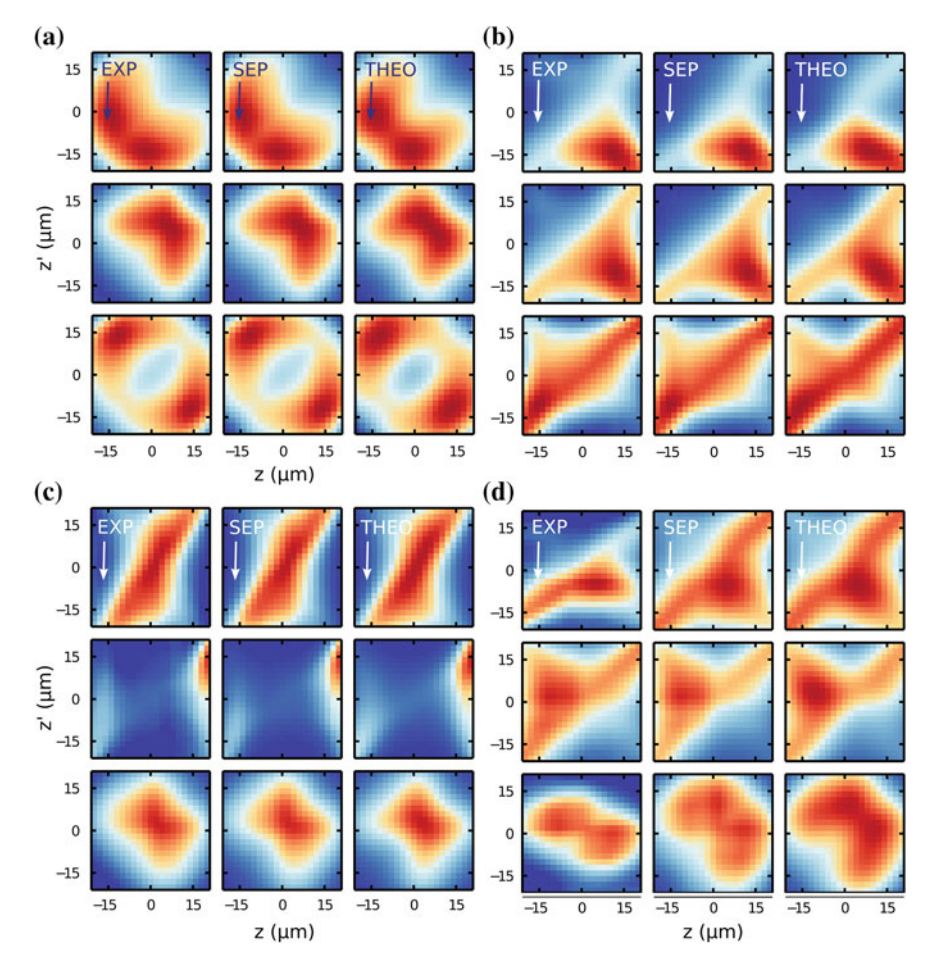


Fig. 6.4 Result of the fitting procedure. Occupation numbers  $n_m$  (in units of  $\epsilon_m/\mu$ ) of the quasiparticle modes with index m for a fit to the data from Fig. 6.2. The fit includes the occupation numbers of individual modes up to m=9, while all higher modes are fit with one common occupation number. The plot clearly reveals how the occupation of the lowest even (odd) modes are increased (decreased) as compared to the single-temperature state from Fig. 6.1, where  $n_m=0.5 \times \mu/\epsilon_m$  (dashed line)

with just one temperature for all modes clearly fails to describe the data (best fit:  $T_{\rm eff} = (0.38 \pm 0.01) \times \mu$ , reduced  $\chi^2 \approx 25$ ).

Notably, our fitting results for the GGE exhibit strong correlations between the different even modes and the different odd modes, respectively. This demonstrates the difficulty in fully and independently determining the parameters of such complex many-body states. In fact, any full tomography of all parameters would require exponentially many measurements. The results thus clearly show the presence of a GGE with at least two, but most likely many more temperatures.

Non-thermal properties of a relaxed quantum many-body system are in general expected to be characterized by higher-order correlation functions. Also, the conserved operators  $\hat{\mathcal{I}}_m$  entering the GGE description (6.1) of an integrable interacting system will in general involve higher-order operator products [33, 34]. For the relaxed states found in our system, the  $\hat{\mathcal{I}}_m$  are assumed to be given, to a good approximation, by the quadratic quasi-particle number operators that describe the occupation numbers of the excitations. Hence, the density operator is Gaussian, and any higher-order correlation function is expected to separate into one- and two-point functions. To provide further evidence for our theoretical description and the presence of a Gaussian GGE, we show in Fig. 6.5 examples of the measured four-point, six-point, ten-point and twenty-point correlation functions (see also Eq. 1.80). As the two-point correlation functions, they are in very good agreement with the theoretical model. In the future, such higher-order correlation functions could be used for a detailed tomography of the dynamical quantum many-body states [35, 36].



**Fig. 6.5** Examples of higher-order correlation functions. **a** Four-point correlation functions C(z, -2, -14, z'), C(z, 6, 6, z'), and C(z, 12, 14, z'). We compare the experimental correlation function (EXP) with a correlation function calculated from experimental two-point correlation functions (SEP) and our theoretical model (THEO), finding very good agreement. **b**, **c** Same for the six-point and ten-point correlation functions C(z, -10, 12, z', -2, -12), C(z, -10, 12, z', 6, 6), C(z, -10, 12, z', 6, 6), C(z, -12, 2, z', -12, -16, -12, z', -16, -14), C(z, 14, 20, z', 2, z', -12, -8, 20, 6) and C(z, -8, -10, 2, z', 2, -12, 0, -4, -14). All coordinates are given in  $\mu$ m and were randomly chosen to illustrate the high-dimensional data. First deviations become visible only in even higher correlation functions, such as the twenty-point correlation functions shown in (**d**). However, an Ornstein-Uhlenbeck simulation suggests that these deviations can be very well explained by the finite statistics of the experimental data, which become more important the higher the order of the correlation function (see also Fig. 5.2). In agreement with this statement, the twenty-point correlation functions constructed from the lower-noise two-point functions (SEP) still show very good agreement with theory

We further experimentally confirm the separation

$$C_{4}(z_{1}, z_{2}, z_{3}, z_{4}) = \frac{C_{12}C_{23}C_{34}C_{14}}{C_{13}C_{24}}$$

$$C_{6}(z_{1}, z_{2}, z_{3}, z_{4}, z_{5}, z_{6}) = \frac{C_{12}C_{23}C_{34}C_{45}C_{56}C_{14}C_{25}C_{36}C_{16}}{C_{13}C_{24}C_{35}C_{46}C_{15}C_{26}}$$

$$\vdots$$

$$(6.5)$$

of the four-point, six-point and higher-order correlation functions into two-point correlation functions. Here, we have used the notation  $C_{ij} \equiv C(z_i, z_j)$  for the two-point correlation functions. This demonstrates the Gaussian nature of the fluctuations. Any deviations from this separation could in the future be used to reveal and characterize interactions between quasi-particles.

#### 6.3 Conclusion

Our work raises the interesting question how many Lagrange multipliers are needed to describe the relaxed state of a realistic integrable quantum system. Similar as in classical mechanics, where N conserved quantities exist for a generic integrable system with N degrees of freedom, integrability in quantum many-body systems has been proposed to be characterized by the fact that the number of independent local conserved quantities scales with the number of particles. Here, we conjecture that far less Lagrange multipliers are needed to describe a quantum state to a given precision [37]. This would have the appeal of a strong similarity to thermodynamics, where also only few parameters are needed to describe the properties of a system on macroscopic scales. In our specific case, given our observables and the optical resolution of the experiment, already 9+1 parameters are sufficient to describe the experimental data.

Addressing even more fundamental issues, the observed near-Gaussian GGE state bears similarity to the approach of a Gaussian fixed point, i.e., a nearly scale-invariant and at the same time non-interacting state of an equilibrium system. While for the relaxed system higher-order terms beyond the Luttinger description vanish, we observe a state at finite effective temperatures. This advocates universality of prethermalized quantum many-body systems. Provided that the final equilibrium state which the system will in principle reach at much greater times (see Sect. 4.5), is described by a non-Gaussian GGE, the prethermalized Gaussian fixed point needs to be at least partially repulsive.

In conclusion, we have observed direct experimental signatures for the emergence of a generalized Gibbs state. This substantiates the importance of the maximum entropy principle and strikingly visualizes the emergence of statistical mechanics from a microscopic unitary quantum evolution. Moreover, the observed tunability of the non-equilibrium states holds important prospects for precision interferometry [29, 30].

#### References

- T. Langen, S. Erne, R. Geiger, B. Rauer, T. Schweigler, M. Kuhnert, W. Rohringer, I.E. Mazets, T. Gasenzer, J. Schmiedmayer, Experimental observation of a generalized Gibbs ensemble. Science 348, 207 (2015)
- 2. E.H. Lieb, W. Liniger, Exact analysis of an interacting Bose gas. I. The general solution and the ground state. Phys. Rev. **130**, 1605–1616 (1963)
- V.E. Korepin, Quantum Inverse Scattering Method and Correlation Functions (Cambridge University Press, Cambridge, 1997)
- A. Polkovnikov, K. Sengupta, A. Silva, M. Vengalattore, Colloquium: nonequilibrium dynamics of closed interacting quantum systems. Rev. Mod. Phys. 83, 863–883 (2011)
- M. Rigol, V. Dunjko, V. Yurovsky, M. Olshanii, Relaxation in a completely integrable manybody quantum system: an ab initio study of the dynamics of the highly excited states of 1D lattice hard-core bosons. Phys. Rev. Lett. 98, 050405 (2007)
- 6. R. Balian, From Microphysics to Macrophysics: Methods and Applications of Statistical Physics (Springer, New York, 2007)
- 7. C.E. Shannon, W. Weaver, *The Mathematical Theory of Communication* (The University of Illinois Press, Urbana, 1949)
- 8. E.T. Jaynes, Information theory and statistical mechanics. Phys. Rev. 106, 620–630 (1957)
- 9. E.T. Jaynes, Information theory and statistical mechanics. II. Phys. Rev. 108, 171–190 (1957)
- M. Greiner, I. Bloch, O. Mandel, T.W. Hänsch, T. Esslinger, Exploring phase coherence in a 2D lattice of Bose-Einstein condensates. Phys. Rev. Lett. 8716, 160405 (2001)
- J. Esteve, J.-B. Trebbia, T. Schumm, A. Aspect, C.I. Westbrook, I. Bouchoule, Observations
  of density fluctuations in an elongated Bose gas: ideal gas and quasicondensate regimes. Phys.
  Rev. Lett. 96, 130403 (2006)
- P. Krüger, S. Hofferberth, I.E. Mazets, I. Lesanovsky, J. Schmiedmayer, Weakly interacting Bose gas in the one-dimensional limit. Phys. Rev. Lett. 105, 265302 (2010)
- 13. T. Kinoshita, T. Wenger, D. Weiss, A quantum Newton's cradle. Nature 440, 900-903 (2006)
- M. Gring, M. Kuhnert, T. Langen, T. Kitagawa, B. Rauer, M. Schreitl, I.E. Mazets, D. Adu Smith, E. Demler, J. Schmiedmayer, Relaxation and prethermalization in an isolated quantum system. Science 337, 1318–1322 (2012)
- T. Langen, R. Geiger, M. Kuhnert, B. Rauer, J. Schmiedmayer, Local emergence of thermal correlations in an isolated quantum many-body system. Nat. Phys. 9, 640–643 (2013)
- J.P. Ronzheimer, M. Schreiber, S. Braun, S.S. Hodgman, S. Langer, I.P. McCulloch, F. Heidrich-Meisner, I. Bloch, U. Schneider, Expansion dynamics of interacting bosons in homogeneous lattices in one and two dimensions. Phys. Rev. Lett. 110, 205301 (2013)
- 17. M.A. Cazalilla, R. Citro, T. Giamarchi, E. Orignac, M. Rigol, One dimensional bosons: from condensed matter systems to ultracold gases. Rev. Mod. Phys. **83**, 1405–1466 (2011)
- T. Schumm, S. Hofferberth, L.M. Andersson, S. Wildermuth, S. Groth, I. Bar-Joseph, J. Schmiedmayer, P. Kruger, Matter-wave interferometry in a double well on an atom chip. Nat. Phys. 1, 57–62 (2005)
- M. Kuhnert, R. Geiger, T. Langen, M. Gring, B. Rauer, T. Kitagawa, E. Demler, D. Adu Smith, J. Schmiedmayer, Multimode dynamics and emergence of a characteristic length scale in a one-dimensional quantum system. Phys. Rev. Lett. 110, 090405 (2013)
- 20. J. Berges, Sz. Borsányi, C. Wetterich, Prethermalization. Phys. Rev. Lett. 93, 142002 (2004)
- M. Eckstein, M. Kollar, P. Werner, Thermalization after an interaction quench in the Hubbard model. Phys. Rev. Lett. 103, 056403 (2009)
- T. Kitagawa, A. Imambekov, J. Schmiedmayer, E. Demler, The dynamics and prethermalization of one-dimensional quantum systems probed through the full distributions of quantum noise. New. J. Phys. 13, 073018 (2011)
- T. Betz, S. Manz, R. Bücker, T. Berrada, C. Koller, G. Kazakov, I.E. Mazets, H.-P. Stimming, A. Perrin, T. Schumm, J. Schmiedmayer, Two-point phase correlations of a one-dimensional bosonic Josephson junction. Phys. Rev. Lett. 106, 020407 (2011)

References 121

- 24. J. Berges, S. Borsanyi, C. Wetterich, Prethermalization. Phys. Rev. Lett. 93, 142002 (2004)
- T. Gasenzer, J. Berges, M.G. Schmidt, M. Seco, Non-perturbative dynamical many-body theory of a Bose-Einstein condensate. Phys. Rev. A 72, 063604 (2005)
- J. Berges, T. Gasenzer, Quantum versus classical statistical dynamics of an ultracold Bose gas. Phys. Rev. A 76, 033604 (2007)
- R. Bistritzer, E. Altman, Intrinsic dephasing in one-dimensional ultracold atom interferometers. Proc. Natl. Acad. Sci. 104, 9955 (2007)
- 28. T. Kitagawa, S. Pielawa, A. Imambekov, J. Schmiedmayer, V. Gritsev, E. Demler, Ramsey interference in one-dimensional systems: the full distribution function of fringe contrast as a probe of many-body dynamics. Phys. Rev. Lett. **104**, 255302 (2010)
- J. Grond, J. Schmiedmayer, U. Hohenester, Optimizing number squeezing when splitting a mesoscopic condensate. Phys. Rev. A 79, 021603 (2009)
- T. Berrada, S. Van Frank, R. Bücker, T. Schumm, J.-F. Schaff, J. Schmiedmayer, Integrated Mach-Zehnder interferometer for Bose-Einstein condensates. Nat. Commun. 2077 (2013)
- 31. H.-D. Meyer, U. Manthe, L.S. Cederbaum, The multi-configurational time-dependent Hartree approach. Chem. Phys. Lett. **165**, 73–78 (1990)
- 32. O. Alon, A. Streltsov, L.S. Cederbaum, Multiconfigurational time-dependent Hartree method for bosons: many-body dynamics of bosonic systems. Phys. Rev. A 77, 033613 (2008)
- 33. M. Kollar, M. Eckstein, Relaxation of a one-dimensional Mott insulator after an interaction quench. Phys. Rev. A 78, 013626 (2008)
- D.M. Gangardt, M. Pustilnik, Correlations in an expanding gas of hard-core bosons. Phys. Rev. A 77, 041604 (2008)
- R. Hübener, A. Mari, J. Eisert, Wick's theorem for matrix product states. Phys. Rev. Lett. 110, 040401 (2013)
- A. Steffens, M. Friesdorf, T. Langen, B. Rauer, T. Schweigler, R. Hübener, J. Schmiedmayer, C.A. Riofrío, J. Eisert, Towards experimental quantum field tomography with ultracold atoms. arXiv:1406.3632 (2014)
- J.-S. Caux, F.H.L. Essler, Time evolution of local observables after quenching to an integrable model. Phys. Rev. Lett. 110, 257203 (2013)

# Chapter 7 Relaxation Dynamics in an Imbalanced Pair of One-Dimensional Bose Gases

We study the relaxation dynamics in a quenched pair of 1D Bose gases with atom number imbalance. As demonstrated in the previous chapters, 1D Bose gases follow completely integrable dynamics via dephasing of their many-body eigenstates. This leads to equilibration, i.e. time-independence of the observables, and to states which can be described by generalized Gibbs ensembles. For the imbalanced pair, we observe that this relaxation strongly depends on the choice of observable. In particular, we find that the dephasing can mimic thermalization if suitable initial conditions are imposed on the system. Furthermore, we explore the potential of imbalanced 1D Bose gases as a model system for the study of spin-charge dynamics within the Luttinger liquid framework.

# 7.1 Quenching an Imbalanced Pair of One-Dimensional Bose Gases

Non-equilibrium dynamics of isolated quantum systems play a central role in many fields of physics [1]. An important question in this context is whether the unitary evolution of an isolated quantum systems can lead to the emergence of thermal properties [2, 3]. For example, the eigenstate thermalization hypothesis (ETH) conjectures that dephasing can lead to thermalization in systems with a chaotic classical limit [4–6]. On the other hand, as we have seen in the previous chapters, so-called integrable systems are expected not to thermalize at all [7]. However, this distinction has to be taken with caution, as the notion of integrability is not clearly defined in the quantum case so far [8].

Recently, cold atom experiments have enabled precise studies of such non-equilibrium dynamics [9–14]. Here, we investigate the dynamics in a pair of slightly atom number imbalanced 1D Bose gases. The 1D Bose gas is known as

a prime example of an integrable system with strongly suppressed thermalization [7, 9, 11, 15]. Nevertheless, we demonstrate that dephasing leads to a state that closely resembles the thermal equilibrium state.

### 7.2 Experimental Results

Our experiment starts with a single phase-fluctuating 1D Bose gas that is prepared on an atom chip. The gas contains approximately 3000–10,000 atoms at tunable temperatures below 120 nK. The principle of the experiment is depicted in Fig. 7.1. A quench is realized by coherently splitting the initial gas into two uncoupled parts by deforming the initial harmonic trapping potential into a tunable double-well potential. Tilting the double-well potential slightly during the splitting, enables the realization of a variable mean atom number imbalance  $\Delta N/N = (N^{(1)} - N^{(2)})/(N^{(1)} + N^{(2)})$  between the two gases (see Fig. 2.14). As the splitting process is coherent, the two gases are created with almost perfectly correlated phase profiles. Over time, interactions in the gas lead to a relaxation of these initial correlations. The dynamics of this relaxation can be directly probed using matter-wave interferometry between

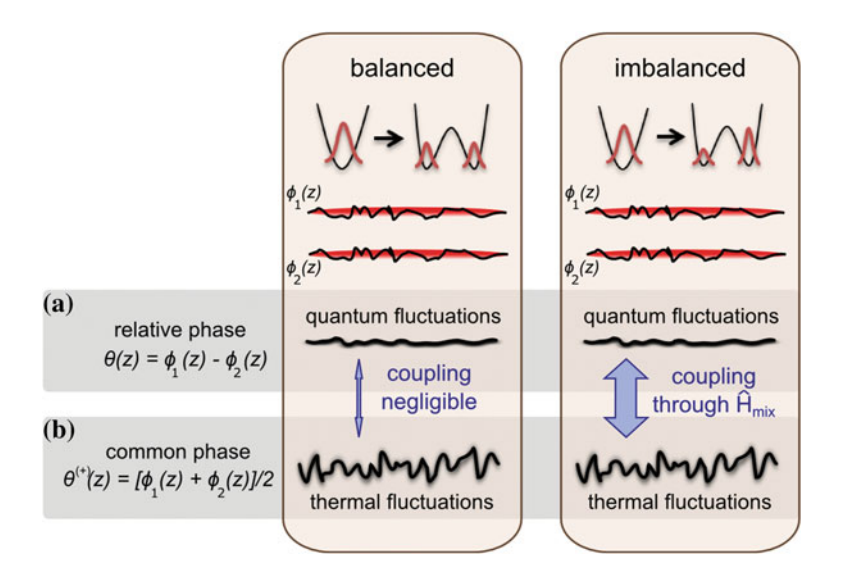
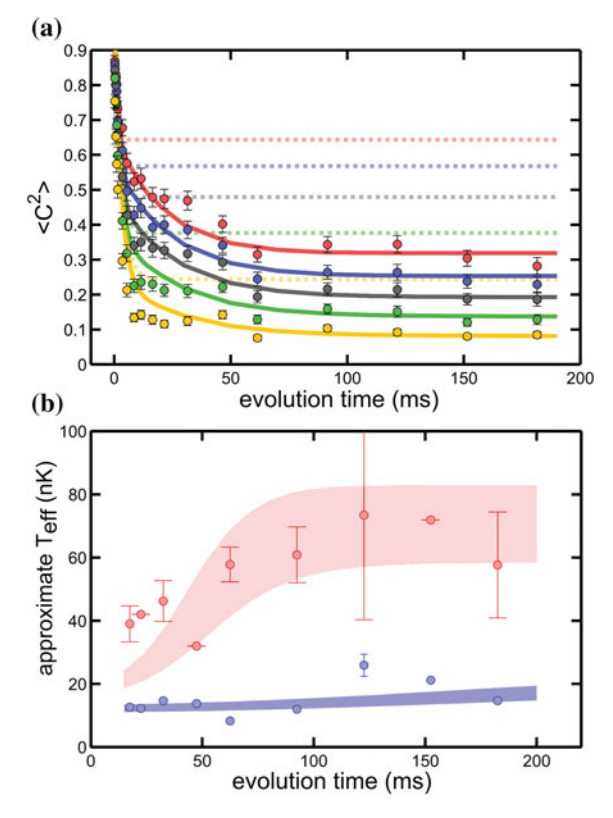


Fig. 7.1 Principle of the experiment. A single 1D Bose gas is coherently split into two parts. In the experiment, the system is probed in terms of anti-symmetric (b) and symmetric (b) superpositions of the eigenmodes in the individual parts. If the two parts have the same mean atom number, anti-symmetric and symmetric degrees of freedom are almost perfectly decoupled, as demonstrated in the previous chapters. If, however, the two parts have different mean atom numbers, the Hamiltonian  $\hat{H}_{\text{mix}}$  mixes the anti-symmetric and symmetric degrees of freedom, leading to an equilibration of the two. Here, we investigate the relaxation dynamics under the influence of this mixing



**Fig. 7.2** Dynamics of an imbalanced pair of 1D Bose gases. **a** Decay of the mean contrast squared for  $L=20, 30, 40, 60, 110 \,\mu\text{m}$  (points from *top* to *bottom*) with a high mean imbalance  $\Delta N/N=8\,\%$  and  $T_{\text{in}}=(114\pm23)\,\text{nK}$ . The experimental values have been corrected for the contrast reduction that is due to imperfections of the imaging system (see Appendix and Refs. [22, 23]). After a very rapid decay to the prethermalized state the system slowly relaxes further to a second steady state. The relaxation is in good agreement with our theoretical model (*solid lines*, see text). *Dashed lines* indicate the expected values for  $\langle |C|^2(L)\rangle$  without imbalance [22]. **b** Evolution of  $T_{\text{eff}}(t)$ . For low imbalance (*blue*,  $\Delta N/N=3\,\%$ ,  $T_{\text{in}}=(30\pm3)\,\text{nK}$ ) the system remains prethermalized for very long evolution times t. For high imbalance (*red*, data from **a**) the system first prethermalizes and then relaxes to a second steady-state. As shown in the theoretical analysis (see Sect. 7.3), the system is only approximately thermal before reaching this final steady state, and can thus only be assigned an approximate effective temperature. The *shaded areas* describe an estimate for this approximate effective temperature based on our theoretical model

the gases. The temperature of the initial gas is small enough such that thermalising two-body collision [16] and other predicted thermalization mechanisms [17–20] can be neglected during this relaxation (see Sect. 4.5).

Preliminary results for the observed evolution of the mean interference contrast squared  $\langle C^2(L) \rangle$  are plotted in Fig. 7.2a. They reveal two distinct time scales of relaxation. Initially, the contrast rapidly decreases in the approach to the prethermalized

state. This is followed by a much slower decay to a second steady state. The effect of the small difference in atom number between the two gases is thus not negligible, but instead leads to completely new dynamics [21].

Due to the similarity of the observations with the behavior of the gas in the 1D/3D crossover (see Sect. 4.5), we characterize the dynamics by extracting an effective temperature  $T_{\rm eff}(t)$  of the dynamical states. To this end, the mean contrast squared  $\langle C^2(L) \rangle$  is fitted as a function of integration length L for various evolution times up to 200 ms [22]. The results are presented in Fig. 7.2b.

For low atom number imbalance we observe the relaxation to a prethermalized steady state. The stability of this state is revealed by a constant effective temperature. However, for high atom number imbalance, the effective temperature rises significantly before reaching a second steady state. In Fig. 7.3, we present the effective temperature of this final state for a set of measurements with varying initial temperatures and densities. For a wide range of parameters we find

$$T_{\rm fin} \approx \frac{T_{\rm in} + T_{\rm eff}(0)}{2}.\tag{7.1}$$

This temperature corresponds exactly to the temperature that is expected in thermal equilibrium. Here,  $T_{\rm in}$  is the temperature of the initial gas before splitting,  $T_{\rm eff}(0)$  is the temperature characterizing the additional amount of energy that is added to the system by the coherent splitting process. From this measurement it thus seems as if the system had thermalized.

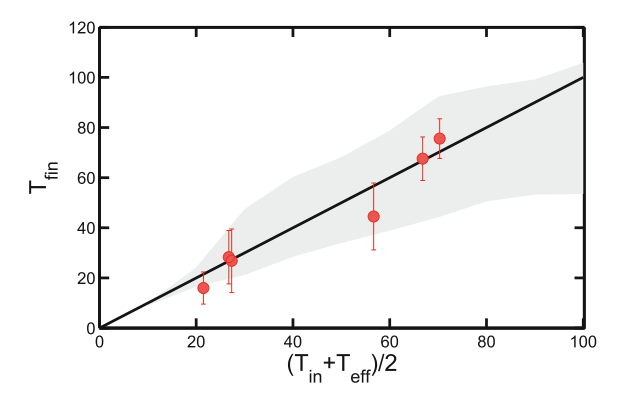


Fig. 7.3 Final temperature of the relaxation. For a given initial temperature  $T_{\rm in}$  and a given initial effective temperature  $T_{\rm eff}(0)$ , the measured final temperature of the anti-symmetric modes (red points) reaches  $T_{\rm fin} = [T_{\rm in} + T_{\rm eff}(0)]/2$ . This value coincides with the value expected in thermal equilibrium (solid line). The shaded area is an estimate of the uncertainty for the theory prediction, based on the experimental resolution, statistics and fitting precision [23]

#### 7.3 Theoretical Discussion and Interpretation

The dynamics of the system can be described by a low-energy Luttinger liquid description. As the tilt of the potential to achieve the atom number imbalance is much smaller than the chemical potential, we neglect it in the following and assume two identical wells. As discussed in detail in Sect. 1.5.1, each of the two gases can in this case be described by a Luttinger Hamiltonian  $H^{(i)}$ , which contains the individual density fluctuations  $\hat{n}^{(i)}(z)$  and phase fluctuations  $\hat{\phi}^{(i)}(z)$ . Here, i=1,2 denotes the two gases. The total Hamiltonian is thus of the form

$$\hat{H} = \hat{H}^{(1)} + \hat{H}^{(2)}. (7.2)$$

In the previous chapters, this situation was studied by transferring into symmetric and anti-symmetric superpositions of the low-energy eigenstates of the individual gases (Eq. 1.63). The reason for this is that the anti-symmetric degrees of freedom can directly be studied in terms of the relative phase  $\theta(z) = \phi^{(1)} - \phi^{(2)}$  and the matterwave interference contrast C(L). The splitting initializes the symmetric degrees of freedom with a high amount of energy, while the anti-symmetric degrees of freedom are only populated by a small amount of energy. In this situation, thermalization is revealed by an equilibration of symmetric and anti-symmetric degrees of freedom to the temperature  $T_{\rm fin}$  (see Sect. 4.5).

The change of basis leads to the new Hamiltonian (see Eq. 1.66)

$$\hat{H} = \hat{H}^{(-)} + \hat{H}^{(+)} + \hat{H}_{\text{mix}},\tag{7.3}$$

where  $H^{(\pm)}$  describes the symmetric and anti-symmetric degrees of freedom, respectively. The new term  $\hat{H}_{\text{mix}}$  describes mixing between symmetric and anti-symmetric degrees of freedom. Its explicit form is discussed in Sect. 1.5.1.

If the mean atom number in both gases is the same,  $\hat{H}_{mix}$  vanishes and only processes beyond the Luttinger description can lead to equilibration, as studied in Sect. 4.5. However, in the presence of an atom number imbalance, anti-symmetric and symmetric degrees of freedom are no longer an eigenbasis of the full Hamiltonian and will mix under the influence of  $\hat{H}_{mix}$ . This mixing depends on the atom number imbalance as well as on temperature.

To describe this situation we diagonalize  $\hat{H}^{(1)}$  and  $\hat{H}^{(2)}$  independently [24]. The results of this diagonalization can then be transferred into the symmetric/antisymmetric basis to compare them with the experiment.

While halving the atom number, the splitting creates an almost identical copy of the initial phase profile. As the thermal correlation length  $\lambda_T$  is proportional to the ratio of  $n_{\rm 1D}/T$  this means that each part of the system contains thermal fluctuations that are equivalent to a temperature  $T_{\rm in}/2$ . Following the classical field model introduced in Sect. 4.4, the phase fluctuations in the gas i=1,2 take the form

$$\langle |\phi_k^{(i)}(t)|^2 \rangle = \frac{m^2 c^{(i)2}}{\hbar^2 k^2 n_{\rm 1D}^{(i)2}} \langle |n_k^{(i)}(0)|^2 \rangle \sin^2(c^{(i)}kt) + \langle |\phi_k^{(i)}(0)|^2 \rangle \cos^2(c^{(i)}kt), \tag{7.4}$$

where  $n_{1D}^{(i)}$  denotes the densities in the individual gases. With  $n_k(0) \equiv n_{k0}$  and  $\phi_k(0) \equiv \phi_{k0}$ , the relative phase fluctuations are given by

$$\langle |\theta_{k}|^{2} \rangle = \langle |\phi_{k}^{(1)} - \phi_{k}^{(2)}|^{2} \rangle$$

$$= \frac{m^{2}c^{(1)2}}{\hbar^{2}k^{2}n_{1D}^{(1)2}} \sin^{2}(c^{(1)}kt) \langle |n_{k0}^{(1)}|^{2} \rangle + \langle |\phi_{k0}^{(1)}|^{2} \rangle \cos^{2}(c^{(1)}kt)$$

$$+ \frac{m^{2}c^{(2)2}}{\hbar^{2}k^{2}n_{1D}^{(2)2}} \sin^{2}(c^{(2)}kt) \langle |n_{k0}^{(2)}|^{2} \rangle + \langle |\phi_{k0}^{(2)}|^{2} \rangle \cos^{2}(c^{(2)}kt)$$

$$- \frac{m^{2}c^{(1)}c^{(2)}}{\hbar^{2}k^{2}n_{1D}^{(1)}n_{1D}^{(2)}} \sin(c^{(1)}kt) \sin(c^{(2)}kt) \left( \langle n_{k0}^{*(1)}n_{k0}^{(2)} \rangle + \langle n_{k0}^{*(2)}n_{k0}^{(1)} \rangle \right)$$

$$- \cos(c^{(1)}kt) \cos(c^{(2)}kt) \left( \langle \phi_{k0}^{*(1)}\phi_{k0}^{(2)} \rangle + \langle \phi_{k0}^{*(2)}\phi_{k0}^{(1)} \rangle \right)$$

$$(7.5)$$

Assuming only a small difference in atom number between the two gases, we make the following approximation

$$\frac{m^2 c^{(1)^2}}{k^2 n_{\rm 1D}^{(1)2}} \approx \frac{m^2 c^{(2)^2}}{k^2 n_{\rm 1D}^{(2)2}} \approx \frac{m^2 c^{(1)} c^{(2)}}{k^2 n_{\rm 1D}^{(1)} n_{\rm 1D}^{(2)}} \approx \frac{m^2 c^2}{k^2 n_{\rm 1D}^2},\tag{7.6}$$

with  $2n_{1D} = n_{1D}^{(1)} + n_{1D}^{(2)}$  and  $c = [c^{(1)} + c^{(2)}]/2$ .

The initial conditions for the density fluctuations in the two gases are given by (see Eqs. 1.84 and 4.4)

$$\langle |n_{k0}^{(1)}|^2 \rangle \approx \langle |n_{k0}^{(2)}|^2 \rangle \approx \frac{k_B T/2}{mc^2} n_{1D} + \frac{n_{1D}}{2}$$
 (7.7)

$$\langle n_{k0}^{*(1)} n_{k0}^{(2)} \rangle \approx \langle n_{k0}^{*(2)} n_{k0}^{(1)} \rangle \approx \frac{k_B T/2}{mc^2} n_{1D} - \frac{n_{1D}}{2}.$$
 (7.8)

In these equations, the first term describes the thermal fluctuations originating from the initial gas, while the second term describes the atomic shot noise that is added to the system in the splitting process. The minus sign in the second equation arises from the anti-correlations of the shot noise (see Fig. 4.6). The shot noise is directly related to the effective temperature of the prethermalized state via  $k_B T_{\text{eff}}(0) \equiv$  $k_B T_{\rm eff} = g n_{\rm 1D}/2$ .

Similarly, we find for the phase fluctuations

$$\langle |\phi_{k0}^{(1)}|^2 \rangle \approx \langle |\phi_{k0}^{(2)}|^2 \rangle \approx \langle \phi_{k0}^{*(1)} \phi_{k0}^{(2)} \rangle \approx \langle \phi_{k0}^{*(2)} \phi_{k0}^{(1)} \rangle \approx \frac{k_B T/2}{4n_{1D} \frac{\hbar^2 k^2}{4m}}$$
(7.9)

This yields

$$\langle |\theta_k|^2 \rangle \approx \frac{mk_B T}{\hbar^2 k^2 n_{1D}} 2 \sin^2(c'kt) + \frac{mk_B T_{\text{eff}}}{\hbar^2 k^2 n_{1D}} 4 [\sin^2(ckt) \cos^2(c'kt)], \tag{7.10}$$

where  $c' = [c^{(1)} - c^{(2)}]/2$ . This expression can be used to calculate the two-point phase correlation function (see Eq. 1.81). The result is presented in Fig. 7.4, and reveals two light-cones. With the integral

$$\int_0^\infty \frac{dk}{\pi} \frac{1}{k^2} \sin^2(ckt) [1 - \cos(kz)] = \frac{1}{4} |z|, \qquad (7.11)$$

which is valid for all  $z \leq 2ct$  within the light-cones, we can identify the respective steady states of the system. Note that this integral gives the same result when the  $\sin^2(ckt)$  term is replaced by  $\cos^2(ckt)$ . Comparing the form of the steady states with the phase correlation function in equilibrium (Eq. 1.85), one clearly observes two thermal-like steady states. The first steady state is the prethermalized one, which is characterized by the coherence length  $\lambda_{T_{\rm eff}} = \hbar^2 n_{\rm 1D}/mk_B T_{\rm eff}$  and the temperature  $T_{\rm eff}$ . It is reached with a fast light-cone characterized by the velocity c. The second thermal state is reached on a timescale set by the much slower velocity c'. Its temperature is given by  $T_{\rm fin}$ . Similar to the two-point correlation function, all higher-order correlation functions relax to these steady states.

In the experiment, the finite optical resolution makes this second light-cone less pronounced. Consequently, the correlation function can be approximated by an exponential decay. This explains why the system appears thermal already during the second stage of relaxation, although it is still relaxing. The corresponding approximate temperature is in good agreement with the experimental observations (Fig. 7.2b). Moreover, Eq. 1.78 can be used to calculate the mean contrast squared, which we find to be in good agreement with our data, as demonstrated in Fig. 7.2a.

Similar dynamics are obtained for the symmetric mode. Again, there is a rapid phase of prethermalization, followed by a slow relaxation with the characteristic velocity c'. Finally, this leads to a state with a temperature

$$T_{\rm fin}^{(+)} = \frac{T + T_{\rm eff}}{2}.$$
 (7.12)

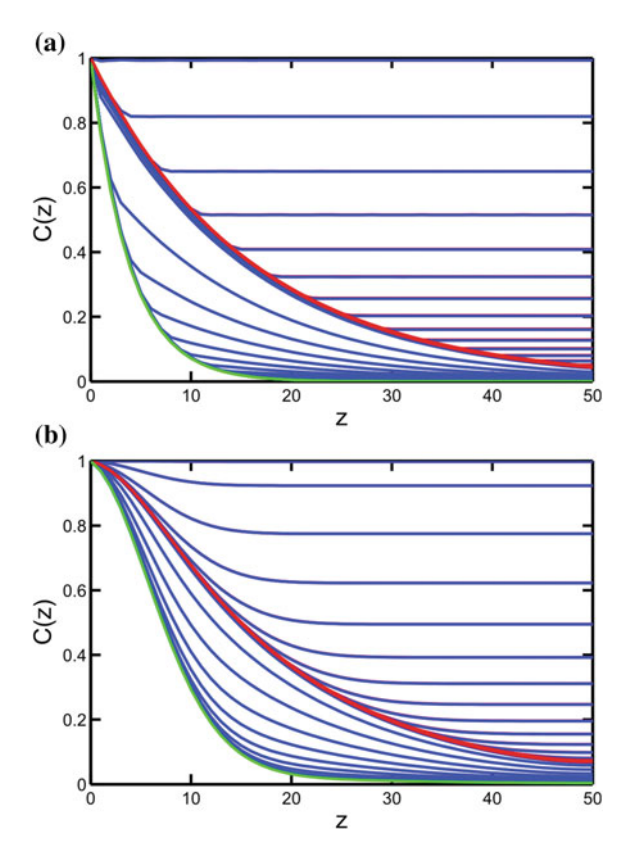


Fig. 7.4 Dynamics of the two-point phase correlation function in the theoretical model. a The two-point phase correlation function reveals a fast light-cone-like decay to the prethermalized state (red line), followed by a much slower second light-cone-like decay to the final relaxed state (green line). Evolution times increase in steps of 1 ms from top to bottom until the prethermalized state is reached, followed by steps of 50 ms in the approach to the final state (blue lines). Parameters are  $n_{1D} = 50/\mu m$ ,  $\Delta N/N = 2.5\%$  and  $T_{in} = 100$  nK. While the characteristic velocity for the first light-cone is given by the mean speed of sound  $c = (c^{(1)} + c^{(2)})/2$  of the excitations in the individual gases, the second light-cone is governed by their difference  $c' = (c^{(1)} - c^{(2)})/2$ . Experimentally, the first light-cone was probed in Chap. 5. Probing the second light-cone directly is precluded by the finite statistics of the experiment (see Fig. 5.2). Instead we calculate the mean contrast squared and compare it to the data in Fig. 7.2. b Taking the resolution of the imaging system into account, the second light-cone becomes close to a exponential decay for all times. When probing the evolution of the mean squared contrast as in Fig. 7.2b, the system thus appears to be thermal at any point in time during this second light-cone

Thus, all degrees of freedom are described by the same temperature.

Calculating the phase correlation functions of the individual gases, one finds from Eq. 7.4

$$\langle |\phi_k^{(i)}|^2 \rangle = \left(\frac{mk_B T}{2\hbar^2 k^2 n_{1D}} + \frac{mk_B T_{\text{eff}}}{\hbar^2 k^2 n_{1D}}\right) \sin^2(ckt) + \frac{mk_B T}{2\hbar^2 k^2 n_{1D}} \cos^2(ckt)$$

$$(7.13)$$

which describes a fast relaxation towards a temperature

$$T_{\rm fin}^{(i)} = \frac{T + T_{\rm eff}}{2}.$$
 (7.14)

Thus, each gas relaxes to the temperature that is expected in thermal equilibrium. However, only dephasing and no true thermalization has taken place. The time scale for this equilibration of the individual gases is identical to the one for the prethermalization of the symmetric and anti-symmetric degrees of freedom. This can be understood from the fact that we add number fluctuations to each gas, bringing it out of equilibrium. The time scale for the dephasing of these number fluctuations corresponds exactly to the time scale for the prethermalization. While the individual gases have already equilibrated, the total system evolves further, because the two gases continue to dephase with respect to each other.

Finally, we note that this system can be interpreted as a tunable quantum simulator for spin-charge physics within the Luttinger liquid framework [25, 26]. In this case, the symmetric degrees of freedom can be identified with the charge degrees of freedom  $\hat{H}^{(c)}$  of a fermionic spin chain, while the anti-symmetric degrees of freedom play the role of the spin  $\hat{H}^{(s)}$ . If the two gases are prepared with identical mean atom numbers, spin and charge degrees of freedom are separated. In the imbalanced case, the mixing term can be identified as a coupling between spin and charge. In the system of two spatially separate 1D Bose gases the characteristic velocities  $c_{s,c} = \sqrt{g_{s,c}n_{1D}/m}$  of spin and charge degrees of freedom are identical, as  $g_s = g_c \equiv g$ . Different velocities for spin and charge can be achieved by replacing the two wells employed in this thesis by two internal atomic states  $|1\rangle$  and  $|2\rangle$  with different interaction constants  $g_{11}$ ,  $g_{22}$  and  $g_{12}$  [27–30]. This situation would lead to  $g_{s,c} = g_{11} + g_{22} \mp 2g_{12}$  and thus different velocities for spin and charge. These velocities could be studied experimentally by probing the propagation of the in situ density fluctuations after a quench of the radial confinement [31, 32].

#### 7.4 Conclusion

We have observed that the dephasing of an imbalanced pair of 1D Bose gases can result in states which are, for all practical purposes, indistinguishable from thermal equilibrium. However, this observation of an apparent thermalization relies on the

thermal-like initial conditions that were imposed on the system by the coherent splitting process. The system always retains a strong memory of the initial conditions and thus has not truly reached thermal equilibrium. For example, if the system was initialized with other initial conditions, such as the ones studied in Chap. 6, it would equilibrate, but never appear thermal in its correlation functions [33]. This theoretical interpretation is supported by our preliminary experimental observations and we expect it to be insightful to experimentally study this effect and its competition with *true* thermalization in systematic detail.

Interestingly, the observed dynamics depends strongly on the measurement. In the experiment, fluctuations of the anti-symmetric degrees of freedom are probed. These degrees of freedom exhibit a rapid relaxation with a single time scale if there is no imbalance, and a relaxation with two distinct time scales if there is imbalance. The same timescales govern the relaxation of the symmetric degrees of freedom. In contrast to that, if the properties of a single gas were accessible in experiment, they would already look completely relaxed after the first, rapid time scale. Whether there is a general connection between the choice of measurement basis and the observed relaxation dynamics will be an interesting topic for future research.

#### References

- A. Polkovnikov, K. Sengupta, A. Silva, M. Vengalattore, Colloquium: nonequilibrium dynamics of closed interacting quantum systems. Rev. Mod. Phys. 83, 863–883 (2011)
- J.V. Neumann, Beweis des Ergodensatzes und des H-Theorems in der neuen Mechanik. Z. Phys. 57, 30–70 (1929)
- P. Reimann, Foundation of statistical mechanics under experimentally realistic conditions. Phys. Rev. Lett. 101, 190403 (2008)
- J.M. Deutsch, Quantum statistical mechanics in a closed system. Phys. Rev. A 43, 2046–2049 (1991)
- 5. M. Srednicki, Chaos and quantum thermalization. Phys. Rev. E 50, 888-901 (1994)
- M. Rigol, V. Dunjko, M. Olshanii, Thermalization and its mechanism for generic isolated quantum systems. Nature 452, 854–858 (2008)
- M. Rigol, Breakdown of thermalization in finite one-dimensional systems. Phys. Rev. Lett. 103, 100403 (2009)
- J.-S. Caux, J. Mossel, Remarks on the notion of quantum integrability. J. Stat. Mech. Theor. Exp. 2011, P02023 (2011)
- 9. T. Kinoshita, T. Wenger, D. Weiss, A quantum Newton's cradle. Nature 440, 900-903 (2006)
- L.E. Sadler, J.M. Higbie, S.R. Leslie, M. Vengalattore, D.M. Stamper-Kurn, Spontaneous symmetry breaking in a quenched ferromagnetic spinor Bose-Einstein condensate. Nature 443, 312–315 (2006)
- 11. M. Gring, M. Kuhnert, T. Langen, T. Kitagawa, B. Rauer, M. Schreitl, I.E. Mazets, D. Adu Smith, E. Demler, J. Schmiedmayer, Relaxation and prethermalization in an isolated quantum system. Science 337, 1318–1322 (2012)
- M. Greiner, O. Mandel, T.W. Hänsch, I. Bloch, Collapse and revival of the matter wave field of a Bose-Einstein condensate. Nature 419, 51 (2002)
- T. Langen, R. Geiger, M. Kuhnert, B. Rauer, J. Schmiedmayer, Local emergence of thermal correlations in an isolated quantum many-body system. Nat. Phys. 9, 640–643 (2013)

References 133

 J.P. Ronzheimer, M. Schreiber, S. Braun, S.S. Hodgman, S. Langer, I.P. McCulloch, F. Heidrich-Meisner, I. Bloch, U. Schneider, Expansion dynamics of interacting Bosons in homogeneous lattices in one and two dimensions. Phys. Rev. Lett. 110, 205301 (2013)

- V.E. Korepin, Quantum inverse scattering method and correlation functions (Cambridge University Press, Cambridge, 1997)
- 16. I.E. Mazets, J. Schmiedmayer, Thermalization in a quasi-one-dimensional ultracold bosonic gas. New J. Phys. **12**, 055023 (2010)
- I.E. Mazets, T. Schumm, J. Schmiedmayer, Breakdown of integrability in a quasi-1D ultracold Bosonic gas. Phys. Rev. Lett. 100, 210403 (2008)
- S. Tan, M. Pustilnik, L.I. Glazman, Relaxation of a high-energy quasiparticle in a onedimensional Bose gas. Phys. Rev. Lett. 105, 090404 (2010)
- H.-P. Stimming, N.J. Mauser, J. Schmiedmayer, I.E. Mazets, Dephasing in coherently split quasicondensates. Phys. Rev. A 83, 023618 (2011)
- 20. I.E. Mazets, private communication
- T. Kitagawa, S. Pielawa, A. Imambekov, J. Schmiedmayer, V. Gritsev, E. Demler, Ramsey interference in one-dimensional systems: the full distribution function of fringe contrast as a probe of many-body dynamics. Phys. Rev. Lett. 104, 255302 (2010)
- M. Kuhnert, R. Geiger, T. Langen, M. Gring, B. Rauer, T. Kitagawa, E. Demler, D. Adu Smith,
   J. Schmiedmayer, Multimode dynamics and emergence of a characteristic length scale in a one-dimensional quantum system. Phys. Rev. Lett. 110, 090405 (2013)
- M. Kuhnert, Thermalization and prethermalization in an ultracold Bose gas. Ph.D. thesis, Vienna University of Technology, 2013
- 24. T. Schweigler, T. Langen, Dynamics of pairs of 1D Bose gases. Unpublished
- 25. T. Giamarchi, Quantum Physics in One Dimension (Clarendon Press, Oxford, 2004)
- T.L. Schmidt, A. Imambekov, L.I. Glazman, Spin-charge separation in one-dimensional fermion systems beyond Luttinger liquid theory. Phys. Rev. B 82, 245104 (2010)
- T. Kitagawa, A. Imambekov, J. Schmiedmayer, E. Demler, The dynamics and prethermalization of one-dimensional quantum systems probed through the full distributions of quantum noise. New. J. Phys. 13, 073018 (2011)
- A. Widera, S. Trotzky, P. Cheinet, S. Fölling, F. Gerbier, I. Bloch, V. Gritsev, M.D. Lukin, E. Demler, Quantum spin dynamics of mode-squeezed Luttinger liquids in two-component atomic gases. Phys. Rev. Lett. 100, 140401 (2008)
- M.B. Zvonarev, V.V. Cheianov, T. Giamarchi, Spin dynamics in a one-dimensional ferromagnetic Bose gas. Phys. Rev. Lett. 99, 240404 (2007)
- 30. J.N. Fuchs, D.M. Gangardt, T. Keilmann, G.V. Shlyapnikov, Spin waves in a one-dimensional Spinor Bose gas. Phys. Rev. Lett. **95**, 150402 (2005)
- J. Esteve, J.-B. Trebbia, T. Schumm, A. Aspect, C.I. Westbrook, I. Bouchoule, Observations
  of density fluctuations in an elongated Bose gas: ideal gas and quasicondensate regimes. Phys.
  Rev. Lett. 96, 130403 (2006)
- 32. C.-L. Hung, V. Gurarie, C. Chin, From cosmology to cold atoms: observation of Sakharov oscillations in a quenched atomic superfluid. Science **341**, 1213–1215 (2013)
- N. Linden, S. Popescu, S.J. Short, A. Winter, Quantum mechanical evolution towards thermal equilibrium. Phys. Rev. E 79, 061103 (2009)

# Chapter 8 Conclusion and Outlook

The experiments that are presented in this thesis span a wide range of topics at the very heart of the field of non-equilibrium dynamics.

The results demonstrate for the first time several characteristic aspects of these dynamics, including the existence of a stable, thermal-like prethermalized state and its dynamical, light-cone-like emergence. Furthermore, the connection of the prethermalized state with generalized statistical ensembles and the subtle difference between thermalization and equilibration are highlighted.

The possibility to manipulate isolated quantum systems in ways as the ones presented here, has sparked a strong theoretical interest in non-equilibrium phenomena. This is further intensified by the striking similarities between the emergence of a statistical description and the emergence of classicality. An interesting future lies ahead, from possible applications of special non-equilibrium states to a profound understanding of the nature of non-equilibrium dynamics.

Our results enable many promising possibilities to further investigate the non-equilibrium dynamics of quantum many-body systems. Some of these possibilities will be briefly presented in the following.

# 8.1 Cooling, Thermalization and Ultracold Mixtures in 1D

The experiments performed so far, indicate that the initial gas before the splitting is thermal. On the other hand, we have shown that, at least for low temperatures, normal thermalization mechanisms are strongly suppressed. A detailed study of the cooling process and the nature of the resulting state is thus crucial. In 1D this cooling process must proceed notably different than in 3D, not only because of the suppression of thermalization, but also because of the important role played by the discrete level structure of the trap [1, 2]. Several theoretical models have been put forward [3–5] and are currently under experimental investigation.

A natural extension of this process, which could be investigated in our setup, is the sympathetic cooling of <sup>87</sup>Rb together with bosonic <sup>39</sup>K or fermionic <sup>40</sup>K.

This is particularly interesting as the different masses and the different statistical properties of bosons and fermions would strongly perturb the integrability of the system. Furthermore, as discussed in Sect. 2.2, the RF double-well potentials are state- and species-selective, allowing for experiments where one species is split while the other one is not [6]. Thus, it is possible to realize a non-equilibrium interferometer with one species, which is coupled to a controllable bath realized by the other species. This would create the opportunity to study the dynamics of open quantum systems.

# **8.2** Using Prethermalized States for Precision Interferometry

The matter-wave interferometer presented in this thesis is also suitable for precision interferometry. A key requirement for this application is a precise control of the relative phase between the two arms of the interferometer. In a general interferometer, interactions lead to a randomization of this relative phase, severely limiting the measurement times and thus its sensitivity. Recent studies indicate that interactions in low-dimensional quantum gases are favorable to achieve long measurement times [7].

However, as we have seen in this thesis, the multimode dynamics of a 1D gas generally lead to an additional loss of coherence. On the other hand, the prethermalized state shows very robust coherence for very long times. This suggests that it could be used as a resource for interferometry, greatly enhancing the possible measurement times. On top of that, the interactions during the splitting process can be used to introduce strong number squeezing, which could significantly improve the sensitive of the interferometer [8–10]. The combination of both effects has been demonstrated in the recent realization of an integrated Mach-Zehnder interferometer on an atom chip [11].

The prerequisite to further exploit these effects is a thorough understanding of the splitting process. A first step, the experimental modification of the initial state after splitting, was already presented in Chap. 6. Further studies, both experimentally and theoretically, are currently in progress.

# 8.3 From the Coherence Dynamics of Coupled 1D Superfluids to Universality Away from Equilibrium

During the splitting the dynamics of the system is affected by a varying tunnel coupling between the two gases. To understand the splitting, it is thus important to understand the dynamics of tunnel-coupled gases. This situation, however, has implications which go far beyond the understanding of the splitting process.

As we have seen in Chap. 2, symmetric and anti-symmetric modes remain decoupled for very long times during the dynamics. In the case of coupling between the

two gases, the anti-symmetric modes can therefore be described by the quantum Sine-Gordon Hamiltonian [12–14]

$$\hat{H}_{\text{SG}} = \frac{\hbar c}{2} \int_{-\mathcal{L}/2}^{\mathcal{L}/2} dz \left[ \frac{\pi}{K} \hat{n}^2(z) + \frac{K}{\pi} \left( \frac{\partial}{\partial z} \hat{\theta}(z) \right)^2 \right] - 2n_{\text{1D}} J \int_{-\mathcal{L}/2}^{\mathcal{L}/2} dz \cos[\sqrt{2} \, \hat{\theta}(z)].$$

The first part of this Hamiltonian is identical to the Luttinger Hamiltonian (Eq. 1.32). The second part leads to a large range of new phenomena, with applications in many different fields of physics [15–17]. In general, the relaxation mechanism and the nature of the steady states in more complicated field theories are still largely unknown [18]. As the Sine-Gordon model is arguably the simplest model with a gapped spectrum there is thus a large interest in studying its properties [12, 14, 19–21]. New tools, like the higher-order correlation functions introduced in Chap. 6 could facilitate important insights into these properties.

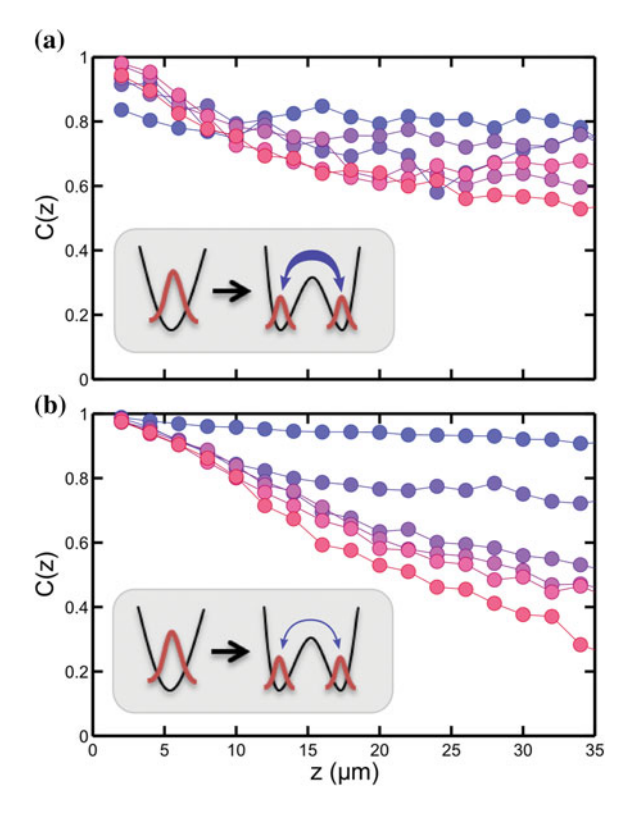
For the parameters realized in our experiments a semi-classical approximation is often applicable, where the cosine term is approximated by its first order expansion. The corresponding excitation spectrum has a gapped and an ungapped branch, which are degenerate for vanishing tunnel coupling [20]. Changing the tunnel coupling in experiments thus allows the realization of various different quenches.

First, an experiment similar to the splitting of the gas in Chap. 4 is performed, but keeping a finite tunnel coupling at the end of the splitting process. This results in initial conditions which are equivalent to the ones studied in the uncoupled case. The ensuing dynamics, however, strongly depends on the value of the coupling, as shown in Fig. 8.1. In terms of the dispersion relation this corresponds to a quench from an infinite gap to a finite one.

In a second experiment, an equilibrium situation in a double well with tunnel coupling is prepared, before the tunnel coupling is turned off by splitting the equilibrium gases further. This situation has the interesting property that two length scales exist in the initial state, one given by the length scale of the tunnel coupling and one by the thermal coherence length. In this procedure the quench connects a situation with finite gap to one with zero gap, with the initial conditions corresponding to a thermal state. Preliminary results are presented in Fig. 8.2.

Finally, two equilibrium gases are combined, realizing a quench from no gap to finite gap. This experiment is particularly interesting, as the cosine term cannot be expanded anymore, making the theoretical description very challenging. As the relative coherence between the initial thermal gases is low because of thermal fluctuations, combining them leads to a growth of the coherence with time. This experiment holds the prospect for novel insights into one of the most fundamental question of non-equilibrium dynamics: is there universality away from equilibrium? To understand what this concept means and why it is so fundamental, we need to ask how much can be learned from our experiments about other complex non-equilibrium systems? While it is clearly most interesting to study non-equilibrium dynamics at

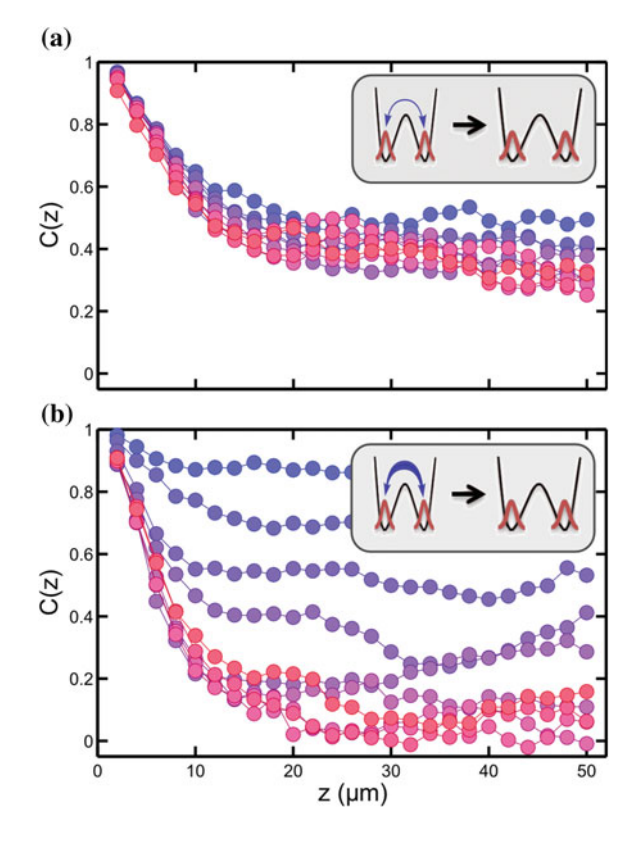
Fig. 8.1 Splitting to a state with finite tunnel coupling. a Coherent splitting of a gas into two parts with a strong tunnel coupling J. The large value of J strongly suppresses the loss of phase coherence with time. **b** Coherent splitting of a gas into two parts with a small tunnel coupling J. A light-cone-like evolution is observed, similar to the results presented in Chap. 5. In both plots  $t = 0, 4, 8, 12, 16, 25 \,\mathrm{ms}$ from top to bottom



such a clean and controllable level as in the experiments presented in this thesis, it is as clear that experiments with a cold gas containing several  $10^3$  atoms can never simulate the whole complexity of the expanding early universe [22]. In equilibrium, such quantum simulations of complex quantum many-body systems are possible [23–25]. The key to this is universality, which is rooted in the independence of the physical laws from the microscopic details of a particular system. Such independence can emerge when classical and quantum corrections are successively included across a range of scales. Universality is well understood in thermal equilibrium, where its mathematical foundations are given by the renormalization group [26]. For example, at a continuous phase transition, characteristic scaling properties of microscopically very different systems can be characterized in terms of a few universality classes relating to common symmetry properties of the systems. No such understanding exists away from equilibrium.

Universal behavior has been predicted for the build-up of coherence between the two gases in the experiment described above. In the given case, the existence of a universal function was conjectured, which, if measured at early evolution times would allow the prediction of the dynamics for any point in time. The emergent energy scale governing the dynamics in this system is predicted to be given by the

Fig. 8.2 Dynamics of tunnel coupled quasi-condensates. a Quench of a pair of gases with small tunnel coupling Jin equilibrium to a situation where J = 0. The dynamics changes the low-coherence initial state only very little. **b** The same experiment for high initial tunnel coupling. A light-cone-like decay of correlations can be observed. Evolution times from top to bottom are 0-5 ms in steps of 1 ms, followed by 10, 12, 17 and 22 ms



gap  $\Delta = (4J\mu)^{\eta}$ , where  $\eta \approx 1/2$  plays the role of a dynamical critical exponent for the quantum Sine-Gordon model.

Observing such universality away from equilibrium would provide fundamentally new insights into the properties of quantum many-body systems.

#### References

- I.E. Mazets, J. Schmiedmayer, Thermalization in a quasi-one-dimensional ultracold bosonic gas. New J. Phys. 12, 055023 (2010)
- I.E. Mazets, T. Schumm, J. Schmiedmayer, Breakdown of integrability in a quasi-1D ultracold bosonic gas. Phys. Rev. Lett. 100, 210403 (2008)
- B. Rauer, Evaporative cooling of one-dimensional Bose gases. Master's thesis, Vienna University of Technology, 2012
- 4. E. Witkowska, P. Deuar, M. Gajda, K. Rzążewski, Solitons as the early stage of quasicondensate formation during evaporative cooling. Phys. Rev. Lett. 106, 135301 (2011)
- P. Grisins, B. Rauer, T. Langen, J. Schmiedmayer, I.E. Mazets, Dissipative cooling of degenerate Bose gases. arxiv:1411.4946 (2014)

- M. Göbel, Low dimensional traps for Bose-Fermi mixtures. Ph.D. thesis, Ruperto-Carola University of Heidelberg, 2008
- J. Grond, U. Hohenester, I. Mazets, J. Schmiedmayer, Atom interferometry with trapped Bose-Einstein condensates: impact of atom-atom interactions. New J. Phys. 12, 065036 (2010)
- 8. J. Grond, J. Schmiedmayer, U. Hohenester, Optimizing number squeezing when splitting a mesoscopic condensate. Phys. Rev. A **79**, 021603 (2009)
- 9. C. Gross, T. Zibold, E. Nicklas, J. Esteve, M.K. Oberthaler, Nonlinear atom interferometer surpasses classical precision limit. Nature **464**, 1165–1169 (2010)
- M.F. Riedel, P. Böhi, Y. Li, T.W. Hänsch, A. Sinatra, P. Treutlein, Atom-chip-based generation of entanglement for quantum metrology. Nature 464, 1170–1173 (2010)
- 11. T. Berrada, S. Van Frank, R. Bücker, T. Schumm, J.-F. Schaff, J. Schmiedmayer, Integrated Mach-Zehnder interferometer for Bose-Einstein condensates. Nat. Commun. 2077 (2013)
- V. Gritsev, A. Polkovnikov, E. Demler, Linear response theory for a pair of coupled onedimensional condensates of interacting atoms. Phys. Rev. B 75, 174511 (2007)
- 13. C. Neuenhahn, Nonequilibrium dynamics of interacting quantum many-body systems. Ph.D. thesis, Friedrich-Alexander-Universität Erlangen-Nürnberg, 2012
- E.G. Dalla Torre, E. Demler, A. Polkovnikov, Universal rephasing dynamics after a quantum quench via sudden coupling of two initially independent condensates. Phys. Rev. Lett. 110, 090404 (2013)
- S. Coleman, Quantum sine-Gordon equation as the massive Thirring model. Phys. Rev. D 11, 2088–2097 (1975)
- M.P.A. Fisher, G. Grinstein, Quantum critical phenomena in charged superconductors. Phys. Rev. Lett. 60, 208–211 (1988)
- J.V. José, L.P. Kadanoff, S. Kirkpatrick, D.R. Nelson, Renormalization, vortices, and symmetrybreaking perturbations in the two-dimensional planar model. Phys. Rev. B 16, 1217–1241 (1977)
- A. Mitra, T. Giamarchi, Mode-coupling-induced dissipative and thermal effects at long times after a quantum quench. Phys. Rev. Lett. 107, 150602 (2011)
- C. Neuenhahn, F. Marquardt, Quantum simulation of expanding space-time with tunnelcoupled condensates. arXiv:1208.2255v1 (2013)
- N.K. Whitlock, I. Bouchoule, Relative phase fluctuations of two coupled one-dimensional condensates. Phys. Rev. A 68, 053609 (2003)
- T. Betz, S. Manz, R. Bücker, T. Berrada, C. Koller, G. Kazakov, I.E. Mazets, H.-P. Stimming, A. Perrin, T. Schumm, J. Schmiedmayer, Two-point phase correlations of a one-dimensional bosonic Josephson junction. Phys. Rev. Lett. 106, 020407 (2011)
- 22. J. Schmiedmayer, J. Berges, Cold atom cosmology. Science 341, 1188–1189 (2013)
- S. Nascimbène, N. Navon, K.J. Jiang, F. Chevy, C. Salomon, Exploring the thermodynamics of a universal Fermi gas. Nature 463, 1057 (2010)
- M.J.H. Ku, A.T. Sommer, L.W. Cheuk, M.W. Zwierlein, Revealing the superfluid lambda transition in the universal thermodynamics of a unitary Fermi gas. Science 335, 563–567 (2012)
- T. Donner, S. Ritter, T. Bourdel, A. Öttl, M. Köhl, T. Esslinger, Critical behavior of a trapped interacting Bose gas. Science 315, 1556–1558 (2007)
- 26. K. Wilson, The renormalization group and the  $\epsilon$  expansion. Phys. Rep. 12, 75–199 (1974)

### **Appendix A: Simulation of Realistic Wire Traps**

The idealized formulas introduced in Chap. 2 give a qualitative feeling for the different trapping geometries that can be created using atom chips. To describe our specific implementation, we employ a numerical calculation that includes the precise position of each wire into the description. The resulting magnetic fields are used to calculate the static, RWA and beyond RWA potentials.

### Magnetic Fields of Extended Wires

To make this simulation an accurate description of the experiment it is essential to take the finite size of the trapping wires into account. The magnetic field of a rectangular wire of width W, height H and length L can be calculated from the Biot-Savart law [1]

$$\mathbf{B}(\mathbf{r}) = \int_{-W/2}^{W/2} \int_{-H/2}^{H/2} \int_{-L/2}^{L/2} d\mathbf{r}' \frac{\mu_0}{4\pi} \frac{\mathbf{j} \times (\mathbf{r} - \mathbf{r}')}{|\mathbf{r} - \mathbf{r}'|^3}, \tag{A.1}$$

where  $\mathbf{j} = I/(WH)\hat{\boldsymbol{e}}_z$  denotes the current density and  $\mu_0$  is the vacuum permeability. The resulting field in the different spatial directions is given by [2]

$$B_x = \frac{\mu_0 I}{4\pi HW} \left[ -f(L, H, W) + f(-L, H, W) - f(-L, -H, W) + f(L, -H, W) \right]$$
(A.2)

$$B_{y} = \frac{\mu_{0}I}{4\pi HW} [f(L, H, W) - f(-L, H, W) + f(-L, -H, W) - f(L, -H, W)]$$
(A.3)

$$B_z = 0, (A.4)$$

with

$$f(L, W, H) = y_{+} \operatorname{arccoth}\left(\frac{z_{+}}{\sqrt{x_{-}^{2} + y_{+}^{2} + z_{+}^{2}}}\right) - x_{-} \operatorname{arccoth}\left(\frac{y_{+}z_{+}}{x_{-}\sqrt{x_{-}^{2} + y_{+}^{2} + z_{+}^{2}}}\right)$$

$$- y_{-} \operatorname{arccoth}\left(\frac{z_{+}}{\sqrt{x_{-}^{2} + y_{+}^{2} + z_{+}^{2}}}\right) + x_{-} \operatorname{arccoth}\left(\frac{y_{-}z_{+}}{x_{-}\sqrt{x_{-}^{2} + y_{+}^{2} + z_{+}^{2}}}\right)$$

$$+ z_{+} \ln\left(\frac{y_{-} - \sqrt{x_{-}^{2} + y_{+}^{2} + z_{+}^{2}}}{y_{+} - \sqrt{x_{-}^{2} + y_{+}^{2} + z_{+}^{2}}}\right). \tag{A.5}$$

Here,  $x_{\pm} = x \pm W/2$ ,  $y_{\pm} = y \pm H/2$  and  $z_{\pm} = z \pm L/2$ .

## Floquet Formalism

To calculate the RF dressed state potentials beyond the rotating-wave approximation, we use the Floquet formalism [3]. The principle of this formalism is to use a time-independent Hamiltonian with infinite dimension, to describe the evolution under a time-dependent Hamiltonian with finite dimension.

More specifically, one aims to solve a Schrödinger equation with the Hamiltonian

$$\hat{H} = \mu_B g_F \left[ B_S(\mathbf{r}) \hat{F}_z + B_{RF} \cos(\omega_{RF} t + \delta) \hat{F}_x \right]$$
 (A.6)

describing the interaction of the atoms with a time-dependent RF field (see Eq. 2.3). Here,  $F_x$  and  $F_z$  are x and z direction of the total angular momentum operator  $\hat{F}$  [4]. This Hamiltonian is periodic,  $\hat{H}(t) = \hat{H}(t+T)$ , with the period  $T = 2\pi/\omega_{RF}$  given by the frequency of the RF radiation.

Similar to the Bloch theorem for the spatially periodic Hamiltonian of a crystal lattice [5], the solution can be written as a superposition of functions  $\Phi_{\alpha}(r,t) = \Phi_{m_F}(r,t+T)$  that are periodic in time. Here,  $m_F = -2, \ldots, +2$  labels the bare atomic Zeeman levels. These functions are the eigenfunctions of the block-diagonal

Floquet Hamiltonian  $\hat{H}_F$ , the matrix elements of which are given by

$$\langle m_F, n | \hat{H}_F | m_F', m \rangle = H_{m_F, m_F'}^{n-m} + n\hbar\omega \delta_{m_F, m_F'} \delta_{n,m}. \tag{A.7}$$

Here  $H_{m_F,m_F'}^k$  denotes the *k*th Fourier component of the respective matrix element of the time-dependent Hamiltonian. These Fourier components are given by

$$H_{m_F,m_F'}^k \sim \begin{cases} (B_S F_z)_{m_F,m_F'} & k = 0\\ (B_{RF} F_x)_{m_F,m_F'} \exp(ik\delta) & k = \pm 1\\ 0, & k > 1 \end{cases}$$
(A.8)

In a fully quantized treatment [3], n and m can be identified with the definite, but very large number of photons in the RF field, i.e. with the dressed-state manifolds introduced in the main text. In practice, transitions between separated manifolds quickly become negligible for increasing difference in photon number. The matrix of the time-independent, infinite Hamiltonian  $\hat{H}_F$  can thus be truncated at an order around n-m=10, which can easily be diagonalized numerically. This directly yields the dressed state energy spectrum.

Our numerical implementation of this procedure, including the realistic wires described above, is based on work by Aurélien Perrin. Exemplary results are shown in Figs. 2.4 and 2.12 of the main text.

## **Appendix B: Estimation of the Tunnel Coupling**

For the coherent splitting process, as well as for the experiments with tunnel coupled gases presented in the outlook, it is important to estimate the tunnel coupling between the gases for a given double-well potential.

A first estimate can be obtained from a generic result for the tunneling frequency [6, 7]

$$\omega_p \simeq \omega_{\perp} \frac{d^2}{4a_{ho}^2} \exp\left(-\frac{d^2}{4a_{ho}^2}\right),$$
 (A.9)

where d is the distance between the two wells,  $\omega_{\perp}$  is the trap frequency in a single well and  $a_{ho} = \sqrt{\hbar/m\omega_{\perp}}$  is the corresponding ground-state size. This frequency is related to the tunnel coupling via  $J = \hbar\omega_p^2/4\mu$  [8].

For a more realistic description it is necessary to numerically calculate the eigenfunctions of the simulated double-well potential. However, the single mode solution of the GPE is no longer a good description of the two gases in the double well. Instead, at least two modes are necessary. To construct these two modes one determines the ground state of the Schrödinger equation in each single well [8]. The two lowest states of the double-well system can be approximated by the symmetric and anti-

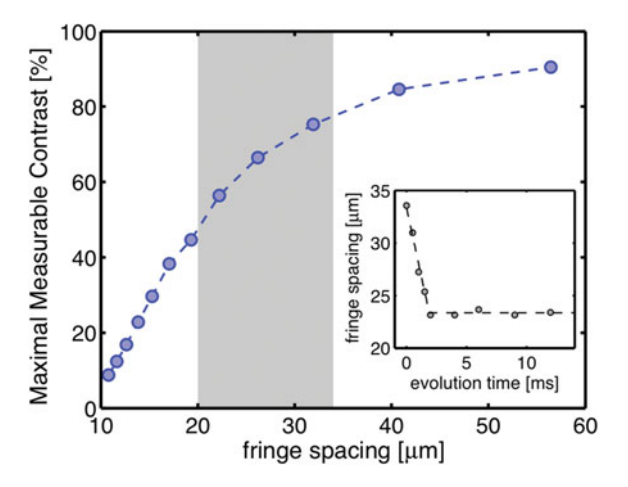
symmetric superpositions of these eigenstates. To further refine them, they can be used as starting values for an imaginary time-propagation using the Gross-Pitaevskii equation. The two eigenstates are separated by a gap  $\Delta$ , which directly corresponds to the tunneling frequency. This two-mode approximation can be further improved by including a nonlinear interaction term in the tunnel coupling energy [9] as described and implemented in [8].

Comparing with the results in Chap. 2 and in Ref. [10], shows that this calculation is very useful as an estimate of the tunnel coupling. For precise values, however, the two-mode approximation is not accurate enough and the tunnel coupling has to be obtained experimentally using measurements of phase correlation functions or using Josephson oscillations.

# **Appendix C: Comparison of the Measured Mean Contrast with Theory**

The contrast observed in experiment is affected by the properties of the vertical imaging system. To compare our results to theory, we model the imaging process using a simulation of the imaging system that includes the measured point spread function, diffraction effects from the chip surface, the finite size of the cloud in time-of-flight and the photon shot noise [11–13]. The resulting maximum measurable contrast is shown in Fig. A.1. These result are in qualitative agreement with an estimate based on the modulation transfer function of the imaging system [12]. For the data presented in Fig. 7.2 we rescaled the data by the corresponding factor. Note that the position of the fringes is independent of the maximal measurable contrast. Consequently, no such rescaling is necessary for measurements of the local relative phase  $\theta(z)$ .

**Fig. A.1** Maximum measurable contrast. Figure taken from [13]



# Appendix D: 87Rb Data

Table A.1	Properties	of 87Rb	[14]
-----------	------------	---------	------

Natural isotopic abundance		27.83 %
Nuclear spin	I	3/2
Mass	m	86.9902 u
D <sub>1</sub> -transition wavelength in vacuum	$\lambda_{D1}$	794.979 nm
D <sub>2</sub> -transition wavelength in vacuum	$\lambda_{D2}$	780.241 nm
D <sub>1</sub> -transition linewidth	$\Gamma_{\mathrm{D1}}$	$2\pi \times 5.58 \mathrm{MHz}$
D <sub>2</sub> -transition linewidth	$\Gamma_{\mathrm{D2}}$	$2\pi \times 6.01 \mathrm{MHz}$
D <sub>1</sub> -transition strength	$f_{\mathrm{D1}}$	0.3421
D <sub>2</sub> -transition strength	$f_{\mathrm{D2}}$	0.6956
doppler limit $T_D = \hbar \Gamma / 2k_B$	$T_D$	146 μΚ
$F = 2$ , $m_F = 2$ s-wave scattering length	$a_s$	$98.99(2)a_0 \simeq 5.238 \mathrm{nm}$

#### References

- 1. J.D. Jackson, Classical Electrodynamics (Wiley, New York, 1998)
- S. Hofferberth, Coherent manipulation of Bose-Einstein condensates with radio-frequency adiabatic potentials on atom chips. Ph.D. thesis, University of Heidelberg, 2007
- J.H. Shirley, Solution of the schrödinger equation with a Hamiltonian periodic in time. Phys. Rev. 138, B979–B987 (1965)
- 4. J.J. Sakurai, Modern quantum mechanics (Addison-Wesley Publishing Company, Reading, 1994)
- 5. F. Bloch, Über die Quantenmechanik der Elektronen in Kristallgittern. Z. Phys. 52, 555 (1929)
- T. Schumm, Bose-Einstein condensates in magnetic double well potentials. Ph.D. thesis, University of Paris 11, 2005
- G.J. Milburn, J. Corney, E.M. Wright, D.F. Walls, Quantum dynamics of an atomic Bose-Einstein condensate in a double-well potential. Phys. Rev. A 55, 4318–24 (1997)
- 8. T. Betz, Phase correlations of coupled one-dimensional Bose gases. Ph.D. thesis, Vienna University of Technology, 2011
- 9. D. Ananikian, T. Bergeman, Gross-Pitaevskii equation for Bose particles in a double-well potential: two-mode models and beyond. Phys. Rev. A 73, 013604 (2006)
- T. Betz, S. Manz, R. Bücker, T. Berrada, C. Koller, G. Kazakov, I.E. Mazets, H.-P. Stimming, A. Perrin, T. Schumm, J. Schmiedmayer, Two-point phase correlations of a one-dimensional Bosonic Josephson junction. Phys. Rev. Lett. 106, 020407 (2011)
- M. Gring, Prethermalization in an isolated many-body system. Ph.D. thesis, Vienna University of Technology, 2012

12. M. Kuhnert, Thermalization and prethermalization in an ultracold Bose gas. Ph.D. thesis, Vienna University of Technology, 2013

- 13. M. Kuhnert, R. Geiger, T. Langen, M. Gring, B. Rauer, T. Kitagawa, E. Demler, D. Adu Smith, J. Schmiedmayer, Multimode dynamics and emergence of a characteristic length scale in a one-dimensional quantum system. Phys. Rev. Lett. **110**, 090405 (2013)
- 14. D.A. Steck, Rubidium 87 D line data (2003), http://steck.us/alkalidata